Immunological responses to emerging phleboviruses

Elizabeth Allen

Brasenose College
Division of Structural Biology
Nuffield Department of Medicine
University of Oxford

A thesis submitted in partial fulfilment of the requirements for the degree of Doctor of Philosophy

Trinity Term 2019

Immunological responses to emerging phleboviruses

Elizabeth Allen, Brasenose College, University of Oxford

Doctor of Philosophy, Division of Structural Biology, Nuffield Department of Medicine.

Trinity term 2019

Abstract

Emerging viruses of the *Phenuiviridae* family threaten human and animal health across the globe. The mosquito-borne phlebovirus, Rift Valley fever virus (RVFV) is widespread across the African continent wherein regular deadly outbreaks amongst livestock constitute a significant economic burden. In 2009, a tick-borne banyangvirus, severe fever with thrombocytopaenia syndrome virus (SFTSV), emerged in China. Since emergence, SFTSV has spread rapidly and become a serious public health concern in China, Korea, and Japan, with human fatality rates reaching 30%. The growing health burden of phenuiviruses is further highlighted by the emergent tick-borne pathogen, Heartland banyangvirus (HRTV), a genetic relative of SFTSV that is responsible for sporadic human disease outbreaks in the USA.

Targeting of the glycoprotein capsomers displayed on the phenuivirus surface by the antibody-mediated immune response is key to controlling infection. To enhance understanding of the molecular basis for immune recognition, we raised monoclonal antibodies (mAbs) against RVFV Gn, one of which exhibited protective efficacy in a mouse infection model. Structural characterisation, using X-ray crystallography, revealed that neutralising antibodies (nAbs) were directed to the membrane-distal domain B of RVFV Gn and likely prevented virus entry into a host cell by blocking the required rearrangements within viral capsomers necessary for membrane fusion. Additionally, we structurally characterised non-neutralising mAbs that target RVFV Gn. These data revealed a previously unreported domain repositioning of RVFV Gn and uncover a potential intermediate that precedes fusogenic rearrangements of the Gn-Gc lattice. These data form a model for antibody-mediated neutralisation of RVFV and provide a blueprint for the rational design of immunotherapeutics and vaccines capable of preventing RVFV infection.

Finally, we generated additional libraries of immunoglobulins that target phlebo- and banyangviruses. A nanobody library was generated by vaccination with a leading RVFV vaccine candidate and recombinant RVFV Gn and Gc, which revealed a neutralising response directed to RVFV Gc. This thesis reports the expression and purification of recombinant banyangvirus Gn glycoproteins from HRTV and SFTSV. A heterologous prime-boost regime with the recombinant Gn glycoproteins was implemented and cross-reactive mAbs binding both SFTSV and HRTV were isolated. These nanobodies and mAbs may constitute key reagents for future structural studies, viral detection, and neutralisation efforts. Furthermore, it is likely that they will provide additional insight into the fundamental biology of the immune response to phenuiviruses.

The work described herein provides a molecular appraisal of key effectors of the immune response to emerging phenuiviruses. Isolation of novel immunoglobulins and elucidation of their modes of action inform aspects of basic phenuiviral biology and enable future rationalised vaccination and treatment strategies.

Approximately 38, 000 words, excluding abstract, table of contents, references and appendix.

Acknowledgements

First and foremost, I would like to thank my supervisors in Oxford, Thomas Bowden and Juha Huiskonen for their excellent guidance. In particular, thanks to Thomas for being attentive, available and patient throughout my time in Strubi. Thanks to my supervisor Roger Hewson, at PHE, for the opportunity to study in his laboratory. I'm also thankful for Stuart Dowall and Victoria Graham who went above and beyond to make sure my trips to Porton Down were fruitful and that I stayed caffeinated. I feel very lucky to have collaborated with such excellent scientists for this project. I'm especially thankful for Katie Doores, and her post-docs Stef and Jeff, without whom much of the work presented here would not have been possible.

My time in Strubi was made most enjoyable by the great company. Thanks to the current and past members of the Bowden group; Antra, Ilona, Ruben, Guido, Yasa and Weng, for their support and scientific guidance. In particular, a huge thanks to Steinar who guided me through my first year in the lab. Margaret, Ollie and Weixen for keeping the Strubi lab in great working condition. I'm grateful for Tom and Karl, for their expertise and help with crystallography, especially Karl who was always willing to help with harvesting crystals. I'm especially thankful for the friendships I have formed over the four years of my DPhil. Thanks to the coffee-breakers, who provided many laughs, and occasional science chat. It has been great to share the experience of a PhD with the Strubi students; Rhys, Serban, Eamon, Rachel, the Helens, Sam, Vojta, and Reinis. Rob, Vicky and Alice, thanks for sharing cat pictures throughout the writing up period.

Outside of work, I've had a great support network. A huge thanks to the residents of 39 St Mary's Road, past and present- in particular Nonie, Katie and Sarah who have truly made my time in Oxford. Thanks for a wonderful four years. Thanks to Cyndi and Oscar, for providing the perfect environment to write a thesis from. Thanks to my family and friends for their support. And finally, thanks to Seb, for encouraging me to keep going and believing I could do this.

Contents

Chapter 1:

Introduction

Chapter 1: Introduction

1.1 Viruses

Viruses are obligate intracellular organisms and a leading cause of human and animal disease worldwide [1, 2]. Single-stranded RNA viruses are a common cause of emergent human illness and represent a significant threat to global health and biodefence. The low fidelity of RNA polymerases results in enhanced mutation rates compared with DNA viruses, leading to higher genetic change and the requirement for small genomes and genetic economy [3, 4]. Such inaccurate replication allows RNA viruses to readily adapt to novel species as well as escape from immunological pressures arising from the host [5].

1.1.1 Zoonotic RNA viruses

Zoonosis describes the process by which an infectious agent is spread from infected animals to humans. In some instances following human infection, viral agents may also be capable of undergoing human-to-human transmission, highlighting the pandemic potential of zoonotic diseases to global health [6-8]. Although animal reservoirs of zoonotic disease are predominantly mammalian (possibly due to their biological and genetic similarity to humans), many zoonotic diseases have an invertebrate transmission vector, such as dengue virus (DENV) and Zika virus (ZIKV) [9, 10]. Importantly, exposure to an animal virus is not always sufficient to generate productive infection, as the virus must be able to replicate within the human host, a process that includes host-cell entry, host immune evasion and escape from the infected cell or organism. A critical determinate of zoonosis is the ability of a virus to specifically interact with a cellular attachment or entry protein at the stage of host-cell entry, which can dictate the species and cell tropism of the virus [11].

1.1.2 Emerging and re-emerging viruses

For a pathogen to be 'emerging', it is broadly defined as having been recently introduced into a population. Historically, emerging and re-emerging zoonotic diseases have had catastrophic effects upon human populations [12]. Outbreak of the 'Spanish flu' is one of the most devastating examples, having been responsible for millions of deaths in 1918 [13]. Despite medical and scientific advances, the emergence and re-emergence of infectious diseases still has a large effect upon human health and economy. For example, in 2009, a global flu pandemic re-emerged from a porcine reservoir and claimed ~18,000 lives. Other examples of emerging viruses that have recently threatened human health include, Ebola virus (EBOV), Nipah virus, ZIKV and MERS-CoV (Middle East respiratory syndrome coronavirus) [14-17]. In recent years, the number of emerging viruses has appeared to increase at a rate that cannot be accounted for by increased viral surveillance and advancements in scientific detection methods alone [18]. Increased instances of zoonotic viral emergence are likely facilitated by changes in human behaviour, such as; damming of rivers, deforestation, population expansion, environmental encroachment, cultural nuances, transportation, globalisation, and changing weather patterns as a result of global warming [19].

1.2 Phlebo- and banyangviruses as human and animal pathogens

The genus *Phlebovirus*, within the family *Phenuiviridae* (formerly *Bunyaviridae)*, constitutes a group of emerging arthropod-borne pathogens that pose a significant threat to human health and animal husbandry. The genetically diverse group of phleboviruses currently contains ten species recognised by the International Committee on the Taxonomy of Viruses (ICTV), as well as 39 tentative species [20, 21]. The viruses can be broadly categorised into two groups, the Sandfly group (sandfly- and mosquito-borne) and the Uukuniemi-like group (tick-borne), which reflect both the genetic similarities and the invertebrate hosts **(Fig. 1.1)**. Of the ten recognised species, four cause disease in humans, including Rift Valley fever virus (RVFV)

and sandfly fever Naples virus (SFNV). Recent reclassification in the *Phenuiviridae* family sees the creation of the *Banyangvirus* genus, which contains three species of human pathogenic viruses, Bhanja virus, Heartland virus (HRTV) and severe fever with thrombocytopenia syndrome virus (SFTSV). The two most well-studied and biomedically important viruses within these genera are RVFV and SFTSV, both of which cause lethal disease in animals and humans [20].

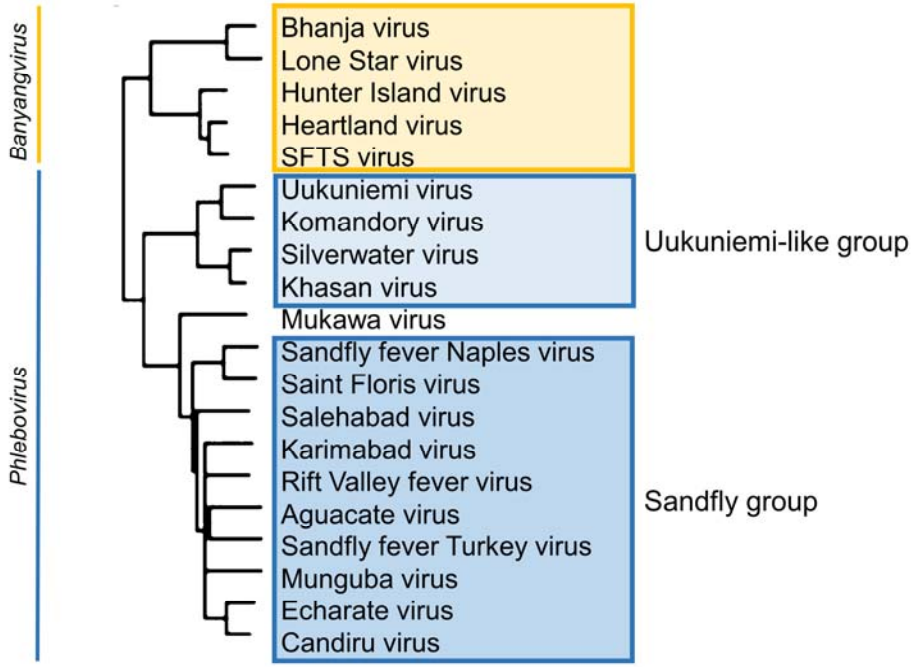

Figure 1.1 Schematic representation of the *Phlebovirus* and related *Banyangvirus* genus.

A phylogenetic tree of representative members of the phlebovirus genus. Constructed by alignment of the M-segment gene. Uukuniemi-like group is highlighted in light blue and Sandfly group in dark blue. The related Banyangviruses (previously classified as phleboviruses) are highlighted in yellow. The newly discovered Mukawa virus is a tick-borne virus which shares common ancestry with the Sandfly group of phleboviruses, thus its serogroup has not been assigned. Adapted from reference [22].

1.2.1 RVFV: a re-emerging phlebovirus

RVFV is a well-established mosquito-borne pathogen discovered in 1930 in the Rift Valley region in Kenya [23] and is now endemic in many parts of Africa and neighbouring regions including the Middle East [24-26]. This zoonotic virus is able to infect and cause disease in

humans, domestic livestock and wildlife species [27]. Upon infection of livestock, such as cattle, sheep, and goats, RVFV constitutes a huge economic burden to the farming industry and is responsible for a high incidence of abortion and neonatal mortality in pregnant livestock [28]. An outbreak in Tanzania in 2006–2007 caused the death of approximately 50,000 livestock. As well as animal mortality, an RVFV outbreak can cause bans on the export of animals, which can cripple local economies which rely upon animal trade [29]. The economic loss in Somalia for the 2006–2007 outbreak has been reported at $471M, approximately 5% of the GDP [30].

Given the high frequency of outbreaks and large geographical distribution of host reservoirs [24, 26, 31], RVFV constitutes a substantial risk to human health. Whilst human disease is most commonly associated with a mild, self-limiting fever [28], in approximately 1% of reported cases severe and potentially lethal, haemorrhagic fever or encephalitis can occur [32]. Indeed, in an outbreak occurring in 1997-1998 in East Africa human cases were estimated at 89,000 with 478 recorded deaths [33].

Aedes and *Culex* mosquito species are the primary vector for RVFV, although numerous mosquito species are capable of RVFV transmission [29, 34]. As mosquito populations rise after a period of heavy rain, an increase in viral amplification between mosquitoes and ruminants occurs [29]. The primary route of infection amongst livestock is through mosquito bite, rather than livestock-livestock transmission [23, 29]. Although human infection may occur following a mosquito bite, the majority of infections arise from contact with infected tissues from animals [35]. The wide distribution of RVFV competent vector species, combined with the concern that climate change may be increasing the spread of mosquito populations further into Europe and northern America, renders RVFV a pressing public health concern [36-39]. RVFV has been classified as a select agent by the CDC (Centre of Disease Control), is on

the list of notifiable diseases by the World Organisation for Animal Health, and has been identified as having potential for misuse as bioterrorism agent.

1.2.2 SFTSV: a recently emerged banyangvirus in China

The banyangvirus, SFTSV (also known as *Huaiyangshan banyangvirus*, and previously classified within the phlebovirus genus) was isolated in the provinces of Henan and Hubei, China, in 2009 [40]. This emerging virus causes disease that is characterised by fever, thrombocytopenia and leukocytopenia as well as a deadly haemorrhagic fever [41]. Compared to other members of the phenuivirus family, the human case fatality rate of SFTSV is relatively high and can range between 5 and 30 % [41, 42].

SFTSV is primarily carried by the *H. longicornis* tick species, which has a widespread geographic distribution covering China, Korea, Japan, Australia, New Zealand and the Pacific islands [43]. Several serological studies indicate that a number of domestic and wild animals have been exposed to the virus, including, boars, rats, and domestic cats [44-48]. The majority of human infections originate following a tick bite and SFTSV has only been reported to undergo human-to-human transmission in cases where direct contact with infectious blood has occurred [49, 50]. Between 2011–2016, approximately 2,500 human cases were reported in China. Additionally, since the discovery of SFTSV in China, hundreds of cases have been reported in Japan and South Korea [45, 51, 52]. Case reporting is highest between April and August [50, 53] with farmers at the greatest risk, due to occupational exposure to ticks.

1.2.3 HRTV: a recently emerged banyangvirus in USA

In 2009, HRTV was identified in two farmers from Missouri, USA, who exhibited leukopenia and thrombocytopaenia count following exposure to ticks. Genetic analysis revealed that the virus is closely related to SFTSV (73% sequence identity across the polymerase protein and

62% across the nucleoprotein) [54]. Between 2009 and 2019, over 40 clinically cases of HRTV infection have been reported in the Midwestern and southern states of USA, with three associated deaths [55]. The distribution of clinical cases reflects the distribution of the *A. americanum* tick, which has been implicated as the primary vector for HRTV [55, 56]. Animals have also been suggested as potential reservoirs of HRTV, and a number of wild animal species, including white-tailed deer, horses, racoons, and coyotes have been shown to be seropositive [57]. Symptoms resulting from HRTV infection in humans are similar to that of SFTSV and include, fever, fatigue, loss of appetite, diarrhoea, leukopenia and, thrombocytopaenia [54].

As reflected by the discovery of HRTV and SFTSV, the number of distinct pathogenic phenuiviridae species has increased over the past ten years. Indeed, other recently discovered phleboviruses include: Viola, Toros and Zerdali viruses [58, 59]. It is likely that more members of the *Phlebovirus* and *Banyangvirus* genera will be discovered in the future with increased genetic and serological surveillance efforts. Given their geographic distribution, diversity, and potential to cause fatal animal and human disease, it is of critical importance to understand both the molecular basis of differing pathogenicity across the phlebo- and banyangviruses and the determinants of protective immune responses.

1.3 Molecular biology and entry mechanism

1.3.1 Overview

Phleboviruses and banyangviruses are tri-segmented RNA viruses that utilise a combination of a negative and ambisense coding strategy **(Fig. 1.2)**. The three RNA segments are termed S, M and L (short, medium and large) and code for five or six proteins, depending on the virus. The S-segment encodes the nucleoprotein (N), which associates with the viral genome, and a non-structural protein (NSs), a virulence factor shown to inhibit interferon signalling [60-64]. The

M segment encodes the glycoprotein precursor which is synthesised as a single polyprotein that requires enzymatic cleavage by the host signal peptidase for maturation, yielding two glycoproteins, Gn and Gc. The M segment of the Sandfly group of phleboviruses also encodes the NSm protein, an anti-apoptotic virulence factor shown to be dispensable for virus replication *in vitro* and *in vivo* [65, 66]. As well as the Gn and Gc, a 78 kDa glycoprotein is encoded on the M segment of RVFV. The function of this protein is not well understood, and may have a role specific to the virus life-cycle in mosquito cells [67, 68]. The L segment encodes the RNA dependent RNA polymerase.

The members of the *Phlebovirus* genus can be genetically categorised into the Uukuniemi-like group (including Uukuniemi virus (UUKV), which is more closely related to the newly classified *Banyangvirus* genus) or the Sandfly group (including RVFV and SFNV). Members of the Uukuniemi-like group and banyangviruses do not possess a non-structural protein NSm, which in the Sandfly group of phleboviruses is present at the 3' of the M segment. In addition to genetic differences, viruses within the Sandfly group are largely spread by mosquitoes or sandflies and those in the Uukuniemi-like group and *Banyangvirus* genus are spread by tick species.

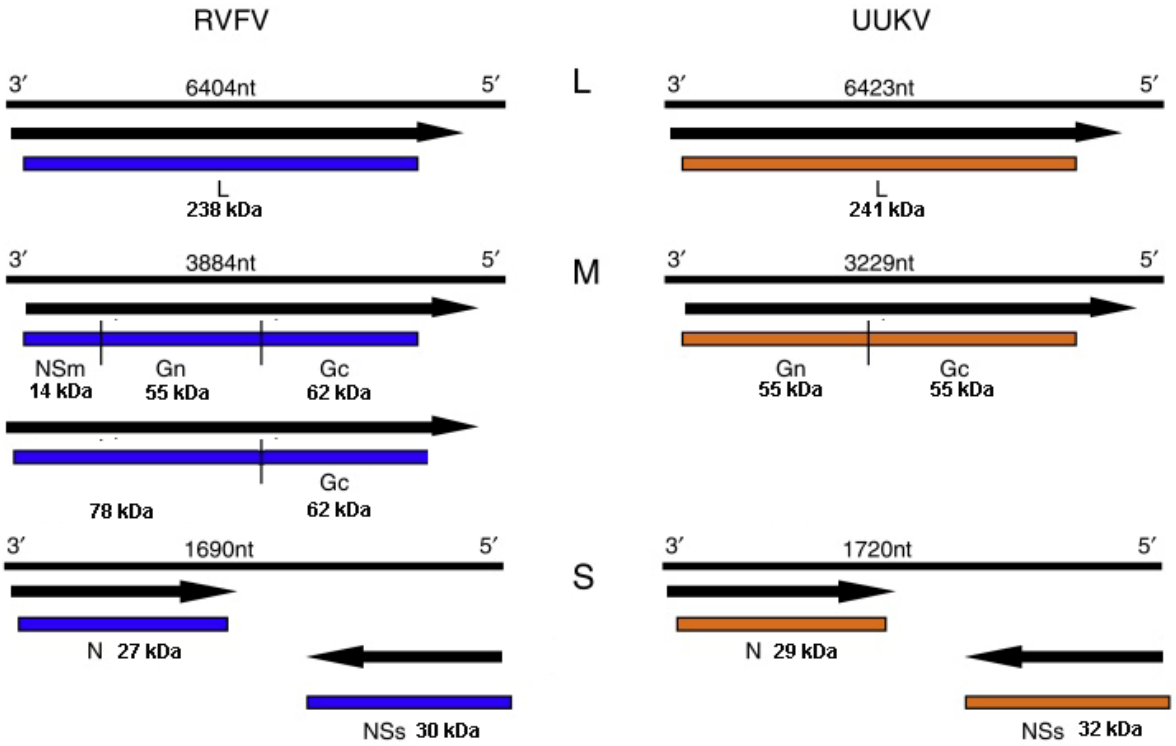

Figure 1.2 Genome organisation of phleboviruses.
Comparison of the coding strategy of the Sandfly group of phleboviruses (RVFV) and the Uukuniemi-like group (UUKV). Banyangvirus genome organisation is identical to the Uukuniemi-like group. RNA is presented as thin black lines with nucleotide length above each segment. mRNAs are presented as black arrows with the orientation shown. Gene products with their apparent molecular mass are shown as coloured boxes. Adapted from reference [20].

1.3.2 Viral architecture and structural proteins

The phlebovirus and banyangvirus virions are approximately 100–120 nm in diameter and enveloped by a lipid bilayer derived from the host-cell surface during the budding process **(Fig. 1.3)** [69]. The virus envelope is decorated by a heterodimer of the two transmembrane glycoproteins, Gn and Gc, which form higher order pentameric and hexameric assemblies [69-72].

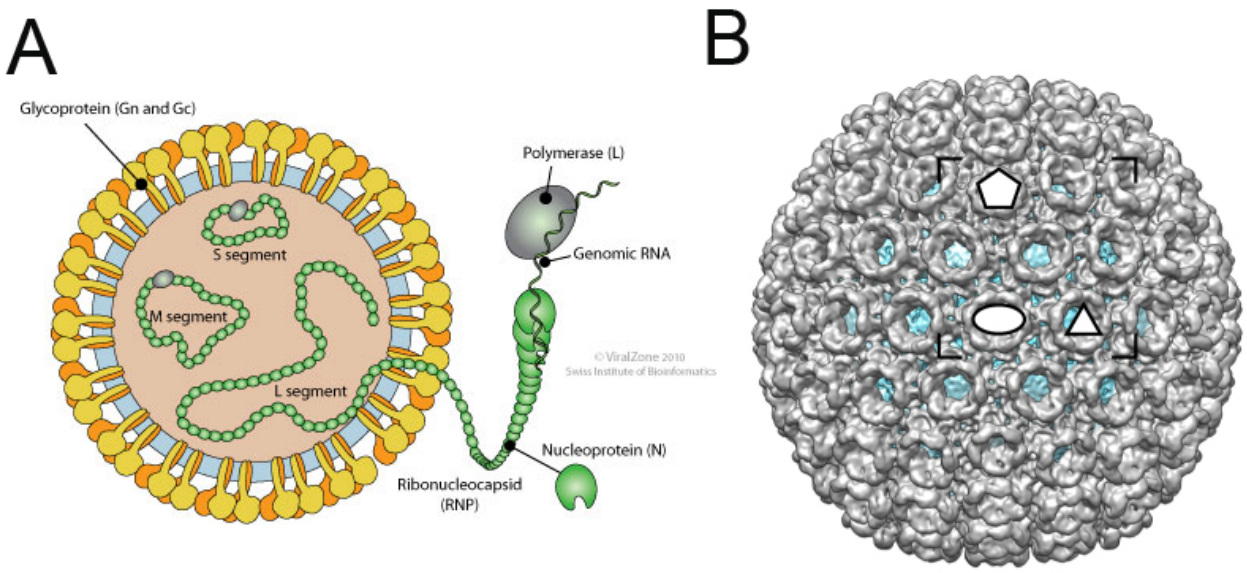

Figure 1.3 Organisation of a phlebovirus particle.
(A) A cartoon representation of the a phlebovirus particle with the three RNA segments S, M and L shown, as well as the nucleoprotein (N), polymerase (L) and Gn/Gc glycoproteins. (Obtained from Viralzone, 2018). (B) A cryo-EM-derived reconstruction of RVFV reveals an icosahedral particle with a *T*=12 symmetry. Heterodimers of the Gn and Gc are arranged on the virus surface as hexameric and pentameric assemblies. Obtained from reference [69].

1.3.2.1 The Gc glycoprotein

The Gc glycoprotein of the *Phenuivirus* family is a class II fusion protein, which facilitates host-cell entry by triggering membrane fusion in a pH dependent manner. Class II fusion proteins adopt a well conserved protein fold, with three domains (termed I, II and III). Domain I is an eight stranded β-barrel, which connects domain II and III. Domain II possesses the hydrophobic fusion loops at the end of a five-stranded beta sandwich. Domain III adopts an immunoglobulin-like fold. The C terminus, which in the full-length protein would extend with a transmembrane region, anchors the protein in the viral envelope.

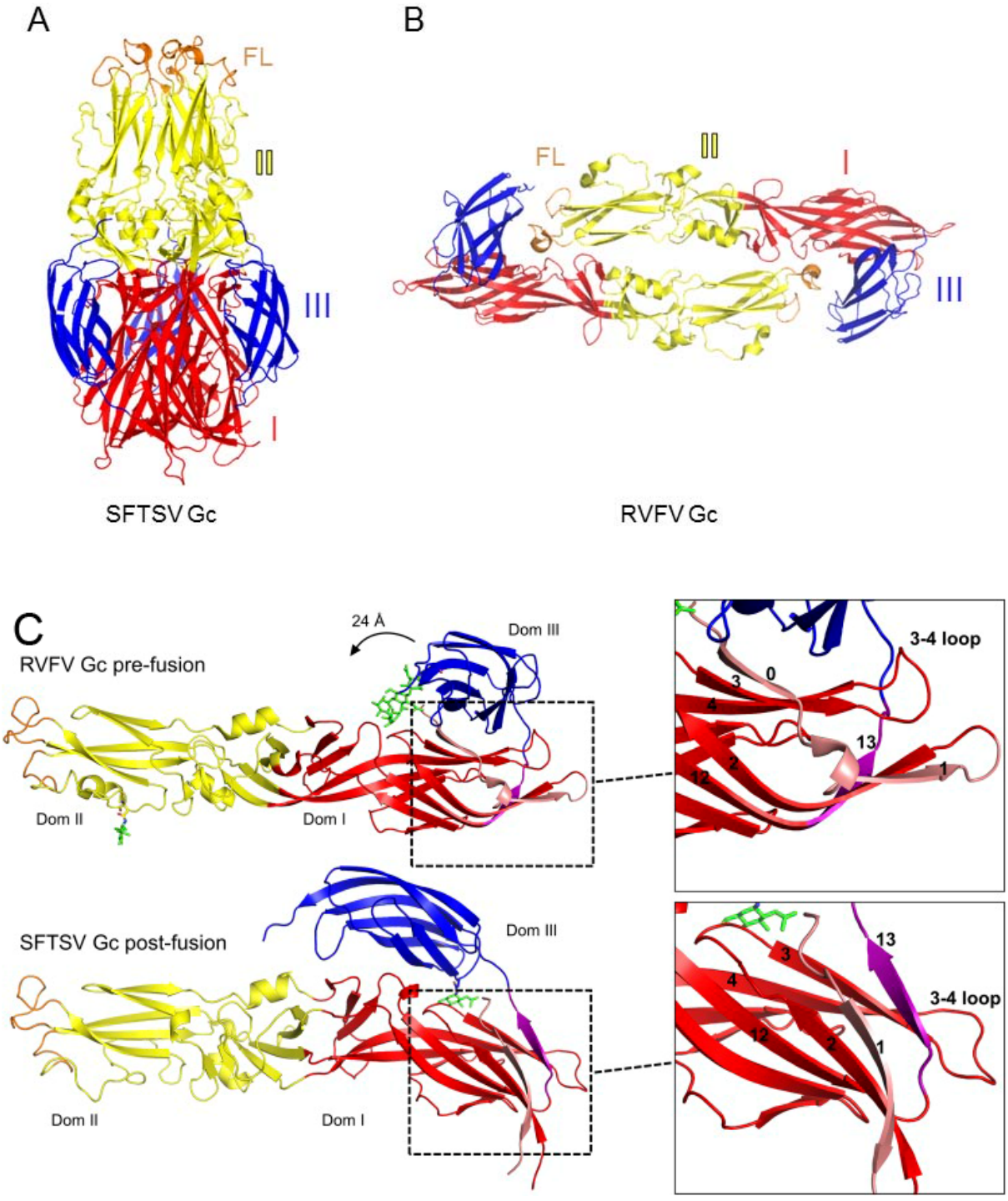

Figure 1.4 Structures of Gc in pre- and post-fusion conformations
Crystal structures of RVFV Gc and SFTSV Gc in the pre- fusion and post-fusion conformations, respectively. Domain I is coloured in red, domain II is coloured in yellow and domain III is coloured in blue. **(A)** The SFTSV Gc trimer generated from PDB: SG47 **(B)** The RVFV Gc (crystallographic) dimer generated from PDB: 4HJI **(C)** Domain positions in the two conformations are compared. In the post-fusion conformation, a 24 Å shift occurs in domain 3 (relative to pre-fusion) and further strand-swapping rearrangements occurs, (zoom in panels). Panel C figure taken from Halldorsson *et al. [73]*.

Within the *Phenuiviridae* family, HRTV, SFTSV and RVFV Gc structures have been elucidated by X-ray crystallography, with SFTSV and HRTV arranged as a putative trimeric post-fusion state and RVFV as a putative pre-fusion dimer. Although the trimerisation of class II fusion proteins upon acidification has been observed elsewhere [74, 75], cryo-electron microscopy (cryo-EM) reconstructions of RVFV in a pre-fusion state show a pentameric or hexameric assembly of Gn-Gc heterodimers, suggesting that the pre-fusion dimer of RVFV Gc may not be physiologically relevant [69]. Comparison of pre- and post-fusion states have revealed that the protein undergoes dramatic conformational rearrangements to facilitate viral fusion **(Fig. 1.4)** [73, 76, 77]**.** In-line with these rearrangements, Halldorsson *et al* used cryo-ET to derive a reconstruction of RVFV particles mixed with liposomes. This work resulted in a model of a putative Gn–Gc intermediate that may be formed during host-cell entry, which suggests that the Gc-encoded fusion loops extend towards the lipid bilayer of the endosome following exposure to acidic environments [69]. Such structural rearrangements to the Gc are also likely accompanied by movement of the cognate Gn, where translational or conformational changes to the protein may be required for the exposure and insertion of Gc fusion loops into the host-cell membrane.

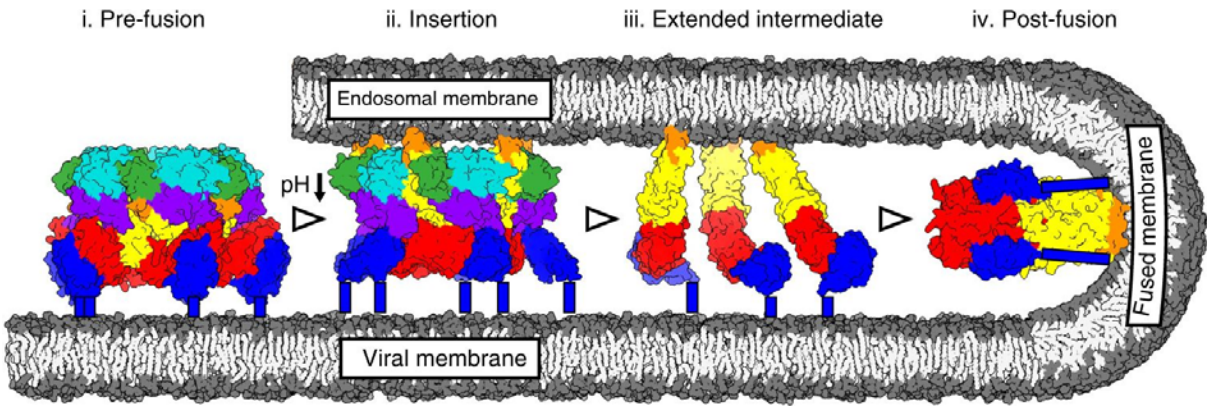

Figure 1.5 A model for phleboviral membrane fusion
(i) At neutral pH, Gn and Gc glycoproteins arrange as pentamers and hexamers on the virus surface (coloured as in Fig. 1.4 and Fig. 1.6). (ii) Upon acidification in the late-endosome, Gn moves aside and allows exposure of the Gc fusion loops and their extension and insertion into the endosomal membrane. (iii) Gn and Gc dimers dissociate, and the extended Gc monomers redistribute. (iv) After membrane fusion, Gc adopts a trimeric conformation. Taken from [69]

1.3.2.2 The Gn glycoprotein

The phlebo- and banyangvirus Gn consists of an N terminal ectodomain, a transmembrane domain and a C-terminal intraviral region. The functional role of the Gn is less clear than that of the Gc. However, all viruses known to use a class II fusion protein also possess an additional membrane protein [78]. The recent structural elucidation of the ectodomains of Gn glycoproteins from RVFV and SFTSV[1] has revealed a three domain globular protein [69, 76], consisting of domain A, domain B, and a β ribbon, which somewhat resembles the fold architecture of the Gn from hantaviruses and the E2 from alphaviruses [77, 79] (**Fig. 1.6)**. The C-terminal region of the Gn remains structurally uncharacterised, although it has been shown to be essential for packaging ribonucleic proteins, a role that is often achieved by a viral matrix protein, which phleboviruses and banyangviruses lack [80, 81]. The C terminal region is also implicated in enabling the formation of Gn dimers through extensive disulphide bonding [76]. However, it remains unclear if these interactions occur in the context of the mature virion.

[1] The structure of SFTSV Gn was published during this project, and was therefore not available to guide the majority of experiments described herein.

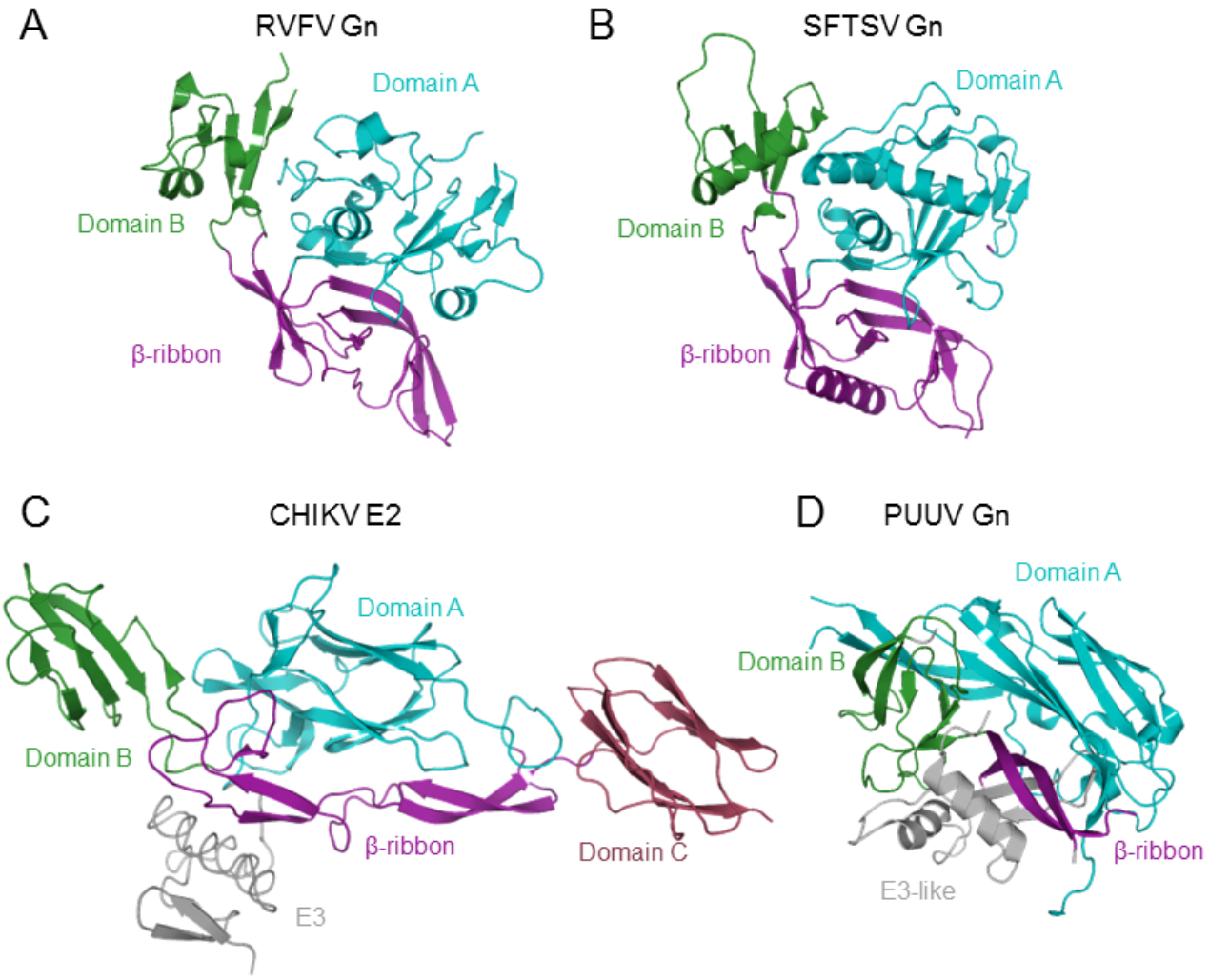

Figure 1.6 Phleboviral Gn glycoproteins and their structural homologues.

The structure of the N-terminal ectodomain of RVFV Gn, as revealed by X-ray crystallography (PDB: 6F8P). **(A)** The prototypic phlebovirus, RVFV Gn, exhibits a novel fold consisting of three domains: domain A is coloured in teal, domain B in green and the β-ribbon in purple (PDB: 6F8P). **(B)** The structure of the prototypic banyangvirus, **SFTSV** Gn[1], reveals a similar domain organisation (PDB: 5Y10). **(C)** Structures of E2 and E3 from Chikungunya virus (CHIKV) (PDB: 4N30) and **(D)** PUUV Gn (PDB: 5FXU), show similarities with the phlebovirus and banyangvirus Gn, suggestive of a shared function as a class II fusion chaperone protein.

Recent cryo-EM investigations have facilitated low-to-medium resolution (8–10 Å) structural maps of the entire RVFV, revealing the putative positions of the Gn and Gc in the context of virions **(Fig. 1.7)** [69]. The N-terminal ectodomain of RVFV Gn glycoprotein lies directly above the fusion loops of RVFV Gc, suggestive of a potential role in preventing premature membrane fusion events.

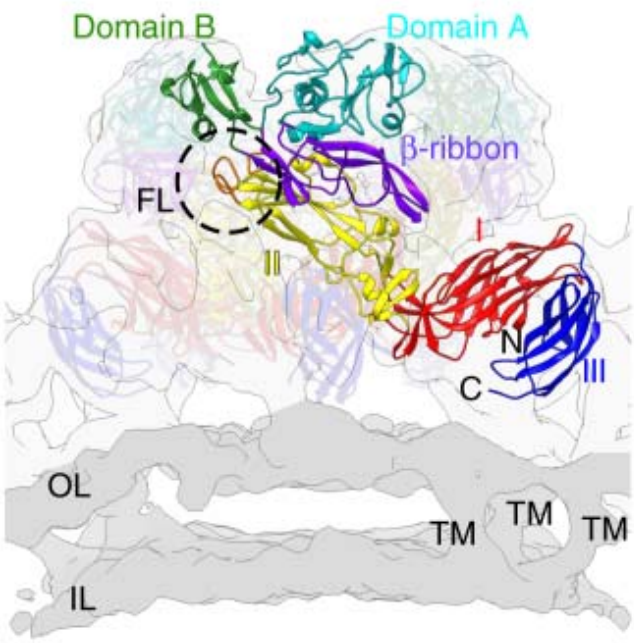

Figure 1.7 Structure of the RVFV Gn and its location on the virus surface.
A cryo-EM reconstruction of RVFV reveals the membrane-distal position of RVFV Gn on the virus surface. A single Gn–Gc heterodimer is highlighted on the pentameric assembly. Gn depicted as in figure 1.6, and Gc as in figure 1.4. The viral fusion loops are displayed in orange and circled. Adapted from [69].

1.3.3 Host-cell entry mechanism

Entry of a phlebovirus or banyangvirus into a host-cell is initiated through the interaction of high-mannose glycans present on both Gn and Gc [82, 83], with DC-SIGN (dendritic cell-specific intercellular adhesion molecule-3-grabbing non-integrin) a C-type lectin almost exclusively presented on dendritic cells [84-86]. As well as DC-SIGN, heparan sulphate (a glycosaminoglycan) and Non-Muscle Myosin Heavy Chain IIA (an actin binding motor protein) promote virus entry [87, 88]. An additional mechanism has been observed for SFTSV, where infected cells produce extra-cellular vesicles containing virus, which are then endocytosed by neighbouring cells, thus propagating the infection [88, 89].

Virus internalisation occurs predominantly through a clathrin-independent endocytic mechanism or caveolae-mediated endocytosis [87, 90] **(Fig. 1.8).** Virions are then transported to late endosomal compartments [91], in which the low pH triggers Gc-mediated fusion with

the endosomal membrane [73, 92, 93]. To facilitate fusion, Gc undergoes dramatic conformational rearrangements. These changes are irreversible and thus premature triggering in the absence of a target membrane can abolish viral infectivity [94].

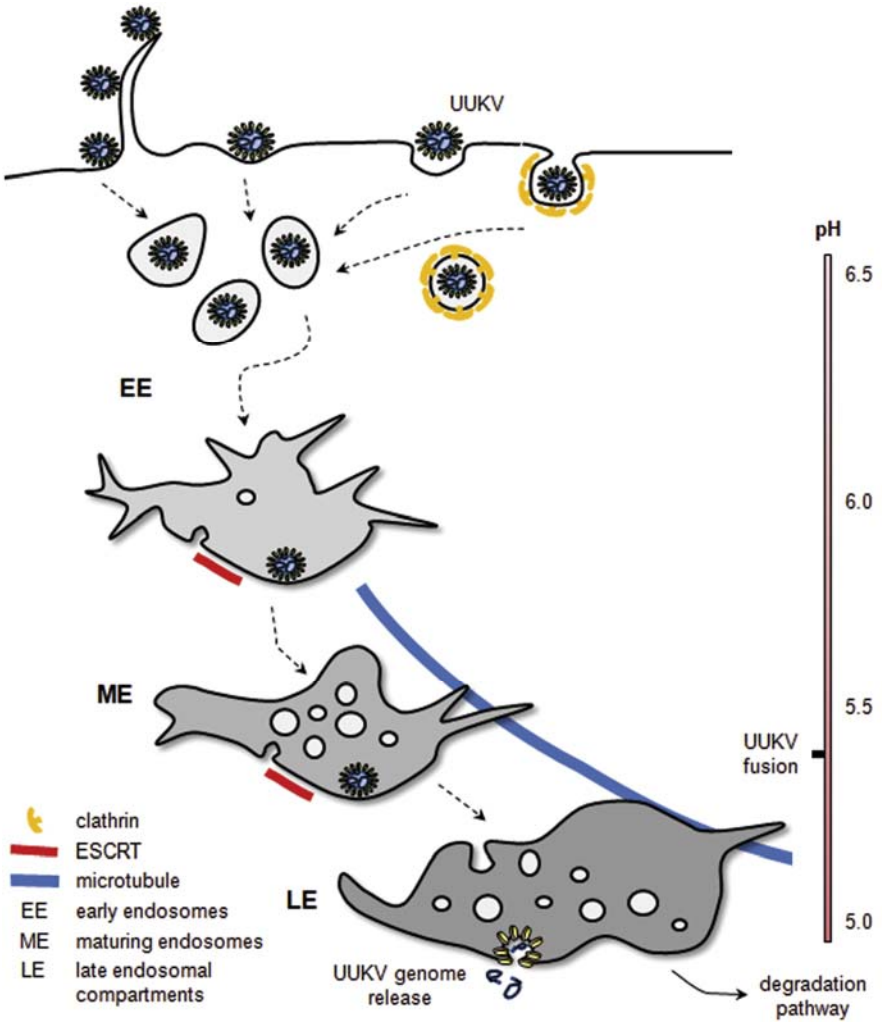

Figure 1.8 Entry pathway of phlebo- and banyangviruses.

Banyangviruses and phleboviruses, such as Uukuniemi virus (UUKV) enter cells through the endocytic pathway. Viruses achieve cell attachment via DC-SIGN expressed on the cell surface [84-86]. The virus is endocytosed by predominantly a caveolae-mediated pathway, and to a lesser extent clathrin-mediated endocytosis, which traffics the virus into the late endosome. As the virus progresses though the endocytic pathway, a drop in pH triggers Gc-mediated fusion of endosome and viral membranes. Adapted from reference [91] (simplified for clarity).

1.3.4 Virus biosynthesis

Following fusion, genome replication and viral mRNA synthesis takes place in the cytoplasm of the host cell. A single polyprotein is produced from the M segment, which is post-translationally cleaved into the Gn and Gc by host cell signal peptidase [95, 96]. The Gn and Gc remain associated, and are guided to the Golgi apparatus by a localisation signal present on the Gn [97, 98]. Virus budding takes place in the Golgi, wherein the viral genome is packaged by association with the cytoplasmic C termini of the Gn and Gc [93, 99]. The virus particle is then trafficked to the plasma membrane for release into the extra cellular milieu.

1.4 Immune responses to phlebo- and banyangvirus

In the early stage of virus infection, the NSs protein suppresses the host innate immune response by downregulating interferon production [61, 100, 101]. Recovery from RVFV infection is associated with the development of high titres of neutralising antibodies, which convey long-lasting protection against further infection [102-104]. The primary target of the antibody response to phlebovirus and banyangvirus infection is the N protein, however the antibodies generated do not have a neutralising effect *in vitro* [105, 106]. Although the response to the N protein is not neutralising, immunisation with the N protein is able to generate protection against RVFV in animal models [107], indicative that recruitment of cellular components of the immune system may be important for protection against infection. The surface-exposed Gn and Gc glycoproteins are the primary target of the neutralising antibody response to RVFV [108-110]. Indeed, immunisation with RVFV Gn and Gc has shown to be effective in generating complete protection in animal models [111]. Furthermore, passive transfer studies indicate that a humoral immunity is sufficient for protection [112]. The role of T cells in the immune response to phlebovirus or banyangvirus infection is not well characterised, however, one study in mice indicates that depletion of CD4+ T cells causes an

increase in viral encephalitis, suggestive that T cell responses could be associated with RVFV infection severity [113].

1.4.1 Antibody-mediated immunity

Antibodies or immunoglobulins (IgGs) are produced in B cells, and are able recognise a huge variety of non-self-molecules. The success of humoral immunity relies on the rapid generation of highly diverse and specific antibodies capable of high affinity binding to any target molecule through the complementarity determining region (CDR). Antibody diversity can be generated through the rearrangement of germline V (variable), D (diversity) and J (joining) gene segments, the pairings of different LC (light chain) and HC (heavy chain) combinations, and affinity maturation. Affinity maturation in the process by which antibodies increase in affinity, avidity and anti-pathogen activity as a result of somatic hypermutation coupled to selection for antigen binding. Resulting antibodies can become highly mutated with an increase in affinity of several orders of magnitude compared to their germline encoded counterparts [114]. Indeed, somatic hypermutation (typically in the range of 20% divergence form germline) has been shown to be essential for a broadly neutralising antibody mediated HIV response [115].

Conventional IgG consists of two heavy chains (HC) and two light chains (HC). HCs are named after their larger molecular weight of ~50 kDa, and comprise three constant domains and one variable domain. LCs are ~25 kDa and consist of one variable and one constant domain. The assembly of the HC and LC generates a forked structure, where there are two identical antigen recognition sites, termed Fab (Fragment antigen binding), which consists of one variable domain and one constant domain from each of the HC and LC. The constant region of the heavy chain, also known as the Fc (fragment crystallisable), is recognised by host Fc receptors which can trigger a cellular signalling cascade to downstream effectors **(Fig. 1.9)**.

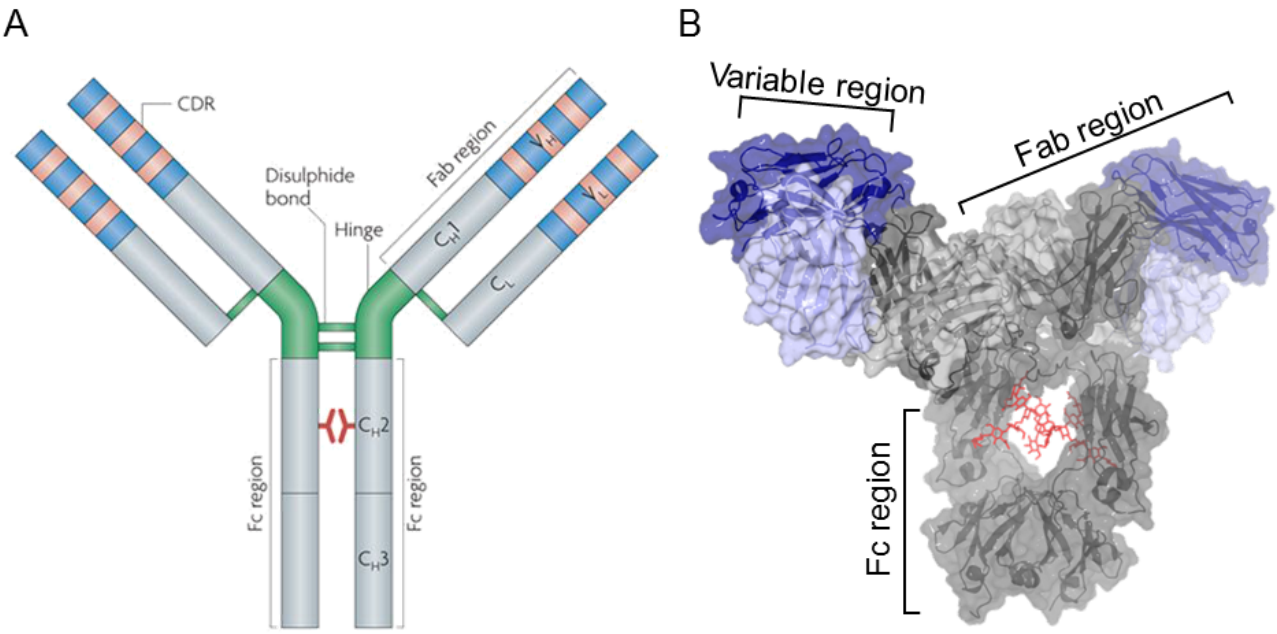

Figure 1.9 Structure of a conventional antibody
(A) A schematic representation of the antibody 'Y' shaped structure, composed of 4 polypeptide chains, generating two identical Fab regions and one Fc region. The Asn297 glycosylation site is marked in red [116]. CDR, complementarity determining region, C_H heavy chain constant domain C_L, light chain constant domain, V_H heavy chain variable domain, V_L light chain variable domain. Adapted from [117] (simplified for clarity). **(B)** Structure of a full length IgG. HC is coloured in dark grey, LC is coloured in light grey, the variable regions are coloured dark blue (HC) and light blue (LC). Glycans are shown in red. (Generated from PDB: 1HZH)

Although recognition of epitopes by the antibody Fab region is critical for antibody-mediated neutralisation, coupling of Fab recognition to Fc-mediated functions has an important role in protective efficacy *in vivo.* Indeed, the importance of Fc-mediated functions of protective antibodies has been described for several viral infections including, HIV-1, influenza A, and respiratory syncytial virus (RSV) [118-120]. Fc effector mediator functions include antibody dependent cellular cytotoxicity (ADCC), antibody-dependent phagocytosis (ADP), antibody-dependent complement-mediated lysis (ADCML), all of which result in destruction of the infected cell **(Fig. 1.10)**. These functions likely explain the protective effect against virus infection that some non-neutralising antibodies exhibit [121-124].

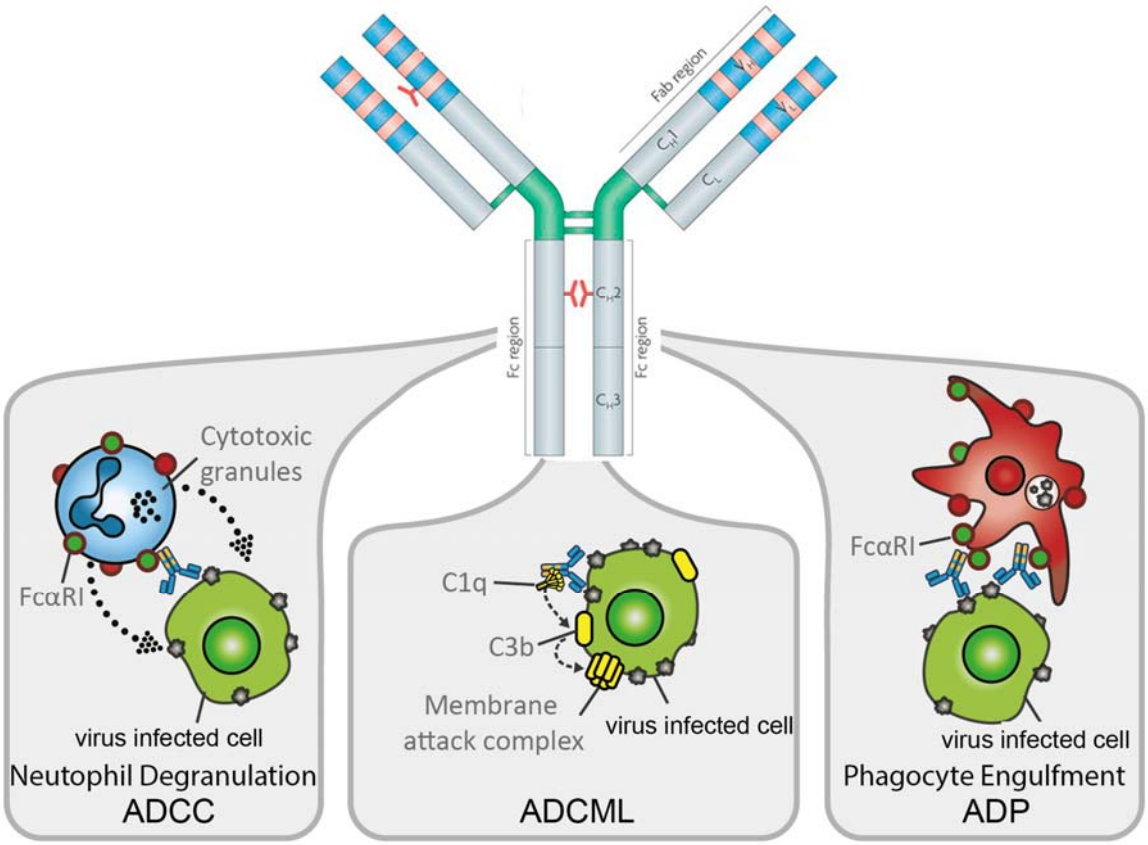

Figure 1.10 Fc-mediated effector functions of immunoglobulins.
Schematic representation of Fc-mediated effector functions in response to a viral infection. ADCC (antibody dependent cellular cytotoxicity), by association with Fc receptors, neutrophils are recruited and cytotoxic granules are released. ADCML (antibody-dependent complement-mediated lysis) Fc regions associated with C1q and generate the membrane attack complex that leads to the lysis of the virus infected cell. ADP (antibody-dependent phagocytosis) Fc regions recruit phagocytes through their Fc receptors leading to phagocytic engulfment of infected cells. Adapted from [117] (simplified for clarity) and [125] (textual changes).

1.4.2 Monoclonal antibodies as anti-viral therapeutics

Research on antiviral monoclonal antibodies (mAbs) has recently expanded due to the rapid development of novel technologies employed in the production of antigen-specific mAbs. mAb therapy is a form of passive immunotherapy which focusses on a rapid and specific anti-pathogen response, rather than the generation of long-lasting protection that may be conveyed by vaccination strategies. The first licensed antiviral mAb therapy was for the treatment of RSV [126]. Since, mAb therapies are in development against several viruses including MERS-

CoV,[127-129], Influenza [130] and EBOV [131, 132] which show therapeutic efficacy in animal models. Additionally mAb therapy against Hendra and Nipah viruses is also under clinical development, having completed Phase-I clinical trials [133, 134]. The use of mAb therapy for emergent viral disease was demonstrated with the development of the ZMapp cocktail of three anti-EBOV mAbs, used against human EBOV infection [131, 132]. The rapid development of mAb therapies makes them promising candidates for future therapeutic response to emerging virus outbreaks.

1.4.3 Current status of phlebovirus and banyangvirus vaccine development

Of the human pathogenic members of the *Phenuiviridae* family, considerable vaccine development has been performed for RVFV. Vaccination is viewed as the only method to prevent RVFV infection of livestock. However, vaccine use is inconsistent across Africa and the Arabian Peninsula, where most countries do not vaccinate due to the sporadic nature of RVFV outbreaks [29]. Although there are vaccines approved for use in animals in the event of RVFV outbreak, there is significant room for improvement of these vaccines, and there are currently no licensed vaccines for human use [135]. The most widely used vaccine for livestock is the Smithburn vaccine, a live attenuated RVFV which induces lasting protection after only one dose. However this vaccine is not suitable for pregnant livestock, due to a high risk of abortion and the possibility of reversion to virulence [136]. Furthermore, live-attenuated vaccines do not fulfil the need to differentiate from infected and vaccinated animals (DIVA). Subunit vaccines which only include the Gn or Gc glycoproteins are therefore attractive as they allow immune response to the N protein as a method to differentiate virus exposed from vaccinated animals [137]. Strategies such as subunit vaccines, DNA vaccines, virus-like particles (VLPs), and viral vectored vaccines are in development by several research groups [135, 138-140].

Although significant progress has been made in the field of RVFV vaccination, these strategies have yet to be applied to SFTSV and HRTV. Recent developments however, include a SFTSV DNA vaccine which was able to protect against lethal SFTSV challenge in animal models [141]. The molecular basis of the protective immune response to phleboviruses and banyangviruses has not yet been elucidated and could give valuable insight into how to rationally improve current vaccine strategies [142].

1.5 **Aims**

This thesis is divided into three primary aims, all of which are focused on characterisation of the antibody immune response generated against pathogenic phenuiviruses:

Aim 1: The first part of this thesis was to evaluate the antibody response generated against a recombinant Gn glycoprotein immunogen and use a structural biology approach to identify sites of vulnerability on RVFV surface that can be targeted by the antibody-mediated immune response.

Aim 2: At the start of my DPhil, only the high resolution structure of the phlebovirus RVFV Gn was known. Therefore, the second aim of my thesis was to explore the structural diversity of the Gn glycoprotein within the genus/family. Due to their importance as therapeutic targets and genetic distance from RVFV Gn, the second part of this thesis focused on structurally characterising the Gn glycoproteins from pathogenic banyangviruses HRTV and SFTSV.

Aim 3: The final aim of this thesis focused on assessing the immune response generated against recombinant viral glycoprotein immunogens and a vaccine candidate. This work commenced by looking at the single-chain antibody response generated in a llama by immunising with the ChAdOx1-GnGc vaccine and both Gn and Gc glycoproteins. This work went on to assess the cross-reactive immune response generated following immunisation of mice with the Gn glycoproteins from HRTV, SFTSV and RVFV.

Combined, these investigations provide an initial blueprint of the antigenic phlebovirus/banyangvirus surface, guiding future recombinant vaccine design and antibody-based antiviral efforts.

Chapter 2

Materials and Methods

Chapter 2: Materials and Methods

2.1 Molecular biology

2.1.1 cDNA templates

Genes of the M-segments of RVFV (UniProt accession no. P21401), HRTV (UniProt accession no. JSPZ8) and SFTSV (UniProt accession no. R4V2Q5), were synthesised by GeneArt (Life Technologies, Germany) and codon optimised for expression in human cell lines. Mutated RVFV Gn constructs (discussed in Chapter 4) were also codon optimised and synthesised by GeneArt. All other cDNA was experimentally derived by either Dr Stephanie Krum (KCL) for the rabbit immunoglobulins or staff from the Steyaert Lab (VIB, Brussels) for the llama immunoglobulins.

2.1.2 Glycoprotein construct design

Glycoprotein construct boundaries were determined by analysis of the only structure of a phlebovirus Gn available at the time (PDB: 6F9F) [69], in combination with disorder prediction using RONN [143], and transmembrane and secondary structure prediction using the Phobius server [144]. Full length and truncated ectodomain constructs were designed based upon the expression construct for RVFV Gn and the resulting fragment that crystallised [69]. See **Appendix 1.5** for phenuiviral Gn sequence alignment.

2.1.3 Plasmids

The cDNA corresponding to phleboviral glycoproteins and Fab fragments was cloned into the pHLSec plasmid [145] with a secretion signal and a hexa-histidine tag (His-tag) for detection and purification. The pHLSec vector is modified from pLEX and contains an ampicillin selection marker, pBR322 origin of replication, chick β-actin promoter, rabbit β-globin polyA signal, multiple cloning site with Kozak sequence, secretion signal, His-tag and termination codon (**Fig. 2.1**)[145]. The AgeI and KpnI restriction sites were used to insert an in-frame

construct 3' of the secretion signal and 5’ of the His-tag. Fab light chains were cloned between Age I and XhoI, so to exclude the His-tag and aid in the purification of authentic heterodimeric recombinant proteins.

For poorly expressing constructs, the pHLSec-SUMO vector (**Fig. 2.1** and mentioned in Chapter 5 and Chapter 6), which encodes a SUMO tag and a 3C protease site at the N terminus of the protein of interest, was used to boost expression [146]. At the C-terminus, a 1d4 tag was included for detection of the final cleaved product [147].

Stable expression cell lines were produced for glycoprotein constructs, which required regular production, adopting the method reported by Seiradake *et al* [148]. The pURD plasmid was used and genes were subcloned from the pHLSec plasmid using the AgeI and XhoI sites, so as to maintain the C-terminal His-tag from pHLSec. The pURD plasmid contains a puromycin resistance marker, which allows for selection of cells that have successful gene integration (**Fig. 2.1)** [148].

Nanobodies were cloned by collaborators in the Steyaert lab (VIB, Brussels, Instruct) into the pMESy4 plasmid for bacterial expression [149].

For production of rabbit Fab fragments, cDNA was amplified by PCR from plasmids containing the full-length antibody sequence generated by Dr Stefanie Krumm and cloned into pHLSec [150]. To isolate rabbit antibody sequences, heavy and light chain Fab amplification primers were adapted from reference and are detailed in appendix 1.6 [150].

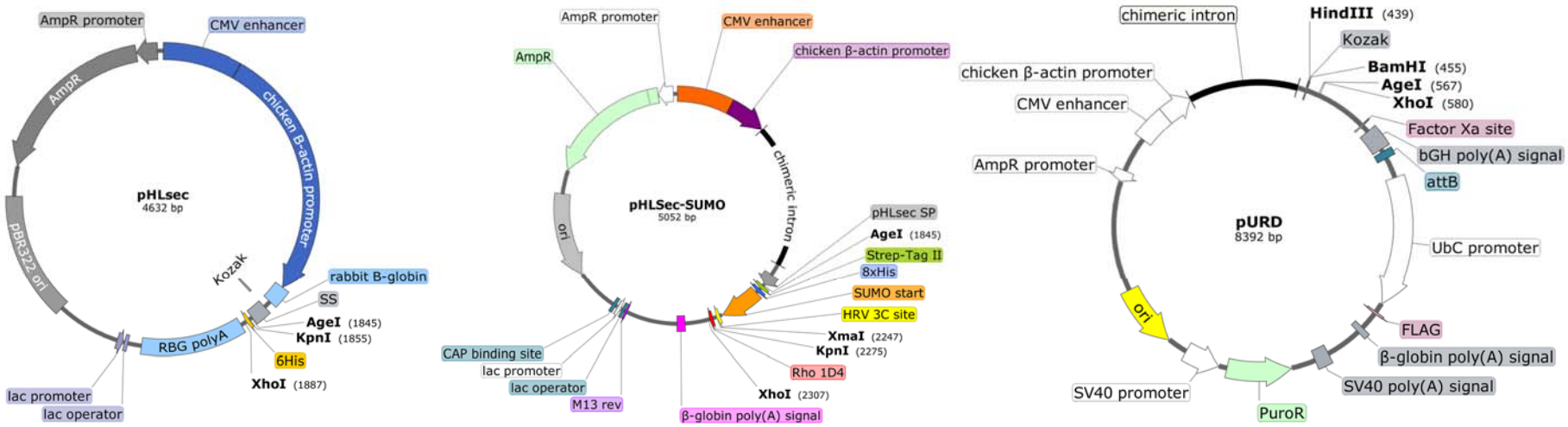

Figure 2.1 Schematic representation of protein expression plasmids
(From left to right) pHLSec, used in standard expression screening, by inserting the gene for the protein of interest between AgeI and KpnI or XhoI. pHLSec-Sumo expression vector with an N-terminal cleavable Sumo tag. Protein of interest gene is inserted between XmaI and KpnI. pURD, expression vector for stable cell line production, genes encoding the protein of interest are inserted between AgeI and XhoI sites

2.1.4 Primers and cloning strategy

Primers were synthesised commercially by Sigma Aldrich. The melting temperature (Tm) of primers was optimised to be between 58 and 60 °C for PCR. Primers were designed with a stabilising region of three nucleotides, restriction site and a sequence complementary to the 3 or 5' region of the protein of interest. Since the expression of all glycoprotein constructs was first tested in pHLSec, sites were chosen to match the pHLSec vector such that the forward primer contained an AgeI site and the reverse primer contained a KpnI site, thus enabling ligation into the pHLSec plasmid by a restriction digest and ligation strategy (as described in **2.1.8**). Fab light chains were cloned between AgeI and XhoI, so to exclude the hexa-histidine tag. Cloning into vectors other than the unmodified pHLSec was achieved by subcloning with restriction digest.

For InFusion cloning, which was used only for generating rabbit Fab in the pHLSec plasmid, primers were designed according to the InFusion (Takara Co. Ltd., USA) manufacture's guidelines. Briefly, the 15 bp primer consists of a region matching the insertion site in the vector, and the beginning/end of the gene to replicate. Primer sequences are detailed in appendix 1.6.

2.1.5 Polymerase chain reaction

Amplification of glycoprotein constructs and antibody Fab regions was performed using a three-step polymerase chain reaction (PCR) protocol. The Pyrobest DNA Polymerase kit (Takara Co. Ltd., Madison, USA) was used for PCR. Oligonucleotide forward primer (200 nM), oligonucleotide reverse primer (200 nM), cDNA template (100–200 pg), dNTP pre-mixture (0.4 mM), Pyrobest buffer II, Pyrobest Polymerase (0.5 µl) and distilled water to a final volume of 50 µl per reaction. DNA amplification took place in a thermal cycler using the following scheme (**Fig. 2.2**): Initial hot-start of 96 °C for 2 min, 30-32 cycles of (i) 96 °C for

30 s, (ii) 55-60 °C for annealing (depending on primers) for 30 s and, (iii) 45 s of 72 °C for extension, then denaturing at 96 °C for 10 min and a final 4 °C holding step.

PCR reactions were analysed by gel electrophoresis to confirm correct amplification and then purified using QIAquick PCR purification (Qiagen, UK) as per the manufacturer's protocol.

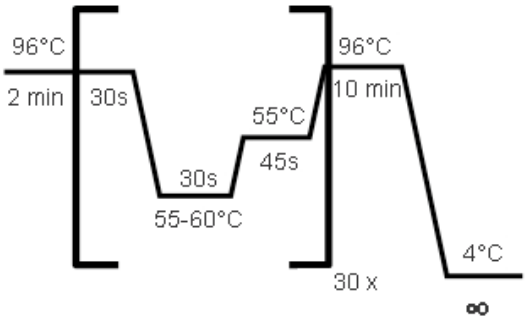

Figure 2.2 PCR cycle schematic

2.1.6 Agarose gel electrophoresis

Agarose gels were made with of 1 % agarose in a TAE (Tris acetate EDTA) buffer and 1x SYBR Safe DNA gel stain (Invitrogen, Paisley, UK). 6x Gel Loading Dye (New England Biolabs, Massachusetts, USA) was added to DNA samples prior to loading. 1 kb plus DNA ladder (Invitrogen) was run alongside samples. Gels were run at 100 V for ~30 min and imaged using the ChemiDoc XRS+ system (Bio-Rad Laboratories, California, USA).

2.1.7 Restriction Digestion

Amplified DNA (PCR products) were PCR purified with the QIAquick PCR Purification Kit (Qiagen, UK). pHLSec vector and PCR fragments were digested in the Cutsmart buffer using XhoI-HF, KpnI-HF and AgeI-HF endonucleases (New England Biolabs, Massachusetts, USA) according to manufacturer's protocols. Reactions were incubated for 30–60 min at 37 °C. The digested materials were isolated by gel electrophoresis, where bands of the correct size were excised and re-purified using the QIAquick PCR Purification Kit (Qiagen, UK) before ligation.

2.1.8 Ligation of digested plasmid and insert

Digested vector and insert were enzymatically ligated using the NEB quick ligation Kit (New England Biolabs, USA). Ligation reactions were prepared such that the insert was in molar excess of 3:1 with 50 ng vector. The vector insert mix was incubated with 10 µl Quick Ligase Buffer and 0.5-1 µl Quick Ligase for 15 mins at RT.

2.1.9 Sub cloning with InFusion

The non-codon optimised rabbit derived antibody sequence had the AgeI and KpnI restriction sequences present in their coding regions, therefore restriction digest could not be used for subcloning into pHLSec. In these cases, infusion cloning was performed using overlapping primers complementary to the target vector. PCR was performed as described in **2.1.4**. PCR amplified DNA inserts (10-200 ng) were added to purified pHLSec vector digested between AgeI and KpnI (with His-tag) or XhoI (without His-tag) (50-200 ng) and reaction volume was adjusted to 10 µl with H_2O. The reaction mix was then added to EcoDry In-Fusion reaction pellet (Takara Co. Ltd., USA) and mixed by pipetting. The reaction was incubated for 15 min at 37 °C, then 15 min at 50 °C. The resulting reaction was diluted with 40 µl TE buffer prior to bacterial transformation.

2.1.10 Transformation of plasmid

3µl of newly ligated plasmid was added to 30µl of DH5α *E. coli* (Invitrogen, Paisley, UK) and incubated on ice for 30 mins. Heat shock at 42 °C was performed for 20 s followed by a 37 °C incubation in super optimal broth (SOC, Invitrogen, Paisley, UK) for 50 min at 180 rpm. Cells were plated on LB agar containing 100 µg/ml ampicillin to select for successful clones.

2.1.11 Plasmid isolation

Colonies were picked from LB agar plates and used to inoculate 5 ml of LB containing 100 µg/ml ampicillin and grown overnight at 37 °C, 180 rpm. Plasmids were isolated from cultures using the QIAprep Spin Miniprep kit (Qiagen, Crawley, UK). Plasmids were then analysed by

restriction digest (**2.1.7**) and gel electrophoresis (**2.1.6**) to check for presence of inserts of the expected size. The purified plasmid DNA was then sequenced by Sanger sequencing (Eurofins, Germany) using sequencing primers detailed in appendix 1.6.

2.1.12 Large scale DNA purification

Subcloning efficiency DH5α *E. coli* cells (Life Technologies, UK) were transformed with plasmid of interest (**2.1.10**). 0.5 or 2 L of LB with selective antibiotic (ampicillin 100ug/ml) were inoculated with transformed colonies and grown overnight for 16–20 h at 37 °C and 180 rpm. Plasmids were isolated using the Plasmid Mega kit or Giga kit (Qiagen, UK) following the manufacturers protocol. The resulting DNA pellet was resuspended in 2 ml or 10 ml of TE buffer (Qiagen, UK) and stored at -20 °C.

2.2 Mammalian protein expression

Recombinant glycoproteins and rabbit Fab fragments were produced by over-expression in a human embryonic kidney-derived immortalised cell line (HEK293T, ATTC® CRL-3216™). Full length antibodies were purified from rabbit hybridoma cultures. Hybridomas were generated commercially by Epitomics (California, USA) [150].

2.2.1 Tissue culture

All mammalian cell culture was performed using aseptic technique within a laminar flow cabinet. HEK 293T cells were cultured in Dulbecco's modified eagle media (DMEM, Sigma Aldrich, UK) supplemented with 10% Foetal Calf Serum (FCS, Sigma, UK), 1% L-glutamine and 2% non-essential amino acids (Life Technologies, UK). Cells were grown at 37 °C with 5% CO_2. For maintenance of cells and expansion, T175 flasks were used (175cm^2 surface area, Corning), and were passaged upon reaching 90% confluency, as assessed by light microscopy. To passage cells, cell culture media was removed, cells were washed in PBS (Life Technologies, UK) and 5 ml Trypsin-EDTA (Life Technologies, UK) was added to each flask

and incubated for 5 min at room temperature until the cell monolayer was disrupted and cells dislodged. Cells were then suspended in 10% FCS supplemented DMEM, and used to seed new flasks, plates or roller bottles.

2.2.2 Small-scale transient transfection

Protein expression was first tested in small scale experiments (of approximately 2 ml) to estimate and compare expression level. 70–90% confluent HEK293T cells were cultured in a 24-well plate containing 0.5 ml DMEM. Lipofectamine 2000 (Thermo Fisher Scientific, UK) was used as the transfection reagent according to manufacturer's protocols. Briefly, 800 µg of purified plasmid DNA (or 400 µg of each heavy chain and light chain of Fab fragments) was diluted in 50 µl of serum-free DMEM (supplemented with L-glut and NEAA), likewise 2 µl of lipofectamine was diluted in 50 µl of supplemented serum-free DMEM. After a 5 min incubation (RT), the solutions were combined and incubated for 20 min (RT) to allow formation of DNA-lipofectamine complexes. After incubation, the DNA-lipofectamine solution was added to 0.5ml fresh DMEM (10% FCS, 1% L-glut, I% NEAA) in each well of the tissue culture plate and mixed by gentle rocking. Cells were incubated for 72 h at 37 °C, 5% CO_2.

After protein expression, the supernatant was aspirated and collected to assess the amount of secreted protein and the remaining cells were dislodged from the flask by addition of 500 µl NuPAGE MES gel running buffer (Thermo Fisher) and repeated pipetting. The supernatant and the cell samples were used in western blotting to assess protein expression. For each transfection, a positive control of RVFV Gn construct residues 154-560, and a negative control where cells were treated with lipofectamine and no plasmid DNA, were collected.

2.2.3 SDS-PAGE

Sodium dodecyl sulphate polyacrylamide gel electrophoresis (SDS-PAGE) was performed to separate proteins according to their apparent molecular mass, for assessment of expression

and/or purity. For most samples, a reducing loading buffer containing (0.25 M Tris-HCl pH 6.8, 15% w/v SDS, 50% v/v glycerol, 25% v/v 2- mercaptoethanol, 0.01% w/v bromophenol blue) was added and incubated for 5 min at 99 °C. In some instances, proteins were run under non-reducing conditions in parallel, utilising a loading buffer that lacked 2-mercaptoethanol. Protein samples were separated using NuPAGE 4–12 % Mini poly-acrylamide gels (Thermo Fisher Scientific, UK) in MES running buffer (Thermo Fisher Scientific, UK), using the NuPAGE Mini gel tank (Thermo Fisher Scientific, UK). Protein samples were run alongside a protein standard ladder for molecular weight estimation. For SDS-PAGE analysis only, 5 µl of Benchmark protein ladder was used in a separate lane (Thermo Fisher Scientific, UK), and gels for further western blot analysis were loaded with 1 µl Benchmark protein ladder and 5 µl of Benchmark pre-stained protein ladder (Thermo Fisher Scientific, UK). Samples were run at 180 V for 45 min. The gel was then removed and stained with Instant Blue fast stain (Expedeon, UK) for 10 min at RT, and then de-stained for 1 h – overnight in deionised water. Gels were imaged using ChemiDoc XRS (BioRad, UK).

2.2.4 Western blot

Western blotting was performed to assess expression of different constructs and determine suitability for large-scale protein production. First, SDS-PAGE was performed (**2.2.3**). Proteins from the unstained gel were transferred to a nitrocellulose membrane using the iBlot2 transfer system (Thermo Fisher Scientific, UK) with iBlot transfer stacks (Thermo Fisher, UK). Blotted membranes were blocked for 1 hr at RT with 5% w/v milk in PBS blocking buffer. Detection of proteins was achieved using the C-terminal His tag and a mouse monoclonal anti –penta His IgG antibody (34660, Qiagen, UK) diluted 1:1000 v/v in blocking buffer with 1 h incubation at RT. Signal amplification and detection was achieved using horse radish peroxidase-conjugated goat anti-mouse IgG (Sigma Aldrich, UK) diluted 1:2000 v/v in blocking buffer with 1hr incubation at RT. Following each incubation step, membranes were washed five times

in PBS containing 0.05% (v/v) Tween 20. Membranes were developed with Clarity Western ECL substrate (Bio-Rad, USA) and imaged with the Chemi-Doc (Bio-Rad, USA) imaging system.

2.2.5 Large scale transient protein expression

For larger scale production of recombinant proteins, HEK 293T cells were seeded into expanded surface (2,125 cm^2) roller bottles (Cellmaster™, Greiner bio-one) with DMEM containing 10% FCS, 1% NEAA and 1% L-glut. When cells reached ~90% confluency (usually four days post seeding) media was removed and replaced with DMEM containing 2% FCS, 1% NEAA, and 1% L-glut. High purity, endotoxin-free plasmid DNA for transfection was first sterilised using chloroform; 10% by volume chloroform was added to the DNA, vigorously mixed and then separated by centrifugation at 13,000 x g for 10 min, after which the DNA was aspirated from the chloroform. A transfection mix was prepared with 50ml serum free DMEM, 500 µg DNA, and 1 mg polyethyleneimine (PEI, polysciences Inc,) per roller bottle. For antibody Fab fragment expression, 250µg of heavy chain DNA and 250 µg light chain DNA were mixed with 1 mg PEI. The DNA and PEI were allowed to complex for 10 min before addition to the cells. In cases where glycosylated proteins were prepared for downstream crystallisation experiments, 250 µM kifunensine (final concentration 5 µM) was added to the DNA-PEI mix. Kifunensine is class I mannosidase inhibitor that restricts glycan processing and results in predominantly $Man_9GlcNAc_2$ high mannose type glycoforms that can be cleaved with the addition of endoglycosidase F_1 (EF_1) [151, 152]. Following transfection, cells were incubated at 37 °C, 5% CO_2, with rolling rotation for 4–5 days or until cells started to dislodge from the surface of the bottle.

2.2.6 Generation of stable expression cell lines

In some instances, where regular production of glycoproteins was required, stable expression HEK 293T cell lines were generated. The gene of interest was cloned into the pURD plasmid

[148] (**2.1.3 and Fig. 2.1)**. HEK 293T cells were seeded into 6 well plates and grown to 90% confluency (**2.2.1**). Upon reaching 90% confluency, cells were transfected with lipofectamine (**2.2.2**), where 1 µg pURD plasmid DNA was used with 3 µg of pURD expression vector encoding integrase (pgk-φC31/pCB92) [148, 153]. The following day, when cells had reached 100% confluency, they were passaged and used to seed a T75 flask (Corning, UK) with 10 ml DMEM, 10% FCS with L-Glu and NEAA (**2.2.1**). Cells were incubated for 3 days and grown to 100% confluency. Puromycin (Thermo Fisher Scientific, UK) was added to a final concentration of 2 µg/ml to select for cells that had successfully integrated the gene of interest and the antibiotic resistance marker into the genome. As expected, a large proportion of the cells treated with puromycin die overnight. Media containing dead cells was removed and replaced with 10 ml DMEM, with 10% FCS, L-Glu and NEAA and 1 µg/ml of puromycin and incubated for 3 days at 37 °C 5% CO_2. For protein production, cells were seeded in roller bottles (**2.2.5**) and supernatant harvested once cells had begun to dislodge from the surface of the bottle (usually after 5-10 days). Stocks of cells were prepared by suspending cells in DMEM, with 10% FCS containing 10% DMSO (Sigma Aldrich, UK) and slow freezing to -80 °C using a Cool Cell® (Biocision, UK). Cells were kept in LN2 for long term storage.

2.3 Protein purification

2.3.1 Buffer exchange by diafiltration

Following mammalian protein expression, cell supernatants were collected and clarified by centrifugation at 3000 x g for 20 min at 4 °C and filtration through a 0.22 µm pore filter unit (Millipore, USA). Filtered supernatants were buffer-exchanged into 10 mM TBS (Tris-buffered Saline comprising of Tris pH 8.0, 150 mM NaCl) using an AKTA Flux (GE healthcare, UK) system fitted with 10 kDa molecular weight cut-off membranes. Supernatants were concentrated to between 100–200 ml and filtered through 0.22 µm pore filter units.

2.3.2 Immobilised metal affinity chromatography

The presence of a hexa-histidine tag on a recombinant protein allows purification by immobilised metal affinity chromatography (IMAC) [154]. 5 ml HisTrap™ HP columns (GE healthcare, UK) were loaded using an AKTA Purifier (GE Healthcare, UK) liquid protein chromatography system. The Unicorn software package (GE Healthcare, UK) was used for machine control, collection and evaluation of chromatography data. Washing of non-specific protein contaminants and elution of protein from the column was achieved by competitive displacement, where 1 M imidazole dissolved in TBS was mixed with TBS to produce a step-wise imidazole gradient of 20 mM to 50 mM. Approximately 120 ml of washing over the gradient was performed in total. After washing, protein was eluted in a buffer containing 250 mM imidazole diluted in TBS.

2.3.3 Size- exclusion chromatography

Size exclusion chromatography (SEC) was used as a final protein purification step to generate pure, monodisperse samples suitable for macromolecular crystallography, *in vitro,* or *in vivo* experiments. An AKTA Purifier (GE Healthcare) was used with a Superdex 200 10/300 Increase column (GE Healthcare), and unless stated otherwise, equilibrated and run in TBS at a flow rate of 0.5 ml/min. Samples were concentrated to ~400 µl using appropriate (at least 3x the MW of the protein of interest) molecular weight cut off (MWCO) Amicon ultra centrifugal filters (Millipore, USA). Prior to loading, proteins were filtered through a 0.22 µm centrifugal unit (Millipore, USA) to remove possible aggregates or precipitate. Samples were loaded into a 500 µl loop prior to injection onto the column. Where possible, SEC was performed on the same AKTA and column for qualitative comparison of elution profiles. Where possible molecular weight standards, (BioRad, UK) were run for the 200 10/300 Increase column, on the primary AKTA of use. Fractions were collected in 500 µl volumes and assessed by SDS-PAGE prior to pooling for downstream applications.

2.3.4 Enzymatic removal of N-linked glycans

Where glycosylated proteins were produced for downstream crystallography experiments, N-linked glycans were removed enzymatically to reduce conformational heterogeneity of the sample [151]. This was achieved by production of the protein in the presence of kifunensine (**2.2.5**) [152], and partial deglycosylation to a single N-acetylglucosamine moiety by overnight incubation at room temperature with endoglycosidase F_1 (EF_1, kindly provided by Dr Ilona Rissannen) at a 1:100 molar ratio (enzyme:glycoprotein). EF_1 is an endoglycosidase that hydrolyses high mannose and non-core-fucosylated hybrid-type glycans [155, 156][157]. The efficiency of deglycosylation was assessed by SDS-PAGE analysis, by comparison with the untreated sample. Subsequent SEC was applied to remove the enzyme from the deglycosylated protein sample and to generate a homogenous sample for crystallography.

2.3.5 Enzymatic removal of SUMO expression tag

Removal of the vector-derived SUMO expression tag was required for some proteins to generate a more native-like protein sample, and was achieved through proteolytic cleavage at the adjacent Human Rhinovirus 3C protease site (**Fig. 2.1**) [158]. 3C protease was kindly provided by Dr Antra Zeltina [159]. For efficient 3C protease activity, proteins were buffer exchanged to remove EDTA or imidazole. This was typically achieved by performing IMAC followed by SEC. 3C protease was added at a 1:100 molar ratio (enzyme:glycoprotein) and incubated overnight at 4°C. Following cleavage, imidazole was added to the mixture to achieve a final concentration of 30 mM. The reaction was then applied to a HisTrap column to separate the His-tag-free protein of interest from the His-tagged SUMO protein and His-tagged 3C protease. The resulting purified protein retained a C-terminal 1d4 tag suitable for detection [147]. The efficiency of SUMO cleavage was assessed by Western blot analysis and detection of the His-tag.

2.3.6 Purification of IgG from hybridoma

Three hybridoma cell lines producing rabbit IgG specific to RVFV Gn were generated commercially by Epitomics, as described in ref [150]. Hybridoma cell cultures were grown in hybridoma SF media (Life Technologies). Cell lines were maintained in a humidified incubator at 37°C, supplied with 5-8% CO_2. Cells were passaged by gentle agitation and aspiration by pipette. Cells in suspension were then used to seed new flasks with fresh media at a ratio of 1:1. Cells were harvested after seven days growth at the desired volume. Cell supernatant was collected and clarified by centrifugation at 3000 x g and filtration through a 0.22 μm pore (Millipore, USA). Full length antibodies were purified using a Protein G column (GE healthcare) and an AKTA purifier. Protein G columns were equilibrated in PBS. Antibodies were eluted from the column with 1M Glycine pH 2.7 into microcentrifuge tubes containing 20% by volume 1M Tris pH 8.0 to neutralise the acid.

2.3.7 Biotinylation of Glycoproteins

Biotinylation was achieved using an EZ-link^{TM} Sulfo-NHS-LC biotinylation kit (ThermoFischer Scientific, UK), according to the manufacturer's protocol. Protein was buffer exchanged into PBS, by application to a PBS-equilibrated desalting column (Zeba Spin Desalting Column, ThermoFischer, UK) and centrifuged for 2 min at 1000 x g. Protein was then incubated for 30 min at RT with a 20-fold excess of 10mM Sulfo-NHS-LC-Biotin, prepared in H_2O immediately prior to use. Buffer exchange using a desalting column was subsequently performed in order to remove any excess biotin (BT) from the reaction. Biotinylation was assessed using a Western blot (**2.2.4**) with a bovine serum albumin (BSA) blocking buffer (5% BSA, in PBS) and an anti-biotin detection antibody (ab19221 Abcam, UK).

2.4 Structure determination by crystallography

2.4.1 Protein crystallisation

High purity, homogeneous proteins of milligram quantities are required for crystallisation trials. Prior to high-throughput screening proteins were concentrated using a 10 kDa MWCO Amicon protein concentrator (Millipore), by centrifugation at 2,500 x g at 4°C, and filtered through a 0.22 μm pore filter. Crystallisation screening was performed using a high-throughput robot screen in which 100 nl protein was mixed with 100 nl precipitant solution, (Cartesian Technologies) and the sitting-drop vapour diffusion method in a 96 well plate [160] (Greiner CrystalQuick). Plates were sealed and housed in a Formulatrix storage vault at 21 °C or 4 °C and images were collected over regular time intervals with automated software. Details of successful crystallisation attempts are detailed relevant chapters. Crystals were cryoprotected in the crystallisation condition supplemented with 25% v/v glycerol, prior to cryo-cooling in liquid nitrogen. Dr Karl Harlos generously provided help and expertise for crystal collection and mounting.

2.4.2 Data collection and processing

X-ray diffraction data were collected at various beamlines at the Diamond Light Source synchrotron (Harwell, UK). Diffraction images were recorded using a PILATUS 6M detector (Dectris, Switzerland). Data were indexed, integrated, and scaled using XIA2 [161]. Resolution limits and data quality were assessed by analysis of CC1/2, I/σI, Rmerge, data completeness, and redundancy. All structures were phased by molecular replacement using PHASER [162]. Tables summarising data collection and refinement for each structure presented in this thesis are presented in the relevant results chapters.

2.4.3 Model building and refinement

Prior to refinement, 5% of reflections were randomly selected and removed to act as a test set of reflections for the generation of the R_{free} statistic. Electron density improvement was achieved by iterative model building and refinement. Real space model improvements were performed using COOT [163]. Reciprocal-space refinement was performed using Refmac5 [164] in the CCP4 suite[165]. TLS (Translation/Libration/Screw) and non-crystallographic symmetry refinement were used, where necessary. Model quality was assessed by the resulting R factors (R_{free} and $R_{work)}$ generated after each round of refinement. These statistics were used to assess model bias and overfitting. Geometry was assessed and improved using COOT, by comparison to known values of bond lengths, angles and torsions [166]. Refined models were validated with MolProbity [167]. The Rv-Gn1−RVFV Gn complex structure was submitted to the PDB for publication (PDB: 6I9I).

2.5 Virology

All virology experiments were performed at Public Health England (PHE), Porton Down, and performed with the invaluable help and expertise of Dr Victoria Graham and Dr Stuart Dowell, without whom these experiments would have not been possible.

2.5.1 Tissue culture and Rift Valley fever virus propagation

Vero cells (ECACC, cat# 8411301) were kindly provided and maintained by Dr Victoria Graham (PHE, Porton Down, UK). Cells were cultured in DMEM with 10% FCS and maintained as described (**2.2.1)**. Cells were grown to 70−80% confluency prior to infection with RVFV. The RVFV strain ZH501 was used in all virus experiments kindly provided by PHE, Porton Down and handled at biosafety containment level 3. Cell supernatant was stored at -80°C for future inoculation or experiments.

2.5.2 Plaque assay

Plaque assays were used to quantify the infectious viral load from viral preparations, Vero cells were grown to 90% confluency in 24-well tissue culture coated plates. Virus was added to the cells in a 10-fold serial dilution and incubated for 1 h at 37°C. After incubation, a liquid overlay comprising MEM with 1% avicel (Sigma Aldrich, UK), 10% FCS (Sigma Aldrich, UK), 1% antibiotic/antimycotic solution (ThermoFischer Scientific, UK), was added. The plates were then incubated for 3–4 days, fixed with PFA (paraformaldehyde, Sigma Aldrich, UK), and washed with H_2O. Monolayer staining was achieved by applying crystal violet to each well of the plate, and incubating at RT for at least 1 h. Plates were washed liberally with H_2O and plaque forming units (pfu) were counted by eye.

2.5.3 Plaque reduction neutralisation test

Plaque reduction neutralisation testing was used to quantify the neutralisation capabilities of antibodies and nanobodies raised against RVFV. 100 µl of a three-fold serial-diluted antibody/nanobody or negative control Ab (anti-HIV monoclonal Ab PG9 [168, 169]) was mixed with an equal volume of 100 plaque forming units (pfu) of RVFV ZH501 at 37 °C for 1 h. The virus–Ab mix was then transferred to 80–90% confluent Vero cells in a 24-well plate and incubated at 37 °C for 1 h. After incubation liquid overlay comprising MEM with (1% avicel, 10% FCS, 1% antibiotic/antimycotic solution) was added. The plates were then incubated for 3–4 days, and fixed and stained, as described above. Plaques were then counted for each well and the neutralisation percentage was calculated relative to the corresponding PG9 mAb negative control. IC50 values were calculated in GraphPad Prism (www.graphpadprism.com) using a least-squares non-linear fit dose-response curve.

2.5.4 RVFV pull down assay

Pierce™ Protein G magnetic beads (ThermoFischer Scientific, UK) were resuspended by vortexing for 30 s before aliquoting 50 µl of beads per microcentrifuge tube. A magnetic rack (NEB, USA) was used for separation of magnetic beads from solution. Beads were washed in 200 µl of sterile PBS (Life Technologies, UK), then 8 µg of mAb was added and incubated for 10 min at RT with rotation. An isotype control (ab1908, rabbit anti-His, Abcam, UK) was used as well as beads prepared only in PBS for negative controls. Beads were then washed three times in PBS, with magnet application to remove solution from the beads. 100 pfu RVFV was then added to the mAb bound beads and incubated at 37 °C for 1 h. Supernatant was then removed from the beads by magnet application and used to prepare a 1 in 5 dilution series in DMEM. 100 µl of each dilution was added to confluent Vero cells and incubated for 1 h at 37 °C. Liquid overlay medium was applied as described in and plated were incubated for 3-4 days before fixing, staining and plaque counting as described (**2.5.3)**. Virus binding was calculated as the inverse percentage of pfu compared to a virus-only control.

2.6 Enzyme-linked immunosorbent assay (ELISA)

96-well Nunc-immuno™ PolySorpR plates (Sigma Aldrich, UK) were coated overnight at 4 °C with 50 µl of 1 µg/ml purified protein in PBS. Wells were washed 3x with PBS-T (0.02% Tween 20). Plates were blocked with 100 µl of 5% (w/v) milk in PBS blocking buffer (Life technologies) for 12 h at RT. Plates were washed 3x in PBS-T. 50 µl of detection antibody/nanobody/Fab fragment was added to the wells and incubated at RT for 1 h. Antibodies are their uses are detailed in **Table 2.1.** Dilution series of protein analyte were prepared in blocking buffer. Wells were washed 5x with PBS-T. 50 µl of HRP conjugated antibody prepared in blocking buffer was added to the wells and incubated for 1 h at RT. Wells were washed 5x with PBS-T. The Pierce HRP ELISA kit (ThermoFischer Scientific, UK) was

used to develop the ELISA for 5–10 mins and neutralised with 2M sulphuric acid, prior to measuring absorbance at 450 nm using an InfinateF200 plate reader (Tecan, Switzerland).

Table 2.1 Detection and conjugated antibodies used in ELISA

	Primary Antibody	**Secondary Antibody**
Rabbit mAb or Fab	Goat anti-rabbit HRP (PI-1000, VectorLabs, UK)	n/a
His-Tagged protein, Glycoprotein Nanobody or Fab	Rabbit anti -His (ab1908, Abcam, UK)	Goat anti-rabbit HRP (PI-1000, VectorLabs, UK)
Glycoprotein-1d4	Mouse anti-1d4 (University of British Columbia)	Horse anti-mouse HRP (MP 7402, VectorLabs, UK)

2.7 Generation of nanobodies specific to RVFV Gn and Gc

2.7.1 Generation of nanobody library- phage display

The generation of anti-RVFV Gn and Gc nanobodies by phage display was performed in collaboration with Dr George Warimwe (Jenner Institute, Oxford) and Jan Steyaert (VIB/VUB, Brussels). ChAdOx1 vaccine encoding RVFV Gn and Gc was produced by the Jenner Institute and provided by Dr George Warimwe [170]. Animal experiments were performed by the Steyaert lab. A llama was vaccinated and boosted twice with ChAdOx1-Gn-Gc before further boosting with recombinant RVFV Gn and Gc glycoproteins, as described in **Fig. 5.1**. Llama serum was collected and used to generate a phage display library in the Steyaert laboratory, as previously described [149]. The library of nanobodies was kindly provided by Dr Els Pardon and colleagues, constructed in the pMESy4 plasmid [149]. A thorough protocol detailing the methods used in the Steyaert lab is available [149]. The plasmid contains an amber stop codon such that the expression of the full-length protein (including the phage protein) occurs only in suppressor cells allowing for phage display. In non-suppressor cells, the amber stop codon generates a truncated protein encoding only the nanobody, which is directed to the periplasmic

space [149]. Phage display libraries were maintained in TG1 *E. coli* (suppressor strain, Lucigen), protein production was achieved in Wk6 *E. coli* (non-suppressor [171])

2.7.2 Selection of nanobodies by Phage-display

Nanobody selection was performed by phage display. ELISA plates were coated and incubated overnight at 4°c with either 1 µg/ml RVFV Gn or RVFV Gc in a sodium carbonate coating buffer. A negative control well was run for each selection, which was coated only with buffer. Plates were washed 5 x with PBS, then blocked with 4% milk in PBS and incubated at RT for 2 h. A solution containing 10 µl of phage library diluted 1/10 with PBS containing 4% milk was added to each well and incubated for 2 h at RT. Wells were washed 15 x with PBS. To elute phage bound to the plate, trypsin was prepared at a final concentration of 25 µg/ well and added to each well for a 30 min incubation at RT. Phage were then collected from each well and mixed with an AEBSF trypsin inhibitor (Carl Roth, Germany). Serial dilutions were prepared from each well and used to inoculate exponential phase TG1 culture, which was then incubated for 30 min at 37°c. The cultures were then plated on selective medium (LB agar plus 100 µg/ml ampicillin + 2% (wt/vol) glucose), and a glycerol stock of the newly enriched library was created with undiluted phage. Plates were incubated overnight at 37 °C. Successful selection was indicated upon observation of an at least 100-fold enrichment of phage (number of colonies on the plate), when compared to the negative control wells. Individual colonies were also picked from agar plates and used to generate glycerol stocks.

2.7.3 Bacterial expression of nanobodies

Nanobodies were produced in bacteria. WK 6 *E. coli* cells (kindly provided by the Steyaert group, VIB/VUB Instruct) were transformed with plasmids encoding nanobodies selected for their binding to RVFV Gn or RVFV Gc. The transformed bacteria were plated on LB agar containing 100 µg/ml ampicillin and 2% glucose (wt/vol) (as per **2.1.10, 2.7.2**) and glycerol

stocks were created after validation with Sanger sequencing. Overnight precultures were grown in LB supplemented with 2% w/v glucose and 100μg/ml ampicillin. The preculture was then used to inoculate (1% of by volume) 1 L of Terrific broth supplemented with 0.1% (wt/vol) glucose and 1 mM $MgCl_2$ in 2 1 L flasks. The cultures were incubated in a shaking incubator at 37 °C, 170 rpm until an optical density of 0.7 at 600nm was recorded (typically after 2-3 hours). Once cultures had grown to the desired optical density, nanobody expression was induced by adding Isopropyl-β-D-thiogalactoside (IPTG Sigma Aldrich, UK) to a final concentration of 1 mM and incubated at 28 °C and 170 rpm overnight. Bacteria were harvested by centrifugation for 15 min at 9,000 x g at RT. Cell pellets were resuspended in 15 ml ice-cold TSE (20 mM of Tris pH 8.0, 6.5 μM EDTA and 0.5 M sucrose) and incubated at 4 °C for 1 h with a magnetic stirrer for gentle agitation. 30 ml of TSE/4 (diluted four-fold in ddH_2O) was then added to each pellet and incubated at 4 °C, while mixing with a magnetic stirrer. Stirring was continued for 1h or overnight. The suspension was then centrifuged for 30 min at 10,000 x g at 4 °C to recover the supernatant as periplasmic extract. Purification of nanobodies from the periplasmic extract was then performed using IMAC (as per **2.3.2)**

2.8 Animal studies

All mouse studies were performed by specialist staff at the animal facility at PHE, Porton Down.

2.8.1 Ethics

All mouse procedures were conducted in accordance with the Animal (Scientific Procedures) Act 1996 (Establishment License 70/1707 and project license P82D9CB4B).

2.8.2 Murine RVFV infection model

Female BALB/c 6–8 week old mice were housed in groups of three. Groups of six mice (randomly assigned, two boxes per group) were treated intravenously with RV-Gn1 (200 μg or 10 μg) or received no treatment. An additional control group of five mice was treated with 200 μg of a non-RVFV rabbit mAb control. This anti-Hantavirus control antibody was kindly provided by Dr Stephanie Krum and Mr Robert Stass. Four to six h post-treatment, mice were challenged subcutaneously with 20 pfu of RVFV, strain ZH501. Mice were monitored six times daily for symptoms of infection and were culled when the determined humane endpoint was reached. Mouse survival was analysed using a Kaplan-Meier test with log-rank using GraphPad Prism.

2.8.3 Murine recombinant Gn immunisation

Animal experiments were performed by facility staff at PHE, Porton Down. Female BALB/c 6-8 week old mice were housed in groups of three. Groups of four mice (or three, where mice were immunised with SFTSV Gn) were randomly assigned to two boxes per group. Mice were immunised according to the schedule depicted in **Fig. 6.4** via intra-muscular injection. 40 μg of purified glycoprotein, buffered in TBS, was mixed 1:1 (v:v) with Aluminum hydroxide adjuvant (kindly provided by PHE, UK) immediately prior to administration. Mice were bled at two intervals to provide serum to assess immunogenicity of the glycoproteins. After two immunisations a robust IgG immune response was observed, mice were sacrificed and spleens were collected for FACS cell sorting.

2.9 FACS and antigen-specific B-cell sorting of PBMCs

Fluorescence-activated cell sorting of peripheral blood mononuclear cells (PBMCs) was performed with Dr Katie Doores at her laboratory in KCL. Spleens were isolated from mice and kept at 4 °C until processing later on the same day. PBMCs were isolated by macerating spleens and passing through a 100 μm cell strainer (Corning, UK). 5 ml of ACK lysis buffer

(ThermoFischer Scientific, UK) was then added for each macerated spleen and incubated for 5 min at RT, then washed with FACS buffer (PBS with 1% BSA) (by centrifugation at 100 x g for 5 min, then resuspension by pipetting). Cells were resuspended in 50 µl FACS buffer with 2 µl Fc block added (catalogue number: 553142, Rat anti-Mouse CD16/CD32 Insight Biotechnology, UK) and incubated for 15 min on ice. PBMCs were stained with a panel of antibodies detailed in **Table 2.2** and then incubated for 45 min on ice and in the dark. Glycoproteins (HRTV Gn, SFTSV Gn, and RVFV Gn) were conjugated to fluorescent antibodies by recognition of either the His-tag or BT using anti-His-FITC (ab1206, Abcam, UK) and anti-BT-APC conjugated antibodies (532362, Life technologies, UK). Glycoproteins were pre-incubated with fluorescent antibody for 30 min at RT. 2 µg of the tagged glycoprotein (at a final concentration of 20 µg /ml) was then added to each of the prepared PBMC samples and incubated on ice for 45 min. Specific sorting regimes were performed as detailed in (**Table 6.3**, and Appendix 1.7). Stained PBMCs were washed with 10ml FACS buffer prior to cell sorting. Sorts were performed on a high-speed BD FACS Melody™.

Table 2.2: Antibodies using in antigen specific B cell sorting.

Supplier	**catalogue number**	**Details**
eBioscience	45-0452-80	Anti-Human/Mouse CD45R (B220) PerCP-Cy5.5 25 µg
eBioscience	45-0193-80	Anti-Mouse CD19 PerCP-Cy5.5 25 µg
Biolegend	102717	PE/Cy7 anti-mouse CD38 Antibody [Clone: 90]
Biolegend	405715	APC/Cy7 anti-mouse IgD Antibody [Clone: 11-26c.2a]
Biolegend	406515	APC/Cy7 anti-mouse IgM Antibody [Clone: RMM-1]
Biolegend	100751	Brilliant Violet 510™ anti-mouse CD8a Antibody [Clone: 53-6.7]
Biolegend	100553	Brilliant Violet 510™ anti-mouse CD4 Antibody [Clone: RM4-5]
eBioscience	48-5931-80	Anti-Mouse Ly-6G (Gr-1) eFluor® 450 25 µg
eBioscience	48-0114-80	Anti-Mouse CD11c eFluor® 450 25 µg
Biolegend	123123	Pacific Blue™ anti-mouse F4/80 Antibody [Clone: BM8]
Abcam	ab1206	anti-His-FITC
Life technologies	532362	anti-BT-APC

2.10 Data representation and statistical analyses

All data plot generation and statistical analysis (Kaplan-Meier with Log-rank) was performed using GraphPad Prism version 5 (GraphPad Software, California, USA). All molecular representations were produced with Pymol (http://www.pymol.org). Sequence alignments were generated using Multalign [172] or ClustalW [173] and formatted with Espript [174].

Chapter 3

Molecular basis of antibody mediated neutralisation of RVFV

Chapter 3: Molecular basis of antibody mediated neutralisation of RVFV

3.1 Preface

Taking place over the past eight years and across multiple institutions, this project was a combined effort involving many contributions other than my own. The preliminary work described in this chapter; the generation of a library of rabbit antibodies was performed prior to my contribution to the project. Prof Thomas Bowden and Dr Katie Doores designed and implemented the rabbit immunisation regime of RVFV Gn at the Scripps Institute. Dr Stefanie Krum (KCL) performed much of the work to isolate the antibody sequences. The two structures presented here were obtained in parallel by myself and Dr Steinar Halldorsson, in the Bowden lab. The RV-Gn3–RVFV Gn complex crystal was harvested by Dr Karl Harlos. The crystal generated by Steinar (RV-Gn1-RVFV Gn) formed nearing the end of his project, therefore I performed structure refinement and analysis of these data. Full length antibody production and competition ELISAs were performed by Dr Stefanie Krum using recombinant proteins I produced, as described in this chapter. Animal experiments were performed by the facility staff at PHE under the study plan designed by myself and Dr Victoria Graham (PHE). dN/dS analysis discussed was the work of Dr Jayna Raghwani. A paper describing these results was published in *Cell Reports* in 2018 [150].

3.2 Summary of Findings

The Gn subcomponent of the Gn-Gc assembly that encapsulates the human and animal pathogen, Rift Valley fever virus (RVFV), is a primary target of the neutralising antibody response raised during infection and immunisation. To better understand the molecular basis for immune recognition, we raised a class of neutralising monoclonal antibodies (nAbs) against

RVFV Gn, which exhibits protective efficacy in a mouse infection model. Structural characterisation reveals that these nAbs are directed to the membrane-distal domain of RVFV Gn and likely prevent virus entry into a host-cell by blocking fusogenic rearrangements of the Gn-Gc lattice that are required for cellular entry. These data provide a blueprint for the rational design of immunotherapeutics and vaccines capable of preventing RVFV infection.

3.3 Study Background

As neutralising Abs raised during infection and immunisation have been shown to target the phleboviral Gn [110], RVFV Gn was tested for its efficacy as a recombinant immunogen for eliciting nAbs capable of controlling viral infection. Prior to my involvement in the project, four New Zealand white rabbits were immunised with recombinant RVFV Gn, in the laboratory of Prof. Dennis Burton (The Scripps Research Institute) (**Fig. 3.1)**. Following the second boost, a potent neutralising IgG response was observed against the glycoprotein (**Fig. 3.1** and **Table 3.1**). Single B cells were isolated from a selected rabbit by antigen-specific fluorescence-activated single-cell sorting (**Fig. 3.2**).

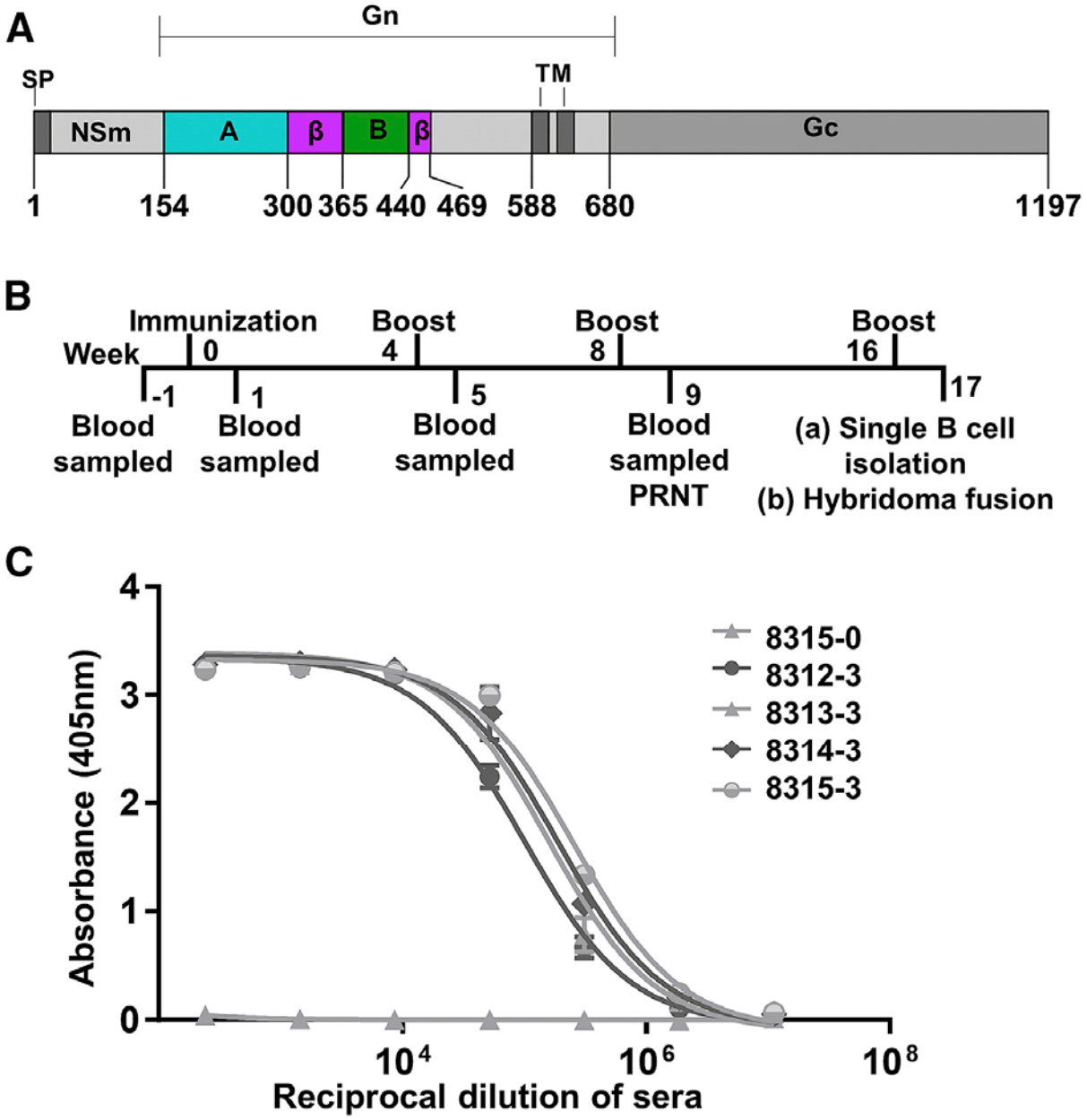

Figure 3.1 Immunisation with recombinant RVFV Gn elicits a robust IgG response
(A) Domain organisation of the RVFV M segment. The full-length ectodomain of RVFV Gn was used for immunisation. The RVFV Gn construct used for crystallisation is coloured according to structural identified domains: domain A (cyan), β-ribbon domain (β, magenta), and domain A (green). The signal peptide (SP), NSm protein, transmembrane region (TM), and Gc glycoprotein are annotated. **(B)** Timeline of rabbit immunisation experiments. Rabbits were immunised with recombinant RVFV Gn and boosted at 4 week intervals. Seven days following the second boost, RVFV Gn binding and neutralisation titres were measured. A splenectomy was performed 7 days following the third boost. mAbs were derived by hybridoma fusion from splenocytes and antigen-specific single B cell sorting of PBMCs. **(C)** ELISA measuring the titres of IgG specific to RVFV Gn for each rabbit (rabbits 8312–8315) following the third boost. Sample 8315-0 is a pre-immunisation sera control derived from rabbit 8315. (Experiments performed by Dr Katie Doores and Prof Thomas Bowden, figure taken from reference [150].)

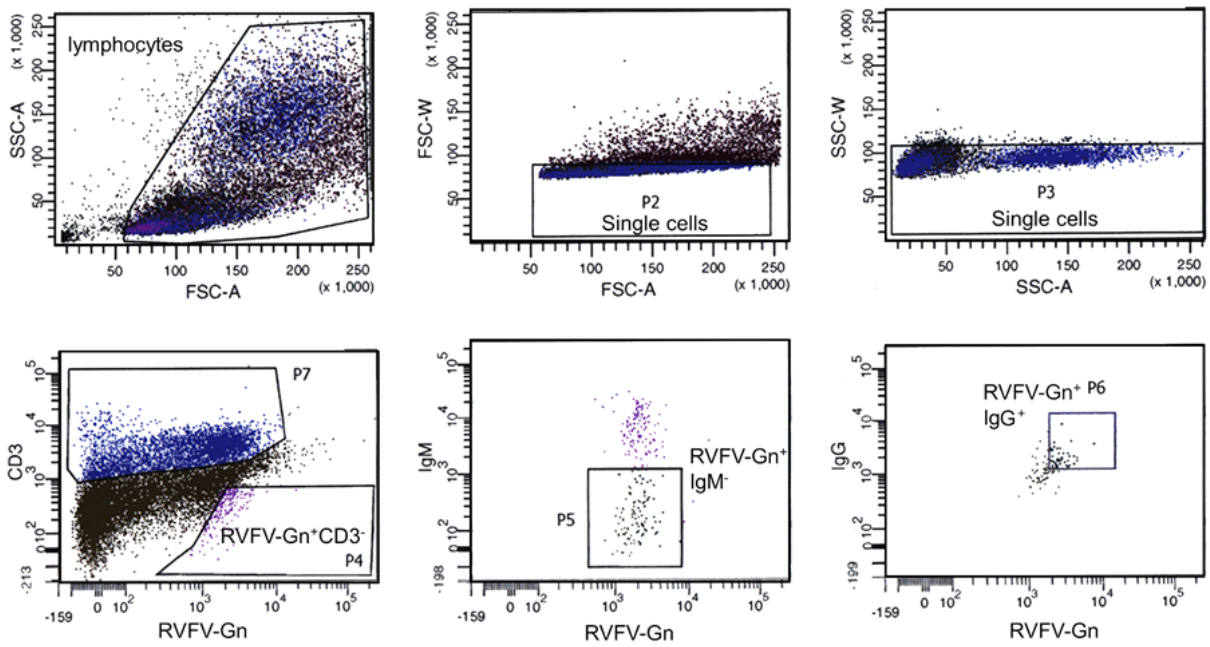

Figure 3.2 Antigen-specific fluorescence-activated cell sorting gating strategy. CD3-IgM-IgG+RVFV Gn+ PBMCs were sorted into single wells of a 96-well plate for subsequent sequence analysis. (Experiments performed by Dr Katie Doores and Prof Thomas Bowden, figure adapted from reference [150].)

Additionally, hybridoma fusion was performed by Epitomics. Approximately 100 hybridomas were isolated and screened for RVFV neutralisation potency. From the isolated neutralising hybridomas, two were sequenced for the heavy- and light-chain pairings termed RV-Gn1 and RV-Gn2. This work is summarised in a publication [150].

Table 3.1. Plaque reduction assay of sera from immunised rabbits with RVFV Gn adapted from [150]

	Serum dilution resulting in a 50% plaque reduction[a]	
Animal ID	**Bleed 2**	**Bleed 3**
8312	1:256	1:4096
8313	1:2048	1:2048
8314	1:512	1:4096
8315	>1:4096	1:8192

[a]These early neutralisation assays were performed by Dr Ben Brennan in the laboratory of Prof. Richard Elliott (University of St Andrews).

This chapter focusses on a class of antibodies derived from the same germline. Chapter 4 will detail additional mAbs that I characterised from this immunisation regime and single-antigen B cell isolation. Two of the antibodies in this class (RV-Gn1 and RV-Gn2) were isolated from the hybridoma fusion and collaborators (Elliott lab, University of St Andrews) have demonstrated neutralisation potential when hybridoma supernatants were screened against RVFV.

3.4 Results

3.4.1 Antibody isolation from single B cells and sequence analysis

This paragraph describes work led by Dr Stefanie Krumm (Doores Lab, KCL). I aided the extraction and amplification of mAb light and heavy chains from one 96 well plate of single B cells. Using antigenic-specific B-cell sorting, a total of 24 pairs of matched heavy and light chains were isolated. The variable regions of these antibodies were sequenced (Appendix 1.3), and cloned into relevant expression vectors.

A library of 27 antibody sequences (24 derived from sorted B cells and 3 from hybridoma fusion), were analysed using the Ig BLAST server [175] and the IMGT-V-quest tool [176]. As CDRH3 has been shown to have the highest contribution to antigen binding on average [177], the similarity of CDRH3 sequences was also considered, to predict which antibodies may bind similar epitopes [177]. The experimental progress for each monoclonal antibody is detailed in **Table 3.2**.

Table 3.2: A summary of the rabbit anti-RVFV Gn monoclonal IgG isolated and experimental characterisation completed thus far.

	Isolation*	**CDRH3 sequence#**	**Fab Expression£**	**Fab Neutralisation %**	**mAb Neutralisation^**	**mAb Protection*!**	**RVFV Gn complex >**	**Structure determined<**
RV-Gn1	H	CATYPNYPTDNLW	Y$	Neutralising	Neutralising	Protective	Y$	Y
RV-Gn2	H	CATYPNYPTDNLW	Y$	Neutralising	Neutralising		Y$	N
RV-Gn3	B	CATYPNYPTDNLW	Y	Neutralising	Neutralising!		Y	Y
RV-Gn4	B	CVRIMAGGCNSW	Y	Non-neutralising	Non-neutralising!		Y	Y
RV-Gn5	B	CGRAPYSRHVGYYICASLW	Y	Non-neutralising	Non-neutralising!		Y	Y
RV-Gn6	B	CVRDAGYSDYSLGLW	Y	Non-neutralising	Non-neutralising!		Y	N
RV-Gn7	B	CARGGATYSSDGYALDYLDVW	Y	Non-neutralising	Non-neutralising!			
RV-Gn8	B	CARGIYMIYDYPSRFNLW	Y	Neutralising	Neutralising!			
RV-Gn9	B	CARSINENDGTVLW	Y	Neutralising				
RV-Gn10	B	CARDGATTGYYFDLW	Y	Non-neutralising				
RV-Gn11	B	CVRVMAGGCNLW	Y	Non-neutralising				
RV-Gn12	B	CVRIMAGGCNLW	Y	Non-neutralising				
RV-Gn13	B	CARDAGSNYYAHYFDFW	Y	Non-neutralising				
RV-Gn14	B	CARDAGSNYYAYYFDFW	Y	Non-neutralising				
RV-Gn15	B	CARDAGSNYYTYYFDFW	Y	Non-neutralising				
RV-Gn16	B	CARDAGSNYYAYYFNFW	Y	Non-neutralising				
RV-Gn17	B	CARDAGSNYYAHYFDFW	Y	Non-neutralising				
RV-Gn18	B	CARDAGYSDYSLGLW	Y	Non-neutralising				
RV-Gn19	B	CARDGGHSDYSLGLW	Y	Non-neutralising				
RV-Gn20	B	CVRSATAASTYTRLDLW	Y	Non-neutralising				
RV-Gn21	B	CVRDLGYSXNLW	Y	Non-neutralising				
RV-Gn22	B	CARSFLDDTNGYYDLW	Y	Non-neutralising				
RV-Gn23	B	CARALDTIKNLW	Y	Non-neutralising				
RV-Gn24	H	CGRDRSTGTMDILDLW	Y$	Neutralising	Neutralising		Y$	N
RV-Gn25	B	CASWTRLDLW	Y	Non-neutralising				
RV-Gn26	B	CGSWTRLDLW	Y	Non-neutralising				
RV-Gn27	B	CASWTPLDLW	Y	Non-neutralising				

* All Abs were derived from a single New Zealand white rabbit immunised with RVFV Gn as described in **Fig.3.1** and reference [150]. H denotes antibodies derived from hybridoma fusion (splenocytes were fused with the Epitomics proprietary fusion partner), B denotes antibodies derived from antigen-specific IgG specific, B cell sorting.
£ All Fabs were generated as recombinant proteins by cloning into the PHLSec expression vector. Expression tested in small scale HEK293T culture, Y denotes detection of soluble secreted protein by Western blot analysis. # Experiments performed by Dr Stefanie Krumm (KCL). ! Rabbit mAbs were generated by cloning the isolated HC and LC sequences into a pHLSec based expression vector. $ Experiments performed by Dr Steinar Halldorsson. % Neutralisation of Fab fragments initial screening using a PRNT assay. ^ Neutralisation of mAb using PRNT assay with dilution series. * Protection experiments performed in BALB/c mice with a lethal RVFV challenge. > Y denotes complex formation with recombinant RVFV Gn as determined by SEC and SDS-PAGE analysis. < Co-crystallisation experiments were performed, those which yielded crystals and subsequent diffraction and structure solution are marked Y, those which did not are marked N. (Throughout: empty cells indicate the experiment was not performed).

This chapter focusses on a single class of mAb. RV-Gn1, RV-Gn2, and RV-Gn3 exhibit high levels of sequence conservation in the complementarity-determining regions (CDRs) of each respective fragment antigen binding (Fab) region (**Fig. 3.3**). Furthermore, analysis of germline V, J, and D segments suggests that these mAbs are likely clonally related, with 8%–12% mutation from germline IGV1S69*01.2 (combined V and J) for both the heavy and light chains **(Table 3.3** and **Fig. 3.3)**.

Table 3.3. Analysis of antibody germlines and CDR loops of antibodies RV-Gn1–3.

HC[&]	**V**	**mutation**	**J**	**mutation**	**D**	**CDRH3**
Rv-Gn1	1S69*01	91.67%	J4*01	83.33%	7-1*01	CATYPNYPTDNLW
Rv-Gn2	1S69*01	91.30%	J4*01	81.25%	7-1*01	CATYPNYPTDNLW
Rv-Gn3	1S69*01	89.86%	J4*01	72.92%	6-1*01	CATYPNYPTDNLW

LC[^]	**V**	**mutation**	**D**	**mutation**	**CDRL3**
Rv-Gn1	1S15*01	92.03%	1-2*01	90.00%	CLGSYDGNSADCLAF
RV-Gn2	1S18*01	93.12%	1-2*01	92.11%	CLGSYDGNSADCLAF
RV-Gn3	1S18*01	92.20%	1-2*02	76.32%	CLGSYDGNSANCLVF

[&] Heavy chain, [^]Light chain
Germline assignments and mutation % from the germlines were calculated using Ig BLAST server [175] and the IMGT-V-quest tool [176]

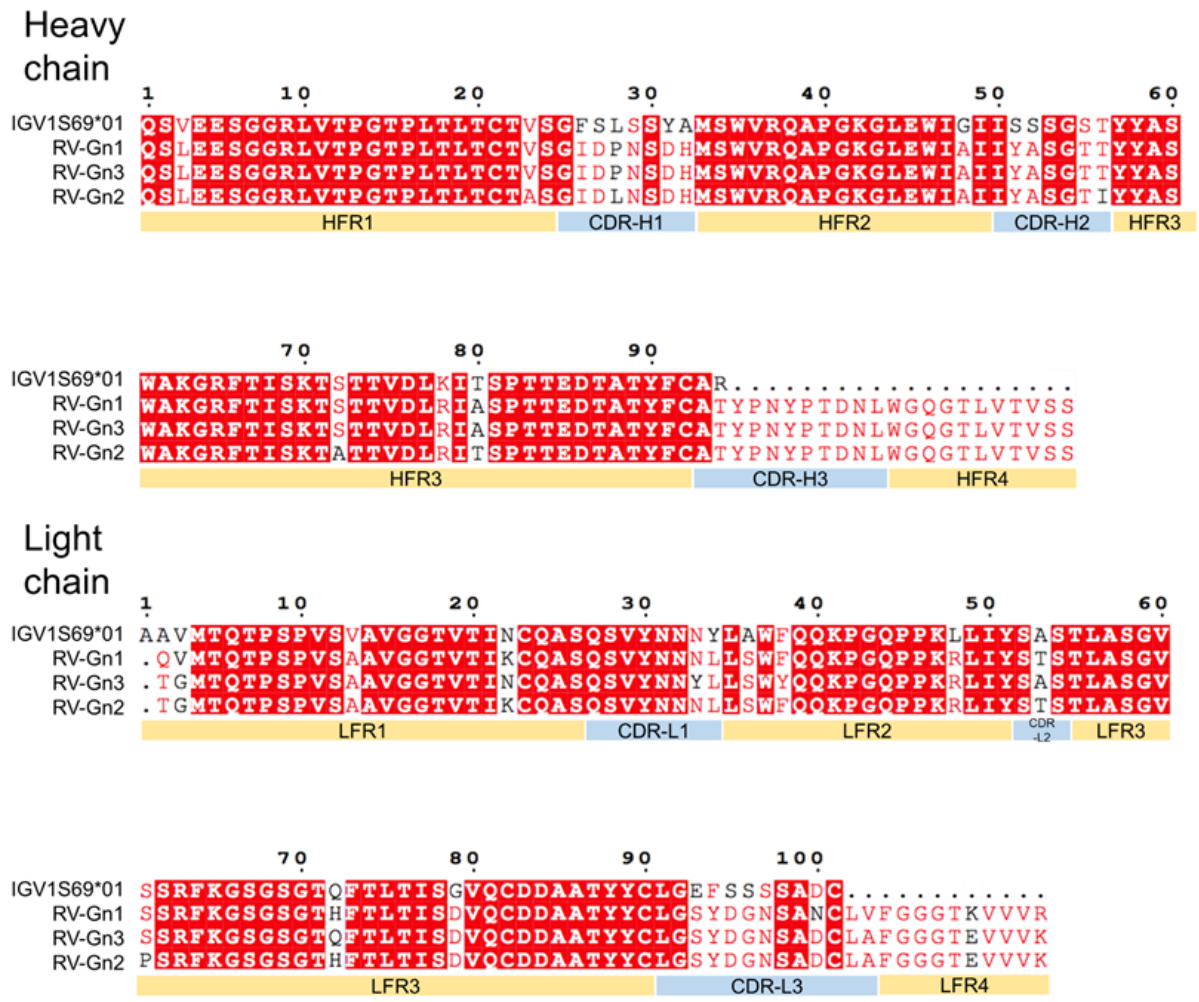

Figure 3.3 Amino acid sequence comparison of three isolated antibodies (RV-Gn1-3) and their corresponding germline sequence.
CDR regions are shown. Top germline V-gene hits were determined using the international immunogenetics information system (IMGT) database [178]. The sequence alignment was determined by Clustal [179] and plotted with ESPRIPT [180], figure adapted from reference [150].

3.4.2 Expression of full-length antibodies

Full-length antibodies were produced for use in binding, neutralisation and protection studies. Dr Stefanie Krum cloned and produced antibodies from the antigen-specific B cell isolation, whilst I purified the RV-Gn1 and RV-Gn2 antibodies from hybridoma cultures by protein G affinity. Cells were expanded for 8–10 days and supernatant collected, clarified, filtered then applied to protein G column. Elution from protein G results in a high purity (>99% purity, as

assessed by SDS-PAGE), homogenous sample. Approximately 0.8 mg of mAb RV-Gn1 was isolated from 250 mL of hybridoma supernatant (**Fig. 3.4**).

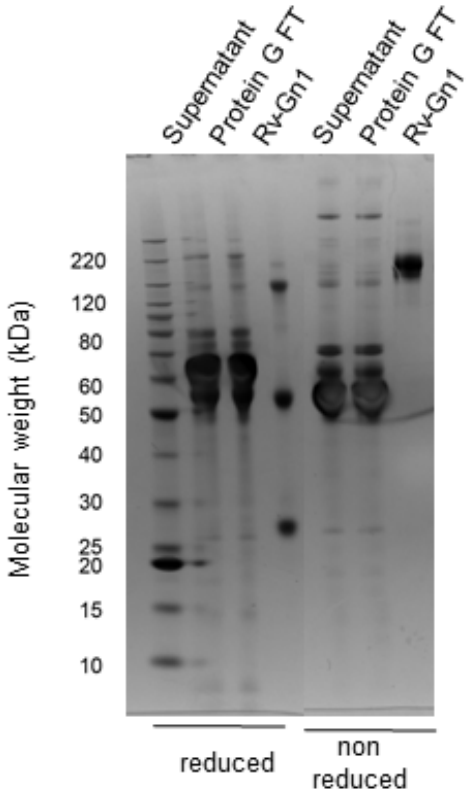

Figure 3.4 SDS-PAGE analysis of Mab Rv-Gn1 from hybridoma supernatant. Samples were prepared both in the presence and absence of reducing agent. Purified RV-Gn1 shows three bands when reduced, the smallest corresponding to the light chain, the middle corresponding to the heavy chain and the largest band corresponding to the intact mAb heterodimer (equivalent to the non-reduced RV-Gn1 single band). High purity sample can be isolated by protein G purification alone with very little contaminant, and little loss of sample from the FT (flow through) of protein G purification.

3.4.3 RV-Gn1, RV-Gn2, and RV-Gn3 exhibit strong binding to recombinant RVFV Gn and compete for the same binding site

Antibody binding was assessed by ELISA. RV-Gn1, RV-Gn2 and RV-Gn3 show remarkably similar binding profiles to the recombinantly produced RVFV Gn ectodomain (residues 154–560). To assess whether these mAbs target similar or overlapping epitopes, a competition analysis was performed by competing Fab fragments with full mAb. This ELISA-based competition assay indicated that these closely related mAbs target a common epitope (**Fig. 3.5**).

The commonalities in CDR sequence and binding affinity, and competition for binding suggest that RV-Gn1, RV-Gn2, and RV-Gn3 can be categorised as a single class of Ab.

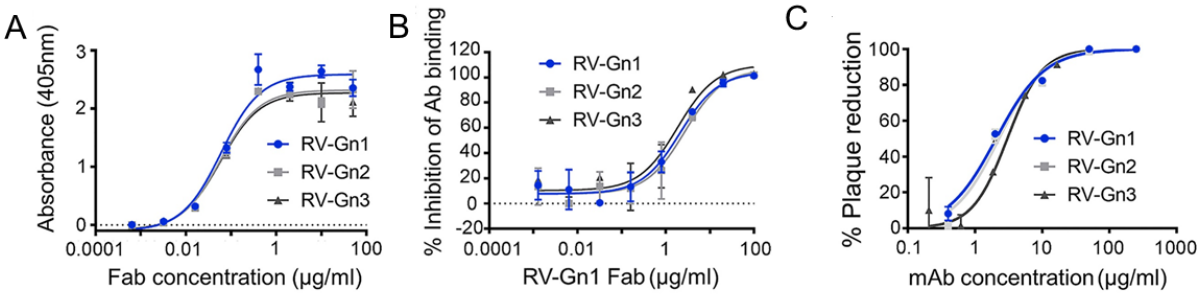

Figure 3.5 High-affinity mAbs RV-Gn1–3 are neutralising and target overlapping epitopes on RVFV Gn
(A) ELISA analysis of mAbs RV-Gn1, RV-Gn2, and RV-Gn3 titrated with RVFV Gn. Experiments were performed in duplicate and repeated three times. A representative dataset is shown. (Performed by Dr Stefanie Krum) **(B)** Competition ELISA analysis: overlap of RV-Gn1–3 epitopes were determined by binding of full-length IgG to RVFV Gn in the presence of RV-Gn1 Fab. Experiments were performed in duplicate and repeated three times. A representative dataset is shown. Dotted line indicates background (Performed by Dr Stefanie Krum) **(C)** RVFV-Gn1, RVFV-Gn2, and RVFV-Gn3 neutralise RVFV in a plaque reduction neutralisation test. Data are shown as percentage reduction in plaques compared with the mAb control (PG9 [168, 169]), and a non-linear regression model is fitted using GraphPad Prism. Experiments were performed in duplicate. Error bars in (A–C) represent the range of the value for experiments performed (not shown when smaller than symbol size). Figure adapted from reference [150].

3.4.4 Assessment of neutralising potency for recombinantly-produced RV-Gn1–3

Supernatants from cells expressing the full-length IgG were first used to screen the neutralising potential of each mAb by plaque reduction neutralisation testing (PRNT). RV-Gn1–3 showed promising neutralisation potential and a further PRNT using a dilution series of purified mAbs demonstrated that each of the RV Gn1–3 mAbs neutralised RVFV with half-maximal inhibitory concentration (IC_{50}) values ranging from 2.1–3.0 µg/mL **(Fig. 3.5)**.

3.4.5 RV-Gn1 is protective in a mouse model of infection

To determine whether this class of anti-RVFV Gn nAb is also protective against disease, we performed a RVFV challenge experiment in mice. Given the levels of RV-Gn1 production from hybridoma cultures, we were able to generate enough mAb for a high and low dose group.

Female BALB/c mice were intravenously administered with 10 μg (low dose) or 200 μg (high dose) of RV-Gn1 eight hours prior to challenge with 20 plaque forming units of RVFV (strain ZH501). Monitoring of mice for disease 14 days post-infection revealed a significant difference between the RV-Gn1 treated mice and the isotype controls ($p=0.03$, Kaplan-Meier with Log-rank). A 60% mortality rate was observed for the IgG isotype control group whilst 100% mortality was observed for the no treatment control. Of the RV-Gn1-treated mice 100% survived RVFV challenge, irrespective of RV-Gn1 dose used (**Fig. 3.6**).

Although we observed increased survival in the isotype control group compared with the no treatment control group, this was not significant ($p=0.08$). We suggest that the unexpectedly high survival rate in the IgG control group may either reflect a feature of the animal system used, as has been observed in other protection studies against emerging viruses [181, 182], or may be a non-specific effect of treatment with IgG [182]. Nevertheless, the 100% survival of mice following treatment with RV-Gn1, with respect to the no-treatment control, indicates the therapeutic potential of anti-RVFV mAbs targeting the RVFV surface.

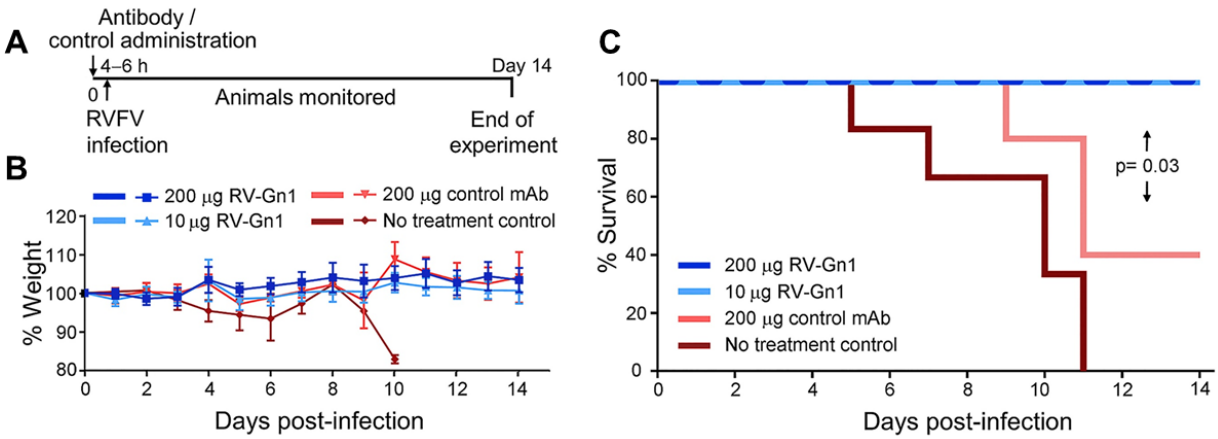

Figure 3.6 RV-Gn1 is protective against RVFV infection in a mouse model.

(A) Timeline of mouse protection experiments. Mice (n = 6) were given RV-Gn1 or control antibody eight hours prior to infection with RVFV. Clinical signs of infection and survival were recorded over 14 days, at the pre-determined experimental end-point. **(B)** Weight loss was recorded over the time course of the experiment. Error bars represent the SEM (not shown when smaller than symbol size). **(C)** Efficacy of antibody protection was assessed by a survival analysis. A Kaplan-Meier log rank test was performed; p = 0.03 between RV-Gn1-treated and mAb control (irrelevant rabbit IgG, Krumm *et al*, unpublished data, section **2.8.2**), p = 0.008 between RV-Gn1-treated and no-treatment control, p = 0.08 between mAb control and no-treatment control. (Experiments performed by facility staff at PHE, Porton Down, figure adapted from reference [150]).

3.4.6 RVFV Gn construct design and expression testing

Although recombinant RVFV Gn previously had been produced for immunisation (construct termed 'Gn_immunogen') and for crystallography (construct termed GnL), I sought to optimise the construct design (**Fig. 3.7, A**). Previous structural studies of the RVFV Gn ectodomain revealed that the C-terminal region of the glycoprotein is conformationally labile and likely poses an obstacle to crystallogenesis [69]. We used this information to create a minimal and hopefully more 'crystallisable' construct of RVFV Gn, which lacked 100 C-terminal residues and included the globular N-terminal region of the protein, which is divided into three domains, domain A, domain B, and the β ribbon. This construct, termed RVFV GnX was derived from a synthetic codon-optimised gene encoding the entire M segment open reading frame (UniProt

accession number P21401). It is interesting to note that recently another group independently identified an identical construct for their crystallisation studies of RVFV Gn [76].

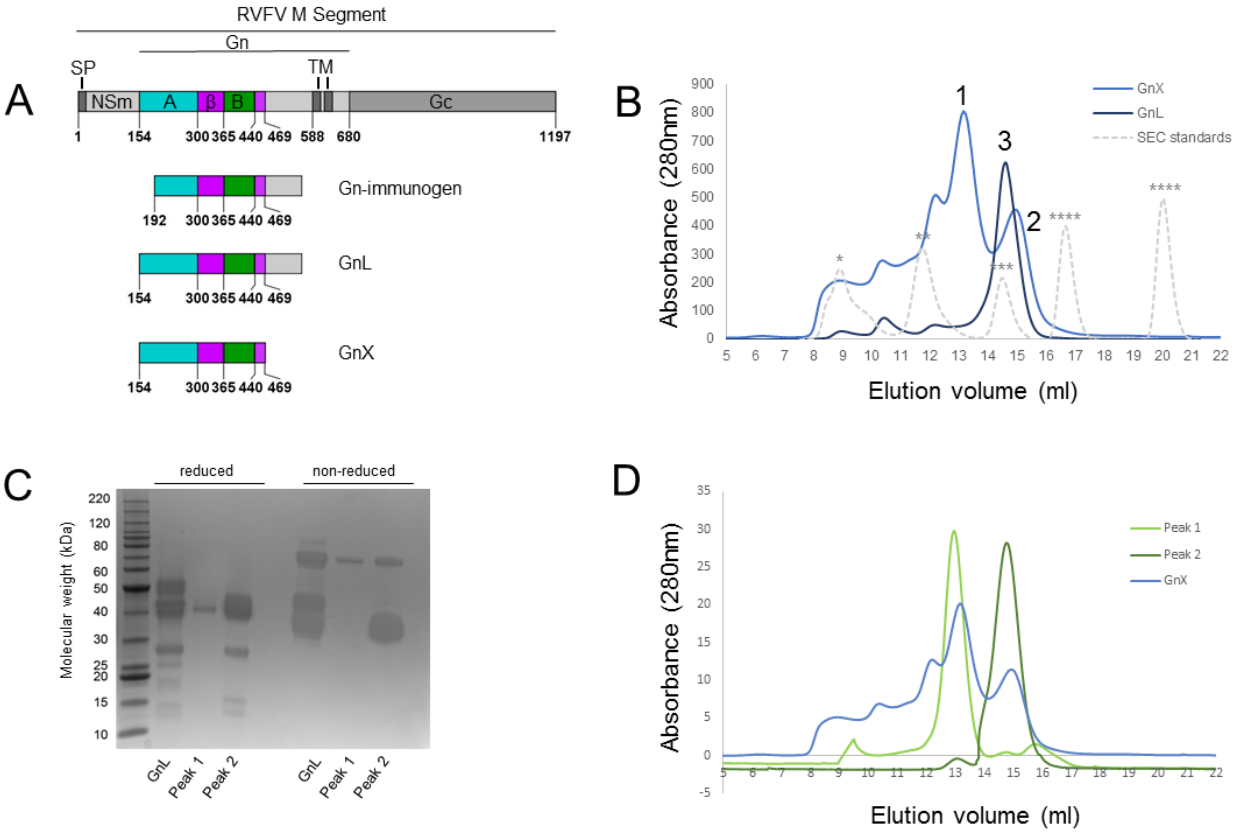

Figure 3.7 RVFV Gn was purified for use in immunisation, ELISA and crystallographic screening.
(A) Schematic representation of the RVFV gene constructs, from top to bottom, the entire M segment, Gn used for immunisation of rabbits, Gn previously utilised for structure determination (PDB:6F8P) and GnX, the new construct for crystallographic study. **(B)** SEC was used to assess the mass and yield of the new GnX protein (light blue). GnX exhibits two peaks of interest, labelled 1 and 2. GnL is overlaid (dark blue) and peak labelled 3. Size exclusion standards are overlaid and shown in dashed grey, asterisks mark the following sizes * 670 kDa, ** 158 kDa, ***44 kDa, ****17 kDa, *****1.4 kDa. **(C)** Purified populations of Gn were assessed by SDS-PAGE analysis. Reduced and non-reduced samples of GnL (Peak 3) and GnX peak 1 and peak 2 were analysed. **(D)** Further size exclusion chromatography was applied to the isolated samples of peak 1 and peak 2 (light and dark green, respectively) overlaid on the original GnX SEC profile (light blue), demonstrating the stability of the two peaks after several days.

3.4.7 Large-scale expression and purification of RVFV Gn

HEK293T cells cultured in roller bottles were transiently transfected with plasmid encoding GnX. Cell culture supernatants were clarified by centrifugation and filtration and then buffer exchanged into TBS. IMAC and SEC were performed, generating a pure sample with an approximate yield of 1 mg/ L of cell culture (**Fig. 3.7, B**). Interestingly, two species were present from the SEC (peak 1 and peak 2 **Fig. 3.7, B**), which corresponded with an approximate molecular weight in the range of ~70 and 35 kDa, respectively. SDS-PAGE analysis revealed only a slight difference between the two species of protein (**Fig. 3.7, C**), where peak 1 runs at the same size as the major component of peak 2. However, peak 2 contains some degradation products similar to those seen in GnL. Given the approximate size, it is likely that the peak 1 is an oligomer, likely a dimer based on the apparent mass by SEC. The stability the 'dimer' product was tested by re-running a diluted fraction of the peak 1 and peak 2, a few days later (**Fig. 3.7, D)**. This analysis resulted in no change in the elution volume, demonstrating that both products remain stable in their oligomeric forms. Since a biological dimer of Gn is not explained by our current understanding of the protein architecture on the virus, as defined by fitting high resolution structures into cryo-EM reconstructions [69], and is not observed when the full length ectodomain of Gn is expressed, I proceeded to use the monomeric RVFV Gn in further experiments.

3.4.8 Recombinant Production and Purification of Fabs

For use in crystallography experiments, the Fab fragment of the RV-Gn1–3 was amplified by PCR from the full-length IgG expression vectors and subsequently cloned into a pHLSec expression vector [183]. Expression was then tested by transient transfection of HEK293T cells by mixing the expression vectors of heavy and light chain 1:1. SDS PAGE and western blot analysis with His-tag. Following confirmation of protein expression, HEK 293T cell cultures were scaled-up to approximately 1L volumes in roller bottles. To enable protein purification,

supernatants were clarified by centrifugation and filtered into a buffer containing TBS (10 mM Tris pH 8.0, 150 mM NaCl). Immobilised metal affinity chromatography (IMAC) and size exclusion chromatography (SEC) were applied to generate a single homogenous peak of RV-Gn3 eluting at approximately 15 mL on a Superdex 200 Increase 10/30 column, corresponding to the molecular mass of ~45 kDa (**Fig. 3.8, A**). This experimental process was also performed by fellow student Dr Steinar Halldorsson, for Fab RV-Gn1.

3.4.9 Generation and purification of RVFV Gn–Fab complexes

The high affinity observed from ELISA indicates that the Fab fragments of RV-Gn1–3 are likely to form a stable complex with RVFV Gn on size exclusion (**Fig. 3.8, A).** Each Fab was added to RVFV Gn at a 1.5-fold molar excess in order to saturate binding and achieve the optimal resolution of the peaks in the SEC trace (**Fig. 3.8, A**). Complex formation yielded a similar SEC profile for each RV-Gn Fab, wherein two species of interest were observed. Consistent with SDS-PAGE analysis, (i) the peak eluting at approximately 13.0 mL corresponded to the newly formed Fab RVFV Gn complex, and (ii) the peak eluting at approximately 15.5 mL corresponded to excess and unliganded RV-Gn Fab (**Fig. 3.8, A**).

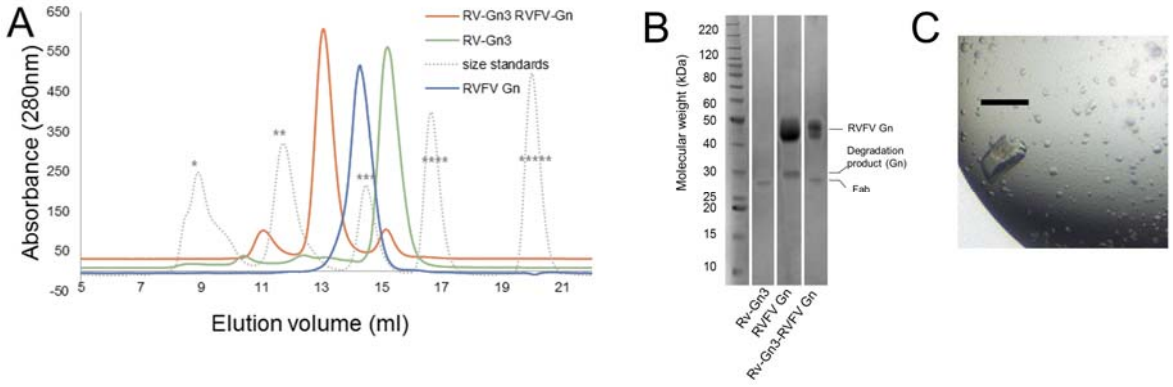

Figure 3.8 RV-Gn3 forms a stable complex with RVFV Gn and generated a single crystal for structural characterisation.
(A) Size exclusion chromatography was used to purify the Fab- RVFV Gn complex. In yellow the SEC profile of RVFV Gn is shown, and Fab RV-Gn3 is shown in green. The complex is shown in blue, with an elution peak centred at approximately 13 ml. Size exclusion standards are overlaid in grey and correspond to the following sizes: * 670 kDa, ** 158 kDa, ***44 kDa, ****17 kDa, *****1.4 kDa. **(B)** SDS-PAGE analysis corroborated estimated molecular masses inferred from SEC. **(C)** A RV-Gn3–RVFV Gn crystal formed after 132 days in a condition comprising 0.2 M lithium sulphate, 0.1 M MES pH 6, and 20% w/v PEG 4000. Black scale bar above crystal represents 100µm.

3.4.10 Crystallisation of RVFV Gn–RV-1 and RVFV Gn–RV-3

The RVFV Gn–RV-Gn3 complex was concentrated to 6.2 mg/mL and subjected to crystallisation screening. Crystal trays were equilibrated and stored at 21°C. Crystals were observed after 132 days in a condition containing 0.1 M, Tris pH 8.0, 2.0 M ammonium sulphate (**Fig. 3.8, C**). Crystallisation screens of RVFV Gn–RV-Gn2 and RVFV Gn–RV-Gn3 were performed in parallel by Dr Steinar Halldorsson. RVFV Gn–RV-Gn2 yielded no diffracting crystals. Crystals arising from screening of the RVFV Gn–RV-Gn3 complex also took considerable time (185 days) to form. The conditions for this crystallisation were 20% w/v PEG 500, 0.1 M bis-Tris pH 6.5.

3.4.11 Structure determination RV-Gn3–RVFV Gn

3.4.11.1 Crystal harvesting and X-ray diffraction data collection

Crystals of both RV-Gn1–RVFV Gn and RV-Gn3–RVFV Gn were cryoprotected in the mother liquor supplemented with 25% glycerol and then flash-cooled in liquid nitrogen. X-ray diffraction data were collected at beamline I03 at Diamond Light Source (Didcot, UK) on a Pilatus 6MF detector (Dectris). Data were indexed, integrated and scaled using xia2 [161]

3.4.11.2 Structure determination of RV-Gn1–RVFV Gn

The crystal structure of the RV-Gn1–RVFV Gn complex was determined at 1.98 Å resolution (**Table 3.4).** Molecular replacement was implemented for phase determination. The structure was solved with PHASER [184], using PDB:4J02 and isolated domains of RVFV Gn (PDB:6F8P) as search models. PDB:4J02 was initially chosen as a search model due to its sequence similarity to RV-Gn1. Iterative rounds of model building and refinement were performed using Refmac5 [185] in the CCP4 suite and COOT [163]. Two copies of the RV-Gn1–RVFV Gn complex populated the asymmetric unit (a.s.u), permitting the implementation of non-crystallographic symmetry restraints during refinement. The two a.s.u copies exhibit near-identical RVFV Gn binding modes (RMSD of 0.5 Å), with only minor differences present on the solvent exposed loops. The final refined structure was validated with MolProbity [186]. Refinement statistics are presented in **Table 3.4**.

3.4.11.3 Structure determination RV-Gn3–RVFV Gn

The crystal structure of the RV-Gn3–RVFV Gn complex was determined at 2.80 Å resolution (**Table 3.4).** Molecular replacement was implemented for phase determination using a method identical to that described for RV-Gn1–RVFV Gn. Iterative rounds of model building and refinement were performed using Refmac5 [185] in the CCP4 suite and COOT [163] then validated with MolProbity [186]. Refinement statistics are presented in **Table 3.4.**

Table 3.4 Crystallographic data and refinement statistics for and RV-Gn3–RVFV Gn.

	RV-Gn1–RVFV Gn	RV-Gn3–RVFV Gn
Data collection statistics		
Beamline	Diamond I03	Diamond I03
Space group	*P*1	*C 2 2 21*
Cell dimensions		
a, *b*, *c* (Å)	51.6, 62.0, 78.9	71.5, 98.5, 172.4
α, β, γ (°)	81.0, 77.5, 84.7	90, 90, 90
Resolution range (Å)	23.6–1.98 (2.03–1.98)[a]	34.6–2.80 (2.90–2.80) [a]
R_{merge}	0.072 (0.651)	0.099 (>1)
I/σ I	5.8 (1.1)	7.0 (0.86)
$CC_{1/2}$	0.98 (0.67)	0.99 (0.44)
Completeness (%)	96.2 (95.3)	97.2 (97.9)
Redundancy	1.8 (1.7)	2.0 (2.0)
Refinement statistics		
Resolution (Å)	23.6–1.98 (2.03–1.98)	34.6–2.8 (2.90–2.80)
No. reflections	59,882	30,747
R_{work} / R_{free}[b] (%)	20.3/24.1	23.6/28.6
No. atoms		
Protein	7,049	3,542
Ligand/ion	n/a	n/a
Water	433	n/a
B-factors		
Protein	48.4	107.4
Ligand/ion	n/a	n/a
Water	49.1	n/a
R.m.s. deviations[c]		
Bond lengths(Å)	0.006	0.008
Bond angles (°)	1.1	1.3
Ramachandran analysis[d]		
Residues in favoured region (%)	98.1	96.8
Residues in allowed region (%)	1.9	3.2

[a]Numbers in parentheses refer to the relevant outer resolution shell.
[b]R_{free} is calculated as for R_{work}, but using only 5% of the data which were sequestered prior to refinement.
[c]r.m.s. deviations: root mean square deviation from ideal geometry.
[d]Determined using the MolProbity server [186].

3.4.12 Structural analysis

3.4.12.1 Structure overview

Interestingly, only residues corresponding to domain B were resolved in both Fab-bound structures (residue numbers: 370–379, 397–437) **(Fig. 3.9)**. Electron density corresponding to both domain A and the β-ribbon domain of RVFV Gn were not visible and could not be sterically accommodated in the RVFV Gn–Fab RV-Gn1 or RVFV Gn–Fab RV-Gn3 crystals, indicating that these regions were likely cleaved during crystallogenesis. Loops 405–431 and 423–431 of domain B in RVFV Gn play a central role in the interaction and maintain a conformation observed in unliganded structures of RVFV Gn, consistent with the high level of structural similarity between nAb-bound and nAb-free RVFV Gn structures (1.1 Å root-mean-square deviation).

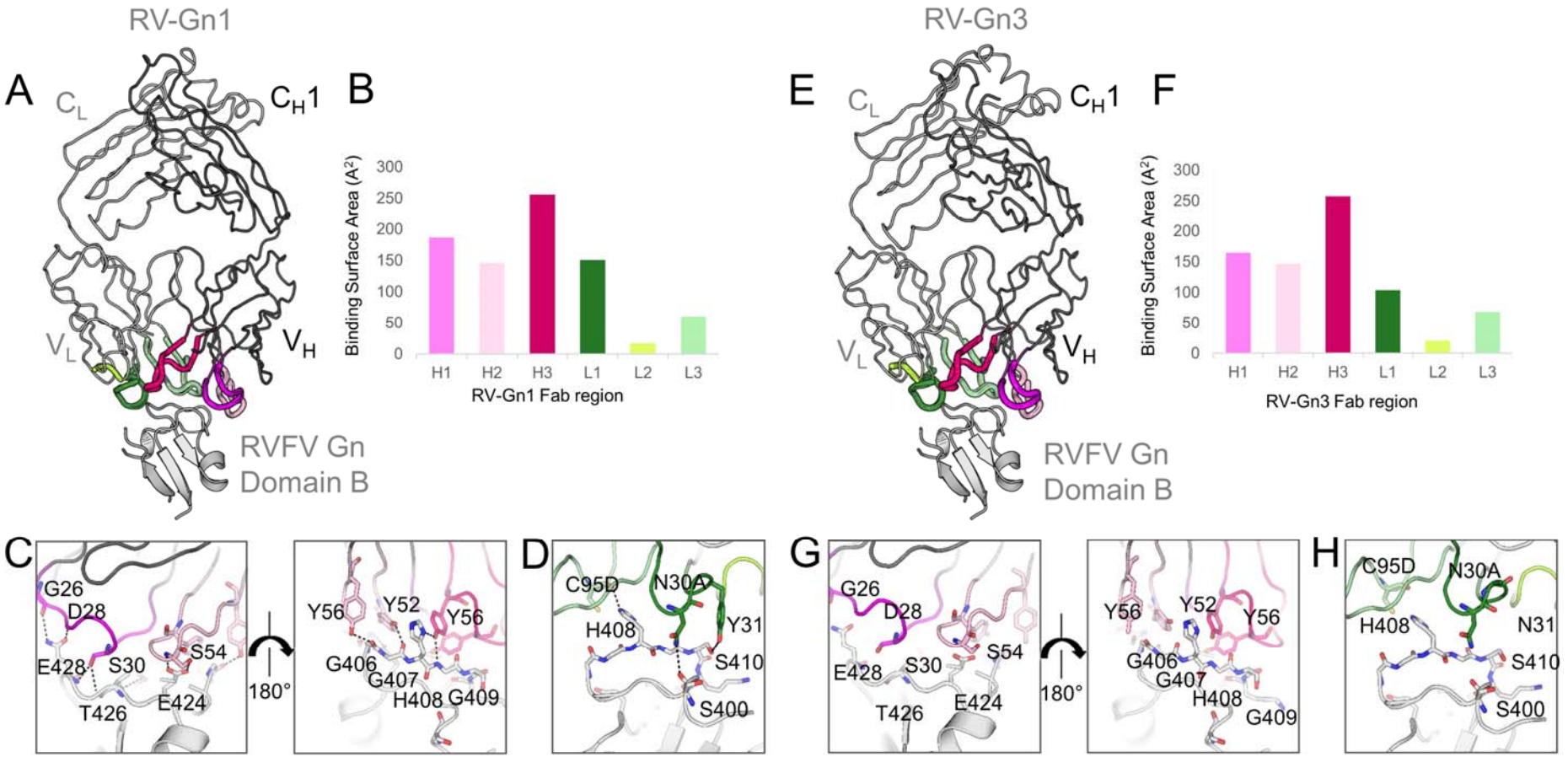

Figure 3.9 Crystal structures of RV-Gn1 and RV-Gn3 bound to RVFV Gn domain B reveal molecular basis of antibody mediated neutralisation. **(A)** V_H, V_L, C_H1, and C_L denote the antibody variable heavy, variable light, constant heavy 1, and constant light chain domains, respectively. Complementarity-determining regions (CDRs) contributing to RVFV recognition are coloured pink (heavy chain) and green (light chain). **(B)** RV-Gn1 recognises RVFV Gn predominantly through the CDR loops of the heavy chain. CDR loop usage by RV-Gn1 in the RVFV Gn complex is shown as a buried surface area ($Å^2$) and was calculated using the PISA EBI server [187]. **(C)** Interactions between the RV-Gn1 V_H residues and the corresponding residues of Gn. **(D)** Interactions between the RV-Gn1 V_L residues and the corresponding residues of Gn. **(E)** Crystal structures of RV-Gn3 bound to RVFV Gn domain B, representation as in (A) **(F)** RV-Gn3 CDR loop usages, analysed and represented as in (B) demonstrates a remarkably similar profile, differing only in CDRL1 usage **(G** and **H)** Interaction between RV-Gn3 and Gn.

3.4.12.2 Epitope analysis

The mode of nAb recognition is essentially identical between RV-Gn1 and RV-Gn3, as would be expected of antibodies from the same class. The RV-Gn1–RVFV Gn structure was solved to a higher resolution (1.98 Å compared with 2.80 Å), consequently, further structural analyses will focus on RV-Gn1, unless otherwise stated.

Salt bridges, hydrogen bonds, and Van der Waals forces contributing to the RV-Gn1–RVFV Gn interactions were identified with the PDBePISA server [188]. The binding interface between RV-Gn1 and RVFV Gn consists of 20 residues from domain B and 31 residues from all CDRs. While each CDR loop from both the heavy and light chains of RV-Gn1 contribute to binding, the heavy chain dominates, with highest contribution to the buried surface area and forms 12 out of 15 hydrogen bonds in the protein–protein interface, typical of an IgG interaction [177] (**Fig. 3.9, B and F**).

Paratope residues recognising Gn are 26–28 and 30–33 from CDR_{H1}, 50, 52–54, 56 and 58 from CDR_{H2}, 95 and 97–100 from CDR_{H3}, 30, 30A, 31 and 32 from CDR_{L1}, 48 and 49 from CDRL2 and 91–95, 95D and 96 from CDR_{L3}. Residues Asn30A, Tyr31, Cys95D from the light chain of RV-Gn3 form hydrogen bonds with RVFV Gn residues Ser400, His408, and Ser410, respectively (**Fig. 3.9**). The heavy chain engages more extensively through its 8 hydrogen bonds from residues Gly26, Asp28, Ser31, Tyr 52, Ser54, Tyr58, Tyr95, Tyr98 and the RVFV Gn residues Gly406, Gly407, His408, Gly409, Glu424, Thr426, Ala427, Gln428 (**Fig. 3.9**). One salt bridge is observed between His33 and Glu424 of RVFV Gn.

The approximately 800 $Å^2$ conformational epitope recognised by the neutralising antibody comprises RVFV Gn residues 400, 401, 403–413, 424–429 and 431. Residues 406–410 of the Gn are contacted by both antibody chains and are therefore likely to be essential for antibody recognition by RV-Gn1. The antibody footprints of RV-Gn1 and RV-Gn3 are remarkably

similar, differences can only be seen when observing the contributions of the antibody light chain (**Fig. 3.9** and **Fig. 3.10**). Indeed, while heavy chain contacts are identical, RV-Gn1 possesses a tyrosine at position 31 of the light chain, which forms a hydrogen bond with Ser410 on domain B on the RVFV Gn. An asparagine in the same position on RV-Gn3 does not participate in the interaction.

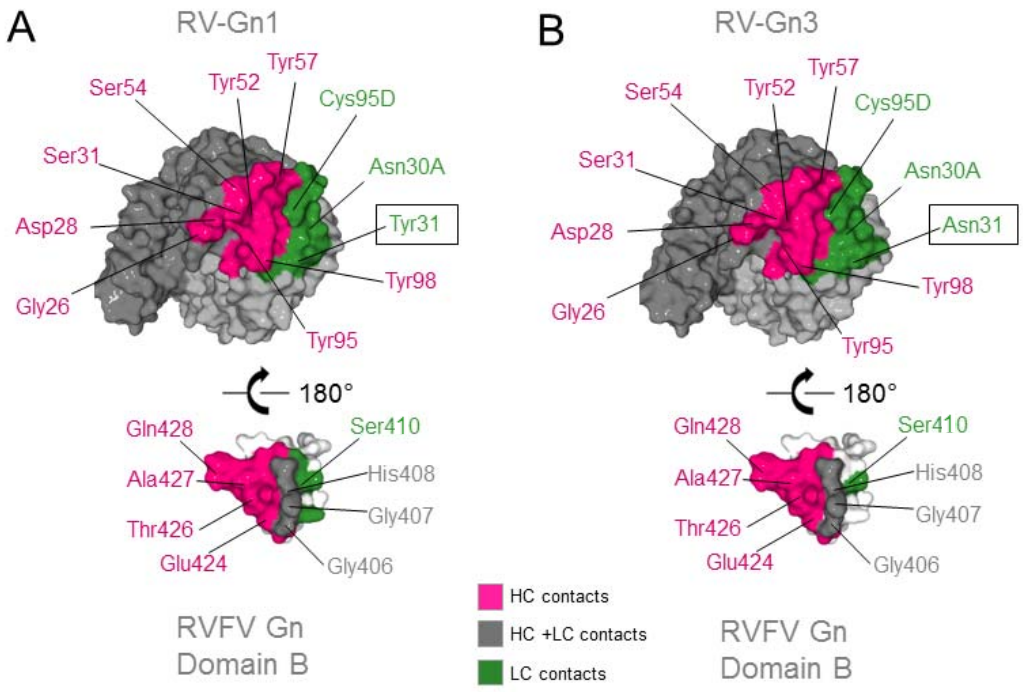

Figure 3.10 Comparative analysis of the paratope and epitope footprints of RV-Gn1 and RV-Gn3
(A) Upper, paratope on the RV-Gn1 Fab recognising Gn. The Fab is represented as a light grey and dark grey surface for the light and heavy chains respectively. Residues from the heavy chain are coloured in pink and residues from the light chain are coloured in green. Residues forming hydrogen bonds in the epitope recognition are labelled. Lower, epitope on the Gn. Gn domain B is represented by white surface. Residues contacted by the LC are coloured in green, residues contacted by the HC are coloured in pink and residues contacted by both chains are coloured in grey.
(B) As for A, showing paratope and epitope for RV-Gn3.

3.4.12.3 Structural analysis in the context of the mature virion

Integration of high resolution crystal structures of RVFV Gn and Gc with lower resolution cryo-electron microscopy (cryo-EM)-derived reconstructions of RVFV virions have enabled the generation of a higher-order Gn–Gc assembly model. In this model, RVFV Gn/Gc forms a T=12 like assembly with Gn located at the membrane-distal region of the virion [69]. To map the location of the RV-Gn1 epitope in the context of the mature RVFV virion, we superimposed the Gn component of our crystallised Fab–Gn complex onto a reported model of assembled RVFV Gn–Gc (**Fig. 3.11**) [69]. This model of the entire RVFV virion reveals that Fab RV-Gn1 targets the membrane distal region of the glycoprotein assembly in a binding mode that extends the Fab perpendicularly from the virion surface (**Fig. 3.11**). Fab fragments were also superposed onto the pentameric and hexameric assembly (PDB no. 6F9B, 6F9C and 6F9F) to evaluate the potential coverage of the virion and the likelihood of bivalent binding in the instance of mAb recognition. Based upon reported structures of full length mAbs, the distance between two Fab regions in one IgG is between 40–52Å (PDB no. 1IGY, 1IGT and 1HZH). The shortest distance between two Fab N termini in the model is 53 Å. Based on the measured distances between RV-Gn1 superposed on the virion assembly, it is possible that a single IgG would be able to bind two Gn molecules at the same time. Although a 1:1 Fab to RVFV Gn stoichiometry might be achieved across the entire virion, given the size of the corresponding Fc region, it is unlikely that this level of occupancy is required to sterically preclude virus–host interactions.

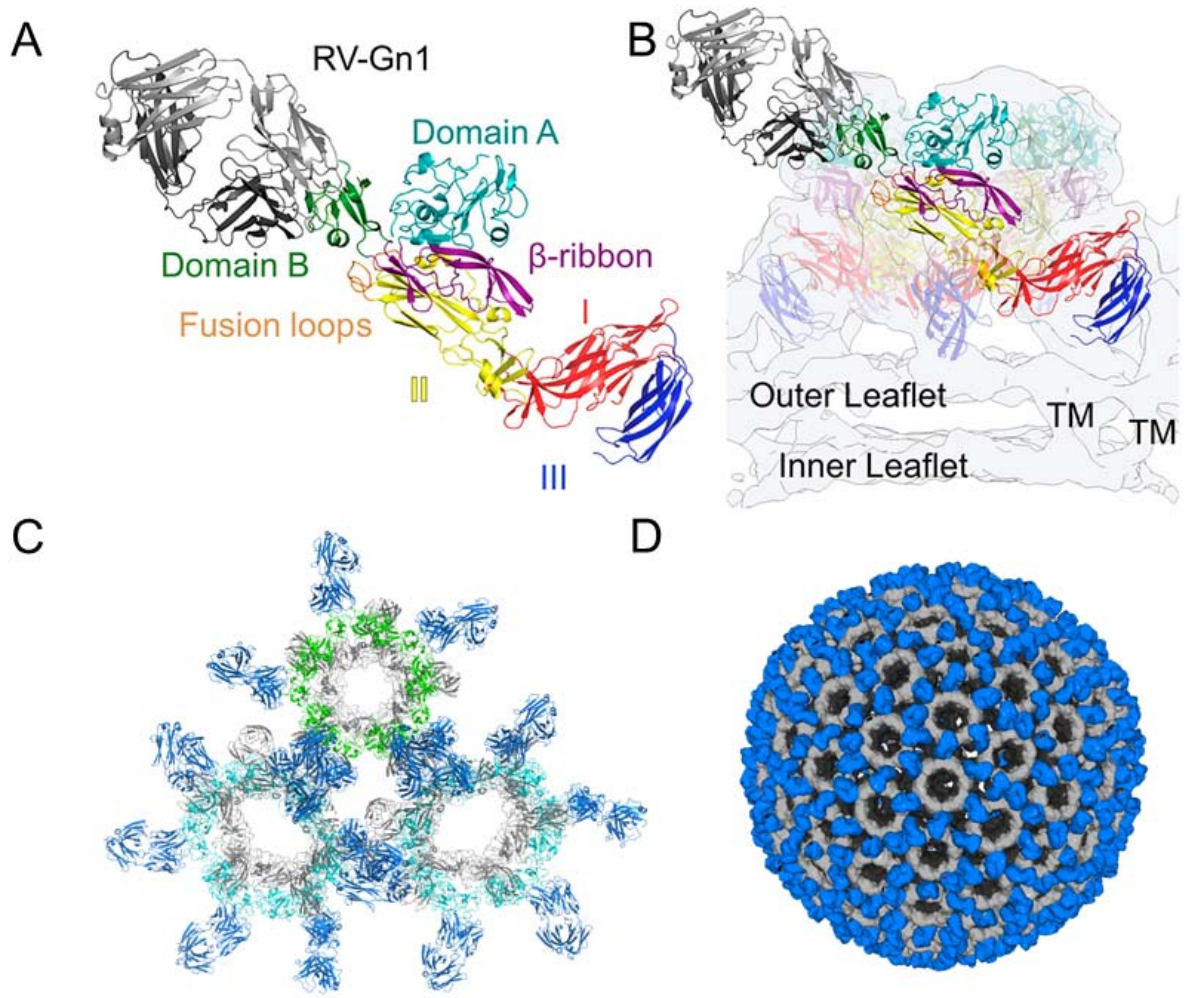

Figure 3.11 RVFV-Gn1 Recognises the Membrane-Distal Surface of the RVFV Gn-Gc Assembly

(A) Modelling RV-Gn1 Fab onto RVFV Gn-Gc heterodimers (PDB: 6F9F) reveals an epitope proximal to Gc-resident hydrophobic fusion loops. RVFV Gc is coloured according to domain, with domain I in red, domain II in yellow, and domain III in blue. RVFV Gn domain A is coloured in teal, domain B in green and the β-sheet in purple. Right: modelling of RV-Gn1 onto the pentameric assembly of RVFV Gn-Gc heterodimers (PDB: 6F9F). Density corresponding to the cryo-electron microscopy-derived reconstruction of the RVFV virion (EMD: 4201) is shown as a transparent surface, with transmembrane regions and leaflets of the virion lipid-bilayer membrane annotated. **(B)** The RV-Gn1 epitope is sterically accessible to full occupancy across the RVFV virion. RV-Gn1 is shown in green, and the Gn-Gc complex assembly of RVFV (EMD: 4197) is shown in grey. **(C)** Complex structure of RV-Gn1 with Gn was docked onto the RVFV pentamer and hexamer maps (PDB No. 6F9B, 6F9C, and 6F9F). RV-Gn1 is shown in marine blue, RVFV Gc is shown in grey, pentameric Gn is shown in lime green and hexameric Gn shown in cyan. **(D)** The RV-Gn1 epitope is sterically accessible to full occupancy across the RVFV virion. RV-Gn1 is shown in blue, and the Gn-Gc complex assembly of RVFV (EMD: 4197) is shown in grey. A and B adapted from reference [150].

3.4.13 Comparison to a neutralising human antibody which targets SFTSV domain B

During the course of this study, an Ab (mAb 4-5) has also been structurally characterised in complex with the Gn of SFTSV [76], a genetically, antigenically, and structurally distal relative of RVFV that shares only 24% sequence identity in Gn (**Fig. 3.12, B–D)** [189, 190]. Interestingly, although RV-Gn1 and mAb 4-5 use distinct modes of binding with dissimilar CDR loop usage and contact antigenically distinctive surfaces, their epitopes localise to domain B of their respective Gn (**Fig. 3.12**), suggesting that the Ab-mediated targeting of this portion of the molecule may be a universal feature of immune responses to the related phlebo- and banyangviruses and therefore an attractive target for immunogen design strategies.

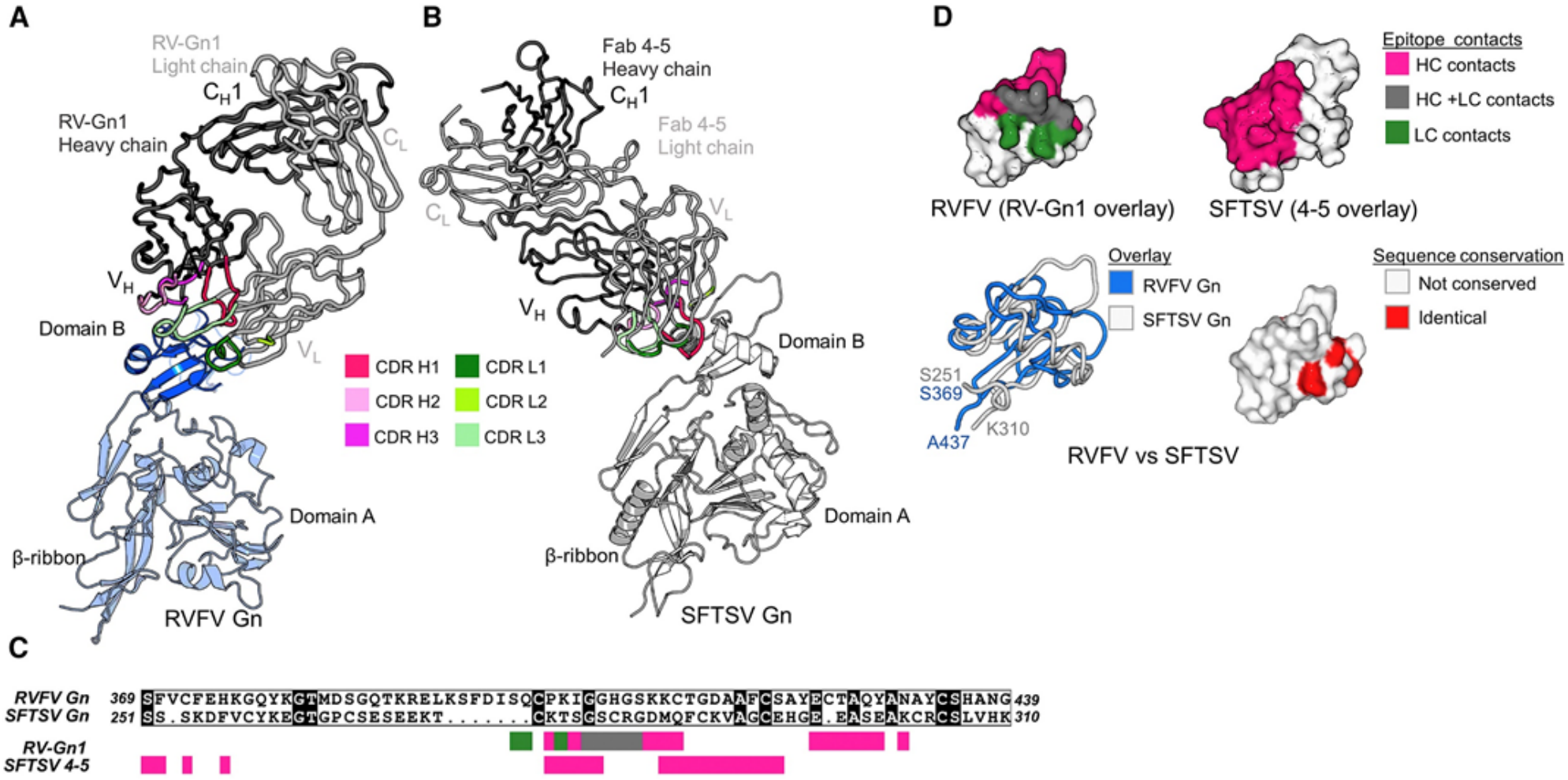
A
RV-Gn1
Light chain
C_H1
RV-Gn1
Heavy chain
C_L
V_H
Domain B
V_L
CDR H1
CDR H2
CDR H3
CDR L1
CDR L2
CDR L3
Domain A
β-ribbon
RVFV Gn
B
Fab 4-5
Heavy chain
C_H1
Fab 4-5
Light chain
C_L
V_L
V_H
Domain B
Domain A
β-ribbon
SFTSV Gn
D
RVFV (RV-Gn1 overlay)
SFTSV (4-5 overlay)
Epitope contacts
HC contacts
HC +LC contacts
LC contacts
Overlay
RVFV Gn
SFTSV Gn
Sequence conservation
Not conserved
Identical
S251
S369
A437
K310
RVFV vs SFTSV
C
RVFV Gn 369 SFVCFEHKGQYKGTMDSGQTKRELKSFDISQCPKIGGHGSKKCTGDAAFCSAYECTAQYANAYCSHANG 439
SFTSV Gn 251 SS.SKDFVCYKEGTGPCSESEEKT.....CKTSGSCRGDMQFCKVAGCEHGE.EASEAKCRCSLVHK 310
RV-Gn1
SFTSV 4-5

Figure 3.12 Comparative analysis of phlebovirus and banyangvirus neutralisation mechanisms

(A) Crystal structure of recombinantly expressed monomeric RVFV Gn in complex with the Fab fragment of RV-Gn1. Domain B of RVFV Gn is shown as a blue cartoon. The β-ribbon domain and domain A (light blue cartoon) were cleaved during crystallogenesis and are modelled by superposition with the previously reported crystal structure of unliganded RVFV Gn (PDB: 6F8P) (Halldorsson et al., 2018). V_H, V_L, C_H1, and C_L denote the antibody variable heavy, variable light, constant heavy 1, and constant light chain domains, respectively. CDRs are coloured shades of pink (heavy chain) and green (light chain). **(B)** Crystal structure of SFTSV Gn in complex with Fab 4-5 (PDB: 5Y11) (Wu et al., 2017), as presented in (A). **(C)** Sequence alignment of SFTSV Gn (residues 251–310) and RVFV Gn (residues 370–439) (calculated by Clustal Omega [179] and plotted with ESPript [180]). Black squares around residues indicate identity. Coloured squares below the sequence mark residues that form contacts with either RV-Gn1 (upper) or SFTSV Gn 4-5 (lower). Residues contacted by the heavy (V_H) chain and light chain (V_L) are shown in pink and green, respectively. Residues contacted by both chains are shown in grey. **(D)** Footprints of RV-Gn1 and Fab 4-5 plotted onto RVFV Gn domain B and SFTSV domain B, respectively, reveal contrasting modes of antigen recognition. Upper: antibody footprints mapped onto domain B of RVFV Gn (RV-Gn1, left) and SFTSV Gn (4-5, right). Structures are shown in surface representation with residues coloured as annotated in (C) Lower left: structure overlay of domain B from RVFV Gn (blue) and SFTSV Gn (white) with a 1.8 Å root-mean-square-deviation (RMSD). Lower right: structure-based mapping of sequence conservation between RVFV Gn and SFTSV Gn. RVFV Gn is shown in surface representation with identical residues coloured red and non-conserved residues coloured white. Figure adapted from reference [150].

3.4.14 Comparison to RVFV human monoclonal antibody structures

A recent study was published detailing the isolation of mAbs from human survivors of RVFV infection [191]. The majority of nAbs target the Gn (only one anti-Gc mAb of the nine reported), supporting the hypothesis proposed by several studies that the Gn is the primary target of a protective and neutralising immune response [108-110]. Furthermore, the derived mAbs/nAbs target 2 distinct epitopes on domain A, which do not overlap with the neutralising epitope targeted by RV-Gn1–3 (**Fig. 3.13**). Indeed, docking of all known antibodies onto the RVFV Gn (PDB: 6f8P) revealed that the RVFV assembly would be able to spatially accommodate our RV-Gn1 and any of the identified human nAbs (**Fig. 3.13**).

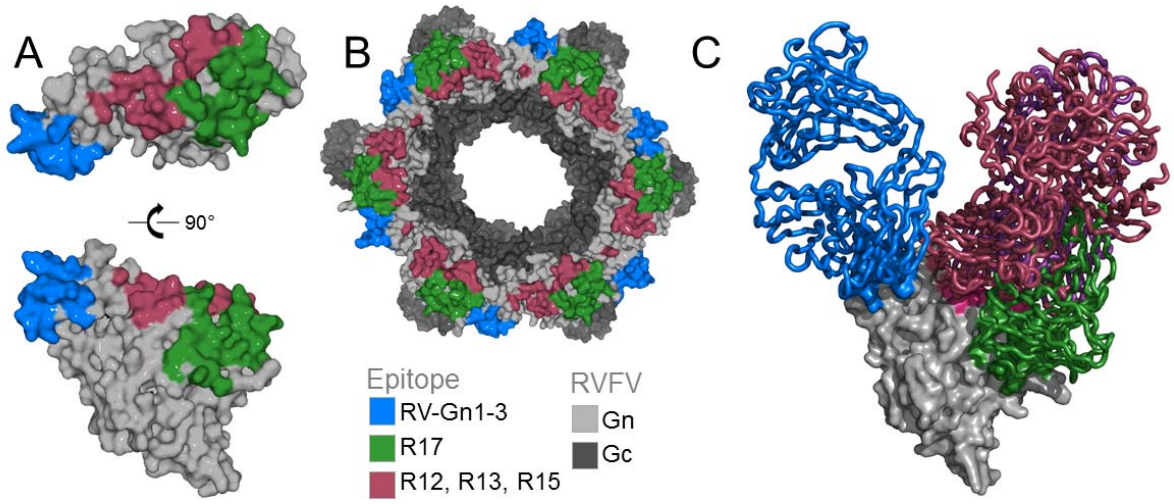

Figure 3.13 RV-Gn1–3 binds a site on RVFV Gn distinct from epitopes targeted by human neutralising mAbs
(A) Neutralising epitope sites mapped onto RVFV Gn (PDB: 6F8C) **(B)** All sites mapped onto the RVFV Gn and Gc hexamer (PDB: 6F9C, 6IEK, 6IEA, 6IEB, 6IEC [191]. **(C)** All known neutralising Fab fragments are mapped onto the Gn structure. Indicating a distinct site for RV-Gn1, likely to be capable of binding in the presence of any of the human monoclonal antibodies.

3.5 Discussion

The assembly of Gn and Gc glycoproteins that encapsulate the surface of RVFV constitutes a primary target of the nAb response generated during both natural infection and immunisation [110]. Immunisation of rabbits with the monomeric N-terminal ectodomain of RVFV Gn was sufficient to elicit a highly neutralising Ab response in rabbits (**Fig. 3.1** and **Table 3.1**).

Monoclonal antibodies were identified from human survivors of RVFV which bind both the Gn and the Gc, however the neutralisation titre on the Gn is much higher *in vitro* and also exhibits *in vivo* protection in mice [191]. These data confirm the Gn glycoprotein as a desirable component of any humoral-based vaccine against RVFV and provide a rational platform for guiding immunogen design efforts for at risk human and animal populations.

We derived RVFV Gn-specific Abs (RV-Gn1–3) using two complementary techniques: hybridoma fusion from spleen and antigen-specific single B cell sorting of PBMCs. Interestingly, these mAbs (RV-Gn1–3) appear to constitute a single class of nAb, as they recognise an overlapping RVFV Gn epitope and likely originate from a single germline (**Fig. 3.3** and **Table 3.3**). Structural elucidation of RV-Gn1 in complex with RVFV Gn revealed an 800 $Å^2$ epitope on domain B of RVFV Gn and provides a molecular basis for immune-mediated neutralisation (**Fig. 3.9**). Interestingly, this region of the Gn has been shown to shield the Gc against premature fusogenic rearrangements. Furthermore it undergoes relocation upon exposure of RVFV to acidic pH [69]. Given the close proximity of the RV-Gn1 epitope to the Gn–Gc interface, it is likely that RV-Gn1 may sterically impede rearrangements to the glycoprotein surface of RVFV, thereby preventing exposure of the RVFV Gc-resident hydrophobic fusion loops in the endosomal membranes following virion uptake into the host cell **(Fig. 3.11** and **Fig. 3.14**). However, we cannot preclude the possibility that RV-Gn1 may also disrupt attachment of DC-SIGN to some of the heterogeneously distributed oligomannose-type glycans presented on RVFV Gn and Gc [82, 86].

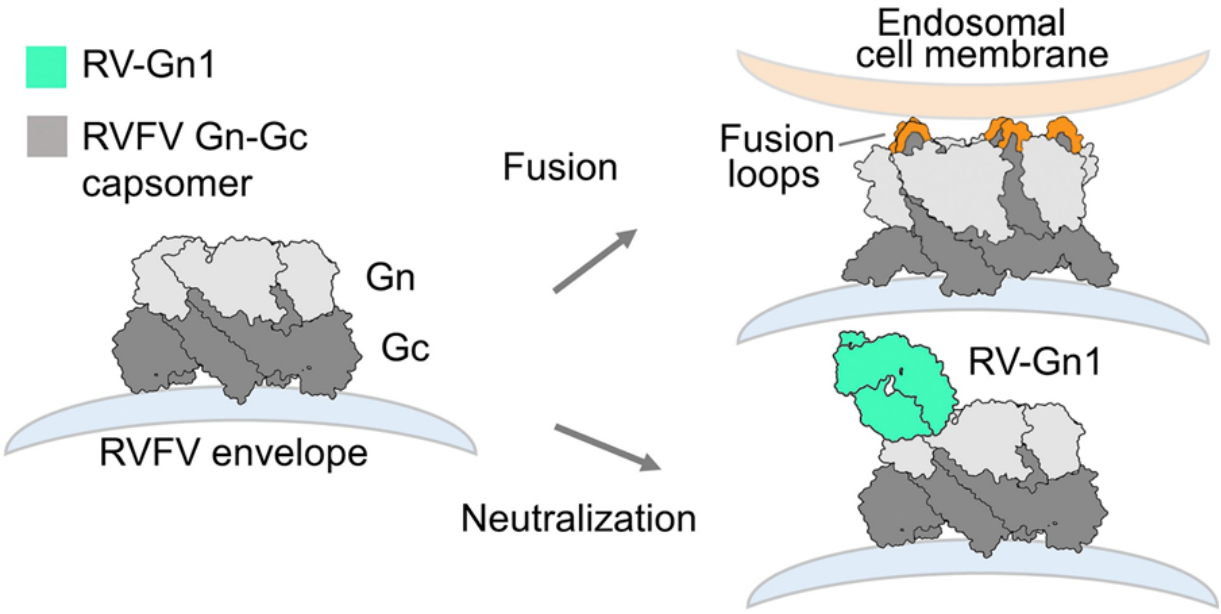

Figure 3.14 A Schematic Model of RV-Gn1-Mediated Neutralisation
Domain B-targeting nAbs (green) sterically impede the exposure of Gc-resident hydrophobic fusion loops (orange). In the absence of RV-Gn1, fusion loops within the Gc glycoprotein are able to extend and insert into endosomal membranes of the host cell, facilitating membrane fusion. Figure adapted from reference [150].

A mouse model of RVFV infection demonstrated that RV-Gn1 was protective against disease **(Fig. 3.6)**. We administered a 'high' and a 'low' dose treatment of antibody, which was calculated from the PRNT assay to be approximately 10% of the neut100% (10 µg) and >neut100% (200 µg), respectively. This experiment did not resolve any additional effects that an antibody might have when used *in vivo,* such as antibody dependent cell cytotoxicity (ADCC) [192] or complement dependent cytotoxicity (CDC). Although the antibody effects *in vivo* would likely originate from the Fc region of the antibody, and these antibodies are not Fc-matched to the host, studies indicate that the mouse FcR is promiscuous and able to interact with rabbit Fc presented on the hybridoma-derived RV-Gn1 [193]. Perhaps as a result of this, the low dose group had an increased level of protection to the RVFV challenge (compared to the dose-matched neutralisation potential), indicating that the neutralisation potential may be an underestimate of the protective efficacy.

Our structural analysis provides a molecular rationale for the way in which RV-Gn1–3 targets and neutralises RVFV (**Fig. 3.9**). We sought to investigate the evolutionary selective pressures acting on RVFV Gn and worked with collaborators to perform a comparative analysis of non-synonymous to synonymous nucleotide substitution ratios (dN/dS), in order to identify regions of the Gn–Gc complex assembly that exhibit greater positive selection for amino acid change (i.e. higher dN/dS ratios)[150]. We therefore subdivided RVFV Gn into its structurally observed A, B, and β-ribbon domains and calculated dN/dS separately for each domain. This additional analysis indicates a significantly higher dN/dS ratio (0.135) for domain B [150], supporting the hypothesis that Gn domain B of the RVFV Gn–Gc complex is subject to the greatest level of immune-mediated selective pressure. Furthermore, the previous observation that this region of SFTSV Gn is also targeted by nAbs (**Fig. 3.12**) [76] suggests that domain B of the Gn may be an important region amongst phenuiviruses more generally. We note that amino acid diversification of this region, although slow, may also be facilitated by a greater level of structural plasticity in RVFV Gn domain B compared to other domains, as has been previously inferred in structural studies of the entire RVFV virion [69].

Despite the genetic, antigenic, and structural differences between the Gn of RVFV and SFTSV (**Fig. 3.12**), the isolation of a nAb from a human SFTSV survivor that targets a similarly-localised neutralising epitope on domain B of SFTSV Gn (**Fig. 3.12, D**) supports a common mechanism of neutralisation and is suggestive that this domain of the Gn may constitute a site of vulnerability for phenuiviruses more broadly. This hypothesis is supported by the evolutionary analysis of RVFV Gn–Gc, which reveals that amino acid diversification of domain B is greater than that of the rest of the Gn–Gc assembly and is likely subjected to a greater level of immune-mediated selective pressure compared to other regions. Interestingly, however, the overall rate of diversification of evolution in domain B (and Gn–Gc) is still

limited compared to other well characterised viruses, including HIV-1 [194], influenza virus [195], and HCV [196], suggesting that a multivalent vaccine, such as that being developed against influenza virus, may protect against immune escape in this region [197]. Given the analogous role of the Gn glycoprotein in protecting the Gc-resident fusion loops in hantaviruses [79], it will be of interest to determine whether this mechanism of neutralisation will also be observed amongst other families within the *Bunyavirales*.

The development of antiviral biologics has proven to be a highly effective strategy to protect against emerging viral pathogens [198]. Our study provides an initial benchmark for the derivation of highly potent therapeutic antibodies from immunisation or convalescent sera that can be used for the treatment or prevention of RVFV infection. Demonstration of the *in vivo* protective efficacy of our mAb, RV-Gn1, in animals, highlights the potential utility of RVFV-specific nAbs as prophylactics. By analogy with mAb cocktails developed against EBOV [199], we anticipate that the identification of nAbs specific to other spatially distinct epitopes on the surface of the RVFV Gn–Gc complex assembly will be an important consideration for the development of synergetic, non-competing combinations of anti-RVFV mAbs.

The elucidation of a neutralising region on the surface of phenuiviruses has important implications for the development of glycoprotein therapeutics. For example, a reverse vaccinology approach [200] that focuses on domain B of the Gn may benefit immunogen design efforts for pathogenic phenuiviruses for which there are no established vaccines, such as SFTSV or Toscana virus. Indeed, the development of such a protein subunit vaccine may also provide an attractive alternative to live-attenuated or inactivated RVFV vaccines, such as MP-12 and Smithburn vaccine, respectively [201], by immunofocusing the antibody response to a vulnerable region of the virion.

Chapter 4

Structural analysis of the non-neutralising antibody response to RVFV

Chapter 4: Structural analysis of the non-neutralising antibody response to RVFV

4.1 Preface

This chapter describes the functional and structural characterisation of two non- neutralising antibodies generated from the rabbit RVFV Gn immunisation described in Chapter 3. Full length antibodies were produced by Dr Stefanie Krum (Doores lab KCL) and ELISAs were performed using glycoprotein produced as described in this thesis.

4.2 Summary of Findings

In this chapter, I sought to characterise epitopes on RVFV Gn which are targeted by non-neutralising antibodies. Combined with knowledge of neutralising epitopes, elucidating regions of the molecule that do not effectively mediate virus neutralisation, these data are important for the rational design of recombinant immunogens. As described in Chapter 3, several Gn-specific rabbit monoclonal Abs (mAbs) were isolated following immunisation of rabbits with a soluble ectodomain portion of RVFV Gn. Two of these mAbs were non-neutralising against live RVFV, *in vitro*. These two antibodies, termed mAb RV-Gn4 and mAb RV-Gn5, were subjected to structural and functional analysis. RV-Gn4 and RV-Gn5 bind two distinct but overlapping epitopes on domain A of RVFV Gn. Intriguingly, this region of the molecule has been a target of neutralising mAbs in a recent structural study by Wang *et al* [191]. Interestingly, mAb RV-Gn4 binds a conformation of RVFV Gn not observed in previous structural studies. To assess the physiological relevance of this novel conformational state of RVFV Gn, and to assess whether the observed epitope is presented in the context of native virions, we subjected mAb RV-Gn4 to a virus pull down assay. To this end, we found that mAb RV-Gn4 bound mature RVFV virions, suggestive that this conformational state is achieved in this context. Combined with cryo-EM studies, these data support a model whereby the observed

RVFV Gn conformation may represent a state natively presented on the native virion surface [69]. In line with previous studies that demonstrate the importance of virus-recognising non-neutralising antibodies in conferring protection [202], this work provides a framework for future *in vivo* investigations that will assess the efficacy of non-neutralising antiviral mAbs in animal models.

4.3 Results

4.3.1 Recombinant mAbs RV-Gn4–7 do not neutralise RVFV *in vitro*

We sought to further characterise the mode of interaction for representative non-neutralising antibodies, chosen based upon genetic diversity of the CDR_{H3} and CDR_{L3} regions **(Table 4.1),** termed RV-Gn4–7. Initial Fab screening indicated that Fabs RV-Gn4–7 were not neutralising. To confirm this result was consistent for the mAbs, mAbs 4–7 (recombinant IgGs) were assessed for neutralisation potency using an *in vitro* PRNT (Plaque Reduction Neutralisation Test) assay. Full-length mAbs (produced by Dr Stefanie Krumm) were tested for neutralisation potency by a PRNT assay. Neutralisation testing revealed no difference in plaque numbers when incubated with a dilution series of antibody (5 ng–100 μg/ml), confirming the results of the Fab neutralisation experiments.

Table 4.1. Analysis of germline and CDR3 loops of non-neutralising antibody heavy and light chains.

HC	V	mutation (%)	J	mutation (%)	D	CDRH3
RV-Gn4	1S69*01	90.58%	J2*01	70.00%	8-1*01	CVRIMAGGCNSW
RV-Gn5	1S69*01	92.75%	J4*01	72.92%	1-1*01	CGRAPYSRHVGYYICASLW
RV-Gn6	1S69*01	93.12%	J4*01	75.00%	7-1*01	CVRDAGYSDYSLGLW
RV-Gn7	1S44*01	89.25%	J5*01	80.39%	6-1*01	CARGGATYSSDGYALDYLDVW

LC	V	% mutation	D	% mutation	CDRL3
RV-Gn4	1S2*01	90.43%	1-2*02	81.08%	CQGSDYGSGWYFTF
RV-Gn5	1S19*01	93.97%	1-2*02	86.11%	CLGGFDDDADNAF
RV-Gn6	1S36*01	90.22%	1-2*02	72.50%	CQCSEFGIYYLGGF
RV-Gn7	1S15*01	91.13%	1-2*02	82.50%	CLGGYHTSTTDTTF

Germline assignments and percentage mutation from the germlines were calculated using Ig BLAST server [175] and the IMGT-V-quest tool [176]

4.3.2 Fabs RV-Gn4–7 form stable complexes with RVFV Gn

We first characterised mAb binding to recombinant RVFV Gn by ELISA (performed by Dr Stefanie Krum, KCL). Plates were coated with RVFV GnL (produced and defined as described in **Chapter 3**) and then incubated with a dilution series of mAb. ELISA data show high affinity of binding of mAbs RV-Gn4,5 and 7 (binding analysis of mAb RV-Gn6 is pending) **(Fig. 4.1)**. The relative binding affinity of RV-Gn4 appeared lower than that of RV-Gn5 and RV-Gn7.

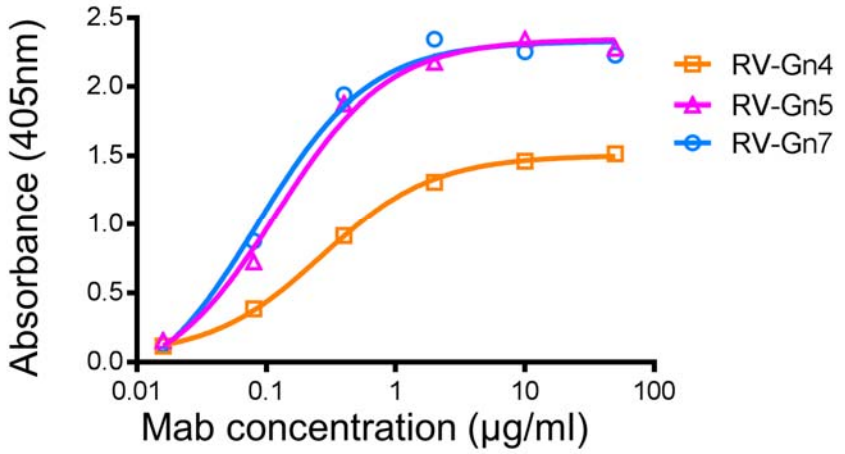

Figure 4.1 mAbs RV-Gn4, RV-Gn5 and RV-Gn7 bind to RVFV Gn.
A dilution series of purified RV-Gn4, 5 and 7 was prepared to probe binding to recombinant RVFV GnL. Curves were fit using GraphPad Prism. Approximate IC50 values are 270 ng/ml, 120 ng/ml and, 90 ng/ml for RV-Gn4, RV-Gn5 and RV-Gn7 respectively. RV-Gn6 binding data is pending. ELISA performed by Dr Stefanie Krum (one experiment), detected with anti-rabbit HRP.

Since the mAbs bound with high affinity, I next tested whether they formed stable complexes with the construct of RVFV Gn identified to be amenable for crystallogenesis (termed GnX, defined in **Fig. 3.7**) [69]. Fab fragments and RVFV GnX were produced, as described in **Chapter 3,** section **3.3.7** and **3.3.8)**. Fabs RV-Gn4, RV-Gn5, and RV-Gn6 (RV-Gn7 was omitted at this stage due to insufficient purification yield) were incubated with RVFV GnX for 1–2 h at RT. Complexes were concentrated and applied to a Superdex 200 Increase 10/30 column for size exclusion chromatography (SEC). SEC revealed stable complex formation for Fabs RV-Gn4, RV-Gn5, and RV-Gn6 Fabs, as indicated by an elution volume in line with the apparent molecular mass (**Fig. 4.2**). All three Fab–Gn complexes were subjected to crystallisation screening, two of which yielded crystals.

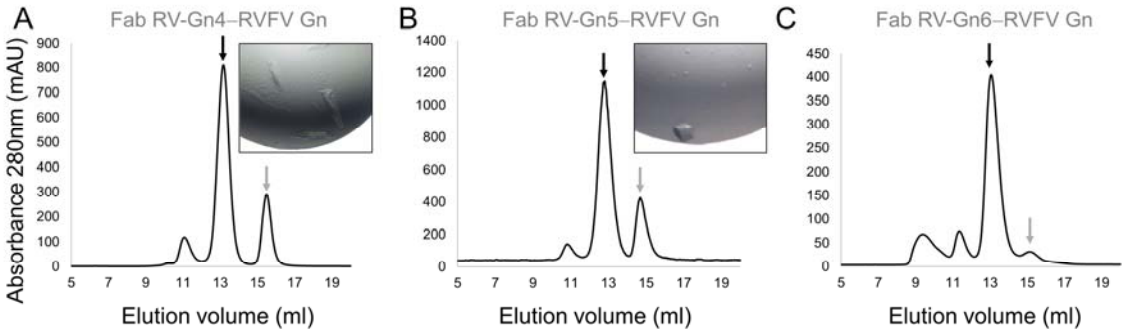

Figure 4.2. Complex formation and crystallogenesis of non-neutralising antibody-RVFV-Gn complexes.
(A) RV-Gn4 complex was purified by size exclusion chromatography, (complex indicated by black arrow, excess Fab indicated by grey arrow) and crystals (inset) formed in a drop containing 0.1 M amino acids (Glu, Ala, Gly, Lys, Ser) 0.1 M (Tris/bicine) pH 8.5, 37.5 % (MPD, PEG 1000, PEG 3350). **(B)** RV-Gn5 complex was purified by size exclusion chromatography (inset) and crystals formed in a drop containing condition containing 0.5 % v/v Jeffamine ED-2001 reagent, 0.1 M HEPES, 1.1 M Sodium Malonate, pH 7.0. **(C)** RV-Gn6 complex was purified by size exclusion chromatography. Crystal screens yielded no diffracting crystals.

4.3.3 Structure determination Fab RV-Gn5–RVFV Gn

4.3.3.1 Crystallisation of the Fab RV-Gn5–RVFV Gn complex

The SEC-purified Fab RV-Gn5–RVFV Gn complex was concentrated to 6.8 mg/ml and subjected to crystallisation screening using the vapour diffusion method. After 280 days, a crystal was observed in a condition containing 0.5 %v/v jeffamine ED-2001 reagent, 0.1 M HEPES, 1.1 M sodium malonate, pH 7.0 **(Fig 4.2, B)**. The crystal was cryoprotected in the mother liquor supplemented with 25% glycerol, and flash-cooled in liquid nitrogen. X-ray diffraction data were collected at beamline I03 at Diamond Light Source (Didcot, UK) on a Pilatus 6MF detector (Dectris). Data were indexed, integrated and scaled with Xia2 [161].

4.3.3.2 Phasing and refinement of Fab RV-Gn5 in complex with RVFV Gn

The RV-Gn5–RVFV Gn structure was solved by molecular replacement with PHASER, using a Fab fragment (PDB 4J02) and truncated RVFV Gn (PDB 6F8P, lacking domain B) as search models [69, 184, 203]. Iterative rounds of model building and refinement were performed using

Refmac5 [185], in the CCP4 suite, with global non-crystallographic symmetry (NCS) restraints (two copies present in the a.s.u. and real-space refinement performed in COOT [163]. The final refined structure was validated with MolProbity [186]. Data collection and structure refinement statistics are presented in **Table 4.2**.

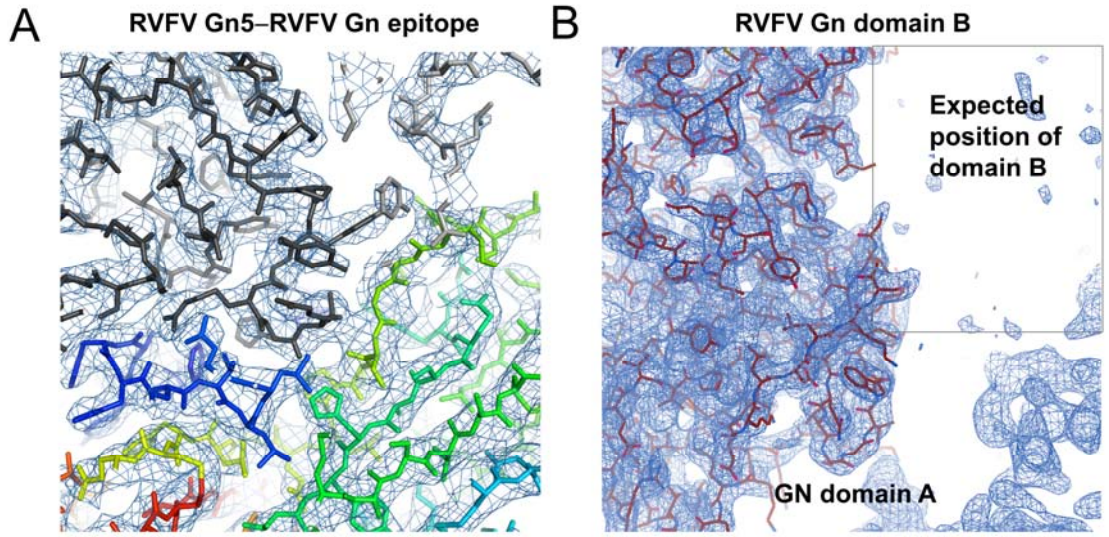

Figure 4.3 Electron density of the RV-Gn5-Gn complex.
(A) Electron density at the RV-Gn5–RVFV Gn interface. A 2Fo-Fc map (blue mesh) is displayed, contoured at 1.0 σ with the model shown as sticks. RVFV Gn is coloured in rainbow, from N- to C-terminus, RV-Gn5 HC in dark grey and LC in light grey. **(B)** Electron density at the expected position of RVFV Gn domain B. A 2Fo-Fc map and model are shown as in A. RVFV Gn is coloured in red. No density is observed in for domain B although there is sufficient space in the a.s.u to accommodate the domain, (boxed area).

Table 4.2. Crystallographic data processing and refinement statistics for RVFV Gn–RV-Gn5.

	RVFV Gn–RV-Gn5
Data collection statistics	
Beamline	Diamond I03
Space group	*P 4 21 2*
Cell dimensions	
a, *b*, *c* (Å)	166.1, 166.1, 145.4
α, β, γ (°)	90 90 90
Resolution range (Å)	51.6–3.1 (3.2–3.1) [a]
R_{merge}	0.27 (>1)
I/σ I	9.9 (1.4)
$CC_{1/2}$	1 (0.6)
Completeness (%)	99.9 (100)
Redundancy	13.2 (13.1)
Refinement statistics	
Resolution (Å)	51.6–3.1 (3.2–3.1)
No. reflections	37,134
R_{work} / R_{free} [b] (%)	21.1 /24.4
No. atoms	
Protein	9,513
Ligand/ion	n/a
Water	n/a
B-factors	
Protein	89.2
Ligand/ion	n/a
Water	n/a
R.m.s. deviations[c]	
Bond lengths(Å)	0.013
Bond angles (°)	1.83
Ramachandran analysis[d]	
Residues in favoured region (%)	95.8
Residues in allowed region (%)	4.2

[a]Numbers in parentheses refer to the relevant outer resolution shell.
[b]R_{free} is calculated as for R_{work}, but using only 5% of the data which were sequestered prior to refinement.
[c]r.m.s. deviations: root mean square deviation from ideal geometry.
[d]Determined using the MolProbity server [186].

4.3.3.3 Structural analysis

4.3.3.3.1 Structural overview

The crystal structure of Fab RV-Gn5–RVFV Gn comprises two copies of the Fab–Gn complex in the asymmetric unit. In both copies, all Fab residues were resolved, whereas for RVFV Gn only residues 193–363 and 441–469 were resolved. There lacked clear density for residues from the N termini (residues 154–193) and domain B (residues 364–440) (**Fig. 4.3**). The two molecules in the asymmetric unit exhibited identical modes of antibody recognition, (0.64 Å RMSD over equivalent 626 Cα positions).

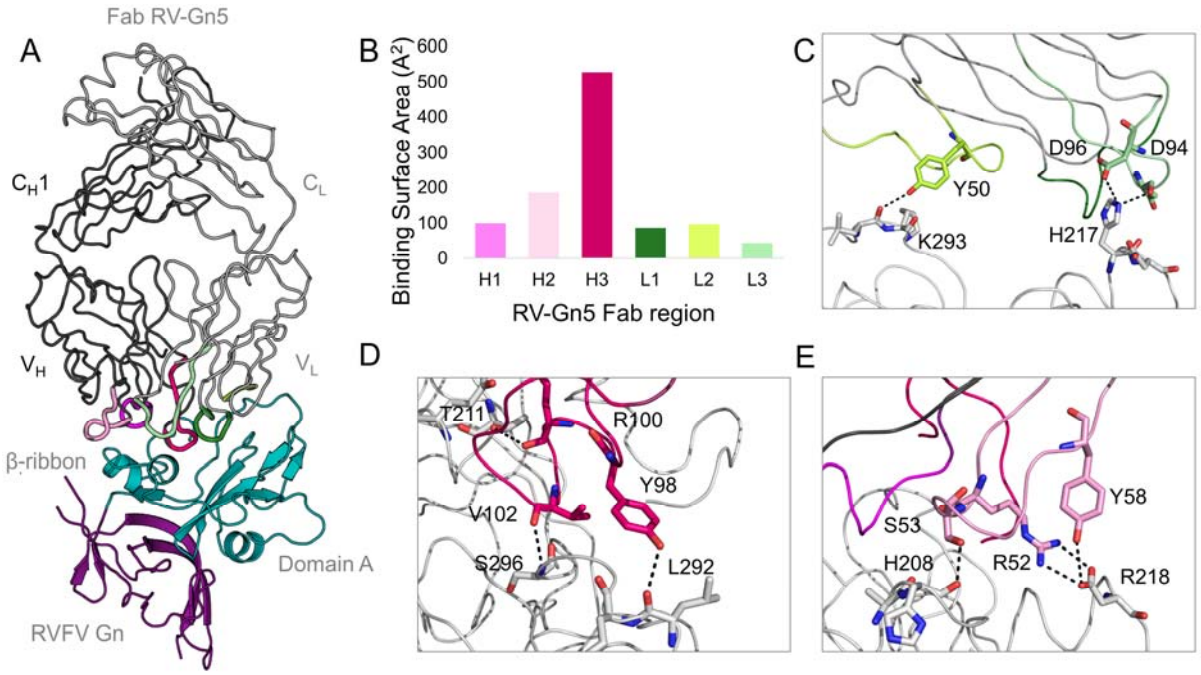

Figure 4.4 The crystal structure of RV-Gn5 bound to RVFV Gn.

(A) Crystal structure of RV-Gn5 bound to RVFV Gn. V_H, V_L, C_H1, and C_L denote the antibody variable heavy, variable light, constant heavy 1, and constant light chain domains, respectively. Complementarity-determining regions (CDRs) contributing to RVFV recognition are coloured pink (heavy chain) and green (light chain). Domain A is shown in teal, and the β-ribbon is shown in purple. **(B)** RV-Gn1 recognises RVFV Gn predominantly through the CDR loops of the heavy chain. CDR loop usage by RV-Gn5 in the RVFV Gn complex is shown as a buried surface area (Å^2), calculated using the PISA EBI server [187]. **(C)** Interactions between the RV-Gn5 V_L residues and the corresponding residues of Gn. **(D and E)** Interactions between the RV-Gn5 V_H residues and the corresponding residues of Gn**.** Dotted lines mark the model predicted hydrogen bonds.

4.3.3.3.2 The Fab RV-Gn5–RVFV Gn epitope

Fab RV-Gn5 recognises domain A of RVFV Gn at an interface that occludes approximately 925 $Å^2$ of the protein surface (as determined by the PDB-ePISA server [187, 188]). Each CDR loop of the heavy and light chain contributes to antigen recognition. The highest proportion of binding is attributed to the CDR3 loop of the heavy chain, which utilises eight residues to make contact with RVFV Gn. The heavy chain also contributes the most hydrogen bonds to the binding interface, specifically: $Thr211^{Gn}$–$Arg99^{HC}$, $Ser296^{Gn}$–$Val100A^{HC}$, $Ala207^{Gn}$–$Arg99^{HC}$, $His208^{Gn}$–$Ser53^{HC}$, $His209^{Gn}$–$Arg99^{HC}$, $Glu214^{Gn}$–$Arg99^{HC}$, $Asp218^{Gn}$–$Arg52^{HC}$, $Asp218^{Gn}$–$Tyr58^{HC}$ and $Leu292^{Gn}$–$Tyr97^{HC}$. Six salt-bridges form between the HC Arg52 and Arg99 and with the Gn Glu214. The HC paratope consists of CDR_{H1}: residues 26– 33, CDR_{H2}: residues 52–58, and CDR_{H3}: residues 97–100D. The epitope contacted by the heavy chain consists of 25 RVFV Gn residues: Val193, Leu195, Lys 197, Phe200, Phe203, Gln204, Ala207, His208, His209, Arg210, Thr211, Leu213, Glu214, His217, Asp218, Tyr 254, His258, Leu 292, Lys293, Lys294, Gly295, Ser296, Tyr297, Pro298, and Gly441.

The light chain recognises eight residues on RVFV Gn: Leu213, Val216, His217, Asp218, Lys223, Leu292, Lys293, Lys294, Gly295. Of these contacts, four are hydrogen bonds: $Leu292^{Gn}$–$Tyr49^{LC}$, $Lys293^{Gn}$–$Asp95^{LC}$, $His217^{Gn}$–$Asp95^{LC}$, $His217^{Gn}$–$Asp95^{LC}$, and one salt-bridge between $His217^{Gn}$–$Asp95^{LC}$. CDR_{L1} residues 30, 30A, CDR_{L2} residues 49–56, and CDR_{L3} residues 92–95 are involved in the binding interface.

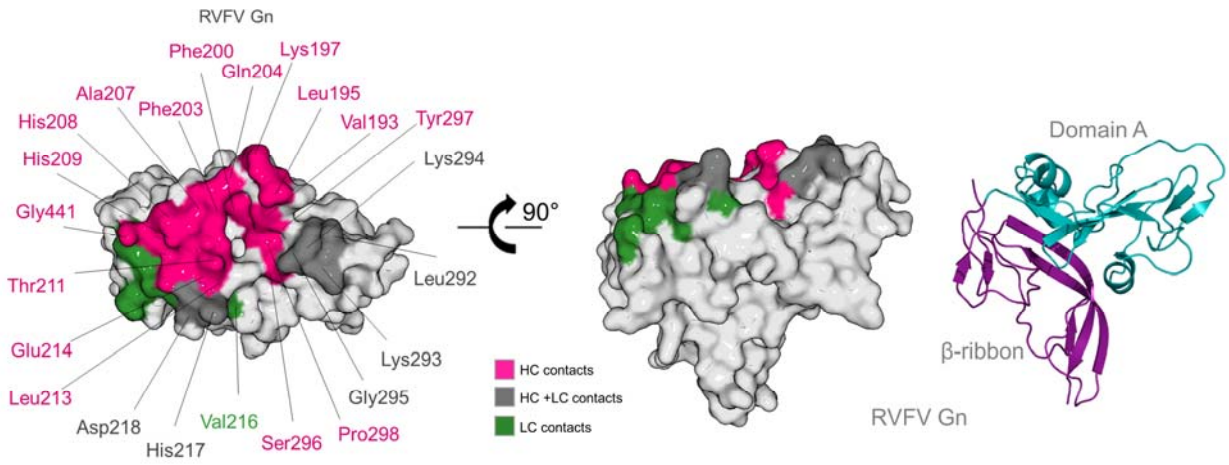

Figure 4.5 Analysis of the epitope footprints of RV-Gn5.
RVFV Gn is shown as a white surface. Residues contacted by the LC are coloured in green, residues contacted by the HC are coloured in pink and residues contacted by both chains are coloured in grey. Epitope contacts were analysed using the PDB-ePISA server. RVFV Gn is also shown in cartoon representation (right) with domains revealed in the complex crystal structure coloured in purple (β ribbon) and teal (domain A).

4.3.4 Structure determination of Fab RV-Gn4 in complex with RVFV Gn

4.3.4.1 Crystallisation of the Fab RV-Gn4–RVFV Gn complex

The SEC-purified Fab RV-Gn4–Gn complex was concentrated to 8.6 mg/ml and subjected to crystal screening using the vapour diffusion method. After 24 hrs, crystals formed in several conditions. Diffraction data suitable for structure determination were collected from crystals formed in a condition containing: a mixture of MPD, PEG 1000, PEG 3350 (37.5 %), 0.1 M amino acids (Glu, Ala, Gly, Lys, Ser), 0.1 M (Tris/bicine) pH 8.5, and 6% 1,6-hexanediol. Crystals were flash-cooled in liquid nitrogen. X-ray diffraction data for Fab RV-Gn4–RVFV Gn were collected at beamline I04 at Diamond Light Source (Didcot, UK) on a Pilatus 6MF detector (Dectris). Data were indexed, integrated and scaled using XIA2 [161].

4.3.4.2 Phasing and refinement of the Fab RV-Gn4–RVFV Gn complex

Several datasets were collected, and their corresponding structures were solved by molecular replacement with PHASER, using Fab fragment (PDB 4J02) and truncated RVFV Gn (PDB

6F8P, lacking domain B) as search models [69, 184, 203]. Unrefined electron density maps were assessed for the presence of domain B and, the highest resolution dataset that exhibited the best overall electron density for the complex, with particular attention to domain B of RVFV Gn was selected for further refinement **(Fig. 4.6)**. Iterative rounds of model building and refinement were performed using Refmac5 [185], in the CCP4 suite, with global NCS restraints (two copies present in the a.s.u.) and real-space refinement performed in COOT [163]. The final refined structure was validated with MolProbity [186]. Data collection and refinement statistics are presented in **Table 4.3**.

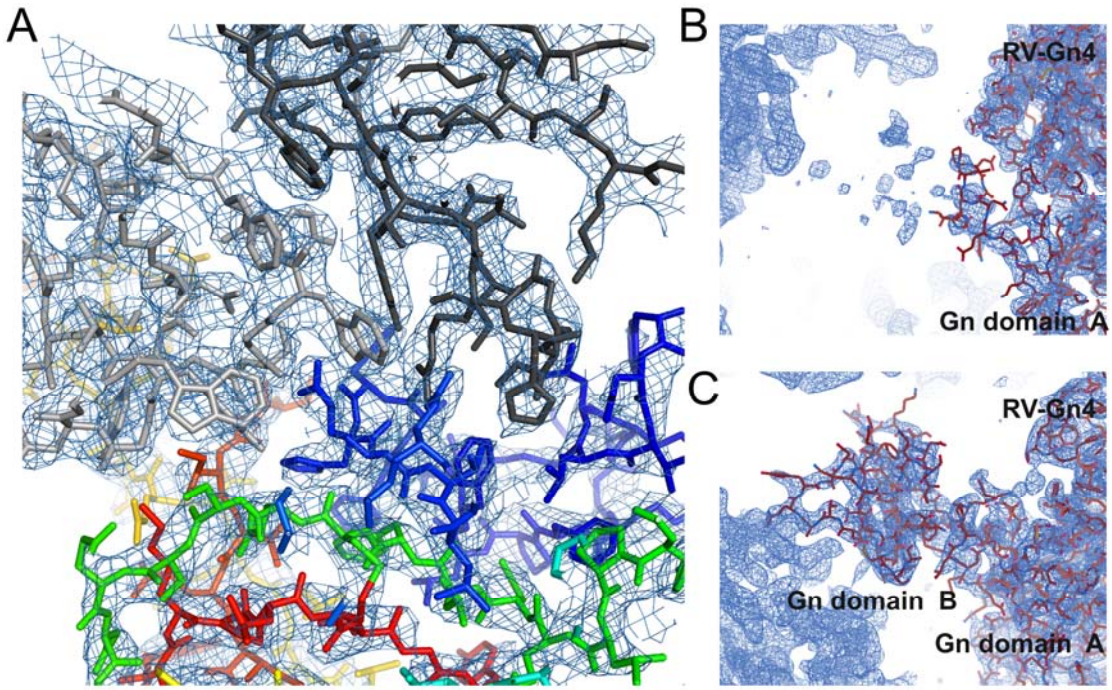

Figure 4.6 Electron density of RV-Gn4 complex with RVFV Gn.
(A) Electron density at the RV-Gn4–RVFV Gn interface. A 2Fo-Fc map (blue mesh) is displayed, contoured at 1.0 σ with the model shown as sticks. Gn is coloured in rainbow, RV-Gn4 HC in dark grey and LC in light grey. **(B** and **C)** Electron density of RVFV Gn domain B. Gn is coloured in red. **(B)** Gn domain has some incomplete density in chain C, that did not improve upon attempts to place domain B. **(C)** Chain D has complete domain B density and a newly observed confirmation of this domain could be placed.

Table 4.3. Crystallographic data processing and refinement statistics for RVFV Gn–RV-Gn4.

	RVFV Gn–RV-Gn4
Data collection statistics	
Beamline	Diamond I04
Space group	*P 21 21 2*
Cell dimensions	
a, *b*, *c* (Å)	102.1, 263.9, 71.4
α, β, γ (°)	90, 90, 90
Resolution range (Å)	71.4 – 2.9 (3.0 – 2.9) [a]
R_{merge}	0.32 (>1)
I/σ I	9.74 (1.1)
$CC_{1/2}$	1.0 (0.5)
Completeness (%)	99.9 (99.8)
Redundancy	19.9 (20.4)
Refinement statistics	
Resolution (Å)	71.4–2.9 (3.0–2.9)
No. reflections	43,775
R_{work} / R_{free} [b] (%)	21.0/24.5
No. atoms	
Protein	10,061
Ligand/ion	n/a
Water	n/a
B-factors	
Protein	82.9
Ligand/ion	n/a
Water	n/a
R.m.s. deviations[c]	
Bond lengths(Å)	0.013
Bond angles (°)	1.9
Ramachandran analysis[d]	
Residues in favoured region (%)	95.6
Residues in allowed region (%)	4.3
Residues in disallowed region (%)	0.01

[a]Numbers in parentheses refer to the relevant outer resolution shell.
[b]R_{free} is calculated as for R_{work}, but using only 5% of the data which were sequestered prior to refinement.
[c]r.m.s. deviations: root mean square deviation from ideal geometry.
[d]Determined using the MolProbity server [186].

4.3.4.3 Structural analysis

4.3.4.3.1 Structural overview of the Fab RV-Gn4–RVFV Gn complex

Similar to the Fab RVGn5–Gn complex, density was missing for the domain B of RVFV Gn in many of the datasets collected. Indeed, in the dataset presented here, electron density corresponding to domain B was observed for only one of the two copies in the asymmetric unit (chain D), with only partial density observed in the other (chain C). Furthermore, residues 191–376 and 393–469 were resolved in chain D and residues 191–371 and 436–469 were resolved in chain C (lacking domain B). Indeed, molecular replacement failed to locate domain B as a single unit separate from the rest of RVFV Gn in chain C. Map improvement strategies, such as solvent flattening, and density modification had no effect, indicative that domain B in chain C may be naturally flexible in the crystal [204]. A crystal contact between RVFV Gn domain B, residue Gln428 and the neighbouring chain C (Gn residues Thr278 and Cys250), likely rationalises why domain B of chain D was visualised. Aside from these differences in the Gn, the two copies observed in the asymmetric unit exhibit near identical Fab recognition modes (RMSD of 0.49 Å, over 645 equivalent Cα residues), where only minor differences were observed in solvent-exposed loops.

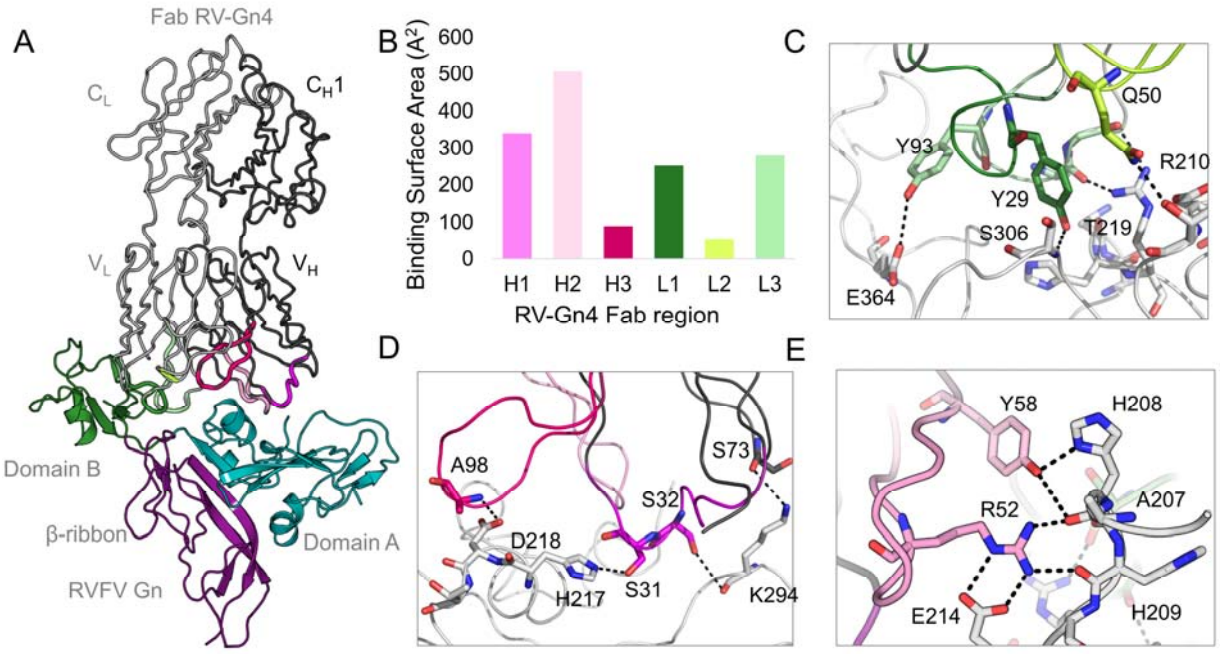

Figure 4.7 The crystal structure of RV-Gn4 bound to RVFV Gn.
(A) Crystal structure of RV-Gn4 bound to RVFV Gn. V_H, V_L, C_H1, and C_L denote the antibody variable heavy, variable light, constant heavy 1, and constant light chain domains, respectively. Complementarity-determining regions (CDRs) contributing to RVFV recognition are coloured pink (HC) and green (LC). Domain A is shown in teal, domain B is shown in green and the β-ribbon is shown in purple. **(B)** RV-Gn1 recognises RVFV Gn predominantly through the CDR loops of the heavy chain. CDR loop usage by RV-Gn4 in the RVFV Gn complex is shown as a buried surface area ($Å^2$) and was calculated using the PISA EBI server [187]. **(C)** Interactions between the RV-Gn4 V_L residues and the corresponding residues of Gn. **(D** and **E)** Interactions between the RV-Gn4 V_H residues and the corresponding residues of Gn. Dotted lines mark the model predicted hydrogen bonds.

4.3.4.3.2 The Fab RV-Gn4–RVFV Gn epitope

Fab RV-Gn4 recognises domain A of RVFV Gn with an interface that occludes approximately 950 $Å^2$ of solvent accessible surface area. Whilst each CDR loop from both the heavy and the light chain contribute to antibody binding, the HC dominates the interaction, forming ten hydrogen bonds and six salt bridges. The LC interactions contribute six hydrogen bonds and one salt bridge **(Fig. 4.7)**.

The hydrogen bonding network utilised by the heavy chain consists of $His217^{Gn}$–$Ser31^{HC}$, $His208^{Gn}$–$Tyr58^{HC}$, $Lys294^{Gn}$–$Ser73^{HC}$, $Ala207^{Gn}$–$Arg52^{HC}$, $Ala207^{Gn}$–$Tyr58^{HC}$,

His209^{Gn}–Arg52^{HC}, Glu214^{Gn}–Arg52^{HC}, Asp218^{Gn}–Ala97^{HC} and Lys294^{Gn}–Ser30^{HC}. The six observed salt bridges occur between residue Glu214 of the Gn and residues Arg52 and His53 of CDR_{H2}. In addition to hydrogen bonds and salt bridges, contacts are established with van der Waals forces. The heavy chain paratope consists of CDR_{H1} residues 28–33, CDR_{H2} residues 52–58, and CDR_{H3} residues 95–98. The Gn residues contacted by the heavy chain are Phe191, Asp192, Leu194, Leu195, Phe203, Ala207, His208, His209, Arg210, Thr211, Leu213, Glu214, His217, Asp218, Thr219, Lys294, Gly295, Ser296 **(Fig. 4.8)**.

Hydrogen bonds arising from Fab RVGn-4 light chain interactions are: Ser306^{Gn}–Try30^{LC}, Thr219^{Gn}–Gln50^{LC}, Asn364^{Gn}–Tyr93^{LC}, Arg210^{Gn}–Ser95^{LC}, Arg210^{Gn}–Ser95A^{LC}, Asp218^{Gn}–Gln50^{LC}. Additional van de Waals contacts are made from each CDR loop, CDR_{L1} contacts with residues 26–32, CDR_{L2} with 49–50 and 53, and CDR_{L3} with residues 92–96. The epitope contacts established by the light chain are Ala207, His208, His209, Arg210, Glu214, Asp218, Thr219, Ile220, Gln305, Ser306, Ser307, Glu308, Glu364, Asn366, Leu368, Pro369, Asp370, Ser400, Lys404, Ser440, Gly441, Ile442, Lys453.

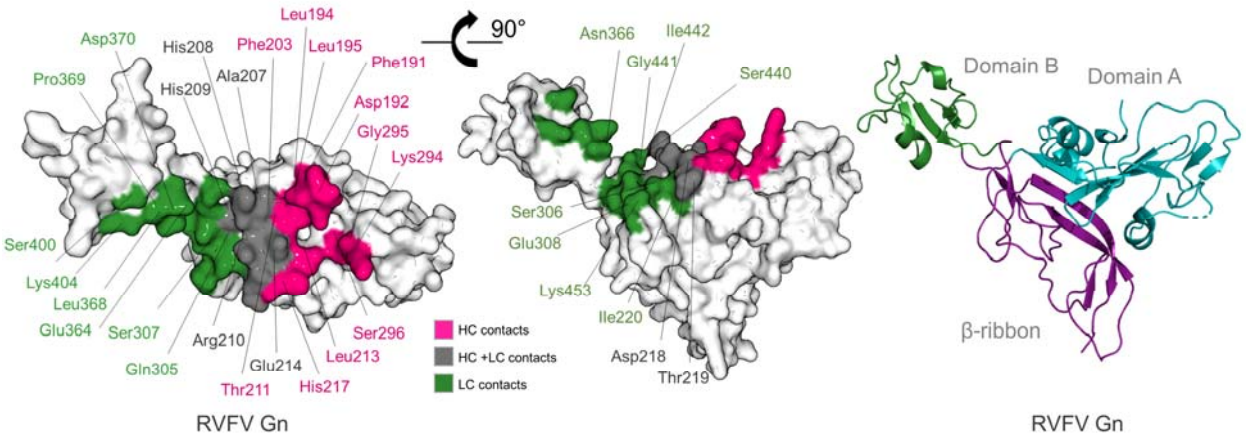

Figure 4.8 Analysis of the epitope footprint of RV-Gn4
Gn is represented in both surface (left) and cartoon representations (right). Residues contacted by the LC are coloured in green, residues contacted by the HC are coloured in pink and residues contacted by both chains are coloured in grey. The cartoon representation of RVFV Gn coloured by domain; the β ribbon is purple, domain A is teal, and domain B is green.

4.3.4.3.3 Structures of RV-Gn4 and RVFV-Gn5 complexes reveal a novel conformation of RVFV Gn

Structure overlay analysis has demonstrated few differences between unbound and nAb-bound states of RVFV Gn [150, 191]. However, comparison of these structures with RVFV Gn in Fab RV-Gn4 and RV-Gn5-bound states reveals that the glycoprotein undergoes a dramatic conformational rearrangement upon recognition of these non-neutralising mAbs (**Fig. 4.7, 4.8** and **4.9**). Interestingly, residues that are occluded within the fold of the previously defined structures of RVFV Gn become accessible and are recognised by both mAb RV-Gn4 and RV-Gn5. Indeed, these epitopes lie beneath N terminal residues of RVFV Gn (residues 154–193), as presented in its unbound form. In both Fab RV-Gn4 and RV-Gn5-bound crystals (**Fig. 4.9**), the orientation of these N-terminal residues is altered, where they are directed into solvent cavities of the crystal and are disordered.

Furthermore, domain B also undergoes a substantial movement to accommodate RV-Gn5 binding, where a hinge-like motion occurring at the domain boundaries of domain B and the β-ribbon (residues Glu364 and Ser441) results in an approximately 60° change in orientation. Given that this domain was observed to be disordered in several of the asymmetric units in RV-Gn4 and RV-Gn5-bound structures, it is likely that crystal contacts stabilise an otherwise dynamic state of domain B formed upon mAb recognition. Additionally, given the amount of time required to crystallise RVFV Gn in the unbound state (>298 days [205]), combined with cryo-EM observations derived from study of the entire Gn–Gc lattice, it is possible that domain B is flexible in the context of the mature virion. Indeed, consistent with the proposed assembly model of RVFV Gn and Gc [205], which suggests that domain B moves to unsheathe hydrophobic fusion loops presented by the cognate Gc during viral fusion, it is possible that domain B flexibility, observed in the crystallographic studies herein, may be physiologically relevant in the context of native virus functionality.

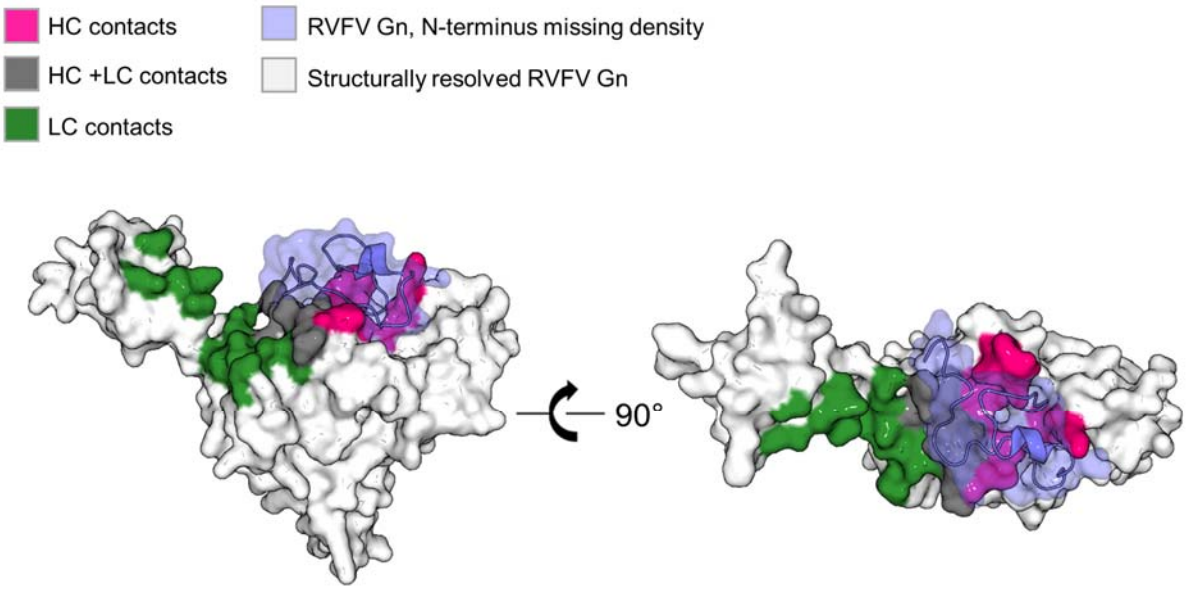

Figure 4.9 Structural rearrangements in RVFV Gn N terminus must occur to allow binding of RV-Gn4.
RVFV Gn (conformation observed in complex with Rv-Gn4) is displayed as a white surface, with the Rv-Gn4 epitope depicted in green (LC contacts), pink (HC contacts) and grey (contacted by both HC and LC). Superposition of the native Gn N terminus (PDB: 6F8P) is displayed as transparent marine surface with cartoon.

4.3.5 mAb RV-Gn4 and mAb RV-Gn5 target a region that is spatially distinct from the neutralising epitope of mAb RV-Gn1

Sequence alignment of RV-Gn4 and RV-Gn5 reveals 77–80% identity across the variable regions, values which are comparable to the similarity between RV-Gn4 or RV-Gn5 with RV-Gn1 **(Fig 4.10)**. However, while RV-Gn4 and RV-Gn5 exhibit distinct modes of recognition to RVFV Gn domain A, approximately 50% of the epitope residues are shared (**Fig 4.11)**.

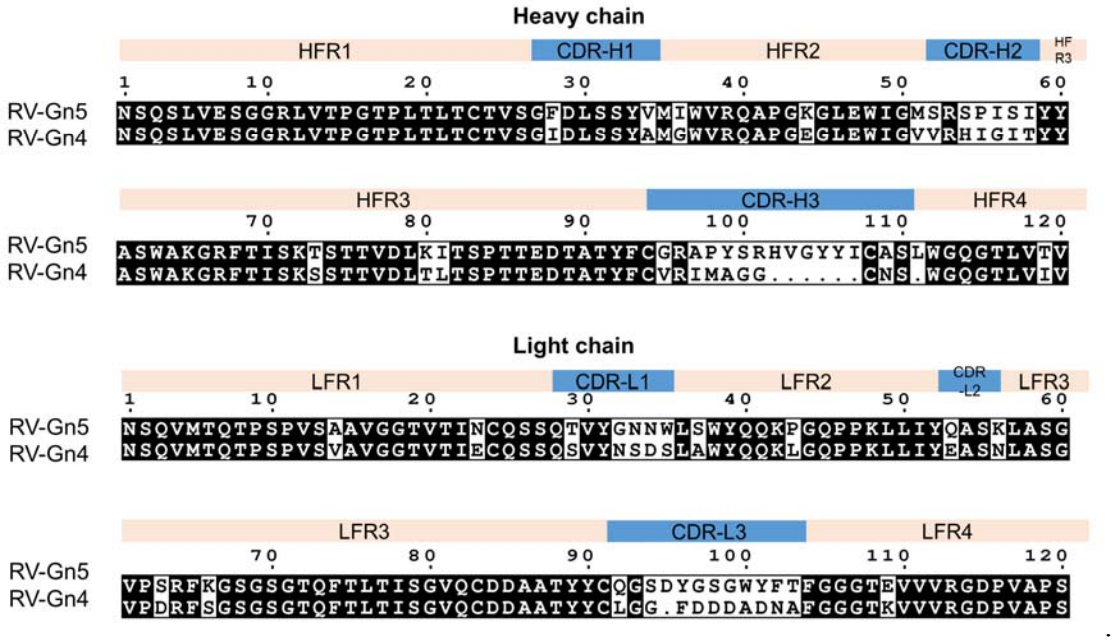

Figure 4.10 Heavy and light chain sequence alignment of the variable regions of RV-Gn4 and RV-Gn5
The sequence alignment was determined by Clustal Omega [179] and plotted with ESPRIPT [180].

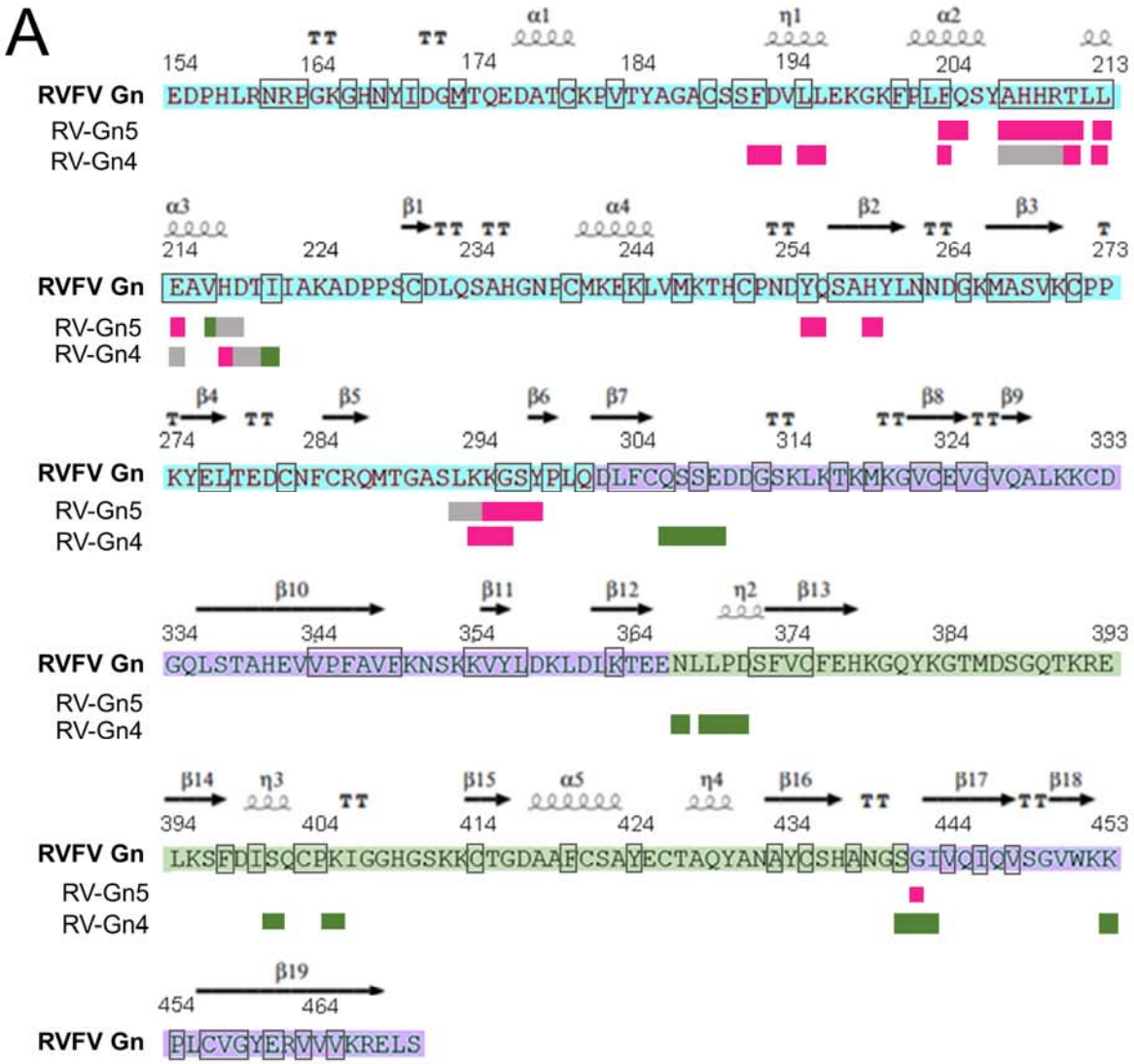

Figure 4.11 Comparative analysis of the RV-Gn4 and RV-Gn5 epitopes

(A) RVFV Gn ectodomain sequence is displayed and coloured according to domain, Domain A is shown in teal, domain B is shown in green and the β-ribbon is shown in purple. Black squares around residues indicate buried surfaces. Coloured squares below the sequence mark residues forming contacts with either RV-Gn5 (upper) or RV-Gn4 (lower). Residues contacted by the heavy (V_H) chain and light chain (V_L) are shown in pink and green, respectively. Residues contacted by both chains are shown in grey. **(B)** Complex crystal structures of RV-Gn5 (left) and RV-Gn4 (right) bound to RVFV Gn. Coloured as is **Fig 4.7**.

Epitope comparison reveals that RV-Gn4 and RV-Gn5 bind to a distinct domain of RVFV Gn, when compared to RV-Gn1 (domains A and B, respectively). Indeed, even when accounting for the extended conformation of domain B observed in the Fab RV-Gn4–RVFV Gn complex both antibodies Fab fragments can be modelled onto RVFV Gn without any steric hindrance (**Fig. 4.12**). Consistent with the structure-based hypothesis of non-competing modes of Fab recognition, complex formation and SEC analysis reveals the stable formation of a ternary Fab RV-Gn1 – Fab RV-Gn4 – RVFV Gn complex (**Fig. 4.12)**.

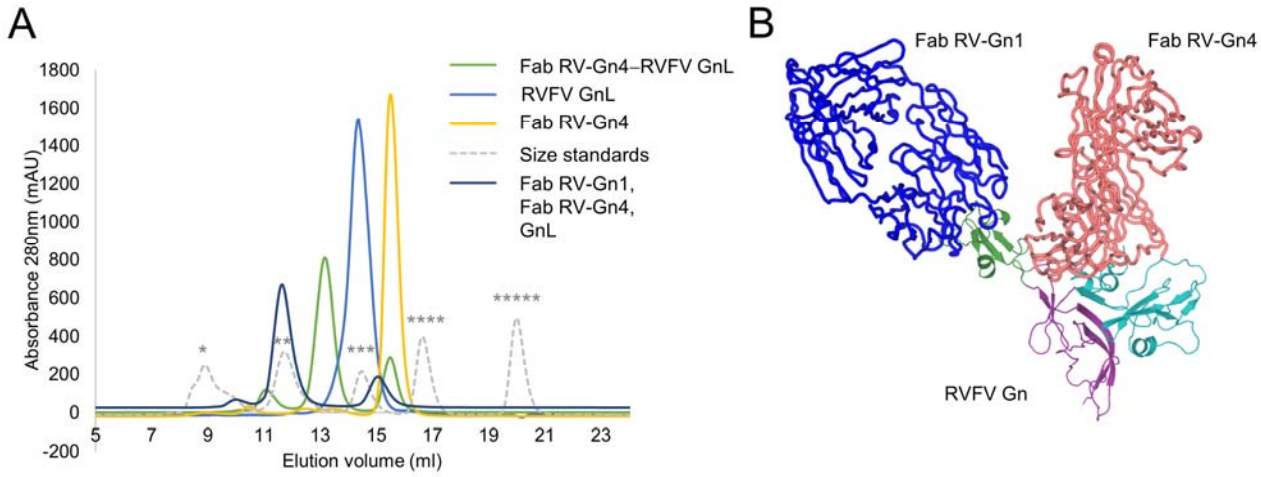

Figure 4.12 RV-Gn1 and RV-Gn4 can simultaneously bind RVFV Gn.
(A) RV-Gn1, RV-Gn4 and GnL were mixed and binding was assessed using size exclusion chromatography (shown in dark blue). This mix of three components appeared to form a ternary complex, eluting consistent with a size standard marker of 158 kDa; the expected mass of two Fabs and one Gn is ~135kDa. Size exclusion profiles of GnL (light blue), RV-Gn4 (yellow) and a complex of one Fab RV-Gn4- GnL (green) are displayed for comparison. Size standards are shown in grey dashed line and are marked with asterisks, corresponding to: *670kDa, **158kDa, ***44kDa, ****17kDa, ****1.4kDa. **(B)** Model of two Fab bound to Gn. RV-Gn1-Gn (structure described in Chapter 3) was docked onto RV-Gn4-Gn structure. The model for simultaneous binding revealed no steric hindrance. Gn shown in cartoon and coloured by domain. Domain A is shown in teal, domain B is shown in green and the β-ribbon is shown in purple. RV-Gn4 is shown as pink ribbon, and RV-Gn1 in marine ribbon.

4.3.6 mAb RV-Gn4 and mAb RV-Gn5 displace the N-terminal epitope targeted by human neutralising mAbs

Recently identified RVFV-neutralising human mAbs also bind domain A of RVFV Gn [191]. The disordered nature of the N terminus in the RV-Gn4 and RV-Gn5 structures indicates that the epitopes targeted by the human nAbs may be disrupted in the presence of mAb RV-Gn4 or RV-Gn5. Indeed, the epitopes identified by *Wang et al*, corresponds to the N terminal residues (154–193) of RVFV Gn that were disordered in Fab RV-Gn4 and RV-Gn5 complexed structures[191]. The differential targeting of domain A may likely be attributed to the method by which these two sets of mAbs were raised. Indeed, while the human mAbs were raised following human exposure to infectious virus, the RVFV Gn immunogen protein used to raise mAbs RV-Gn4 and RV-Gn5 solely included residues 192–560, and lacked N-terminal residues 154–191 (**Fig. 4.9** and **Fig. 3.7**). These data suggest that the inclusion of these residues in future immunisation experiments may increase the proportion of neutralising mAbs elicited that target this region of the molecule. However, it is unknown whether such an optimised immunogen will allow the isolation of mAbs that trap domain B in the observed extended state.

4.3.7 Investigating the likelihood of domain B rearrangements in the context of mature RVFV particles

Low resolution (approximately 1 nm) cryo-EM studies of intact RVFV particles have revealed that the virus forms a flexible icosahedral (T=12) structure formed of Gn–Gc hexamers and pentamers. Fitting of unbound RVFV Gn and Gc crystal structures into these reconstructions have provided a model for Gn–Gc assembly, wherein Gn shields the cognate Gc [69]. To assess whether the novel conformation of RVFV Gn, observed in the RV-Gn4 bound crystal structure, is sterically allowed within these assembly models, the Fab RV-Gn4–RVFV Gn structure was fitted onto previously reported Gn–Gc hexamers (from PDB no. 6F9B, 6F9C and 6F9F). This

fitting analysis revealed that the extended domain B conformation is likely compatible with the surrounding protein environment, especially given the observed mobility of the Gc-encoded fusion loop (**Fig. 4.13**). Furthermore, Fab RV-Gn4 can also be accommodated in this assembly model (**Fig. 4.15**), suggestive that it may be able to recognise the mature virus. Although this fitting analysis does not unambiguously confirm the existence of native flexibility in domain B of RVFV Gn, it shows that it is possible and is consistent with a cryo-ET study by Halldorsson *et al*, which observed relocation of domain B upon acidification of RVFV [69].

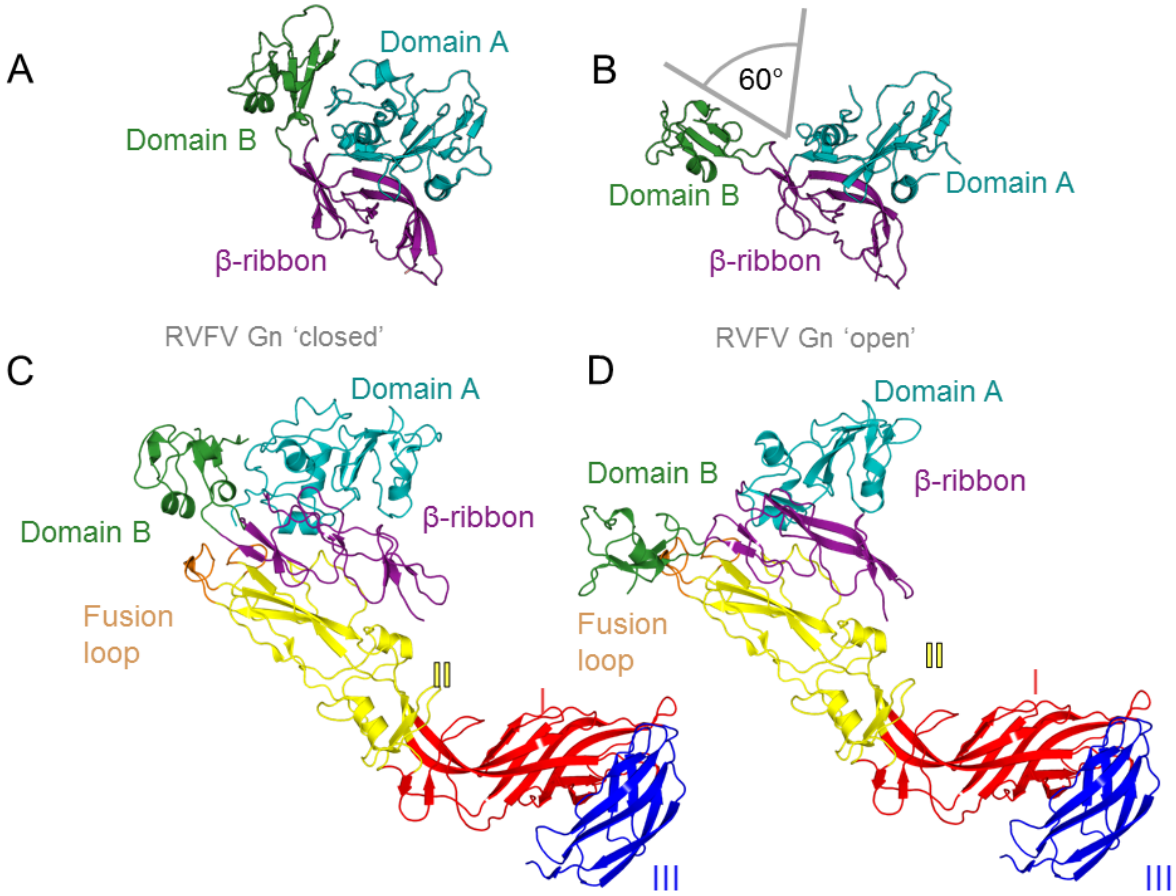

Figure 4.13 Domain B undergoes a 60° hinge motion upon binding to Rv-Gn4, which is modelled in the context of Gc.
(A) RVFV Gn (unbound) structure (PDB: 6F8P), demonstrating a 'closed' conformation and **(B)** RVFV Gn bound by RV-Gn4. Domain B undergoes a 60° movement, where the two strands which connect domain A and B act as a hinge, and an 'open' conformation is observed. Domain A is shown in teal, domain B is shown in green and the β-ribbon is shown in purple. **(C)** Electron microscopy reconstructions reveal Gn and Gc heterodimer in the context of the entire virion. (PDB: 6F9F). **(D)** RV-Gn4 bound Gn is modelled as a heterodimer of Gn and Gc. Domain B movement may affect the Gc fusion loop.

4.3.8 RV-Gn4 binds RVFV particles but does not prevent infection *in vitro*

To address whether non-neutralising mAbs RV-Gn4 and RV-Gn5 are able recognise intact RVFV, and not only recombinantly-derived RVFV Gn, binding of mAb RV-Gn4 to infectious RVFV was investigated using an adapted plaque assay. Briefly, protein G conjugated magnetic beads were incubated with mAb RV-Gn4, mAb RV-Gn2 (a nAb available at the time of experiment) and negative controls (ab1908 and beads only) before addition of 50 pfu RVFV. Magnet application to the beads separated any mAb-bound virus from the supernatant, which was plated onto Vero cells in an PRNT assay. This experiment revealed that RV-Gn4 sequestered the virus particles and thus resulted in a significantly reduced plaque count, with respect to the negative-controls ab1908 and beads only, which showed no effect on plaque number **(Fig. 4.14)**. Although mAb RV-Gn5 has not yet been tested in this assay, the similarity in epitope would suggest that virus binding is also possible.

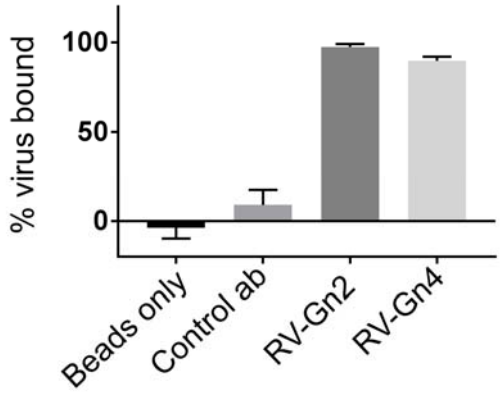

Figure 4.14 RV-Gn4 binds Rift Valley fever virus particles
Magnetic protein G beads were used to capture 50 pfu RVFV. The following samples were compared in triplicates: either beads only, control ab (ab1908), neutralising mAb RV-Gn2 and non-neutralising mAb RV-Gn4. Binding was assessed by counting pfu after bead incubation. % binding was calculated compared with a virus only control.

4.3.9 RV-Gn4 and RV-Gn5 are likely able use bivalent binding to contact RVFV

Assuming the position of RVFV Gn domain A does not change in the context of the RVFV hexamer to allow mAb RV-Gn4 and RV-Gn5 binding, structure-based overlay analysis

suggests that a full occupancy of these mAbs could be achieved across the entire virion **(Fig. 4.15)**. Furthermore, the measured distances of the neighbouring Fab fragments fall within the range expected to allow bivalent binding of both respective mAbs (within 40–52 Å, PDB no. 1IGY, 1IGT and 1HZH) between neighbouring RVFV Gn–Gc hexameric and pentameric assemblies **(Fig. 4.15)**. However, further cryo-EM and molecular dynamics studies would be necessary to explore these hypotheses further.

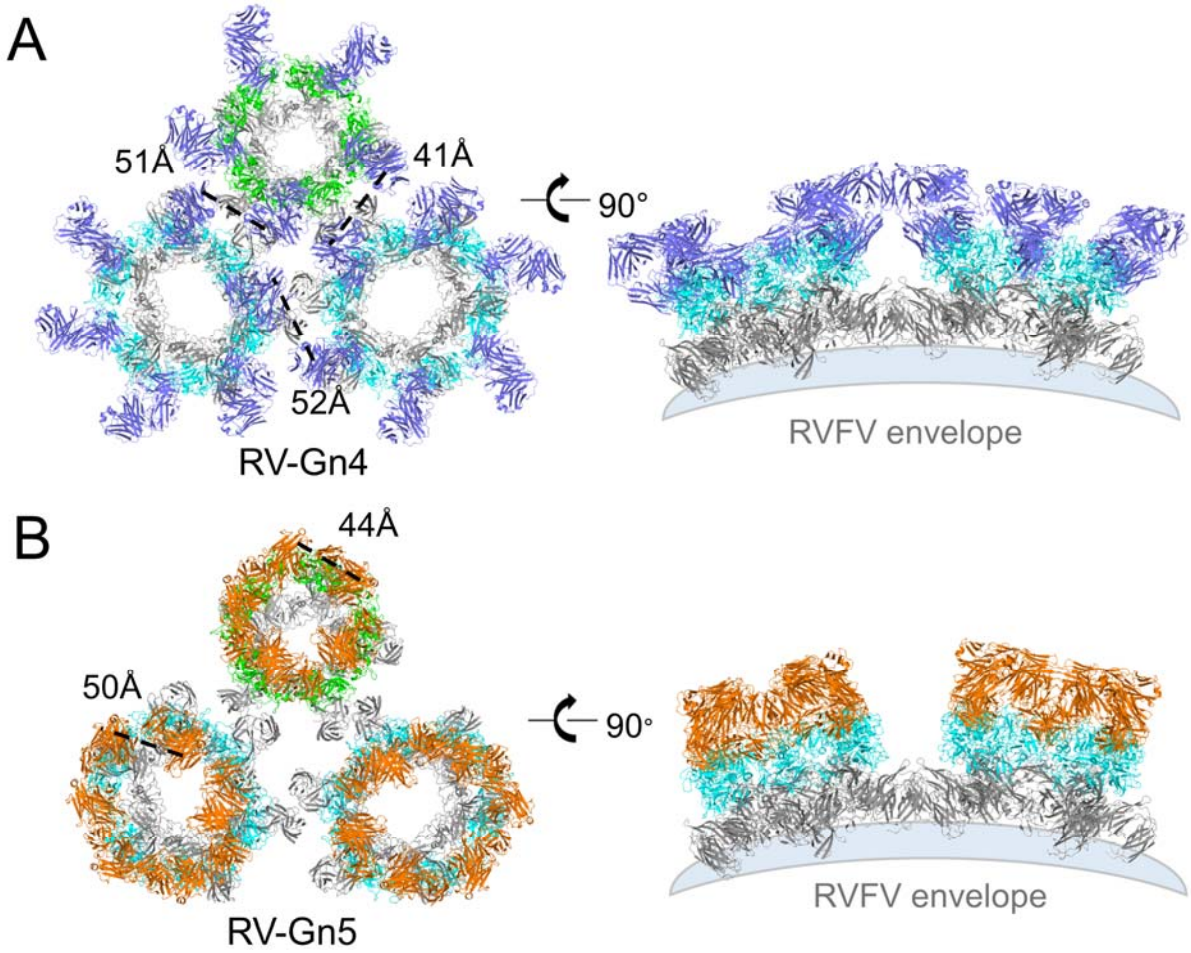

Figure 4.15 Mapping of RV-Gn4 and RV-Gn5 to RVFV glycoprotein assemblies suggests the potential for bivalent mAb binding.
Complex structures of RV-Gn4 and RV-Gn5 were superposed onto the RVFV pentamer and hexamer maps (PDB No. 6F9B, 6F9C, and 6F9F). RVFV Gc is shown in grey, pentameric Gn is shown in green and hexameric Gn shown in cyan. **(A)** RV-Gn4 is shown in marine blue, distances between Fab where bivalent mAb binding could occur are marked with dashed lines and distances between the Fab. **(B)** RV-Gn5 is shown in orange, distances between Fab where bivalent mAb binding could occur are marked with dashed lines and distances between representative Fabs of the pentamer and hexamer.

4.3.10 Preliminary investigations into domain B flexibility

Comparison of RVFV Gn crystal structures derived here and elsewhere, combined with cryo-EM analysis of the entire RVFV virion, suggests that domain B of RVFV Gn is natively flexible and can rearrange to 'open' and 'closed' states [69], (**Fig. 4.13**). Given that known neutralising mAb epitopes have been defined on only the 'closed' state of RVFV[191], we sought to assess whether stabilisation of this state, through the introduction of disulphide bonds, would result in a more effective immunogen. Five structure-guided mutations, D155C-N437C, Y184C-Q389C, Y184C-K242C, N160C-V373C, and Y184C-L394C of RVFV GnL were designed, with the aim of creating inter-domain stabilising disulphide bonds between domain B and domain A (**Fig. 4.16**). Expression was tested in 2 ml HEK293T culture and tested using Western blotting with His-tag detection. Secreted protein could be detected for two of the site-directed mutants tested, D155C-N437C and Y184C-Q389C (**Fig. 4.16**). Mutant Y184C-Q389C (D155C-N437C has yet to be characterised) was then purified in 1 L of HEK293T cell culture, as described above. Protein was purified by IMAC followed by SEC. Although the yield was lower (approximately 1 mg/L vs 2–4 mg/L purified protein) than that of wt RVFV GnL, the SEC profiles looked identical **(Fig. 4.16).** I sought to verify if the incorporated mutations resulted in the formation of a disulphide bond by ELISA binding analysis, mass spectroscopy, thermal unfolding, and crystallography. While the Y184C-Q389C RVFV Gn construct has not yet crystallised and mass spectrometry and thermal unfolding have yet to verify the presence or absence of the putative new disulphide bond, an ELISA analysis demonstrated that mAb RV-Gn4 and Fab RV-Gn5 are both able to bind the engineered protein, suggestive that the open conformation of RVFV Gn domain B is still available. Interestingly, mAb RV-Gn3, which is specific to an epitope on RVFV Gn domain B, exhibited weaker binding affinity to Y184C-Q389C RVFV Gn than the wt protein **(Fig. 4.16)**, suggestive that the substitution may have resulted in yet uncharacterised structural differences. Following

confirmation that a disulphide bond has been introduced, small angle X-ray scattering experiments could be used to compare the relative flexibility of domain B in the wt and disulphide mutant RVFV Gn. The identification and characterisation of a RVFV Gn domain B stabilised mutant will justify future immunogenicity analyses, *in vivo*.

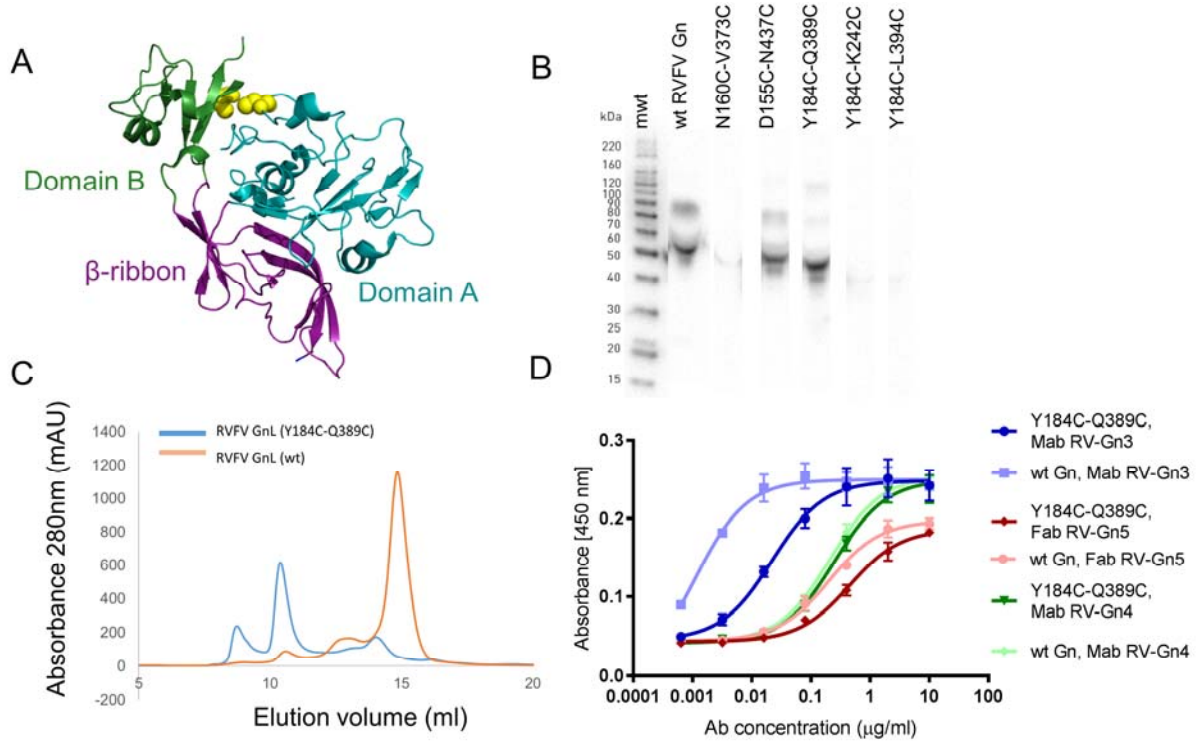

Figure 4.16 Engineering of RVFV Gn to modulate protein flexibility and epitope availability
(A) Five mutated RVFV Gn were designed by introducing new cysteine pairs. Y184C-Q389C is shown as a representative. Residues mutated to cysteine are shown in yellow spheres. RVFV Gn is coloured according to domain: Domain A is shown in teal, domain B is shown in green and the β-ribbon is shown in purple. **(B)** Small scale expression testing of five mutant GnL proteins. Cell supernatants transfected with the RVFV Gn proteins were analysed by Western blot (reducing) with anti-His tag detection. Molecular weight marker (mwt) is shown. **(C)** RVFV GnL mutant Y184C-Q389C was expressed in 1 L of HEK293T cells and then purified by SEC (blue). The wt RVFV Gn protein is overlaid in orange. **(D)** ELISA analysis of wt and mutant Y184C-Q389C demonstrates differential binding of RV-Gn3 and comparable levels of binding for RV-Gn4 and RV-Gn5. Data were collected in triplicate. Error bars display the standard error of the mean.

4.4 Discussion

In Chapter 3, we show that RVFV Gn acts as an effective immunogen capable of generating a potent neutralising antibody response. In this chapter, we have evaluated a library of mAbs elicited against this immunogen that are able to bind RVFV Gn but not neutralise RVFV *in vitro* **(Fig. 4.14).** Three of these mAbs were complexed with RVFV GnX and subjected to crystal screening. I structurally characterised two of the non-neutralising antibodies. Structural elucidation reveals overlapping yet distinct epitopes that differ in the CDR usage and angle of Fab binding (**Fig. 4.4, 4.7** and **4.15)**. Further structural evaluation and competitive binding analysis would be needed to elucidate if other epitopes may be contacted by other non-neutralising mAbs derived from our library.

4.4.1 The observed rearrangements to RVFV Gn may be relevant to native virus functionality

Structural characterisation revealed that a large movement of RVFV Gn domain B was required to accommodate mAb RV-Gn4 binding. Although unable to neutralise, the ability of mAb RV-Gn4 to bind infectious RVFV revealed that the crystallographically observed conformation of RVFV Gn may exist on the surface of the mature virion. Consistent with this hypothesis, cryo-ET-derived reconstructions of RVFV reveals that domain B may be mobile and able to extend in the manner similar to that observed in the Fab RV-Gn4–RVFV Gn crystal structure upon acidification [69]. However, given the low resolution of this region of the reconstruction (presumably due to intrinsic mobility of the glycoprotein lattice), it is not possible to confirm whether such rearrangements are equal to the 60° movement observed between unbound and Fab RV-Gn4-complexed RVFV Gn crystal structures.

While RVFV Gc functions as an established class II fusion protein, the functional role of RVFV Gn remains unclear. However, class II fusion proteins are presented on a multitude of viruses,

some of which have a 'chaperone' type protein similar to RVFV Gn. For example, the alphavirus E2 glycoprotein has a similar domain architecture to RVFV Gn and protects the hydrophobic fusion loops of the cognate E1 glycoprotein [78]. This shielding functionality has been suggested for RVFV Gn, and is supported by structural studies of viral fusion intermediates that demonstrate that de-shielding of the fusion loops occurs upon virus exposure to acidic environments, such as those existing in endosomes [69]. Inspection of RVFV Gn–Gc assembly predicted from flexible fitting of crystal structures into a low resolution cryo-EM reconstruction of RVFV suggests that domain B of RVFV Gn lies on top of the fusion loop of Gc. It is possible that domain B flexibility is required to allow Gc extension and fusion loop insertion into the host cell membrane. Further studies are required to confirm if RVFV Gn domain B flexibility is a feature of native RVFV functionality. The inter-domain disulphide substitutions presented may provide a platform for this work (**Fig. 4.16)**. In addition to leading to less flexible (and more crystallisable) recombinantly-derived RVFV Gn, such substitutions could be introduced into virus-like particles (VLPs) or genetically modified viruses for future studies that will clarify RVFV Gn functionality.

As well a large movement of domain B, a rearrangement of the Gn N terminus is required for mAb RV-Gn4 and RV-Gn5 binding. As with many recombinant viral immunogens, the RVFV Gn glycoprotein used to raise mAbs in this study presented non-native surfaces. Most notably, the RVFV Gn immunogen used in this study lacks N-terminal residues 154–191. The Gn glycoprotein did possess these residues for ELISA and complex formation experiments, therefore recombinant Gn must be able to accommodate antibody binding and reveal the epitope that lies beneath the N terminus. Furthermore, as mAb RV-Gn4 is able to bind the mature virus, these residues must be able to relocate on the native virion. Interestingly, the N-terminal residues that are disrupted by mAb RV-Gn4 form the major region of the neutralising epitope described by Wang *et al* [191]. Wang *et al* further demonstrate antibodies that bind the

N terminus are able to inhibit attachment *in vitro*. It is therefore curious that RVFV is able to bind and replicate *in vitro* in the presence of mAb RV-Gn4 or mAb RV-Gn5 (as demonstrated by non-neutralising PRNT results). It seems possible mAb RV-Gn4 and RV-Gn5 binding to RVFV presents the N-terminus in a conformation which is still available for host-cell recognition.

4.4.2 Non-neutralising antibodies may still be protective

Neutralisation efficacy as measured by PRNT does not always accurately predict mAb-mediated protection, *in vivo*, as has been demonstrated and described for several viruses, including Lassa virus, HIV and RVFV [107, 206, 207]. Indeed, although neutralising antibody titres can correlate well with protection, many studies indicate that non-neutralising antibodies can also be protective [122, 124, 208] . For example, Dunand *et al* report that Fc-mediated effector cell-mediated protection against influenza virus was conferred by a non-neutralising antibody that binds to the hemagglutinin surface glycoprotein [209]. Furthermore, a non-neutralising mAb specific to the influenza virus nucleoprotein conferred protection in wild-type mice, but no protection in antibody-deficient mice, suggestive that the mechanism did not rely upon CD8 killer T cells. However, while PRNT assays alone are not sufficient to describe the therapeutic effects of an antibody *in vivo*, they remain an invaluable technique for aiding the identification of neutralising epitopes that interfere with viral entry, fusion and replication in a host cell. In light of these previously reported observations, it is possible that many anti-RVFV Gn mAbs that were shown as non-neutralising in the PRNT assay may also exhibit protective efficacy in animal models. This seems especially plausible for mAb RV-Gn4, as it has been shown to recognise mature RVFV particles (**Fig. 4.14**), and supports the need for *in vivo* studies that will establish the protective efficacy of non-neutralising anti-RVFV mAbs.

4.4.3 Implications for immunogen design

Immunisation of rabbits with a RVFV Gn ectodomain construct (residues 192–560) was performed in 2010, prior to the structural elucidation of RVFV Gn glycoprotein fold, and elicited both a neutralising and non-neutralising mAb response. Given that the immunogen used in these experiments did not constitute the entirety of what is now known to be the globular fold of RVFV Gn (residues 154–469), it is unsurprising that a number of the mAbs isolated and characterised in this thesis did not appear to neutralise live RVFV, *in vitro*. Indeed, although testing of bulk IgG from immunised rabbits demonstrated a robust neutralising response, only approximately 30% of the hybridoma cells tested at the onset of the immunisation work produced IgG capable of potently neutralising RVFV, *in vitro*.

When considered with the structural characterisation of two non-neutralising mAbs derived from this immunisation, as described here, these data indicate several possible pathways for immunogen optimisation. Indeed, an obvious approach, which is presented in Chapters 5 and 6, is to prepare an elongated immunogen that includes N-terminal residues 154–192. Alternatively, given that neutralising and protective mAbs can target RVFV Gn domain B alone (as demonstrated Chapter 3), it seems conceivable that a reverse-immunology design approach relying on a minimal immunogenic subunit may be all that is required to induce a protective immune response. However, given that the non-neutralising antibodies presented here are capable of binding the mature virion, it is important not to neglect the potential for protection via cellular-mediated immunity. Indeed, experiments are currently ongoing to assess whether the derived non-neutralising mAb RV-Gn4 is capable of protecting against RVFV infection in a live animal model. If protection is observed, the truncated immunogen used may be more optimal than expected, as it would likely elicit mAbs capable of functioning by both blocking virus-host interactions (as described for mAb RV-Gn1) and inducing cellular immunity (as predicted for mAb RV-Gn4). Thus, in the context of recombinant subunit vaccine

design, it would likely be worthwhile to assess the protection levels conferred by RVFV Gn immunogens of various lengths.

4.5 Conclusions

In this chapter, I characterised several non-neutralising mAbs that were elicited following immunisation of rabbits with recombinant RVFV Gn. One of the non-neutralising complex structures reported in this chapter shows that RVFV Gn is able to adopt a conformation of domain B that had not been observed in previously reported crystal structures. Interestingly, similar inter-domain dynamics have been observed in a cryo-ET study of acidified RVFV, and such movements may support the conformational rearrangements of the RVFV Gn–Gc lattice required for Gc-mediated fusion of the viral and host membranes. Although the mAbs characterised in this chapter are not able to protect against RVFV infection of cells, I was able to show binding of one such mAb (mAb RV-Gn4) to mature virus, an analysis which demonstrates that the Gn- rearrangements required to accommodate mAb binding occur on the surface of the native virion. It is unclear whether binding of such non-neutralising mAbs confers protection against RVFV infection, *in vivo*. Animal experiment are being planned to assess this possibility. Such studies are important for guiding the design of improved immunogens and identifying spatially distinct sites on the RVFV surface that can be targeted by antibody-based immune-therapeutics.

Chapter 5

Developing and characterising a library of nanobodies that bind RVFV Gn and Gc

Chapter 5: Developing and characterising a library of nanobodies that bind RVFV

5.1 Preface

The ChAdOx1-GnGc vaccine was provided by Dr George Warimwe and Daniel Wright (University of Oxford). Nanobody screening was performed in the lab of Prof Jan Steyaert as part of a course funded by Instruct. The aims of this project were to generate and characterise the nanobody response to RVFV generated through a viral-vectored vaccine regime.

5.2 Summary of findings

A robust antibody-based immune response was generated by immunising llamas with an adenovirus-based vaccine encoding the RVFV Gn–Gc polyprotein and boosting with recombinantly-produced RVFV Gn and Gc. A library of 33 nanobodies was generated and selection was performed against RVFV Gn and Gc. Of the reactive members identified, several nanobodies were recombinantly produced for biochemical and biophysical study. Binding to recombinant RVFV Gn and Gc was assessed by ELISA and neutralisation was tested using a PRNT assay (plaque reduction neutralisation testing). Four nanobodies appeared to exhibit mild neutralising activity. Structural studies of nanobody complexed with recombinant RVFV Gn and Gc are ongoing, with the aim of elucidating neutralising and non-neutralising epitopes.

5.3 Introduction

Since the discovery of RVFV in 1930 in Kenya there has been significant research into the generation of vaccines that are both safe for human and animal use, and comply with DIVA regulations (differentiation of infected from vaccinated animals) [110]. Although there are currently no vaccines licensed for human use, a number of promising candidates have been identified, using various vaccine platforms [135, 138-140]. One such vaccine is the adenovirus-vectored vaccine which encodes the RVFV Gn and Gc glycoproteins known as ChAdOx1-

GnGc developed by *Warimwe et al* [210, 211]. ChAdOx1-GnGc conveys multi-species protection in sheep, cattle, and goats, and elicits neutralising antibodies in dromedary camels [210, 211]. Furthermore, the ChAdOx1 vaccine platform is well tolerated in humans [212-214], and the exclusion of the RVFV N protein allows differentiation of vaccinated versus infected animals. Therefore, this preclinical vaccine shows promise for future licensing.

Camelids are naturally exposed to RVFV, with symptoms including abortion amongst pregnant animals, haemorrhagic septicaemia and sudden death [215, 216]. Thus, camels are an important target species for RVFV vaccination [217]. Interestingly, the humoral arm of the camelid immune response includes a repertoire of single-chain antibodies, which are only known to be present in camelids and sharks [218, 219]. Single-chain antibodies typically possess a large CDR3 loop, compact shape, and a convex paratope, which combine to enable recognition of small pockets on protein surfaces that conventional antibodies are often unable to reach [220-223]. Furthermore, the variable domain of the single chain antibody, known as a nanobody, has been demonstrated to be an effective crystallisation chaperone [220, 224-228]. Recently the bioengineering of nanobodies to a larger, rigid scaffold protein, generating what is termed as a 'megabody' have demonstrated potential to overcome challenges in cryo-EM. Coupling to a larger protein allows structural resolution of small proteins, which otherwise are not able to generate enough signal-to-noise ratio [229]. Indeed, as well as their use in structural biology, recent studies have demonstrated their potential for engineering of therapeutic antibodies, by linking two different nanobody domains with human IgG1 which resulted in greater potency and cross-reactivity when used against influenza A [230].

5.4 Results

5.4.1 A single llama was immunised with ChAdOx1-GnGc and recombinantly produced RVFV Gn and RVFV Gc

The work described in this section was performed by the lab of Prof Jan Steyaert. A single llama was vaccinated with an adenovirus vectored vaccine encoding the RVFV Gn–Gc polyprotein (ChAdOx1-GnGc) kindly provided by Dr George Warimwe (University of Oxford) (**Fig. 5.1**). Initially, the llama was immunised according to the vaccine regime described by Warimwe *et al* [211]. Serum binding analysis deemed the titre too low to proceed with nanobody selection. After an 8-month interval, the llama was boosted again with ChAdOx1-GnGc, followed by a boost 6 weeks later with recombinant glycoproteins RVFV GnL and Gc (production described below). The second and third boost resulted in a titre of immunoglobulin suitable for nanobody isolation.

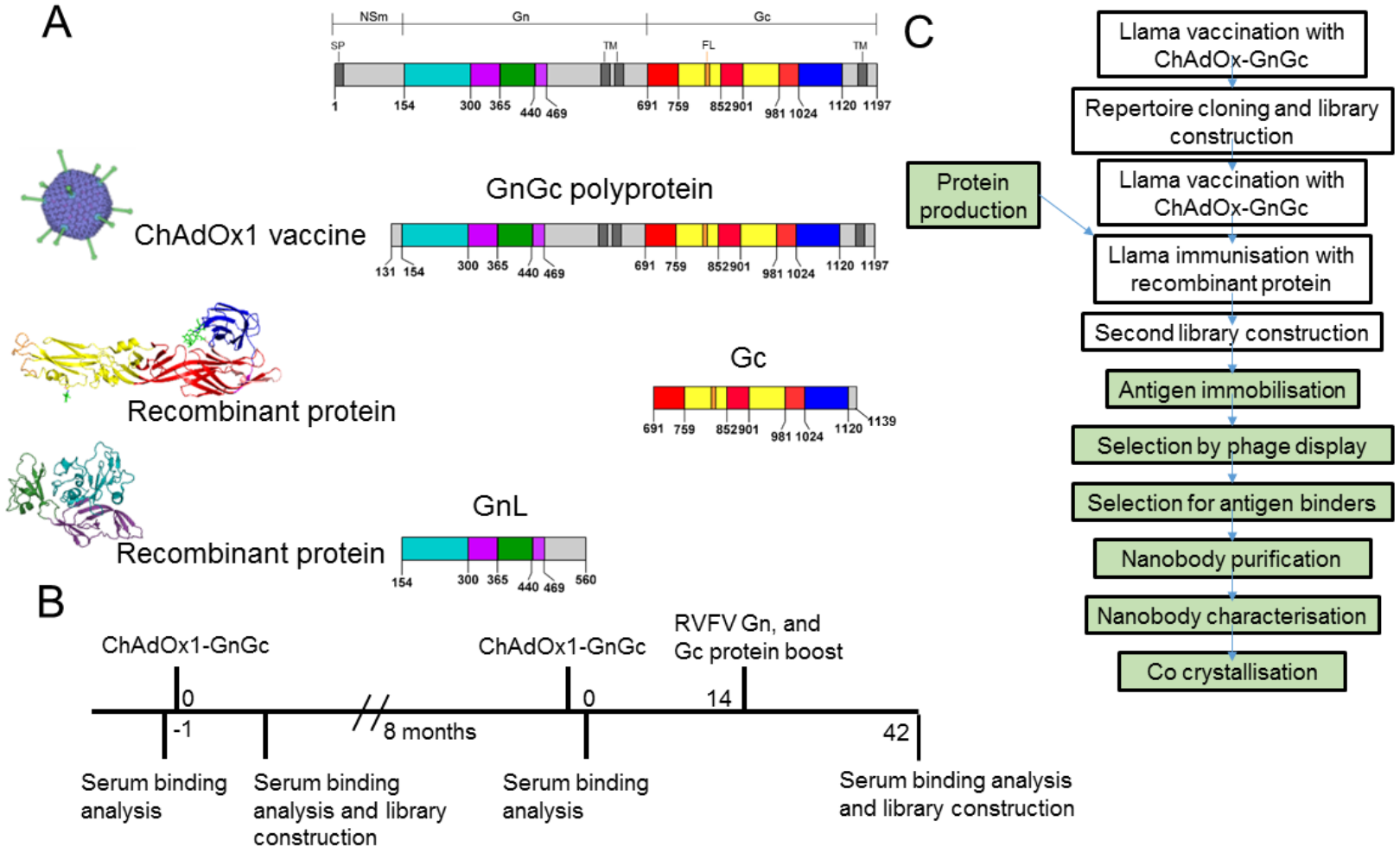

Figure 5.1 llama immunisation constructs, immunisation regime, and nanobody isolation workflow.
(A) Constructs used for llama immunisation. From top to bottom: the RVFV Gn-Gc polyprotein from residues 131–1197 delivered in a chimpanzee adenovirus vectored backbone [210], recombinant RVFV Gc residues 691–1139, and recombinant RVFV Gn residues 154–560. RVFV Gn and Gc structurally resolved domains are coloured. RVFV Gc domain I is coloured in red, domain II in yellow and domain III in blue, the fusion loop is marked in orange. RVFV Gn domain A is coloured in teal, domain B in green and the β-ribbon in purple. **(B)** Llama immunisation schedule, numbers mark the days between immunisations (8 months elapsed between ChAdOx1 immunisations. **(C)** A schematic representation of the experimental processes undertaken. Green highlights denote the areas performed by myself, described in this chapter. (Adapted from [220])

5.4.2 Generating a library of nanobodies against RVFV glycoproteins Gn and Gc

Phage display library generation was performed by the lab of Prof Jan Steyaert (VIB Brussels), by Dr Els Pardon, as previously described [220]. Briefly, after the first and third immunisations (**Fig. 5.1**), peripheral blood mononuclear cells (PBMCs) were isolated from llama-derived sera. Total RNA was purified, reverse-transcribed into cDNA, and nanobody genes were amplified by PCR and cloned into a phage display vector (pMESy4) [220]. The libraries were pooled for the selection.

5.4.3 Protein production for immunisation and crystallisation screening

5.4.3.1 RVFV GnL production for immunisation

RVFV GnL (residues 154–560) was recombinantly expressed in HEK 293T cells and purified by diafiltration, IMAC (via His-tag), and SEC using a Superdex increase s200 10/30 column (**Fig. 5.2**). RVFV GnL expressed relatively well, with a yield of at least 2 mg/L (over multiple independent purifications). The resultant SEC peak corresponded to the mass of a putative RVFV GnL monomer. Fractions were analysed by SDS-PAGE, which indicated two bands. The first band migrated to a molecular mass of approximately ~45 kDa, and likely corresponds to RVFV GnL. The second band corresponds to approximately 30 kDa and may constitute a breakdown product of RVFV GnL. His-tag detection Western blot analysis indicated that this truncated product lacked the C-terminus, on which the His-tag is present **(Fig. 5.2, B)**.

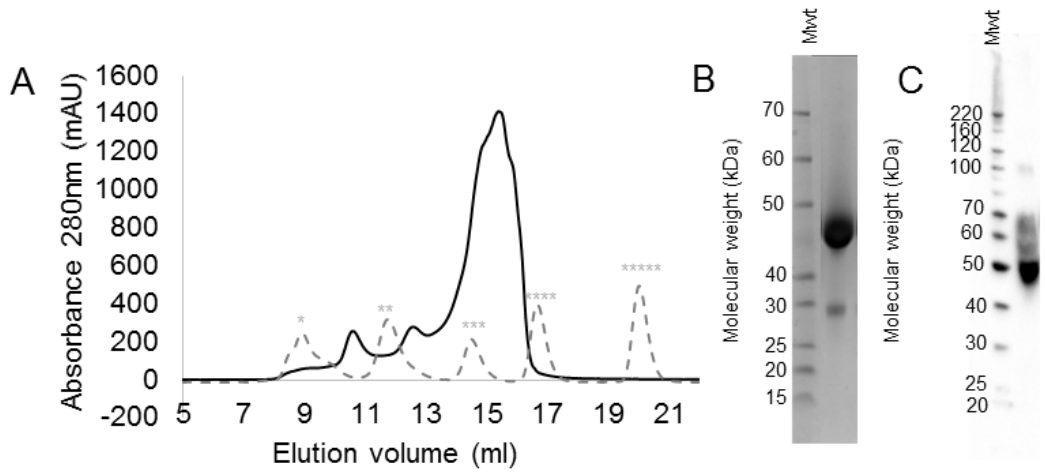

Figure 5.2 RVFV GnL (154-560) was produced for the boost immunisation of the llama and the selection of nanobodies.
(A) Size exclusion chromatography trace of RVFV Gn reveals a large peak eluting at approximately 15 ml. The broadness of the peak is likely due to heterogeneous glycosylation. Molecular weight markers are shown in grey and correspond to: * 670 kDa, ** 158 kDa, ***44 kDa, ****17 kDa, *****1.4 kDa. The fraction eluting at 15.5 ml was used for immunisation and analysed by SDS-PAGE **(B)** and His-tag detection Western blot **(C).** Molecular weight markers are shown (Mwt).

5.4.3.2 Optimising the expression of RVFV Gc

5.4.3.2.1 Construct optimisation and AviTag expression screening

The soluble expression and structural characterisation of the RVFV-Gc ectodomain (residues C691–P1119) has been previously reported [231] **(Fig. 5.1, A)**. Despite this, initial attempts to produce this protein construct, utilising the pHLSec vector in our HEK293T expression system, were unsuccessful. The resulting yield was very low and indicated that construct optimisation was required (<0.1mg per litre of cell culture supernatant). In an attempt to increase the yield, I cloned a range of constructs, including one which corresponded to the crystallised domains reported by *Dessau et al* [231], into the pHLSec vector with a C-terminal AviTag [232]. Small-scale expression testing of the AviTagged constructs demonstrated increased expression relative to the pHLSec C691–S1139 **(Fig. 5.3)**. Although C691–P1119 did show soluble expression, albeit a lower yield than the AviTagged C691–S1139, it appeared that there was

some intracellularly-retained protein. Therefore, large-scale purification was performed with C691–S1139-AviTag. Hereafter, all references to RVFV Gc relate to construct C691–S1139. RVFV Gc-AviTag was expressed in a 1 L culture of HEK 293T cells, and purified by IMAC and SEC, as described above. The addition of the AviTag did result in secreted protein (**Fig. 5.3**), although there were multiple peaks in which RVFV Gc was identified, indicating potential aggregation.

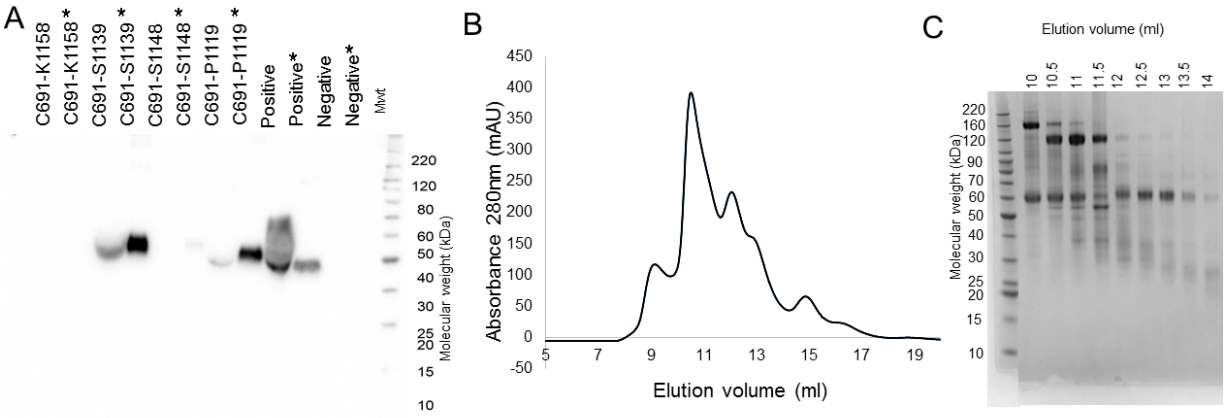

Figure 5.3 Initial expression for RVFV Gc failed to generate a homogenous sample of sufficient yield suitable for immunisation
(A) Several constructs with different C- termini were tested for expression in the modified pHLSec vector which encodes a C terminal AviTag. Expression was tested in 2 ml HEK293T cell cultures and the cell and supernatant fractions (marked by asterisk) were collected after three days and analysed by Western blotting with His-tag detection. Construct labels refer to the N- and C-terminal amino acids. Molecular weight markers (Mwt) are shown and their masses indicated in kDa. **(B)** Expression of RVFV Gc S1139-avi tested for expression in 1 L HEK293 T cell cultures. Several peaks were identified, none with sufficient yield or purity suitable for further experiments. **(C)** SDS-PAGE SEC trace shown in (B) reveals impure RVFV Gc protein eluting in all peaks at approximately 50-60 kDa. Molecular weight markers (Mwt) are shown and their masses in kDa.

5.4.3.2.2 The SUMO tag boosts secreted expression of RVFV Gc

I hypothesised that expression and purification of RVFV Gc was hampered by the absence of the RVFV Gn, which may natively act as a chaperone and shield the hydrophobic fusion loops on RVFV Gc [69]. In attempt to further increase the yield of RVFV Gc, whilst avoiding introducing RVFV Gn as a potential contaminant (that has not shown strong binding to RVFV

Gc in solution), I introduced an expression enhancing chaperone tag, SUMO, to the N-terminus of the protein. Sumoylation of proteins has been shown to enhance soluble expression of aggregation-prone proteins by promoting correct folding [146, 233, 234]. RVFV Gc was cloned into a modified pHLSec expression vector, where an N-terminal SUMO tag is linked to the protein of interest (**Fig. 5.4, A**) [158]. Small-scale expression tests indicated detectable secreted protein in the cell supernatant. Large-scale expression was tested in 8 L of HEK293T cells in roller bottles. Supernatant was harvested five days post-transfection, buffer exchanged and purified using IMAC. Protein was then incubated with 3C protease overnight to remove the SUMO tag. Applying the cleaved protein to a His-trap column revealed a portion of eluting protein that was no longer bound to the Ni resin, which was likely to be the RVFV Gc. This eluting protein was applied to a Superdex s200 10/30 Increase column for purification by SEC **(Fig. 5.4, E).** The SEC revealed several peaks, the peak of highest magnitude eluted in the region of the expected molecular weight for a monomer of RVFV Gc. The yield of the RVFV Gc monomer was approximately 1 mg/L cell culture supernatant.

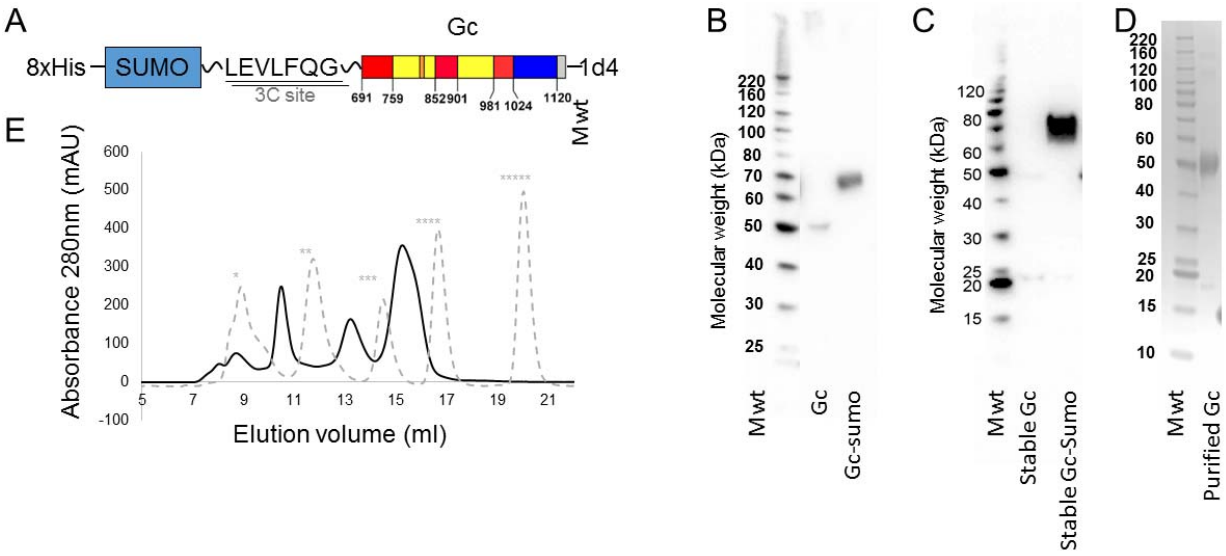

Figure 5.4 Stable production of RVFV Gc in cell lines permitted llama immunisation
(A) Schematic of the Sumo-tagged protein construct. A C-terminal His-tag is present, the SUMO protein is depicted as a blue box, the 3c cleavage site and residues are underlined and the Gc protein is coloured according to the structural domains: domain 1 is red, 2 is yellow and 3 is blue. The fusion loops are coloured in orange. **(B)** Western blot analysis of the Gc and Gc-SUMO protein indicated an increase in yield of secreted protein when produced with the SUMO tag. **(C)** Stable cell lines were generated encoding the Gc and Gc-SUMO. Supernatant was harvested and analysed by western blot analysis indicating detectable secreted protein consistent with the expected mass of the Gc-Sumo construct (~60-70kDa). **(D)** SDS-PAGE analysis of the peak at 15ml as shown in (E). **(E)** RVFV Gc is purified with size exclusion chromatography (post enzymatic removal of the SUMO tag). The protein eluted at a volume of around 15 ml, consistent with a monomeric form of the Gc glycoprotein. Molecular weight markers are shown in grey corresponding to the following sizes: * 670 kDa, ** 158 kDa, ***44 kDa, ****17 kDa, *****1.4 kDa.

5.4.3.2.3 A stable cell line expressing RVFV Gc-SUMO enhances the yield of RVFV Gc

To further increase yield of RVFV Gc, the plasmid DNA encoding RVFV Gc-SUMO was subcloned into the pURD expression vector for stable cell line generation [148]. The experimental process was performed, as described in Chapter 2, section **2.2.6**. Once the cell line had demonstrated stable expression **(Fig. 5.4, C)**, HEK 293T cells were grown in roller bottles. Kifunensine was added for cases where protein was required for crystallography [151]. Protein for immunisation was produced with the native HEK 293T glycosylation. Stable cell line expression yielded approximately 1 mg/L cell culture supernatant. Where RVFV Gc was required for crystallography, enzymatic de-glycosylation was performed by addition of endoglycosidase F1 (EF_1). As assessed by SDS-PAGE, EF_1 treatment resulted in a decrease in

mass of ~5 kDa, indicating removal of the three putative N-linked glycans (**Fig. 5.5, C**). Given the boost in expression of RVFV Gc afforded by this approach, a similar strategy was developed for the production of RVFV Gn (construct RVFV GnX-SUMO), which similarly boosted expression **(Fig. 5.5)**.

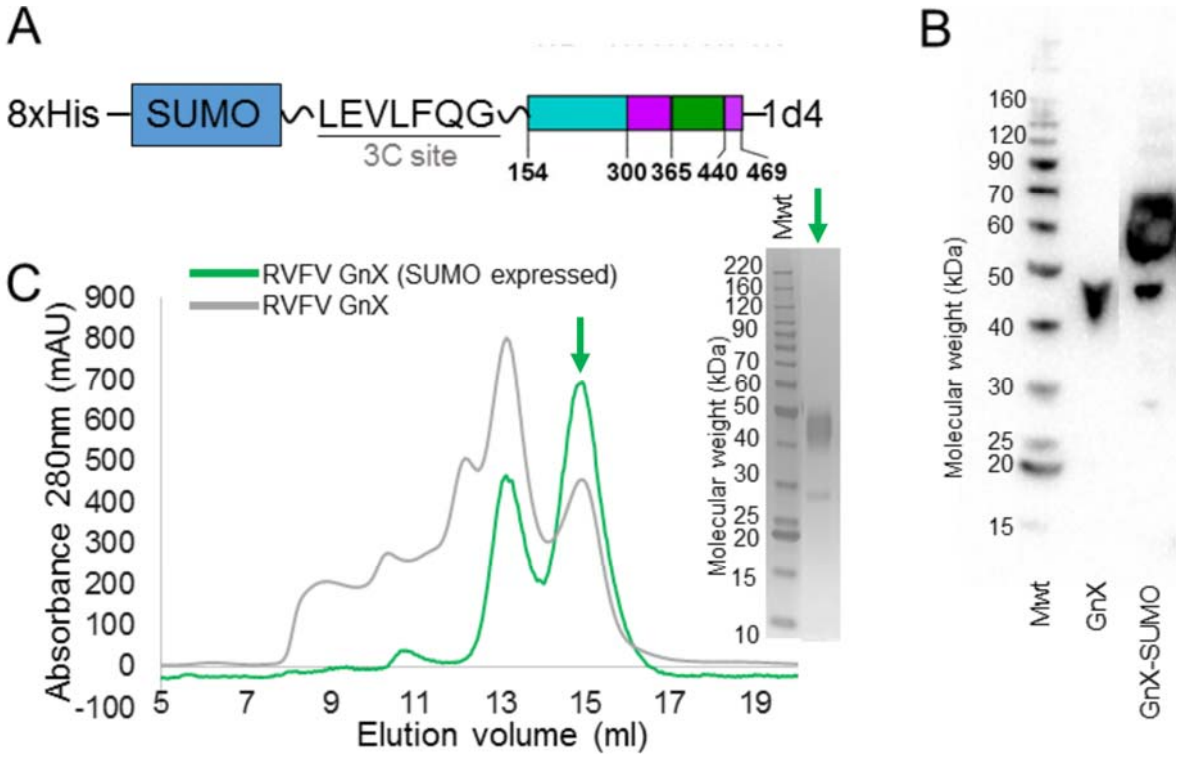

Figure 5.5 The RVFV GnX-SUMO stable cell line was generated for use in Nb co-crystallisation experiments
(A) Schematic of the Sumo-tagged protein construct. A C-terminal His-tag is present, the SUMO protein is depicted as a blue box, the 3C cleavage site and residues are shown and the Gn protein is coloured according to the structural domains: domain A is cyan, B is green and the β-sheet is purple. **(B)** Stable cell lines were generated for both the GnX and GnX-SUMO construct. Secreted protein expression was compared using a Western blot analysis. **(C)** RVFV GnX (SUMO expressed) was purified with size exclusion chromatography (post enzymatic removal of the SUMO tag) shown in green. The protein elutes at 15 ml, consistent with a monomeric form of the Gn glycoprotein (indicated by a green arrow). The GnX (purified without SUMO tag, as described in Chapter 3) is shown in grey for comparison. The monomeric peak of GnX (sumo expressed) (indicated by a green arrow) was collected for further experiments and analysed by SDS-PAGE (inset). Molecular weight markers are shown (Mwt).

5.4.4 Selection and sequence analysis of nanobodies against RVFV Gn and Gc

The experiments presented in this section were performed in the lab of Jan Steyaert, VIB, Brussels. Two separate selections were performed to isolate RVFV Gn- and Gc-specific nanobodies, respectively (as described in Chapter 2, section **2.7.2**). Following the first round of selection for both proteins, an enrichment of binding to both RVFV Gn and Gc was observed. The phage library was then plated onto selective agar and 48 RVFV Gn-specific and 48 RVFV Gc-specific colonies expressing an individual phage were isolated. Each phage colony was expanded and assessed for RVFV Gn and Gc binding by ELISA. ELISA revealed that 16/48 colonies were positive for RVFV Gn and 32/48 colonies were positive for RVFV Gc. The plasmid DNA was then isolated by miniprep and sequenced.

Of the 48 nanobody expressing colonies sequenced, 18 unique sequences were isolated from the Gc-specific library and 15 unique sequences from the Gn-specific library. Since llama single-chain antibody sequences are less well-characterised than rabbit, mouse and human repertoires, germline annotation tools are not available, making germline analysis challenging. Instead, the nanobodies were grouped together into 'families' based upon their overall sequence identity (using DNAstar Lasergene software) shown in **Table 5.1** and Appendix 1.4.

Table 5.1. Summary of nanobody characterisation.

		Family Grouping[a]	Expression tested[b]	Binding affinity[c] (μg/ml)	RVFV neutralisation[d]	Crystallisation screening
Gn selected	Nb1	10				
	Nb2	10		no binding		
	Nb3	10	✓		non-neutralising	
	Nb4	10				
	Nb5	10a				
	Nb6	10b				
	Nb7	10c				
	Nb8	11	✓	1.20	non-neutralising	Nb8–Gn
	Nb9	11				
	Nb10	11				
	Nb11	11				
	Nb12	12	✓	0.15	weak neutralisation	Nb12–Gn
	Nb13	12				
	Nb14	13				
	Nb15	14				
Gc selected	Nb17	1a	✓	1.00	non-neutralising	
	Nb18	1a				
	Nb19	1a				
	Nb20	1a				
	Nb21	1a				
	Nb22	1b				
	Nb23	1b	✓	0.96	neutralising	Nb23–Gc
	Nb24	1b				
	Nb25	1b				
	Nb26	1b				
	Nb27	2				
	Nb28	3	✓	2.29	non-neutralising	
	Nb29	4	✓	0.96	non-neutralising	
	Nb30	5	✗	no binding	non-neutralising	
	Nb31	6				
	Nb32	7	✓	1.12	non-neutralising	
	Nb33	8	✓	6.69	neutralising	Nb33–Gc
	Nb34	9				
	Nb16	irrelevant control	✓	no binding	non-neutralising	

[a]Nanobody sequences were grouped together based upon amino acid sequence alignment (presented in the Appendix 1.4)

[b] Representatives of Nb families were tested for expression. Nb expression was performed in Wk6 *E.coli.* Ticks indicate soluble expression and crosses indicate no detectable protein expression.

[c]Relative binding affinity was estimated by calculating the IC50 value from an ELISA analysis.

[d]Neutralisation potency was estimated by an *in vitro* PRNT assay performed at 1 mg/mL purified nanobody, as presented in **Fig. 5.8**.

Throughout: a blank cell indicates the experiment was not performed

5.4.5 Nanobody expression in Wk6 *E. coli*

Wk6 *E. coli* were transformed with the plasmids provided by the Steyaert lab and sequenced to verify correct gene plasmids were present. Three representatives of the five families of anti-RVFV Gn nanobodies were successfully transformed (Nb3, Nb8 and Nb12). Representatives from the remaining two were transformed yet the sequences did not match those provided, despite three attempts. Similarly, seven representatives of the nine families of anti-RVFV Gc nanobody sequences were rescued in Wk6 *E. coli* (Nb17, Nb23, Nb28, Nb29, Nb30 and Nb33). A plasmid containing DNA for an unrelated nanobody was kindly provided by Dr Els Pardon (Steyaert lab, Brussels). IPTG-induced expression was performed as described in Chapter 2 (**2.7.3**). All nanobodies were purified by IMAC. Analysis by SDS-PAGE revealed a pure protein after IMAC, negating the need for a further purification by SEC. To remove the imidazole elution reagent, nanobodies were then buffer exchanged into TBS. A representative nanobody, Nb12, was also purified by SEC on a Superdex s75 column 10/30. As expected, Nb12 eluted as a single peak corresponding to a putative monomer **(Fig. 5.6)**. The yield of purified nanobodies varied between 1–5 mg/L bacterial culture. Expression of Nb30 did not yield any protein, and should therefore be repeated.

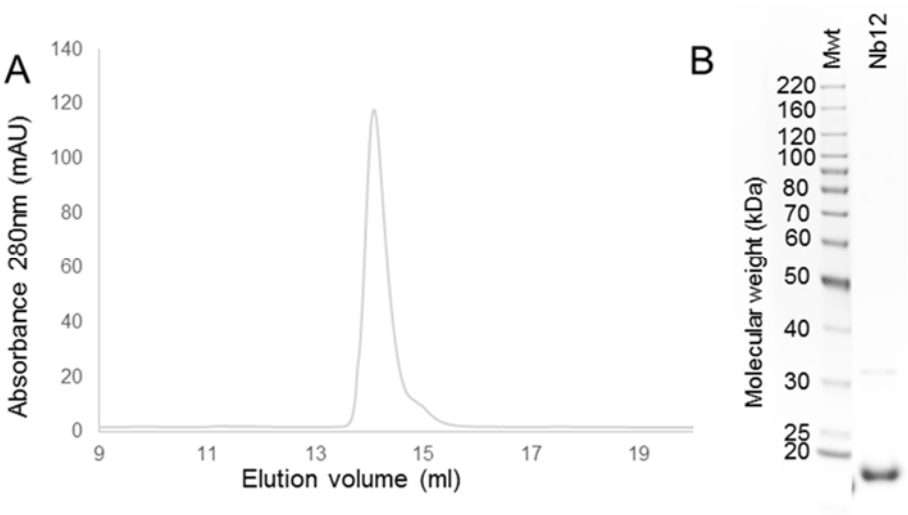

Figure 5.6 Nanobodies were expressed in *E. coli* and purified by IMAC for binding, neutralisation and co-complex crystallisation screening.
(A) A single homogenous peak of Nb12 was identified by SEC analysis on a Superdex s75 column **(B)** SDS-PAGE analysis of nanobody (Nb12) purified by Ni-affinity, reveals a highly pure protein sample (gel edited- removed irrelevant samples in neighbouring lanes).

5.4.6 Purified nanobodies bind RVFV Gn and Gc

Binding of purified nanobodies to RVFV GnX and RVFV Gc was assessed by ELISA. Plates were coated with RVFV GnX-1d4 and RVFV Gc-1d4 and titrated with a triplicate dilution series of nanobody. Surprisingly, a Gc-selected nanobody, Nb17, bound to RVFV Gn, albeit only at a high concentration. An expanded range of concentrations was therefore tested for Nb17 binding to RVFV Gn. No other nanobodies indicated cross-reactivity when prepared at 1 mg/ml. To provide an initial assessment of nanobody binding affinity, curves were fit using GraphPad (Prism) and half maximal binding concentrations (IC50) were calculated to assess the relative affinity of the isolated nanobodies. For the RVFV Gn binders, Nb12 bound with the highest apparent IC50 of 0.15 µg/ml, followed by Nb8 at 1.2 µg/ml and the Gc-selected Nb17 bound with an affinity of 75 µg/ml. Nb29 showed the highest apparent IC50 for RVFV Gc at 0.96 µg/ml. The IC50 values of the remaining Gc-selected nanobodies are as follows; Nb17 1.0 µg/ml, Nb23, 1.0 µg/ml, Nb28 2.3 µg/ml, Nb32 1.2 µg/ml and Nb 33 6.7 µg/ml. Nb3

did not show binding to RVFV Gn (or Gc) and Nb32 did not show binding to RVFV Gc (or Gn).

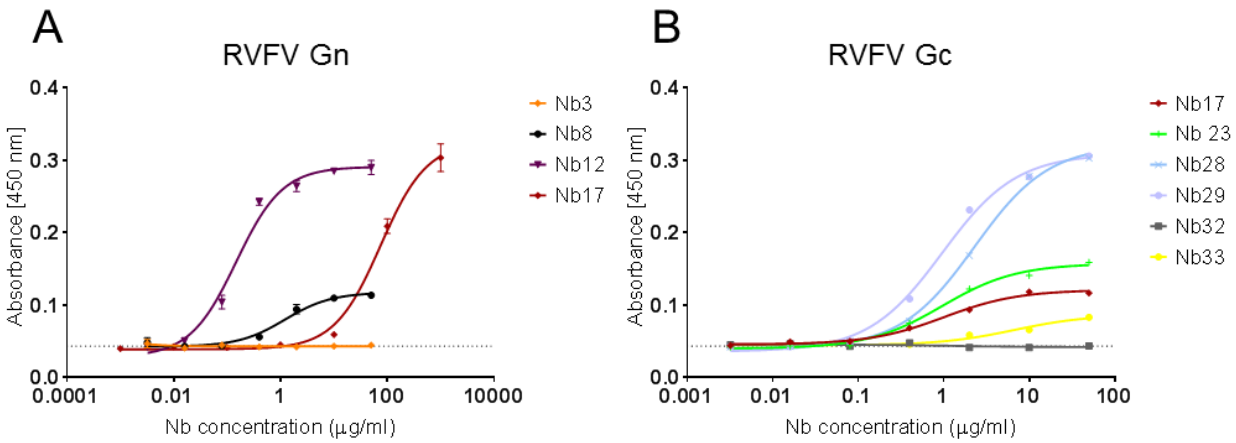

Figure 5.7 Binding of purified nanobodies to RVFV Gn and Gc.
ELISA analysis of nanobody binding. Wells were coated with RVFV GnX **(A)** or RVFV Gc **(B)** and titrated with each nanobody (performed in triplicate). The dotted line indicates background binding observed in the negative control (Nb16). Error bars represent the SEM (not shown when smaller than symbol size). Curve fitting and approximate IC50 values were calculated using GraphPad Prism. The different observed maximum binding capacity may be possibly be attributed to the accessibility of the conformational states that have been observed for RVFV Gn and Gc [69, 231, 235].

5.4.7 Identification of neutralising and non-neutralising nanobodies

Nanobody neutralisation potential was assessed by PRNT assays. A preliminary test was performed by mixing 1.0 mg/ml nanobody with a stock of RVFV before adding to a monolayer of confluent Vero cells. After three days cells were stained and assessed by eye (**Fig. 5.8, A**). Nb12, Nb23 and Nb33 exhibited neutralising activity at high concentrations. A further PRNT assay was performed with these nanobodies, along with Nb17, which appeared to bind both Gn and Gc **(Fig. 5.8, B)**. A 1 in 3 nanobody dilution series were generated (1 mg to 50 ng/ml) prior to mixing with 50 pfu. RVFV. Mixtures were plated onto confluent Vero cells and incubated for three days before fixing, staining and counting plaques. Despite the poor binding affinity to the recombinant Gc **(Fig. 5.8, B)**, the PRNT assay revealed a low level of neutralisation from

nanobodies Nb23 and Nb33. Even at concentrations as high as 1 mg/ml virus neutralisation did not reach 100%, and therefore a reliable neut50% could not be calculated. As expected, the control nanobody, Nb16, showed no neutralisation potency at 1 mg/ml. Nb12 and Nb17 appeared to show signs of neutralisation only at the highest tested concentration, 1 mg/ml. A higher concentration and further replicates of this assay may be required to assess the neutralising potential of all isolated nanobodies, however there was insufficient time and sample quantity to repeat the experiment for this thesis. The potency of neutralisation observed for nanobodies was much lower than that of RV-Gn1–3 **(Fig. 5.8** and Chapter 3 **Fig. 3.5).**

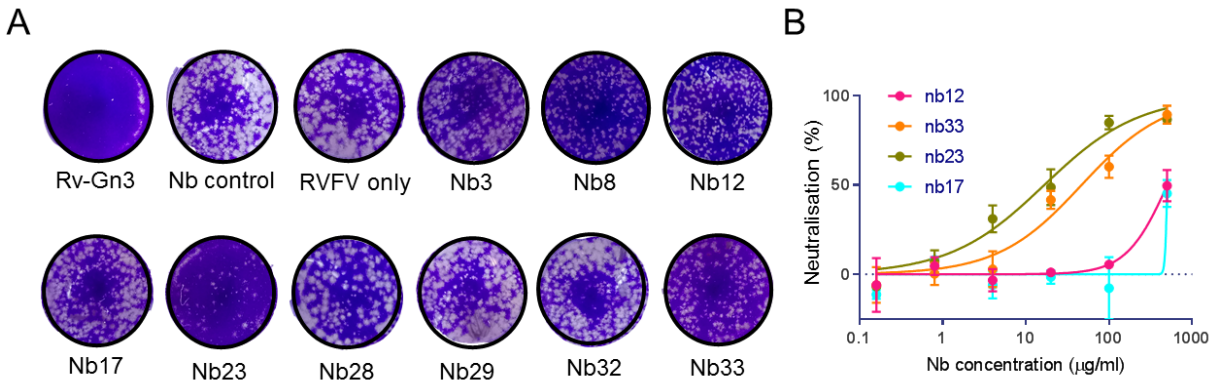

Figure 5.8 Nanobodies 3/9 Nb exhibited neutralisation potency against RVFV *in vitro*. **(A)** Preliminary plaque reduction neutralisation testing. 1mg/ml nanobody was mixed with RVFV and then plated onto confluent Vero cells. An irrelevant nanobody (Nb16) was used as a negative control, and RV-Gn3 at 20 µg/ml was used as a positive control. Nb12, Nb33, Nb23 and Nb17 gave promising neutralisation results. **(B)** A dilution series of nanobody was prepared in duplicate and PRNT assay performed. Percentage neutralisation was calculated relative to a virus only control. Dotted line indicated neutralisation achieved using the irrelevant nanobody (Nb16). Error bars represent the SEM (not shown when smaller than symbol size).

5.4.8 Complex generation and crystallisation screening

Purified and deglycosylated RVFV glycoproteins were mixed with a 1.5-fold molar excess of nanobody and incubated for one to four hours at RT. The concentrated samples were then subjected to SEC on a Superdex s75 10/30 Increase column. Due to the small molecular mass of nanobodies (~15kDa), and the resolution of the technique, assessing complex formation by a peak shift was difficult to determine. 'Complex' peaks were assessed by SDS-PAGE gel analysis to confirm the presence of both the glycoprotein and nanobody **(Fig. 5.9** and **Fig. 5.10)**. Complexes were concentrated before being subjected to crystallisation screening at RT, as detailed in **Table 5.2**. RVFV GnX and Nb complexes appeared to have many components when analysed using SDS-PAGE. Methods to reduce these potential contaminants should be performed in order to improve purity and increase likelihood of crystallisation.

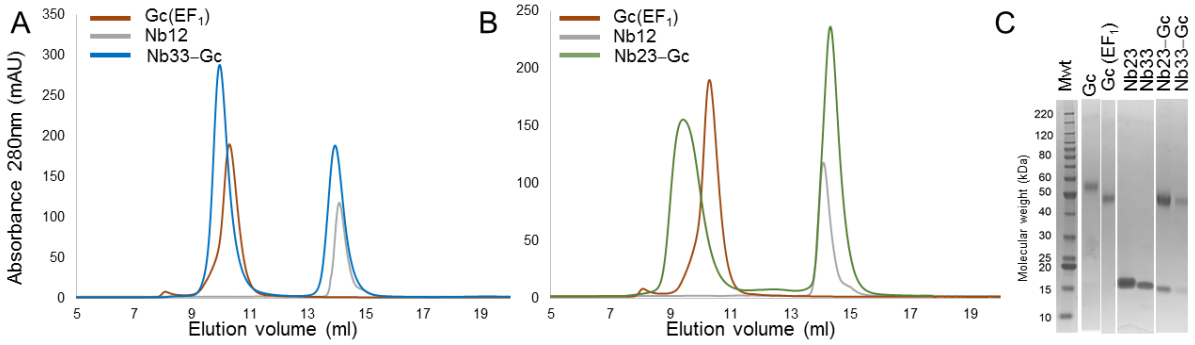

Figure 5.9 RVFV Gc-Nb complex generation for crystallisation screening
(A) Nb33 and deglycosylated RVFV Gc, labelled Gc(EF_1) were complexed and purified by SEC (blue trace). Gc(EF_1) is shown in red and Nb12 is shown in grey for comparison. **(B)** Nb23 and deglycosylated RVFV Gc, were complexed and purified by SEC (green). Gc(EF_1) and Nb12 are displayed as in (A). **(C)** SDS-PAGE analysis of Nb–Gc complexes confirmed the presence of both Gc and nanobody in the purified sample, with no contaminant or degradation products. RVFV Gc and the endoglycosidase treated Gc (EF_1) are shown, demonstrating an apparent ~5kDa reduction in mass. Molecular weight markers are shown (Mwt)

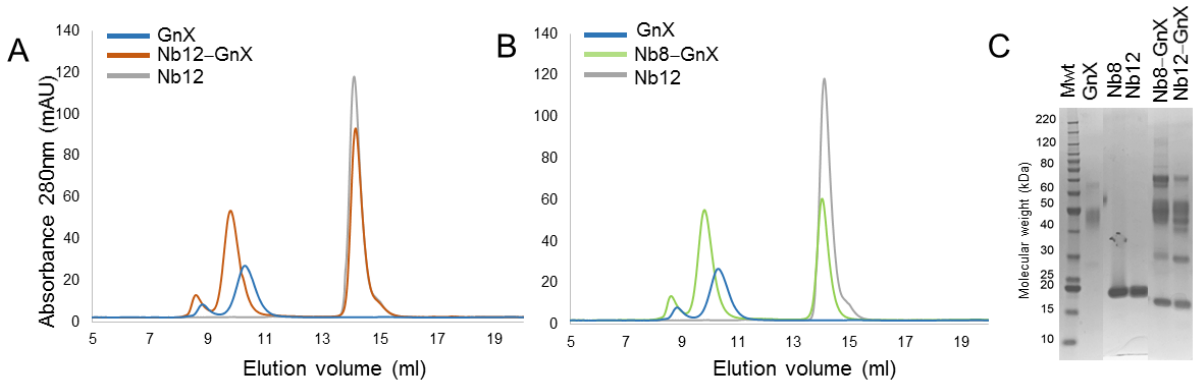

Figure 5.10 RVFV Gn-Nb complex generation for crystallisation screening
(A) Nb12 and RVFV GnX were complexed and purified by SEC, shown in orange. GnX is shown in blue and Nb12 is shown in grey for comparison. **(B)** Nb8 and RVFV GnX, were complexed and purified by SEC, shown in green. GnX and Nb12 are displayed as in (A). **(C)** SDS-PAGE analysis of Nb–Gn complexes confirmed the presence of both Gn and nanobody in the purified sample. The purified complex has many unidentified components that may include breakdown products of RVFV Gn. Molecular weight markers are shown (Mwt)

Table 5.2 A summary of the preliminary crystallisation screening performed for nanobody–glycoprotein complexes.

Complex	Concentration	Screens/conditions tested
Nb8–RVFV Gn	6.3 mg/ml	3/288
Nb12–RVFV Gn	6.5 mg/ml	3/288
Nb23–RVFV Gc	10.7 mg/ml	2/192
Nb33–RVFV Gc	10.3 mg/ml	2/192

5.4.9 Nb17 forms a stable complex with RVFV Gc, but not a ternary complex with Gn and Gc

Given that the Gc selected Nb, Nb17, also showed reactivity towards Gn, I tested whether a ternary complex of Nb17, RVFV Gn and Gc would form and remain stable in SEC. The three independently purified proteins were mixed before being subjected to SEC analysis, using a Superdex S57 column. SEC revealed a peak eluting at volume consistent with the expected mass of RVFV Gc-Nb complexes **(Fig. 5.11)**. The peak exhibited a slight shoulder that corresponds roughly with the expected elution volume of RVFV Gn. A peak was not present at a lower elution volume (and larger apparent mass) as would be expected of a complex

comprising of Gn, Gc and Nb. Therefore, the ternary complex was either too low affinity to withstand SEC or Nb17 is unable to bind both Gn and Gc simultaneously. Additionally, Nb17 did not appear to form a SEC-stable complex with RVFV Gn, in-line with the low apparent affinity (75 µg/ml).

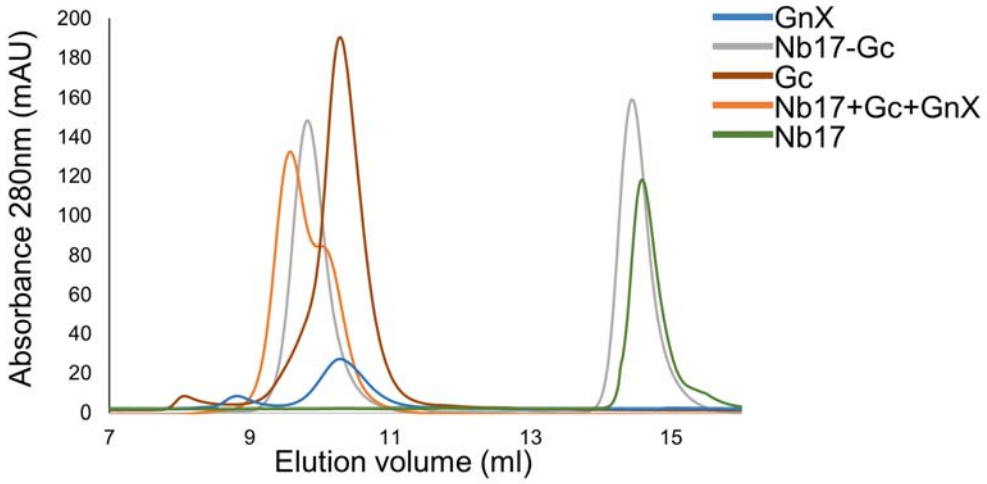

Figure 5.11 Nb17 does not form a stable ternary complex with RVFV Gn and Gc, but complexes with RVFV Gc alone
SEC analysis was performed to determine if a SEC-resistant complex of Gn, Gc and Nb17 could be generated. The mixture of Gc, Gn and Nb17 is shown in orange. A peak shift to a lower elution volume would be expected for a complex of 3 components. Gc–Nb17 complex is displayed in grey showing both a complex and a nanobody peak, GnX is shown in blue, Gc in burgundy and Nb17 in green.

5.5 Discussion

Here, I describe the use of a combined viral vector vaccine and recombinant protein immunisation to generate a phage display library of anti-RVFV Gn and Gc nanobodies. Characterisation of this library identified both neutralising and non-neutralising nanobodies. Preliminary experiments were performed to structurally characterise the nanobody epitopes and protocols have been optimised for future large-scale crystallisation screening.

5.5.1 Pure, homogenous RVFV Gn and Gc were produced for immunisation, binding and crystallographic screening

Purification of the RVFV Gn has been described extensively in this thesis and has been vital to the ongoing work. Purification of RVFV Gc was much less straightforward than RVFV Gn. Here, I demonstrated that an N-terminal SUMO tag was needed in order to produce a homogenous and pure sample of RVFV Gc. The yield of this protein was low, in comparison to Gn, and limited the extent of crystallisation screening of nanobody complexes performed thus far. Generation of a stable cell line expressing RVFV Gc resulted in improved protein yields and thus enabled further experiments.

There are multiple possible explanations for the difficulty in expressing RVFV Gc. In a viral infection, the RVFV Gc would be expressed as a polyprotein with RVFV Gn, wherein RVFV Gn may be required for the correct folding of cognate Gc. Another possibility is that the lack of RVFV Gn causes premature exposure of the hydrophobic RVFV Gc fusion loops, which may result in protein aggregation and cytotoxic effects to the expression cell line. RVFV Gn likely shields the fusion loops on the surface of the virus and prevents premature fusion[69]. Indeed, for the Gc of severe fever with thrombocytopenia syndrome virus (SFTSV), Halldorsson *et al* demonstrated an increase in recombinant protein expression levels after knocking out the fusion loops with hydrophobic-to-hydrophilic residue substitutions [73]. Such substitutions may also aid in increasing protein solubility.

5.5.2 Boosting with recombinant RVFV Gn and Gc was needed to generate an immune response suitable nanobody isolation

Our data suggest that immunisation with the ChAdOx1-GnGc vaccine was insufficient for eliciting the level of immune response necessary for nanobody isolation and that boosting with recombinantly-derived RVFV Gn and Gc rendered the experiment successful. This experiment

was not performed with the intention to evaluate different immunisation regimes, and as there is only one animal subject, these results are not significant. However, it would be interesting to evaluate if this response would also be observed in a larger cohort of animals and furthermore, if the increased antibody titre to recombinant RVFV Gn and Gc correlates well with neutralisation and/or protection. Such experiments would be in-line with assessment of the therapeutic potential of recombinantly-derived RVFV Gn and Gc as immunogens described in Chapter 4.

5.5.3 Potential mechanisms of nanobody-mediated neutralisation

Only four of the nine nanobodies tested were found to neutralise RVFV. Moreover, the neutralisation titres were significantly lower than those of the rabbit mAbs presented in Chapter 3. Aside from the routes via which these reagents were generated, the relative low neutralisation titre of the nanobodies could be attributed to the absence of an avidity effect arising from having two binding sites on a full-length mAb. Furthermore, as single-domain nanobodies (average molecular mass of 12–15 kDa) are about a tenth of the mass of a full-length mAb (~150 kDa), it is likely that they are less able to sterically hinder virus–host interactions, as proposed for mAbs RV-Gn1–3 in Chapter 3.

The relatively small size of single chain antibodies may allow the targeting of sites on the virion surface that the bulkier IgG may not be able to access. Additionally, it would be interesting to identify where the neutralising nanobodies bind, as they could be functioning through a mechanism other than steric hindrance, such as triggering premature fusion and/or disassembly of the RVFV Gn–Gc lattice. Considering the cryo-EM derived reconstruction of the entire RVFV particle [69] and the reported isolation of anti-Gc mAbs [191], there are a number of sites on the Gc that may be accessible to single chain antibodies .

5.5.4 Nanobodies provide a platform for studying the structural basis of anti-Gc-mediated neutralisation

Despite the majority of studies of phleboviral immunity identifying the Gn as the primary target of the neutralising antibody response [110, 191], the nanobody response appears to show more neutralising potential against the RVFV Gc. This may be attributed to the immunisation approach utilised or an incomplete assessment of the derived nanobody repertoire (e.g. there are a further two anti-Gn nanobodies remaining to be characterised). Nonetheless, as there are few reported anti-phlebovirus Gc mAbs, and nothing is known about the structural basis for anti-Gc-mediated neutralisation. The nanobodies reported herein therefore constitute valuable reagents for studying the molecular basis for antibody-mediated targeting of the phleboviral Gc.

5.5.5 Nb17: a nanobody that binds RVFV Gn and Gc

As described in section **5.4.4**, Nb17 was selected against RVFV Gn and was found to bind both RVFV Gn and Gc with nanomolar and micromolar affinities (respectively) **(Fig. 5.7**). The identification of a putatively cross-reactive nanobody is promising, as attempts to form stable complexes of recombinant RVFV Gn and Gc have been unsuccessful. Given the apparent weak affinity of RVFV Gn and Gc, it is unlikely that the two proteins complexed upon mixing for immunisation. Rather, it is more likely that the ChAdOx1-GnGc viral vector vaccine encoding the polyprotein may have resulted in a RVFV Gn–Gc complex.

I tried to form a Nb17–RVFV GnX–Gc complex by mixing the three independently purified proteins. However, the affinity of the potential ternary complex may have been too low to withstand SEC [236]. In-line with the low apparent IC50 (75 μg/ml, as reported above), Nb17 did not appear to form a SEC-stable complex with RVFV Gn alone. Further analysis into the nature of these interactions are necessary. Furthermore, if Nb17 is able to recognise a multi-

component RVFV Gn and Gc epitope, it could be a useful reagent for future structural studies of the RVFV Gn–Gc heterodimer, as current cryo-EM-derived models of RVFV Gn–Gc interactions are limited by the low resolution (approximately 8 Å) of the reconstructions.

5.6 Future directions

5.6.1 Obtaining a higher yield of purified RVFV Gc

In this chapter, I described the process of optimising protein expression protocols, demonstrating an increase in expression from a starting point of <0.2 mg to around 1 mg/L cell culture. Although this work enabled llama immunisation and preliminary characterisation of nanobodies, the improved yield was not sufficient for extensive crystallisation screening of nanobody complexes. To further increase the yield of RVFV Gc, it would be worthwhile to implement recently described lentivirus-transduced cellular expression systems, which have been shown to dramatically increase protein yield [237]. Additionally, co-expression with the purified nanobodies isolated here may help stabilise the protein and increase soluble expression, which could then be used for crystallisation. Indeed, a co-expression strategy could also be applied to the generation of Nb–RVFV Gn complexes and may result in improved homogeneity and purity of complexes (**Fig. 5.10)**

5.6.2 Assessment of RVFV binding using a magnetic bead adapted PRNT assay

While neutralisation potency and binding to recombinant RVFV Gn and Gc was explored, it would also be important to investigate if the isolated nanobodies are able to bind the glycoproteins in the context of a mature virion. In Chapter 4, a virus pull-down assay was implemented to assess binding of a non-neutralising mAb, RV-Gn4, to RVFV. This assay could be adapted for these nanobody reagents, where instead of using protein G conjugated magnetic

beads for IgG capture, His capture magnetic beads (e.g. dynabeads, ThermoFischer Scientific, UK) could be used nanobody binding.

5.6.3 Structural characterisation of nanobodies in complex with RVFV by cryo-EM

In addition to X-ray crystallography, these derived nanobodies could be used in cryo-EM projects. Indeed, it is conceivable that RVFV Gn and Gc-specific nanobodies, when expressed as a more EM-compatible megabody (molecular mass of 60+ kDa [229]), may contribute to a more rigidified RVFV Gn–Gc lattice, and thus enable reconstructions beyond the current ~8 Å resolution barrier [69]. Such an achievement would enhance our understanding of Gn–Gc assembly and reveal the structure of regions of RVFV Gn and Gc that have not yet been elucidated by X-ray crystallography.

5.6.4 Panning for nanobodies that target higher-order RVFV Gn–Gc assemblies

Due to the absence of high-resolution structural information, the intricacies of Gn and Gc assembly on the native RVFV surface (i.e. Gn–Gn, Gn–Gc, and Gc–Gc interactions), remain unknown. Nanobodies that stabilise these higher order interactions could constitute valuable reagents for clarifying these unknown structural features. Future work focused on isolating nanobodies that target multi-subunit RVFV glycoprotein epitopes could employ an adapted phage display selection protocol. Ideally, purified RVFV would be used to select nanobodies, however, the containment facilities used during my project do not currently have the infrastructure for this work. Chemically inactivation of RVFV through paraformaldehyde fixation is possible, although cross-linkages on the virion surface may affect native epitope presentation. Alternatively, a RVFV virus-like particle (VLP) system has been reported and could be very beneficial for this work [238]. Indeed, selection with a non-infectious reagent could be performed on our existing phage library and may help evaluate and take advantage of a multi-glycoprotein subunit RVFV nanobody response.

5.7 Concluding remarks

We sought to generate and characterise a library of nanobody reagents directed to RVFV Gn and Gc. Considerable progress has been made in identifying nanobodies of interest and structural characterisation is ongoing. We demonstrate a neutralising response to RVFV Gc and have characterised a nanobody that recognises both RVFV Gn and Gc subunits. These experiments pave the way for future structural and functional studies.

Chapter 6

Immunological responses to banyangviruses

Chapter 6: Immunological responses to banyangviruses

6.1 Preface

The focus of this thesis thus far has been on the prototypic member of the phlebovirus genus, RVFV. This chapter aims to investigate the immune response mounted against Gn glycoproteins of the emerging and related, banyangviruses, Heartland virus (HRTV) and severe fever with thrombocytopenia syndrome virus (SFTSV). Here, I describe the process by which the expression of HRTV Gn and SFTSV Gn glycoprotein constructs were optimised, and detail preliminary crystallisation trials. Despite construct optimisation and extensive crystal screening, I have yet to structurally characterise HRTV Gn. I achieved successful expression of milligram quantities of highly pure samples of these glycoproteins that are amenable for crystallisation and immunisation studies This chapter details my contributions towards a collaboration, in which we are in the process of generating a library of mAbs that may be used to define neutralising epitopes on the surface of HRTV and SFTSV. A key focus of this work was to isolate cross-reactive mAbs capable of neutralising both HRTV and SFTSV. Animal experiments were designed and planned by myself and Dr Victoria Graham, and performed by the facility staff at PHE. FACS experiments were performed with Dr Katie Doores (KCL) and ELISAs were performed by Dr Jeff Seow (Doores lab, KCL), using the proteins described in this thesis.

6.2 Summary of Findings

In this chapter, we sought to study the antibody-mediated immune response generated against the Gn glycoprotein of three viruses from the phlebovirus and banyangvirus genera: HRTV, SFTSV and RVFV. By optimising expression of Gn glycoproteins from each virus, I was able to obtain sufficient yield to immunise mice. In addition to immunisation of mice with only RVFV, HRTV or SFTSV Gn, we investigated a heterologous prime-boost strategy with HRTV

Gn and SFTSV Gn, with the aim of generating cross-reactive mAbs. We successfully produced a pool of mAbs that recognise SFTSV Gn and HRTV Gn. This work provides a platform for elucidating common features of a protective immune response across phleboviruses and banyangviruses. Indeed, work is currently ongoing to characterise the mAb response using a workflow similar to that described in Chapters 3 and 4 with the goal of identifying cross-reactive, neutralising, and protective epitopes on the surface of HRTV Gn and SFTSV Gn.

6.3 Introduction

In recent years, two novel tick-borne banyangviruses have been identified that cause disease in humans [239]. Severe fever with thrombocytopenia syndrome virus (SFTSV) was discovered in China, in 2009, and has since been responsible for several outbreaks, and thousands of human infections in China, Japan, and South Korea [240]. In the absence of licensed antivirals or vaccines, mortality rate can reach 30% in a clinical setting, with symptoms of febrile illness, thrombocytopenia, leukocytopenia, and encephalitis [41]. SFTSV transmission is principally associated with the tick species *Haemaphysalis longicornis,* however, several studies have indicated the risk of human-to-human transmission [241, 242].

Heartland virus (HRTV), a banyangvirus that is genetically similar to SFTSV is carried by the tick species, *Amblyomma americanum*. HRTV was identified in 2009 after causing disease in two humans that presented with leukopenia and thrombocytopenia [54, 56]. Serological studies of antibodies (Abs) against HRTV in animals have implicated racoons and white-tailed deer as candidate reservoir species [243]. Unlike SFTSV, HRTV has not been implicated in large outbreaks; infections have only been reported in 40 humans in Missouri, Tennessee, and Oklahoma, with no evidence of human-to-human transmission.

To date, there have been no published immunogenicity studies for HRTV virus and few vaccine candidates have been tested for SFTSV. A DNA vaccine encoding SFTSV NSs and N [141],

and a recombinantly-derived SFTSV NsS protein immunogen [244], have been tested in mice, where neither gave a promising outcome. More recently DNA vaccines encoding each protein of SFTSV, have provided protective immunity, and demonstrated the Gn and Gc glycoproteins to be the most effective immunogens [141], in line with vaccine studies for RVFV [110].

A recently reported crystal structure of SFTSV Gn in complex with a human-derived mAb delineated a neutralising epitope located on domain B (discussed in detail in Chapter 3) [76]. The elucidation of the structure of the SFTSV Gn demonstrated that the protein presents the same fold as RVFV Gn. Structural comparison revealed a 3.1 RMSD between RVFV Gn, suggesting that the two proteins are antigenically dissimilar [245].

6.4 Results

6.4.1 Expression of pure, homogenous protein was optimised for both immunisation and crystallographic screening

6.4.1.1 HRTV Gn

6.4.1.1.1 Construct design and small scale expression trials

HRTV Gn possesses only 21% sequence identity to RVFV Gn (the only related Gn glycoprotein structure known at the time of construct optimisation PDB: 6F8P [69]). Several constructs were designed, using the known RVFV Gn structure as a guide **(Appendix 1.5** - phenuivirus Gn sequence alignment) and were cloned into the pHLSec vector and were screened for soluble expression in HEK 293T cells. Western blot analysis revealed that 8/9 of the constructs demonstrated soluble expression **(Fig. 6.1)**. The construct that best aligned to the known domain boundaries of RVFV Gn was chosen for large-scale production, and is hereafter referred to as HRTV Gn (residues C27–K358).

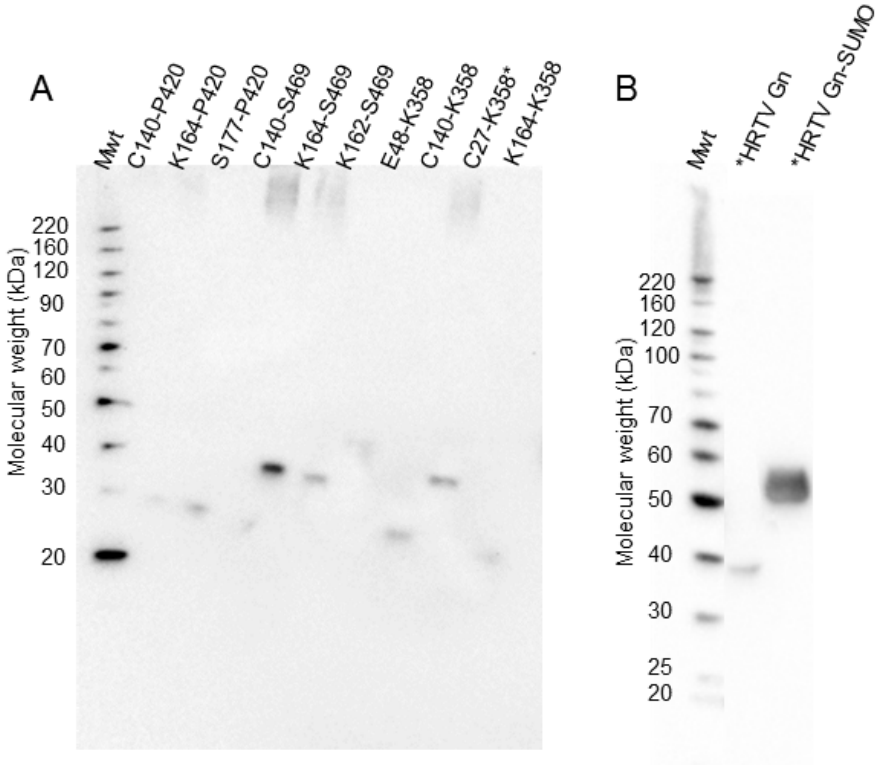

Figure 6.1 Expression testing of HRTV Gn revealed soluble protein expression
(A) Several constructs were tested for soluble expression using the pHLSec expression plasmid (see also **Appendix 1.5** for a sequence alignment of HRTV, SFTSV and RVFV Gn). His-tag detection was used in a Western blot of cell supernatants. Construct boundaries are listed above. Molecular weight marker is shown (Mwt). The construct that best aligned to the known domain boundaries of RVFV Gn was chosen for large-scale production, and is hereafter referred to as HRTV Gn (residues C27–K358) and marked with an asterisk. **(B)** Expression trials were also performed for a SUMO tagged version of HRTV Gn (see also **Fig. 6.2)**

6.4.1.1.2 Crystallisation screening of purified HRTV Gn

HEK 293T cells were transfected with pHLSec plasmid encoding HRTV Gn, in the presence of kifunensine (an N-linked glycosylation inhibitor) [152]. Five days following transfection, cell supernatant was harvested, buffer exchanged, and purified by IMAC and SEC. After the first round of size exclusion, a homogenous peak corresponding to the apparent molecular mass of a HRTV Gn monomer was observed **(Fig. 6.2, B)**. The protein was then enzymatically deglycosylated with endoglycosidase F1 (EF_1) and subjected to a final SEC step. Surprisingly, two peaks were observed following deglycosylation, where the low molecular mass peak

corresponded to the original monomer and the higher molecular mass peak corresponded to a possible dimer or trimer **(Fig. 6.2, C)**. SDS-PAGE analysis of these peaks revealed that the deglycosylated sample was present in the higher molecular weight peak and that enzymatic deglycosylation was only partially achieved **(Fig. 6.2, C)**. Nevertheless, both peaks were separately concentrated and prepared for crystallisation screening. In order to produce a sample with more homogeneous, yet limited glycosylation ($Man_5GlcNAc_2$), HRTV Gn was also produced in HEK 293S cells, which lack the N-acetylglucosaminyltransferase I (GNTI) gene [157]. The protein was purified by size exclusion, revealing a single peak consistent with a HRTV Gn monomer, then concentrated to 6.1 mg/ml for crystallisation screening. A summary of the crystallisation screens attempted is provided in **Table 6.1**. Although some screens yielded crystals **(Fig. 6.2, B)**, X-ray diffraction data collection is pending. Future attempts to solve the HRTV Gn structure may benefit from crystallographic screening of other constructs that demonstrated soluble protein expression.

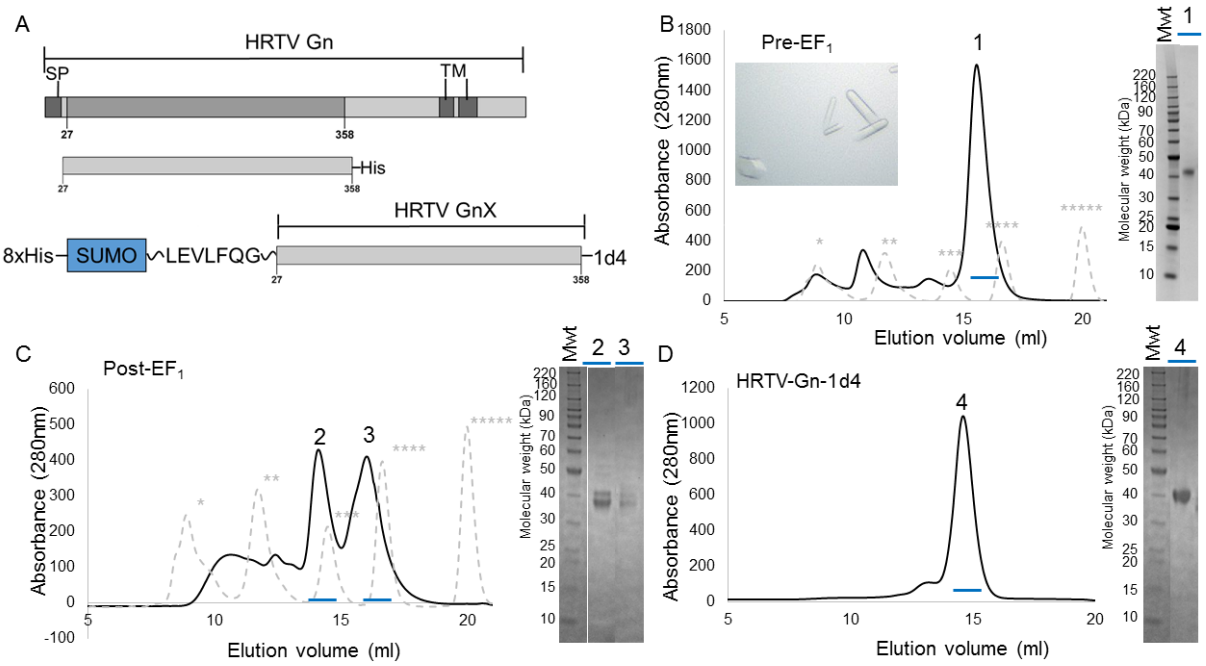

Figure 6.2 HRTV Gn was produced for crystallisation screening as well as immunisation, ELISA and antigen specific B cell sorting.
(A) Schematic of the HRTV Gn glycoprotein and the construct used for expression. The structure of HRTV Gn remains unknown and is therefore shown in grey. SP denotes the signal peptide and TM denotes the transmembrane regions. A C-terminal His-tag was used for purification and detection. A HRTV Gn-SUMO construct was generated for use in B cell sorting, where a protein without the His-tag was required. **(B)** HRTV Gn was expressed in the presence of kifunensine, a first round of size exclusion was performed and SDS-PAGE was used to assess the homogeneity and purity. Size standards are shown in grey dashed lines and asterisks mark the following sizes: * 670 kDa **158 kDa ***44 kDa ****17 kDa ****1.4 kDa. Right, SDS PAGE analysis of the resulting HRTV Gn protein evidenced incomplete deglycosylation (peaks labelled 2 and 3 on the SEC trace). Molecular weight markers are show (Mwt). Inset, crystals formed after 350 days in a condition containing 0.8 M succinic acid, pH 7.0. **(C)** Enzymatic glycosylation of HRTV Gn (produced in panel B) resulted in the generation of an additional peak of higher apparent molecular mass. SDS-PAGE analysis of the peaks labelled 1 and 2 indicate incomplete deglycosylation **(D)** HRTV Gn was also expressed with a SUMO tag. Post enzymatic removal of the sumo tag using 3C protease SEC was performed and the resulting peak (numbered 4) was analysed by SDS-PAGE.

Table 6.1. Summary of HRTV Gn preparations used for crystallisation screening.

Construct	Apparent Oligomeric state[#]	Enzymatic deglycosylation	Tag	Concentration (mg/ml)	Crystallisation screens/conditions
23–344	monomer	native*	1d4	14.0	5/480
23–344	monomer	native, HEK293S[&]	His	6.1	5/480
23–344	monomer	kifunensine^	His	9.5	12/1152
23–344	dimer/trimer	Kifunensine, EF_1[%]	His	4.5	4/384
23–344	dimer/trimer	kifunensine, EF_1[%]	His	7.3	6/576
23–344	monomer	kifunensine^	1d4	8.0	4/384
23–344	monomer	kifunensine, EF_1[%]	His	3.9	4/384
23–344	monomer	kifunensine^	His	5.0	10/960

[#] as assessed by SEC analysis
*HEK293T native glycosylation is complex and heterogeneous [151, 246-248]
& HEK293S GNTI$^-$ glycosylation produces Man5GlcNac2 glycoforms [249]
^ HEK293T and kifunensine treatment produces predominantly Man9GlcNac2 glycoforms [157]
% HEK293T, produced with kifunensine then enzymatically deglycosylated with EF_1 produces predominantly GlcNAc glycoforms [157].

6.4.1.1.3 Large-scale expression and purification of HRTV Gn for immunisation and antigen-specific B cell sorting

Expression trials were performed with the SUMO tag in order to generate protein with a cleavable His-Tag and to test for an increase in protein yield. Large-scale expression was performed in 2 L of HEK 293T cells in roller bottles (in the absence of kifunensine in an effort to maintain more native-like glycosylation) and then purified, as described for RVFV Gc-SUMO (Chapter 5, section **5.4.3**). The resulting protein appeared identical to its non-SUMO counterpart (His tagged HRTV Gn) in solution and yielded 2–3 mg per L cell culture **(Fig. 6.2, D).** The SUMO-derived HRTV Gn protein encodes the 1d4 tag instead of the His-tag, enabling antigen specific labelling for the subsequent B-cell sorting described below. This 1d4 tagged HRTV Gn was used in the immunisation, ELISA and antigen specific B cell sorting.

6.4.1.2 SFTSV Gn production for immunisation, ELISA and B cell isolation

The recently reported structure of SFTSV Gn [76] (PDB: 5Y10) was used to guide construct design of a soluble construct that could be used for immunisation and future structural studies

[76]. cDNA encoding SFTSV residues D21–342 was cloned into the pHLSec vector [145] and small-scale test expression analysis in HEK 293T cells revealed that the protein was successfully secreted. For large-scale expression, SFTSV Gn was transfected into HEK 293T cells in roller bottles. Cell supernatant was harvested 4–5 days post-transfection and buffer exchanged. SFTSV Gn was subsequently purified by IMAC and SEC **(Fig. 6.3)**. The yield of this protein was low (average of ~0.2–0.5 mg/L over independent purifications), however, sufficient sample quantity and quality was obtained for immunisation and ELISA experiments **(Fig. 6.3).**

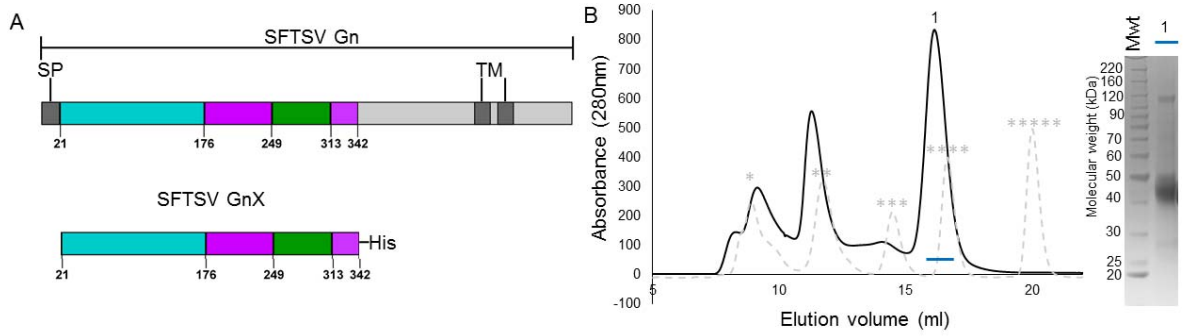

Figure 6.3 SFTSV Gn was produced for immunisation, ELISA and antigen specific B cell sorting.
(A) Schematic describing the construct used for SFTSV Gn. Upper shows the entire Gn protein organisation with domains coloured according to domain: (domain A is teal, domain B is green and the β ribbon is purple). SP denotes the signal peptide and TM denotes transmembrane domains. Below shows the construct used for expression which spans from G21 to N342 with a C-terminal His-tag for purification and detection. **(B)** Size exclusion chromatography was performed from 2L culture supernatant of construct Asp53-Asn356, size standards are shown in grey dashed lines and asterisks mark the following sizes: * 670 kDa **158 kDa ***44 kDa ****17k Da ****1.4 kDa. Inset, SDS PAGE analysis of the resulting SFTSV GnX protein as marked with blue line on SEC trace. Molecular weight markers are show (Mwt).

6.4.1.3 RVFV Gn production for immunisation, ELISA and B cell isolation

RVFV Gn was also used for a murine immunisation regime. The RVFV GnX was produced using the stable expression cell line reported in Chapter 5 and was used for immunisation, ELISA analysis and B cell sorting. The GnX construct was used as it matches the construct

range used for both SFTSV and HRTV Gn, and additionally immune responses to this C terminal truncated RVFV Gn have not yet been characterised. **(Chapter 5, Fig. 5.5, C)** details the protein used in this study.

6.4.2 Mice were immunised with recombinant phlebo- and banyangvirus Gn glycoprotein

The animal work described in this section was performed by the facility staff at PHE. 14 female BALB/c mice were immunised with 40 µg recombinant Gn at two-week intervals using the immunisation scheme presented in **(Fig. 6.4)**. Mice were divided into four groups, according to their immunisation regime. Group 1 consisted of four mice (numbered 1–4), immunised with RVFV Gn (GnX construct), boosted three times in two-week intervals. Group 2 consisted of four mice (numbered 5–8), each immunised with HRTV Gn, boosted three times. Due to an insufficient yield of protein **(Fig. 6.4)**, group 3 consisted of only three mice (numbered 9–11) immunised with SFTSV Gn and boosted only twice. The fourth and final group of three mice (numbered 12–14) were immunised once with SFTSV Gn, followed by HRTV Gn boosted three times. Proteins for immunisation were prepared in 10 mM Tris-pH 8.0, 150 mM NaCl, sterile filtered and adjuvanted with alum in a 1:1 vol/vol ratio immediately prior to injection. Mice were injected subcutaneously with a total volume of 100 µl. Serum samples were obtained prior to the first immunisation (bleed 1) and after the first boost (bleed 2). After bleed 2 (day 27), six mice were selected based on their response to glycoprotein immunogens, as assessed by a serum ELISA **(Fig. 6.5)**. Three mice were culled at day 41 (mouse 3, 6 and 10) and three at day 58 (mouse 7, 12 and 13) **(Fig. 6.4, C)**.

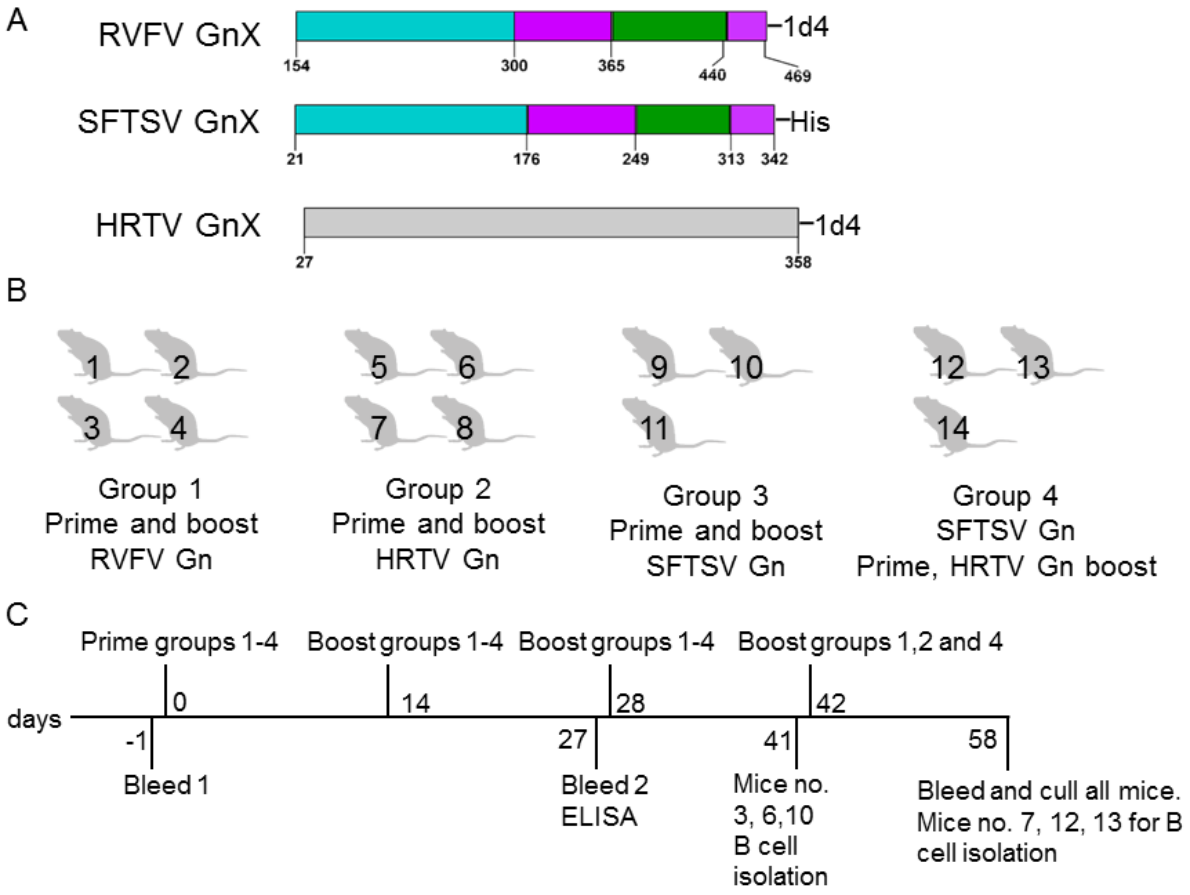

Figure 6.4 Mice were immunised with Gn glycoproteins.
(A) Schematic describing immunisation regimes. Protein constructs are displayed, where structural information is available domains are coloured (domain A in teal, domain B in green and the β ribbon in purple), unknown protein structure is depicted in grey. Domain and construct boundaries are numbered. The C-terminal tag present on each protein is also shown. **(B)** Group 1 consisted of four mice receiving three doses of 40 µg/mouse RVFV Gn, Group 2 consisted of four mice, each received three doses of 40 µg/mouse HRTV Gn, group 3 consisted three mice and received two doses of 40µg/mouse SFTSV Gn and group 4 consisted of three mice and received one dose of SFTSV Gn followed by two doses of HRTV Gn both at 40 µg/mouse. Proteins were adjuvanted in alum. Mouse identification numbers for each group are depicted by the number shown on each mouse. **(C)** Immunisation schedule.

6.4.3 A potent humoral immune response was elicited in mice

Immunogenicity and cross-reactivity resulting from the glycoprotein immunisation was assessed by ELISA analysis, performed by Dr Jeff Seow (Doores laboratory, KCL), using the proteins produced as described in this chapter. Serum was tested from bleed 2, (as depicted in **Fig. 6.5)**. These data were used to select mice for mAb isolation. All mice generated a strong response to the immunisation glycoprotein immunogen/s. The heterologous prime-boost

regime for SFTSV Gn and HRTV Gn (group 4, **Fig. 6.5, D)** resulted in a strong response to both SFTSV Gn and HRTV Gn, which was comparable to the response generated when using the single glycoprotein immunogens (group 2, **Fig. 6.5, B** and group 3, **Fig. 6.5, C)**. Additionally, serum from mice immunised with HRTV Gn alone was able to recognise SFTSV Gn and vice versa (group 2 **Fig. 6.5, B** and group 3, **Fig. 6.5, C)**. Surprisingly, two mice in group 4 mounted a response to RVFV Gn. Additionally, SFTSV Gn-immunised group 3 exhibited a weak immune response to RVFV Gn and RVFV Gn-immunised group 1 exhibited a weak immune response to SFTSV Gn. Further binding analysis from the terminal bleed will be performed to evaluate the effect of the second boost in groups 1, 2 and 4 and confirm the evidence of cross-reactivity observed from bleed 2. Future experiments with a larger study number would be useful to evaluate whether the prime-boost regime was beneficial in immunofocussing towards conserved epitopes across the virus species.

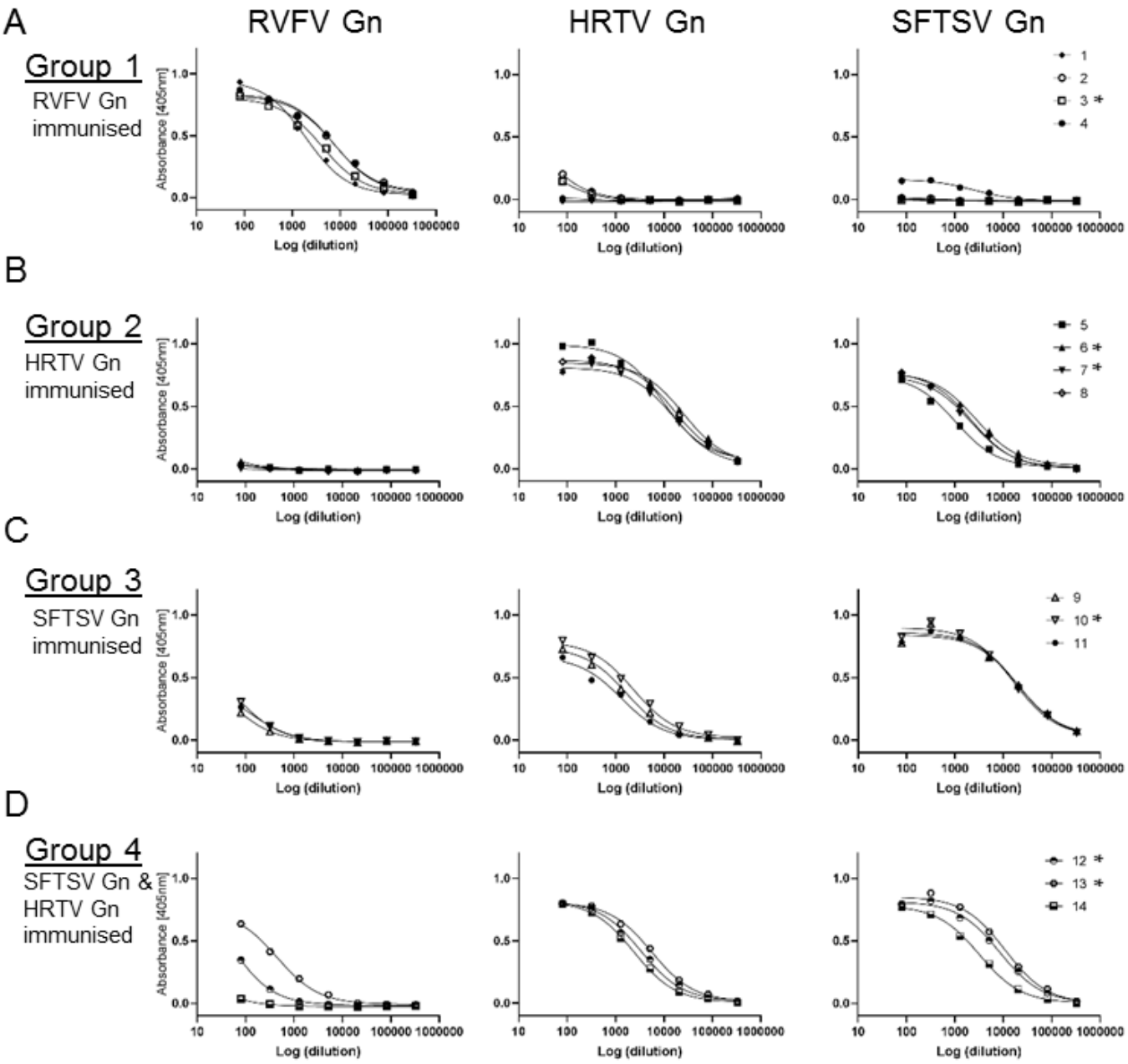

Figure 6.5 Immunisation with phleboviral Gn glycoproteins produces a robust antibody response.

Serum from each immunised mouse was used to test binding against RVFV Gn (left panel), HRTV Gn (centre panel) and SFTSV Gn (right panel),

(A) Serum from group 1 (RVFV Gn immunised) mice numbered 1-4 **(B)** Serum from group 2 (HRTV Gn immunised) mice numbered 5-8 **(C)** Serum from group 3 (SFTSV Gn immunised) mice numbered 9-11 **(D)** Serum from group 3 (SFTSV Gn prime and HRTV Gn boost) mice numbered 12-14.

Data are shown from bleed 2, results only performed as single dilutions (triplicate ELISA data from terminal bleed is in progress) ELISAs were performed by Dr Jeff Seow (KCL) using proteins produced in this thesis.

6.4.4 Single antigen-specific B cells were isolated by fluorescent associated cell sorting (FACS)

6.4.4.1 Gn glycoproteins were conjugated to fluorophores

To isolate single B cells displaying IgG specific to the Gn antigens from the spleens of the immunised mice, fluorescently-labelled Gn glycoproteins were generated for antigen-specific cell sorting **(Table 6.2)**. Multiple labelling strategies were employed to allow sorting of single B cells specific to more than one phenuivirus Gn antigen (i.e. looking for cells that bind to both SFTSV Gn and HRTV Gn, for example). Firstly, a FITC-conjugated anti-His mAb (emission: 520nm) was used to label Gn presenting a His-tag by incubation of fluorescent antibody with the glycoprotein. Secondly, lysine residues on the protein surface of RVFV Gn and HRTV Gn were non-specifically, chemically biotinylated (i.e. NHS-Sulfo linked biotinylation). Successful biotinylation was confirmed by western blot analysis using anti-biotin detection, and biotinylated Gn was labelled by incubation with anti-biotin APC (emission: 660nm). Although unavailable at the time of this experiment, a site specific biotinylation approach [145, 232] such as using AviTagged protein, would be optimal to ensure that biotinylation does not occlude or disrupt antibody epitopes.

Table 6.2. Fluorophores conjugated glycoproteins for antigen-specific B cell sorting

	APC conjugated	FITC conjugated
HRTV Gn	HRTV-Gn-1d4-BT **Fig. 6.2, D**	HRTV-Gn-His **Fig. 6.2, B**
SFTSV Gn	not available	SFTSV-Gn-His **Fig. 6.3, B**
RVFV Gn	RVFV-Gn-1d4-BT **Fig. 5.5, C**	RVFV-Gn-His **Fig. 5.2, A**

6.4.4.2 Gn specific single B cells were isolated by FACS

We sought to isolate mAbs that recognise the phlebovirus and banyangvirus Gn immunogens. Working with Dr Katie Doores, we used fluorescence activated cell-sorting (FACS) to identify

and isolate Gn-specific B cells. Spleens were isolated from mice identified to have a promising IgG response (as measured by ELISA) after the bleed 2 **(Fig. 6.5)**. The selected mice are detailed in **Table 6.3**. PBMCs were isolated from spleens by maceration and then incubated with fluorescently tagged protein(s) and antibodies, as detailed in **Table 6.2.** The gating strategy for B cell isolation is presented in **(Fig. 6.6)**. A naïve mouse spleen was also prepared with the FITC fluorescent Gn probes to assess non-specific binding of B cells to the probes **(Fig. 6.6, F)**. For all other fluorophores, compensation was run prior to the experiment, by members of the Doores lab. Sorting gates were defined in relation to the negative control and are presented in Appendix 1.7 and summarised in **Table 6.3**. Typically, 40–80 single B cells were isolated for each sort.

Table 6.3: Summary of B cell isolation strategy for each mouse

Mouse ID	Immunisation regime	Sort 1	Sort 2	Sort 3
3	RVFV Gn	RVFV-FITC		
6	HRTV Gn	HRTV- FITC		
7	HRTV Gn	SFTSV- FITC and HRTV-APC		
10	SFTSV Gn	HRTV- FITC	SFTSV- FITC	
12	HRTV Gn /SFTSV Gn	HRTV -APC and SFTSV-FITC		
13	HRTV Gn /SFTSV Gn	RVFV- FITC	HRTV- FITC	SFTSV- FITC

The FACS strategy confirmed the results obtained by serum binding ELISA, showing that a cross-reactive response was generated between the HRTV Gn and SFTSV Gn immunised groups. B cells were isolated that bound to fluorescent HRTV Gn and SFTSV Gn from mouse 7, 10, 12, and 13. These results will be confirmed by cloning the mAbs from single B cells then performing ELISA analysis with the purified mAbs, (**Fig. 6.7).**

Given the relatively high level of sequence conservation across the immunised Gn glycoprotein (63%), it is likely that antibodies isolated using HRTV Gn from mice immunised with SFTSV Gn (and vice versa) will be cross-reactive and able to bind glycoproteins present on both viruses.

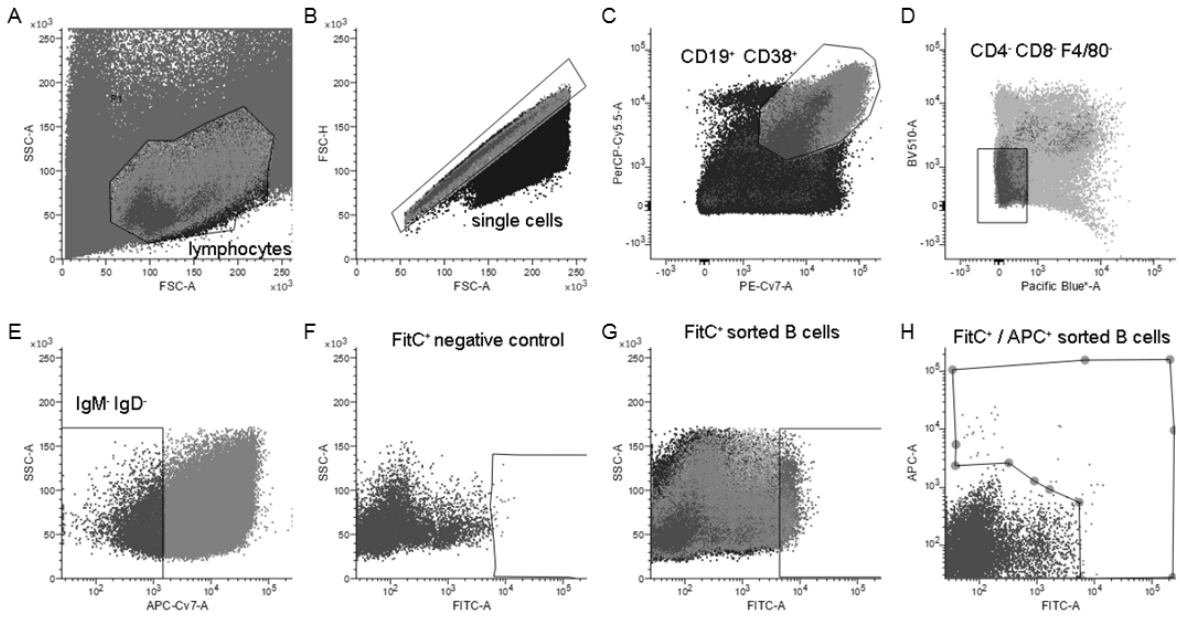

Figure 6. 6 Antigen specific single B cells were isolated using FACS.

Lymphocytes and single cells were identified according to their granularity and size as measured by the forward and side scatter (**A** and **B**). B cells were identified by expression of CD19 and CD38 **(C)**, and negative selection of CD4+, CD8+ T cells and F4/80+ macrophages **(D)**. IgM and IgD markers were used to ensure IgG specific B cells were selected **(E)**. The FITC negative control is shown, where a small amount of background is observed which falls within the gates for antigen specific B cell selection. This was used to set the gate for the Gn-binding B cells **(F)**. B cell selection gates are displayed for FITC+ **(G)** and FITC and APC+ **(H)**
(This figure depicts representatives, sorting details for each mouse are displayed in Appendix 1.7)

6.4.5 mAbs isolated from antigen specific B -cell sorting recognise SFTSV Gn and HRTV Gn

Further work is ongoing to isolate and characterise the mAbs obtained in the single B cell sorting regimes described in this chapter. Preliminary results are available from Dr Jeff Seow

(KCL), which indicate successful isolation of mAbs (from mouse 7 and 10) specific to SFTSV Gn, HRTV Gn or both SFTSV Gn and HRTV Gn, as assessed by ELISA **(Fig. 6.7)**. The characterisation of RVFV Gn-specific mAbs from mouse 3 is of relatively low priority, given that many such mAbs have already been characterised in Chapter 3 and 4 of this thesis. Additionally, further work is needed to verify the specificity of the RVFV-specific mAbs isolated from mouse 13.

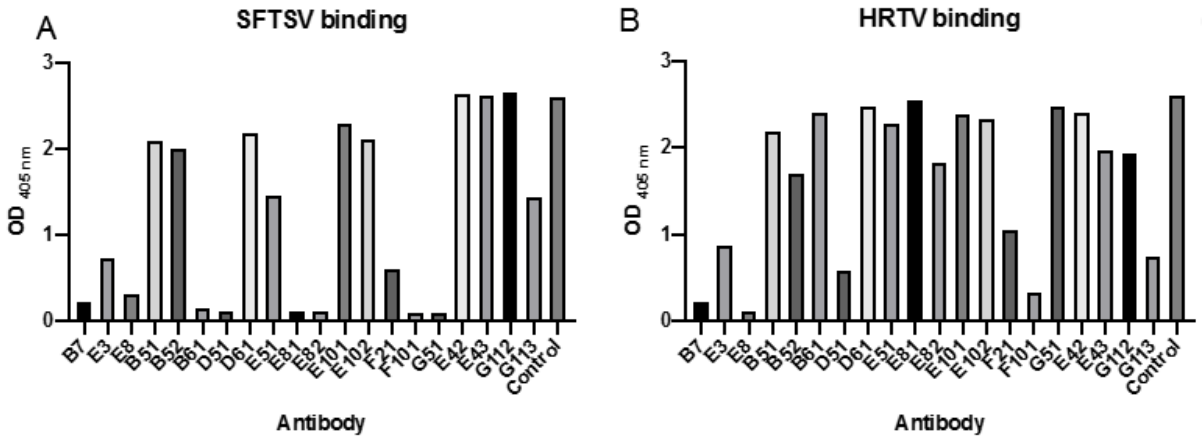

Figure 6. 7 mAbs were isolated which bind to HRTV Gn and SFTSV Gn.
mAbs were isolated from mice immunised with HRTV (mouse 7; antibodies B7, E3 and E8) and immunised with SFTSV Gn (mouse 10; all remaining antibodies B51-G113), and tested for their binding to SFTSV Gn **(A)** and HRTV Gn **(B)**.
Isolation, ELISA and figure performed and produced by Dr Jeff Seow, using Gn glycoproteins described in this chapter.

6.4.6 Domain A and the β-ribbon of the Gn present surfaces with the greatest level of sequence conservation between SFTSV Gn and HRTV Gn.

While future structural studies will be necessary to identify conserved and potentially neutralising epitopes on the phlebovirus and banyangvirus surface, I performed a structure-based sequence mapping approach to identify regions that exhibit the greatest level of identity and thus may constitute cross-reactive SFTSV and HRTV Gn epitopes. Amino acid sequences of SFTSV Gn and HRTV Gn were aligned and compared using the Multalin server [172]. The regions with the highest level of sequence identity appear to be distal to the regions where

neutralising epitopes have been identified on phenuivirus Gn glycoproteins [76, 150, 191]. Indeed, domain B, where mAb RV-Gn1–3 and mAb 4-5 (against SFTSV Gn) bind, appears to be the most sequence divergent (52% identity) region between HRTV and SFTSV Gn. In-line with this observation, examination of the SFTSV Gn–Fab 4-5 structure determined by *Wu et al* [76], reveals that only 8 of the 16 residues comprising the Fab 4-5 epitope are conserved with HRTV, suggestive that mAb 4-5 is unlikely to also neutralise HRTV. Interestingly, the region of the Gn exhibiting the highest level of sequence identity between SFTSV Gn and HRTV Gn is located in the β-ribbon domain, for which no mAbs have yet been shown to bind **(Fig. 6.8, A)**. Finally, given the low level of overall sequence identity, it seems unlikely that there may be epitopes conserved between RVFV Gn, SFTSV Gn and HRTV Gn **(Fig. 6.8, B)**. However, given that a cross-reactive RVFV Gn response was observed from one mouse which had been immunised with both HRTV Gn and SFTSV Gn **(Fig. 6.6, D),** the presence a small patch of residues conserved between these residues on the Gn surface, it would be worthwhile for this hypothesis to be tested in future investigations.

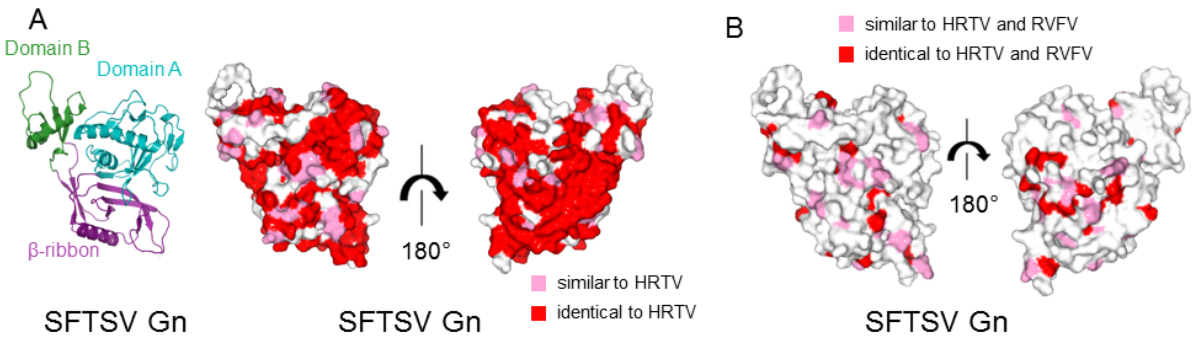

Figure 6.8 Sequence analysis of HRTV and SFTSV identifies patches of elevated conservation.
(A) SFTSV (PDB: 5Y10) domain organisation is depicted as a cartoon, with domain A coloured in teal, domain B coloured in green and the β- ribbon in purple. Sequence identity is plotted onto SFTSV Gn shown in surface representation. Residues shown in red are identical between HRTV and SFTSV, residues shown in pink differ, but have similar chemical properties and remaining non-conserved residues are shown in white. **(B)** As presented for (A), except sequence alignment is across HRTV, SFTSV and RVFV.
Sequence alignments were performed using Clustal [173].

6.5 Discussion

6.5.1 SFTSV Gn and HRTV Gn were produced with sufficient yield and purity for mouse immunisation

This chapter reports the expression and purification of banyangvirus glycoproteins in quantities and purity sufficient for crystallisation screening, immunisation, and mAb isolation. However, it should be noted that the experimental design for immunisation and mAb isolation was limited due to a low yield of SFTSV Gn, and more protein will be required for downstream experiments. Future production of this protein could be improved by adopting expression optimisation strategies, such as sumoylation and stable cell line generation, as performed for HRTV Gn (this chapter) and RVFV Gn/Gc (Chapter 5).

As the structure of HRTV Gn is unknown, purified protein was subjected to crystallisation screening. Ideally, a homogenous sample with limited or no glycosylation would be used. However, enzymatic deglycosylation with EF_1 resulted in only partial deglycosylation and the generation of higher order Gn oligomers **(Fig. 6.2, C)**, which are unlikely to represent biological assemblies on the virion [69, 250]. Alternative deglycosylation strategies should be implemented for HRTV Gn. For example the use of PNGaseF could be explored to assess if this approach results in complete deglycosylation and/or the formation of presumably undesirable higher oligomeric states of HRTV Gn [157]. Furthermore, increased crystallisation screening (e.g. at different temperatures) of HRTV presenting Man_5Glc_2 or Man_9Glc_2 glycosylation [151], may also provide a route to the identification of diffracting crystals.

RVFV Gn has been previously shown to generate a robust immune response (described in Chapter 3–5, and [110, 135, 138-140]. We further show that the RVFV GnX construct (lacking the C terminal amino acids 470–560) is also capable of generating a robust IgG response. At the time of writing, the use of HRTV Gn and SFTSV Gn glycoproteins as recombinant vaccine

candidates has not been reported [42]. This work is therefore the first to demonstrate that these proteins are capable of generating a robust IgG antibody response. It is important to note, however, that it has yet to be established whether this response is neutralising.

6.5.2 A cross reactive IgG response was generated against SFTSV Gn and HRTV Gn

Both ELISA and flow cytometry data indicate that a cross reactive antibody response was generated following our Gn immunisation. It did not appear that a heterologous prime-boost regime was required to generate cross-reactivity between HRTV Gn and SFTSV Gn and immunisation with Gn from one species generated IgGs able to detect of the second species' Gn **(Fig. 6.6).** Surprisingly, antibodies against RVFV Gn were detectable amongst some mice immunised solely with HRTV Gn and SFTSV Gn **(Fig. 6.6, D)**. This is surprising given that the neutralising mAb RV-Gn1 (described in Chapter 3) did not recognise SFTSV Gn, nor did the human anti-SFTSV mAb 4-5 recognise RVFV Gn. Indeed, there is only a 22% amino acid identity between SFTSV Gn and RVFV Gn (21% comparing Gn of HRTV and RVFV). By looking at the sequences of all three of the glycoproteins, I was able to identify a limited patch of conservation **(Fig. 6.8),** where I predict that such antibodies might bind. Attempts to isolate doubly and triply cross-reactive SFTSV, RVFV and HRTV Gn-specific mAbs is ongoing, and when combined with structural analysis, may reveal conserved sites of vulnerability that can be targeted in mAb based-antiviral and immunogen design efforts.

6.6 Conclusion and future directions

In this chapter, I have explored the use of SFTSV Gn and HRTV Gn as immunogens. I successfully produced recombinant protein for use in this study and we were able to generate an antibody response in mice. Antigen-specific B cell sorting resulted in hundreds of B cells for which mAb isolation could be performed. Experiments are ongoing to characterise their

sequence, binding affinities, and neutralisation potential. Further work will also aim to structurally characterise the epitopes targeted by these new reagents.

Although the aim of structurally characterising HRTV Gn has not been met, I am hopeful that the generation of mAbs that bind the glycoprotein may aid in crystallogenesis. Indeed, in Chapter 4, I demonstrated that complex formation of mAb RV-Gn4 with RVFV Gn resulted in crystals in less than 24 hours, which contrasts the many months required to form the unliganded crystal of RVFV Gn [69].

To follow up on the use of HRTV and SFTSV Gn as recombinant subunit vaccine candidates, an animal study of protection should be performed, whereby immunisation with recombinant glycoproteins would be followed by an infection with either RVFV, SFTSV or HRTV. Animal models of SFTSV infection have recently been developed [251-255], however, further work may be necessary to generate models of animal disease that mimic SFTSV and HRTV disease progression in humans [42].

Finally, the generation of SFTSV, RVFV and HRTV virus-like particles (VLP) would be highly beneficial to this line of work. Working with containment level 3 viruses requires specialist facilities and restrictive workflows, whereas the use of VLPs would enable us to perform FACS without a containment facility. This would increase the proportion of isolated mAbs that recognise the native assembly of glycoproteins on the virus surface.

Chapter 7
Conclusions and future directions

Chapter 7: Conclusions and future directions

7.1 Foreword

This final chapter brings together the results presented in the previous chapters. As each chapter had their own discussion section, I will focus on the impact of these findings when taken together. I will also discuss the future perspectives of this project and what they may bring to further the understanding of the immunological response to phlebo- and banyangviruses.

7.2 Summary

The first aim of this thesis was to use structural biology as an approach to characterise the immune response to recombinant RVFV Gn immunogen. This aim was successfully met, with the structural elucidation of a single neutralising epitope on domain B of RVFV Gn. This work was accepted for publication in *Cell Reports* in 2018, and was the first published structural description of a neutralising antibody against RVFV. In addition to the neutralising response, a further two related non-neutralising epitopes were identified on domain A of RVFV Gn. Together, these findings provide a blue-print for future vaccine design. Fortuitously, the structural characterisation of the non-neutralising antibody identified a domain rearrangement within the RVFV Gn that has not been described by our current understanding of the phlebovirus structure. We posit that the observed rearrangement of domain B is required for RV-Gn4 recognition and have shown binding RV-Gn4 to the mature virus suggesting this must occur.

The second aim of this thesis was to determine the structure of Gn from the pathogenic members of the Banyangviruses. Over the course of my studies the SFTSV Gn structure was published, therefore I focussed on HRTV Gn using a crystallographic approach. This aim has only been partially met. In Chapter 6, I presented crystals that had formed after 350 days. Data

collection from these crystals (occurring within two weeks prior to the submission of this thesis) yielded diffraction to ~3.2 Å. Elucidation of the HRTV Gn glycoprotein will build upon our current understanding of the antigenic similarities and differences across the banyangviruses.

The final aim of this thesis is assessing the immune response to a RVFV candidate vaccine and HRTV Gn and SFTSV Gn recombinant protein immunogens. For both of these projects successful generation of immunoglobulin reagents was performed. Anti RVFV Gn and Gc nanobodies were isolated. Anti-Gc neutralising nanobodies were identified, which will be the priority candidates to crystallise, as neutralising epitopes of the phlebovirus Gc have yet to have been structurally characterised. I demonstrated that a cross-reactive immune response was generated between SFTSV and HRTV. mAbs were isolated and future studies will aim to broaden the knowledge of neutralising and cross-reactive sites on the phlebovirus and banyangvirus surface.

7.3 Contributions to the structural characterisation of phenuivirus glycoproteins

Over the course of this doctoral project (2015-2019) the structural understanding of phlebovirus and banyangvirus glycoproteins has greatly expanded. The structural information available in 2015 consisted of cryo-EM maps of UUKV [250, 256] and RVFV [70] at 59 Å and 22 Å angstrom, respectively. These maps provided basic details of the viral envelope such as the overall pentameric and hexameric assemblies of Gn and Gc, however the orientation of glycoproteins could not be confidently placed within these, nor was a higher resolution structure of a phlebovirus Gn available for fitting. Of the Gn and Gc glycoproteins only the pre-fusion crystal structure of RVFV Gc was available [231]. At the time of writing, there are a further four crystal structures of the phenuivirus glycoproteins [73, 76, 257], a cryo-EM reconstruction of RVFV at 7.7–8.6 Å [69] and six structures of neutralising antibodies bound

to the Gn glycoprotein [76, 191]. Using X-ray crystallography, the work presented herein has contributed to the expanding field of structural studies of phenuiviruses in the following ways:

1. Characterisation of a protective epitope on RVFV Gn that implicates domain B as a site of vulnerability on the phlebovirus surface.

2. Structural characterisation of non-neutralising epitopes on RVFV Gn, reveal the intrinsic flexibility of domain B that may be important for virus-host cell interactions.

3. I recently obtained diffraction data which will elucidate the structure of HRTV Gn which will likely expand our appreciation of the antigenic surface of banyangviruses.

7.4 Future directions

7.4.1 Elucidating the mechanism of virus neutralisation and fusion

The results presented in this thesis have identified a neutralising epitope present on domain B of RVFV Gn. However, our study has yet to determine a mechanism of RVFV neutralisation. As the function of Gn is not well-characterised, structure-based hypotheses will require experimental validation. Nevertheless, I propose a potential mechanism based upon the structures of the neutralising and non-neutralising antibody response to RVFV, with some possible future experiments that may be able to test these hypotheses.

By considering the position of Gn domain B in the glycoprotein assembly on the viral surface, we note proximity to the fusion loops of RVFV Gc. Class II fusion proteins present on the surface of viruses often have a chaperone protein. Indeed, the domain topology of the phenuiviral Gn is most similar to that of Puumala virus Gn and Chikungunya virus E2 fusion protein, suggesting that the RVFV Gn may also act as a class II fusion chaperone [69]. We propose that RV-Gn1–3 may be preventing the rearrangements of RVFV Gn and Gc required

for unveiling the Gc-resident fusion loops. Indeed, we have shown that the RV-Gn4 antibody, which may induce or stabilise the 'open' position of RVFV Gn, allows virus propagation and entry *in vivo*, supporting the hypothesis that arrangements of domain B are required for uncovering the fusion loop of Gc and are involved in the dynamic process of fusion.

Ideally, the contribution of RVFV Gn in the viral fusion process would be investigated by cryo-EM using experiments similar to those performed by Halldorsson *et al* [69], whereby acidification of RVFV in the presence of lipid bilayer with which to fuse could be performed in the presence or absence of the monoclonal antibodies derived herein. These experiments, however, are non-trivial and come with many limitations, including capturing enough fusion events for a dataset large enough for structural characterisation at a sufficient resolution, and working with mAbs which are highly flexible and do not lend themselves well to structural characterisation with cryo-EM. Indeed, preliminary experiments performed with Fab fragment of RV-Gn2 for whole virus EM (performed by Dr Steiner Halldorsson, unpublished data) resulted in only partial resolution of the Fab, indicating flexibility and/or partial occupancy. Perhaps if one was determined to test this hypothesis using cryo-EM, panning for a nanobody which binds RVFV Gn domain B from the library presented in Chapter 5, and coupling it to a rigid, and large scaffold protein for generation of a cryo-EM suitable nanobody would be worth pursuing.

In light of the limitations of structurally characterising this interaction, I considered a different approach to elucidate the importance of domain B flexibility. As described in Chapter 4, I generated mutations in the RVFV Gn in an attempt to introduce a disulphide bond between domain A and domain B, and thereby lock Gn in the closed conformation. Although these structure guided mutations resulted in correctly folded secreted protein with the correct folding (determined by ELISA binding to the three classes of mAbs derived in this thesis), the

preliminary data thus far were neither able to confirm nor deny the presence of the engineered disulphide bond. Future work to generate a larger panel of potential mutations that generate a disulphide bond would hopefully result in mutant with a confirmed disulphide between domain A and B. To characterise if this mutation affected the flexibility of domain B as intended, small angle X-ray scattering (SAXS) [258] might be used to compare flexibility between the wild-type and mutated RVFV Gn.

Investigating the effects of conformation restricted RVFV Gn on the infectivity of RVFV will reveal the importance of domain B flexibility in the context of the virus lifecycle. A reverse genetics system for phenuiviruses has been described which could be used to investigate this [258] [60]. Indeed this technique was implemented to investigate the importance of the residues of the Gc-resident fusion loops [73], whereby the mutated viruses encoding site-directed mutations could not be rescued. If flexibility of Gn is required for fusion, the mutated virus with a conformationally locked Gn, will not be able to replicate *in vitro*.

7.4.2 Development of therapeutic mAbs

Generation of immunoglobulins by immunising animals with viral glycoproteins proved an effective, virus-free, and fast process, which could be applied in the event of a viral outbreak. Although we demonstrated RV-Gn1 had a protective effect when administered prior to viral infection we have yet to test its potential as a post-exposure treatment. These studies performed in animals would indicate the potential of RV-Gn1 to be developed as a therapeutic agent. Further development by exchanging the rabbit Fc with a human Fc would be required for its potential application in humans. Indeed, humanised antibodies (or antibody cocktails) are promising reagents for the treatment of emergent viral infections [131, 259].

In Chapter 5, I described the generation of a library of nanobodies which are able to neutralise RVFV by binding Gc. Although only preliminary crystallisation trials were performed due to

limited reagents, structural characterisation of the neutralising epitopes is tractable using the workflow described. Nanobodies may be not be attractive as therapeutic reagents, due to their relatively small size and lack of Fc region. However, when coupling two distinct nanobodies to a human IgG Fc region to generate a multi-domain antibody Laursen *et al* were able to increase potency, protective efficacy, and cross reactivity against Influenza A and B [230]. Thus this strategy may be applicable for generating a pan-phleboviral multi-domain antibody.

7.4.3 Improving immunogen and vaccine design

It is currently unknown if the non-neutralising mAb RV-Gn4 has protective efficacy. A mouse Fc chimeric RV-Gn4 has been developed by the Doores lab and will be tested in the coming months in a mouse model of RVFV infection. In the event that there is protective efficacy we would hope to structurally characterise this system to obtain mechanistic insight. However, if there is no effect upon the RVFV infection, then the non-productive antibody response could be minimised by future Gn immunogen design. Prevention of exposure to non-neutralising epitopes may improve the neutralising and protective immune response of Gn. Such immunofocussing could be achieved through protein engineering to introduce a disulphide bond as described above. Using recombinant phleboviral glycoproteins however will inevitably result in the exposure of non-native epitopes, (such as those sequestered by the quaternary lattice arrangement on native virions). Therefore, in order to minimise the generation of non-neutralising antibodies which bind non-native epitopes the immune system should be presented with the correct biological assembly, namely pentamers and hexamers of RVFV Gn and Gc for phleboviruses. Indeed, introducing inter-dimer disulphide bonds in the recombinant E-protein of Zika virus (ZIKV), was required to generate an antibody which recognised the dimer interface, which was cross-reactive between DENV and ZIKV and did not generate antibody

dependent enhancement [260]. An attractive vaccine strategy, which presents the higher-order biological assembly of RVFV Gn and Gc might be VLPs [238, 261] .

7.4.4 Characterising the immune response to HRTV Gn and SFTSV Gn

Although many of the aims of this thesis were met, I was unable to present a novel structure of the banyangviral Gn glycoprotein. Over the course of my studies, SFTSV Gn was reported by another group, yet the structure of HRTV Gn remains unknown. In the final fortnight of my doctoral project, I was finally able to obtain X-ray diffraction data for HRTV Gn. Unfortunately, there was insufficient time to process and refine the data to an acceptable quality for presentation herein. Structure solution and refinement is therefore a future priority.

At the time of writing the use of HRTV and SFTSV Gn recombinant glycoproteins as immunogens has not been reported. We have shown that these proteins are able to generate a humoral antibody response, which may be protective against banyangvirus infection. A potential aspect for future research would be an animal study of protection, whereby immunisation with recombinant glycoproteins would be followed up by an infection with either RVFV, SFTSV or HRTV. These experiments might indicate the success or limitations of the heterologous prime-boost regime used in this thesis.

7.5 Final concluding remarks

The experiments and analyses performed in this thesis have revealed novel structural and functional insights into the immune response to phlebo- and banyangviruses. The identification of a neutralising epitopes on RVFV Gn represents an important advancement that may influence the generation of future therapeutics. The discovery of a flexible region on RVFV Gn may provide biological insight on the process of phleboviral host-cell entry and constitutes a potentially novel target for immunogen design. Although there has been a recent spark in

interest in this area, the structural characterisation of the phlebo/banyangviral surface remains an important avenue for future research. I hope that in determining the structure of HRTV Gn, and in isolating mAbs against both HRTV Gn and SFTSV Gn, we may identify important immunological sites that can be targeted across pathogenic phenuiviruses more generally. I hope the work presented herein will be valuable for the field of phenuiviruses.

Bibliography

1. Suttle, C.A., *Viruses in the sea.* Nature, 2005. **437**(7057): p. 356-61.
2. Breitbart, M. and F. Rohwer, *Here a virus, there a virus, everywhere the same virus?* Trends in Microbiology, 2005. **13**(6): p. 278-284.
3. Drake, J.W. and J.J. Holland, *Mutation rates among RNA viruses.* Proceedings of the National Academy of Sciences of the United States of America, 1999. **96**(24): p. 13910-13913.
4. Duffy, S., L.A. Shackelton, and E.C. Holmes, *Rates of evolutionary change in viruses: patterns and determinants.* Nature Reviews Genetics, 2008. **9**(4): p. 267-276.
5. Nichol, S.T., J. Arikawa, and Y. Kawaoka, *Emerging viral diseases.* Proceedings of the National Academy of Sciences of the United States of America, 2000. **97**(23): p. 12411-12412.
6. Gurley, E.S., et al., *Person-to-person transmission of Nipah virus in a Bangladeshi community.* Emerging Infectious Diseases, 2007. **13**(7): p. 1031-1037.
7. Lawrence, P., et al., *Human transmission of Ebola virus.* Current Opinion in Virology, 2017. **22**: p. 51-58.
8. Herfst, S., et al., *Drivers of airborne human-to-human pathogen transmission.* Current Opinion in Virology, 2017. **22**: p. 22-29.
9. Kilpatrick, A.M. and S.E. Randolph, *Drivers, dynamics, and control of emerging vector-borne zoonotic diseases.* Lancet, 2012. **380**(9857): p. 1946-1955.
10. Li, C.X., et al., *Unprecedented genomic diversity of RNA viruses in arthropods reveals the ancestry of negative-sense RNA viruses.* Elife, 2015. **4**.
11. Bae, S.E. and H.S. Son, *Classification of viral zoonosis through receptor pattern analysis.* Bmc Bioinformatics, 2011. **12**.
12. Krause, R.M., *The Origin of Plagues - Old and New.* Science, 1992. **257**(5073): p. 1073-1078.
13. Wever, P.C. and L. van Bergen, *Death from 1918 pandemic influenza during the First World War: a perspective from personal and anecdotal evidence.* Influenza and Other Respiratory Viruses, 2014. **8**(5): p. 538-546.
14. Angeletti, S., et al., *Molecular epidemiology and phylogeny of Nipah virus infection: A mini review.* Asian Pacific Journal of Tropical Medicine, 2016. **9**(7): p. 610-615.
15. Baud, D., et al., *An update on Zika virus infection.* Lancet, 2017. **390**(10107): p. 2099-2109.
16. de Wit, E., et al., *SARS and MERS: recent insights into emerging coronaviruses.* Nature Reviews Microbiology, 2016. **14**(8): p. 523-534.
17. Holmes, E.C., et al., *The evolution of Ebola virus: Insights from the 2013-2016 epidemic.* Nature, 2016. **538**(7624): p. 193-200.
18. Jones, K.E., et al., *Global trends in emerging infectious diseases.* Nature, 2008. **451**(7181): p. 990-U4.
19. Parvez, M.K. and S. Parveen, *Evolution and Emergence of Pathogenic Viruses: Past, Present, and Future.* Intervirology, 2017. **60**(1-2): p. 1-7.
20. Elliott, R.M. and B. Brennan, *Emerging phleboviruses.* Current Opinion in Virology, 2014. **5**: p. 50-57.
21. Adams, M.J., et al., *Changes to taxonomy and the International Code of Virus Classification and Nomenclature ratified by the International Committee on Taxonomy of Viruses (2017).* Arch Virol, 2017. **162**(8): p. 2505-2538.
22. Matsuno, K., et al., *The Unique Phylogenetic Position of a Novel Tick-Borne Phlebovirus Ensures an Ixodid Origin of the Genus Phlebovirus.* Msphere, 2018. **3**(3).
23. Daubney, R., J.R. Hudson, and P.C. Garnham, *Enzootic hepatitis of Rift Valley Fever, an undescriptible virus disease of sheep, cattle and man from East Africa. .* Journal of Pathology and Bacteriology, 1931. **34**(4): p. 543-79.
24. Al-Hazmi, M., et al., *Epidemic Rift Valley fever in Saudi Arabia: a clinical study of severe illness in humans.* Clin Infect Dis, 2003. **36**(3): p. 245-52.
25. Sow, A., et al., *Rift Valley fever outbreak, southern Mauritania, 2012.* Emerg Infect Dis, 2014. **20**(2): p. 296-9.
26. Mohamed, M., et al., *Epidemiologic and clinical aspects of a Rift Valley fever outbreak in humans in Tanzania, 2007.* Am J Trop Med Hyg, 2010. **83**(2 Suppl): p. 22-7.

27. Clark, M.H.A., et al., *Systematic literature review of Rift Valley fever virus seroprevalence in livestock, wildlife and humans in Africa from 1968 to 2016.* Plos Neglected Tropical Diseases, 2018. **12**(7).
28. Ikegami, T. and S. Makino, *The Pathogenesis of Rift Valley Fever.* Viruses-Basel, 2011. **3**(5): p. 493-519.
29. Wright, D., et al., *Rift Valley fever: biology and epidemiology.* J Gen Virol, 2019. **100**(8): p. 1187-1199.
30. Peyre, M., et al., *A Systematic Scoping Study of the Socio-Economic Impact of Rift Valley Fever: Research Gaps and Needs.* Zoonoses and Public Health, 2015. **62**(5): p. 309-325.
31. El Mamy, A.B., et al., *Unexpected Rift Valley fever outbreak, northern Mauritania.* Emerg Infect Dis, 2011. **17**(10): p. 1894-6.
32. Nguku, P.M., et al., *An Investigation of a Major Outbreak of Rift Valley Fever in Kenya: 2006-2007.* American Journal of Tropical Medicine and Hygiene, 2010. **83**(2): p. 5-13.
33. *An outbreak of Rift Valley Fever, eastern Africa, 1997-1998.* Can Commun Dis Rep, 1998. **24**(12): p. 101-4.
34. Lumley, S., et al., *Rift Valley fever virus: strategies for maintenance, survival and vertical transmission in mosquitoes.* J Gen Virol, 2017. **98**(5): p. 875-887.
35. Nicholas, D.E., K.H. Jacobsen, and N.M. Waters, *Risk factors associated with human Rift Valley fever infection: systematic review and meta-analysis.* Tropical Medicine & International Health, 2014. **19**(12): p. 1420-1429.
36. Turell, M.J., et al., *Potential for Stable Flies and House Flies (Diptera: Muscidae) to Transmit Rift Valley Fever Virus.* Journal of the American Mosquito Control Association, 2010. **26**(4): p. 445-448.
37. Turell, M.J., et al., *Potential for Psorophora columbiae and Psorophora ciliata Mosquitoes (Diptera: Culicidae) to Transmit Rift Valley Fever Virus.* Journal of Medical Entomology, 2015. **52**(5): p. 1111-1116.
38. Golnar, A.J., R.C. Kading, and G.L. Hamer, *Quantifying the potential pathways and locations of Rift Valley fever virus entry into the United States.* Transboundary and Emerging Diseases, 2018. **65**(1): p. 85-95.
39. Golnar, A.J., et al., *Predicting the Mosquito Species and Vertebrate Species Involved in the Theoretical Transmission of Rift Valley Fever Virus in the United States.* Plos Neglected Tropical Diseases, 2014. **8**(9).
40. Yu, X.J., et al., *Fever with Thrombocytopenia Associated with a Novel Bunyavirus in China.* New England Journal of Medicine, 2011. **364**(16): p. 1523-1532.
41. Zhang, Y.Z., et al., *Hemorrhagic fever caused by a novel Bunyavirus in China: pathogenesis and correlates of fatal outcome.* Clin Infect Dis, 2012. **54**(4): p. 527-33.
42. Reece, L.M., et al., *Current status of Severe Fever with Thrombocytopenia Syndrome vaccine development.* Curr Opin Virol, 2018. **29**: p. 72-78.
43. Lohmeyer, K.H., et al., *Distribution of Rhipicephalus (Boophilus) microplus and Rhipicephalus (Boophilus) annulatus (Acari: Ixodidae) infestations detected in the United States along the Texas/Mexico border.* J Med Entomol, 2011. **48**(4): p. 770-4.
44. Matsuu, A., et al., *Natural severe fever with thrombocytopenia syndrome virus infection in domestic cats in Japan.* Vet Microbiol, 2019. **236**: p. 108346.
45. Yun, S.M., et al., *Severe fever with thrombocytopenia syndrome virus in ticks collected from humans, South Korea, 2013.* Emerg Infect Dis, 2014. **20**(8): p. 1358-61.
46. Wang, S., et al., *SFTS virus in ticks in an endemic area of China.* Am J Trop Med Hyg, 2015. **92**(4): p. 684-9.
47. Hayasaka, D., et al., *Seroepidemiological evidence of severe fever with thrombocytopenia syndrome virus infections in wild boars in Nagasaki, Japan.* Trop Med Health, 2016. **44**: p. 6.
48. Oh, S.S., et al., *Detection of Severe Fever with Thrombocytopenia Syndrome Virus from Wild Animals and Ixodidae Ticks in the Republic of Korea.* Vector Borne Zoonotic Dis, 2016. **16**(6): p. 408-14.
49. Tang, X.Y., et al., *Human-to-Human Transmission of Severe Fever With Thrombocytopenia Syndrome Bunyavirus Through Contact With Infectious Blood.* Journal of Infectious Diseases, 2013. **207**(5): p. 736-739.

50. Zhan, J.B., et al., *Current status of severe fever with thrombocytopenia syndrome in China.* Virologica Sinica, 2017. **32**(1): p. 51-62.
51. Choi, S.J., et al., *Severe Fever with Thrombocytopenia Syndrome in South Korea, 2013-2015.* PLoS Negl Trop Dis, 2016. **10**(12): p. e0005264.
52. Kato, H., et al., *Epidemiological and Clinical Features of Severe Fever with Thrombocytopenia Syndrome in Japan, 2013-2014.* PLoS One, 2016. **11**(10): p. e0165207.
53. Takahashi, T., et al., *The First Identification and Retrospective Study of Severe Fever With Thrombocytopenia Syndrome in Japan.* Journal of Infectious Diseases, 2014. **209**(6): p. 816-827.
54. McMullan, L.K., et al., *A new phlebovirus associated with severe febrile illness in Missouri.* N Engl J Med, 2012. **367**(9): p. 834-41.
55. Brault, A.C., et al., *Heartland Virus Epidemiology, Vector Association, and Disease Potential.* Viruses-Basel, 2018. **10**(9).
56. Savage, H.M., et al., *First Detection of Heartland Virus (Bunyaviridae: Phlebovirus) from Field Collected Arthropods.* American Journal of Tropical Medicine and Hygiene, 2013. **89**(3): p. 445-452.
57. Riemersma, K.K. and N. Komar, *Heartland Virus Neutralizing Antibodies in Vertebrate Wildlife, United States, 2009-2014.* Emerg Infect Dis, 2015. **21**(10): p. 1830-3.
58. de Carvalho, M.S., et al., *Viola phlebovirus is a novel Phlebotomus fever serogroup member identified in Lutzomyia (Lutzomyia) longipalpis from Brazilian Pantanal.* Parasites & Vectors, 2018. **11**.
59. Alkan, C., et al., *Sandfly-Borne Phlebovirus Isolations from Turkey: New Insight into the Sandfly fever Sicilian and Sandfly fever Naples Species.* Plos Neglected Tropical Diseases, 2016. **10**(3).
60. Bouloy, M., et al., *Genetic evidence for an interferon-antagonistic function of rift valley fever virus nonstructural protein NSs.* J Virol, 2001. **75**(3): p. 1371-7.
61. Billecocq, A., et al., *NSs protein of Rift Valley fever virus blocks interferon production by inhibiting host gene transcription.* J Virol, 2004. **78**(18): p. 9798-806.
62. Le May, N., et al., *A SAP30 complex inhibits IFN-beta expression in Rift valley fever virus infected cells.* Plos Pathogens, 2008. **4**(1).
63. Habjan, M., et al., *NSs Protein of Rift Valley Fever Virus Induces the Specific Degradation of the Double-Stranded RNA-Dependent Protein Kinase.* Journal of Virology, 2009. **83**(9): p. 4365-4375.
64. Ikegami, T., et al., *Rift Valley Fever Virus NSs Protein Promotes Post-Transcriptional Downregulation of Protein Kinase PKR and Inhibits eIF2 alpha Phosphorylation.* Plos Pathogens, 2009. **5**(2).
65. Terasaki, K., S. Won, and S. Makino, *The C-Terminal Region of Rift Valley Fever Virus NSm Protein Targets the Protein to the Mitochondrial Outer Membrane and Exerts Antiapoptotic Function.* Journal of Virology, 2013. **87**(1): p. 676-682.
66. Gerrard, S.R., et al., *The NSm proteins of Rift Valley fever virus are dispensable for maturation, replication and infection.* Virology, 2007. **359**(2): p. 459-465.
67. Weingartl, H.M., et al., *Rift Valley Fever Virus Incorporates the 78 kDa Glycoprotein into Virions Matured in Mosquito C6/36 Cells.* Plos One, 2014. **9**(1).
68. Kreher, F., et al., *The Rift Valley fever accessory proteins NSm and P78/NSm-GN are distinct determinants of virus propagation in vertebrate and invertebrate hosts.* Emerg Microbes Infect, 2014. **3**(10): p. e71.
69. Halldorsson, S., et al., *Shielding and activation of a viral membrane fusion protein.* Nat Commun, 2018. **9**(1): p. 349.
70. Huiskonen, J.T., et al., *Electron cryo-microscopy and single-particle averaging of Rift Valley fever virus: evidence for GN-GC glycoprotein heterodimers.* J Virol, 2009. **83**(8): p. 3762-9.
71. Freiberg, A.N., et al., *Three-dimensional organization of Rift Valley fever virus revealed by cryoelectron tomography.* J Virol, 2008. **82**(21): p. 10341-8.
72. Sherman, M.B., et al., *Single-particle cryo-electron microscopy of Rift Valley fever virus.* Virology, 2009. **387**(1): p. 11-5.

73. Halldorsson, S., et al., *Structure of a phleboviral envelope glycoprotein reveals a consolidated model of membrane fusion.* Proc Natl Acad Sci U S A, 2016. **113**(26): p. 7154-9.
74. Modis, Y., et al., *Structure of the dengue virus envelope protein after membrane fusion.* Nature, 2004. **427**(6972): p. 313-319.
75. Gibbons, D.L., et al., *Conformational change and protein protein interactions of the fusion protein of Semliki Forest virus.* Nature, 2004. **427**(6972): p. 320-325.
76. Wu, Y., et al., *Structures of phlebovirus glycoprotein Gn and identification of a neutralizing antibody epitope.* Proc Natl Acad Sci U S A, 2017. **114**(36): p. E7564-E7573.
77. Voss, J.E., et al., *Glycoprotein organization of Chikungunya virus particles revealed by X-ray crystallography.* Nature, 2010. **468**(7324): p. 709-U137.
78. Ge, P. and Z.H. Zhou, *Chaperone fusion proteins aid entropy-driven maturation of class II viral fusion proteins.* Trends in Microbiology, 2014. **22**(2): p. 100-106.
79. Li, S., et al., *A Molecular-Level Account of the Antigenic Hantaviral Surface.* Cell Reports, 2016. **15**(5): p. 959-967.
80. Strandin, T., J. Hepojoki, and A. Vaheri, *Cytoplasmic tails of bunyavirus Gn glycoproteins-Could they act as matrix protein surrogates?* Virology, 2013. **437**(2): p. 73-80.
81. Overby, A.K., R.F. Pettersson, and E.P.A. Neve, *The glycoprotein cytoplasmic tail of Uukuniemi virus (Bunyaviridae) interacts with ribonucleoproteins and is critical for genome packaging.* Journal of Virology, 2007. **81**(7): p. 3198-3205.
82. Phoenix, I., et al., *N-Glycans on the Rift Valley Fever Virus Envelope Glycoproteins Gn and Gc Redundantly Support Viral Infection via DC-SIGN.* Viruses-Basel, 2016. **8**(5).
83. Crispin, M., et al., *Uukuniemi Phlebovirus Assembly and Secretion Leave a Functional Imprint on the Virion Glycome.* Journal of Virology, 2014. **88**(17): p. 10244-10251.
84. Svajger, U., et al., *C-type lectin DC-SIGN: An adhesion, signalling and antigen-uptake molecule that guides dendritic cells in immunity.* Cellular Signalling, 2010. **22**(10): p. 1397-1405.
85. Hofmann, H., et al., *Severe Fever with Thrombocytopenia Virus Glycoproteins Are Targeted by Neutralizing Antibodies and Can Use DC-SIGN as a Receptor for pH-Dependent Entry into Human and Animal Cell Lines.* Journal of Virology, 2013. **87**(8): p. 4384-4394.
86. Lozach, P.Y., et al., *DC-SIGN as a Receptor for Phleboviruses.* Cell Host & Microbe, 2011. **10**(1): p. 75-88.
87. Spiegel, M., T. Plegge, and S. Pohlmann, *The Role of Phlebovirus Glycoproteins in Viral Entry, Assembly and Release.* Viruses, 2016. **8**(7).
88. Sun, Y.Y., et al., *Nonmuscle Myosin Heavy Chain IIA Is a Critical Factor Contributing to the Efficiency of Early Infection of Severe Fever with Thrombocytopenia Syndrome Virus.* Journal of Virology, 2014. **88**(1): p. 237-248.
89. Silvas, J.A., et al., *Extracellular Vesicles Mediate Receptor-Independent Transmission of Novel Tick-Borne Bunyavirus.* J Virol, 2016. **90**(2): p. 873-86.
90. Harmon, B., et al., *Rift Valley Fever Virus Strain MP-12 Enters Mammalian Host Cells via Caveola-Mediated Endocytosis.* Journal of Virology, 2012. **86**(23): p. 12954-12970.
91. Lozach, P.Y., et al., *Entry of Bunyaviruses into Mammalian Cells.* Cell Host & Microbe, 2010. **7**(6): p. 488-499.
92. Melin, L., et al., *The membrane glycoprotein G1 of Uukuniemi virus contains a signal for localization to the Golgi complex.* Virus Res, 1995. **36**(1): p. 49-66.
93. Mir, M.A. and A.T. Panganiban, *The bunyavirus nucleocapsid protein is an RNA chaperone: Possible roles in viral RNA panhandle formation and genome replication.* Rna, 2006. **12**(2): p. 272-282.
94. de Boer, S.M., et al., *Acid-Activated Structural Reorganization of the Rift Valley Fever Virus Gc Fusion Protein.* Journal of Virology, 2012. **86**(24): p. 13642-13652.
95. Plegge, T., et al., *Evidence that Processing of the Severe Fever with Thrombocytopenia Syndrome Virus Gn/Gc Polyprotein Is Critical for Viral Infectivity and Requires an Internal Gc Signal Peptide.* Plos One, 2016. **11**(11).
96. Ulmanen, I., P. Seppala, and R.F. Pettersson, *Invitro Translation of Uukuniemi Virus-Specific Rnas - Identification of a Nonstructural Protein and a Precursor to the Membrane-Glycoproteins.* Journal of Virology, 1981. **37**(1): p. 72-79.

97. Gerrard, S.R. and S.T. Nichol, *Characterization of the Golgi retention motif of Rift Valley fever virus G(N) glycoprotein.* Journal of Virology, 2002. **76**(23): p. 12200-12210.
98. Melin, L., et al., *The Membrane Glycoprotein G1 of Uukuniemi Virus Contains a Signal for Localization to the Golgi-Complex.* Virus Research, 1995. **36**(1): p. 49-66.
99. Piper, M.E., D.R. Sorenson, and S.R. Gerrard, *Efficient Cellular Release of Rift Valley Fever Virus Requires Genomic RNA.* Plos One, 2011. **6**(3).
100. Weber, F. and R.M. Elliott, *Bunyaviruses and Innate Immunity.* Cellular Signaling and Innate Immune Responses to Rna Virus Infections, 2009: p. 287-299.
101. Qu, B., et al., *Suppression of the interferon and NF-kappaB responses by severe fever with thrombocytopenia syndrome virus.* J Virol, 2012. **86**(16): p. 8388-401.
102. Bird, B.H. and S.T. Nichol, *Breaking the chain: Rift Valley fever virus control via livestock vaccination.* Current Opinion in Virology, 2012. **2**(3): p. 315-323.
103. Madani, T.A., et al., *Rift Valley fever epidemic in Saudi Arabia: Epidemiological, clinical, and laboratory characteristics.* Clinical Infectious Diseases, 2003. **37**(8): p. 1084-1092.
104. Sabin, A.B. and R.W. Blumberg, *Human infection with Rift Valley fever virus and immunity twelve years after single attack.* Proc Soc Exp Biol Med, 1947. **64**(4): p. 385-9.
105. Bosco-Lauth, A.M., et al., *Vertebrate Host Susceptibility to Heartland Virus.* Emerging Infectious Diseases, 2016. **22**(12): p. 2070-2077.
106. Fernandez, J.C., et al., *The Nonstructural Protein NSs Induces a Variable Antibody Response in Domestic Ruminants Naturally Infected with Rift Valley Fever Virus.* Clinical and Vaccine Immunology, 2012. **19**(1): p. 5-10.
107. Lorenzo, G., et al., *Protection against lethal Rift Valley fever virus (RVFV) infection in transgenic IFNAR(-/-) mice induced by different DNA vaccination regimens.* Vaccine, 2010. **28**(17): p. 2937-2944.
108. Besselaar, T.G. and N.K. Blackburn, *The effect of neutralizing monoclonal antibodies on early events in Rift Valley fever virus infectivity.* Res Virol, 1994. **145**(1): p. 13-9.
109. Besselaar, T.G. and N.K. Blackburn, *The synergistic neutralization of Rift Valley fever virus by monoclonal antibodies to the envelope glycoproteins.* Arch Virol, 1992. **125**(1-4): p. 239-50.
110. Faburay, B., et al., *Current Status of Rift Valley Fever Vaccine Development.* Vaccines (Basel), 2017. **5**(3).
111. Faburay, B., et al., *Development of a sheep challenge model for Rift Valley fever.* Virology, 2016. **489**: p. 128-40.
112. Labeaud, D., *Towards a safe, effective vaccine for Rift Valley fever virus.* Future Virol, 2010. **5**(6): p. 675-678.
113. Harmon, J.R., et al., *CD4 T Cells, CD8 T Cells, and Monocytes Coordinate To Prevent Rift Valley Fever Virus Encephalitis.* J Virol, 2018. **92**(24).
114. Doria-Rose, N.A. and M.G. Joyce, *Strategies to guide the antibody affinity maturation process.* Curr Opin Virol, 2015. **11**: p. 137-47.
115. Sok, D., et al., *The effects of somatic hypermutation on neutralization and binding in the PGT121 family of broadly neutralizing HIV antibodies.* PLoS Pathog, 2013. **9**(11): p. e1003754.
116. Jennewein, M.F. and G. Alter, *The Immunoregulatory Roles of Antibody Glycosylation.* Trends Immunol, 2017. **38**(5): p. 358-372.
117. Beck, A., et al., *Strategies and challenges for the next generation of therapeutic antibodies.* Nat Rev Immunol, 2010. **10**(5): p. 345-52.
118. Hiatt, A., et al., *Glycan variants of a respiratory syncytial virus antibody with enhanced effector function and in vivo efficacy.* Proc Natl Acad Sci U S A, 2014. **111**(16): p. 5992-7.
119. El Bakkouri, K., et al., *Universal vaccine based on ectodomain of matrix protein 2 of influenza A: Fc receptors and alveolar macrophages mediate protection.* J Immunol, 2011. **186**(2): p. 1022-31.
120. Parsons, M.S., A.W. Chung, and S.J. Kent, *Importance of Fc-mediated functions of anti-HIV-1 broadly neutralizing antibodies.* Retrovirology, 2018. **15**.
121. Horwitz, J.A., et al., *Non-neutralizing Antibodies Alter the Course of HIV-1 Infection In Vivo.* Cell, 2017. **170**(4): p. 637-+.

122. Mayr, L.M., B. Su, and C. Moog, *Non-Neutralizing Antibodies Directed against HIV and Their Functions.* Frontiers in Immunology, 2017. **8**.
123. Dunand, C.J.H., et al., *Both Neutralizing and Non-Neutralizing Human H7N9 Influenza Vaccine-Induced Monoclonal Antibodies Confer Protection.* Cell Host & Microbe, 2016. **19**(6): p. 800-813.
124. Bootz, A., et al., *Protective capacity of neutralizing and non-neutralizing antibodies against glycoprotein B of cytomegalovirus.* Plos Pathogens, 2017. **13**(8).
125. Kelton, W., et al., *IgGA: A "Cross-Isotype" Engineered Human Fc Antibody Domain that Displays Both IgG-like and IgA-like Effector Functions.* Chemistry & Biology, 2014. **21**(12): p. 1603-1609.
126. Correia, B.E., et al., *Proof of principle for epitope-focused vaccine design.* Nature, 2014. **507**(7491): p. 201-206.
127. Jiang, L.W., et al., *Potent Neutralization of MERS-CoV by Human Neutralizing Monoclonal Antibodies to the Viral Spike Glycoprotein.* Science Translational Medicine, 2014. **6**(234).
128. Tang, X.C., et al., *Identification of human neutralizing antibodies against MERS-CoV and their role in virus adaptive evolution.* Proceedings of the National Academy of Sciences of the United States of America, 2014. **111**(19): p. 6863-6863.
129. Ying, T.L., et al., *Exceptionally Potent Neutralization of Middle East Respiratory Syndrome Coronavirus by Human Monoclonal Antibodies.* Journal of Virology, 2014. **88**(14): p. 7796-7805.
130. Chaisri, U. and W. Chaicumpa, *Evolution of Therapeutic Antibodies, Influenza Virus Biology, Influenza, and Influenza Immunotherapy.* Biomed Research International, 2018.
131. Qiu, X.G., et al., *Reversion of advanced Ebola virus disease in nonhuman primates with ZMapp.* Nature, 2014. **514**(7520): p. 47-+.
132. Lyon, G.M., et al., *Clinical Care of Two Patients with Ebola Virus Disease in the United States.* New England Journal of Medicine, 2014. **371**(25): p. 2402-2409.
133. Bossart, K.N., et al., *A Neutralizing Human Monoclonal Antibody Protects African Green Monkeys from Hendra Virus Challenge.* Science Translational Medicine, 2011. **3**(105).
134. Geisbert, T.W., et al., *Therapeutic Treatment of Nipah Virus Infection in Nonhuman Primates with a Neutralizing Human Monoclonal Antibody.* Science Translational Medicine, 2014. **6**(242).
135. Faburay, B., et al., *A Recombinant Rift Valley Fever Virus Glycoprotein Subunit Vaccine Confers Full Protection against Rift Valley Fever Challenge in Sheep.* Sci Rep, 2016. **6**: p. 27719.
136. Botros, B., et al., *Adverse response of non-indigenous cattle of European breeds to live attenuated Smithburn rift valley fever vaccine.* Journal of Medical Virology, 2006. **78**(6): p. 787-791.
137. Bird, B.H., et al., *Rift valley fever virus lacking the NSs and NSm genes is highly attenuated, confers protective immunity from virulent virus challenge, and allows for differential identification of infected and vaccinated animals.* Journal of Virology, 2008. **82**(6): p. 2681-2691.
138. Kortekaas, J., et al., *Efficacy of three candidate Rift Valley fever vaccines in sheep.* Vaccine, 2012. **30**(23): p. 3423-9.
139. Schmaljohn, C.S., et al., *Baculovirus Expression of the M-Genome Segment of Rift-Valley Fever Virus and Examination of Antigenic and Immunogenic Properties of the Expressed Proteins.* Virology, 1989. **170**(1): p. 184-192.
140. de Boer, S.M., et al., *Rift Valley fever virus subunit vaccines confer complete protection against a lethal virus challenge.* Vaccine, 2010. **28**(11): p. 2330-2339.
141. Kwak, J.E., et al., *Development of a SFTSV DNA vaccine that confers complete protection against lethal infection in ferrets.* Nature Communications, 2019. **10**.
142. Crowe, J.E., *Principles of Broad and Potent Antiviral Human Antibodies: Insights for Vaccine Design.* Cell Host & Microbe, 2017. **22**(2): p. 193-206.
143. Yang, Z.R., et al., *RONN: the bio-basis function neural network technique applied to the detection of natively disordered regions in proteins.* Bioinformatics, 2005. **21**(16): p. 3369-76.

144. Kall, L., A. Krogh, and E.L. Sonnhammer, *Advantages of combined transmembrane topology and signal peptide prediction--the Phobius web server.* Nucleic Acids Res, 2007. **35**(Web Server issue): p. W429-32.
145. Aricescu, A.R., W. Lu, and E.Y. Jones, *A time- and cost-efficient system for high-level protein production in mammalian cells.* Acta Crystallogr D Biol Crystallogr, 2006. **62**(Pt 10): p. 1243-50.
146. Melchior, F., *SUMO - Nonclassical ubiquitin.* Annual Review of Cell and Developmental Biology, 2000. **16**: p. 591-+.
147. Molday, L.L. and R.S. Molday, *1D4: a versatile epitope tag for the purification and characterization of expressed membrane and soluble proteins.* Methods Mol Biol, 2014. **1177**: p. 1-15.
148. Seiradake, E., et al., *Production of cell surface and secreted glycoproteins in mammalian cells.* Methods Mol Biol, 2015. **1261**: p. 115-27.
149. Pardon, E., et al., *A general protocol for the generation of Nanobodies for structural biology.* Nat Protoc, 2014. **9**(3): p. 674-93.
150. Allen, E.R., et al., *A Protective Monoclonal Antibody Targets a Site of Vulnerability on the Surface of Rift Valley Fever Virus.* Cell Rep, 2018. **25**(13): p. 3750-3758 e4.
151. Chang, V.T., et al., *Glycoprotein structural genomics: solving the glycosylation problem.* Structure, 2007. **15**(3): p. 267-273.
152. Elbein, A.D., et al., *Kifunensine, a potent inhibitor of the glycoprotein processing mannosidase I.* Journal of Biological Chemistry, 1990. **265**(26): p. 15599-15605.
153. Chen, C.M., et al., *A comparison of exogenous promoter activity at the ROSA26 locus using a PhiiC31 integrase mediated cassette exchange approach in mouse ES cells.* PLoS One, 2011. **6**(8): p. e23376.
154. Block, H., et al., *Immobilized-Metal Affinity Chromatography (Imac): A Review.* Guide to Protein Purification, Second Edition, 2009. **463**: p. 439-473.
155. Trimble, R.B. and A.L. Tarentino, *Identification of distinct endoglycosidase (endo) activities in Flavobacterium meningosepticum: endo F1, endo F2, and endo F3. Endo F1 and endo H hydrolyze only high mannose and hybrid glycans.* J Biol Chem, 1991. **266**(3): p. 1646-51.
156. Grueninger-Leitch, F., et al., *Deglycosylation of proteins for crystallization using recombinant fusion protein glycosidases.* Protein Sci, 1996. **5**(12): p. 2617-22.
157. Maley, F., et al., *Characterization of Glycoproteins and Their Associated Oligosaccharides through the Use of Endoglycosidases.* Analytical Biochemistry, 1989. **180**(2): p. 195-204.
158. Chang, T.H., et al., *Structure and functional properties of Norrin mimic Wnt for signalling with Frizzled4, Lrp5/6, and proteoglycan.* Elife, 2015. **4**.
159. Waugh, D.S., *An overview of enzymatic reagents for the removal of affinity tags.* Protein Expression and Purification, 2011. **80**(2): p. 283-293.
160. Walter, T.S., et al., *A procedure for setting up high-throughput nanolitre crystallization experiments. Crystallization workflow for initial screening, automated storage, imaging and optimization.* Acta Crystallographica Section D-Structural Biology, 2005. **61**: p. 651-657.
161. Winter, G., *xia2: an expert system for macromolecular crystallography data reduction.* Journal of Applied Crystallography, 2010. **43**: p. 186-190.
162. McCoy, A.J., et al., *Phaser crystallographic software.* J. Appl. Cryst., 2007. **40**: p. 658-674.
163. Emsley, P. and K. Cowtan, *Coot: model-building tools for molecular graphics.* Acta Crystallogr D Biol Crystallogr, 2004. **60**(Pt 12 Pt 1): p. 2126-32.
164. Winn, M.D., G.N. Murshudov, and M.Z. Papiz, *Macromolecular TLS refinement in REFMAC at moderate resolutions.* Methods Enzymol., 2003. **374**: p. 300-321.
165. *The CCP4 suite: programs for protein crystallography.* Acta Crystallogr. D Biol. Crystallogr., 1994. **50**(Pt 5): p. 760-763.
166. Ramachandran, G.N., C. Ramakrishnan, and V. Sasisekharan, *Stereochemistry of polypeptide chain configurations.* J Mol Biol, 1963. **7**: p. 95-9.
167. Davis, I.W., et al., *MolProbity: all-atom contacts and structure validation for proteins and nucleic acids.* Nucleic Acids Res., 2007. **35**(Web Server issue): p. W375-383.
168. Walker, L.M., et al., *Broad and potent neutralizing antibodies from an African donor reveal a new HIV-1 vaccine target.* Science, 2009. **326**(5950): p. 285-9.

169. Walker, L.M., et al., *Broad neutralization coverage of HIV by multiple highly potent antibodies.* Nature, 2011. **477**(7365): p. 466-70.
170. Warimwe, G.M., et al., *Chimpanzee Adenovirus Vaccine Provides Multispecies Protection against Rift Valley Fever.* Sci Rep, 2016. **6**: p. 20617.
171. Zell, R. and H.J. Fritz, *DNA mismatch-repair in Escherichia coli counteracting the hydrolytic deamination of 5-methyl-cytosine residues.* EMBO J, 1987. **6**(6): p. 1809-15.
172. Corpet, F., *Multiple Sequence Alignment with Hierarchical-Clustering.* Nucleic Acids Research, 1988. **16**(22): p. 10881-10890.
173. Chenna, R., et al., *Multiple sequence alignment with the Clustal series of programs.* Nucleic Acids Research, 2003. **31**(13): p. 3497-3500.
174. Gouet, P., et al., *ESPript: analysis of multiple sequence alignments in PostScript.* Bioinformatics, 1999. **15**(4): p. 305-308.
175. Ye, J., et al., *IgBLAST: an immunoglobulin variable domain sequence analysis tool.* Nucleic Acids Res, 2013. **41**(Web Server issue): p. W34-40.
176. Giudicelli, V., X. Brochet, and M.P. Lefranc, *IMGT/V-QUEST: IMGT standardized analysis of the immunoglobulin (IG) and T cell receptor (TR) nucleotide sequences.* Cold Spring Harb Protoc, 2011. **2011**(6): p. 695-715.
177. D'Angelo, S., et al., *Many Routes to an Antibody Heavy-Chain CDR3: Necessary, Yet Insufficient, for Specific Binding.* Front Immunol, 2018. **9**: p. 395.
178. Lefranc, M.P., et al., *IMGT, the international ImMunoGeneTics database.* Nucleic Acids Res, 1999. **27**(1): p. 209-12.
179. Sievers, F., et al., *Fast, scalable generation of high-quality protein multiple sequence alignments using Clustal Omega.* Molecular Systems Biology, 2011. **7**.
180. Robert, X. and P. Gouet, *Deciphering key features in protein structures with the new ENDscript server.* Nucleic Acids Research, 2014. **42**(W1): p. W320-W324.
181. Zhao, X., et al., *Immunization-Elicited Broadly Protective Antibody Reveals Ebolavirus Fusion Loop as a Site of Vulnerability.* Cell, 2017. **169**(5): p. 891-904 e15.
182. van Doremalen, N., et al., *A single-dose ChAdOx1-vectored vaccine provides complete protection against Nipah Bangladesh and Malaysia in Syrian golden hamsters.* PLoS Negl Trop Dis, 2019. **13**(6): p. e0007462.
183. Aricescu, A.R., W.X. Lu, and E.Y. Jones, *A time- and cost-efficient system for high-level protein production in mammalian cells.* Acta Crystallographica Section D-Structural Biology, 2006. **62**: p. 1243-1250.
184. McCoy, A.J., et al., *Phaser crystallographic software.* J Appl Crystallogr, 2007. **40**(Pt 4): p. 658-674.
185. Murshudov, G.N., et al., *REFMAC5 for the refinement of macromolecular crystal structures.* Acta Crystallogr D Biol Crystallogr, 2011. **67**(Pt 4): p. 355-67.
186. Chen, V.B., et al., *MolProbity: all-atom structure validation for macromolecular crystallography.* Acta Crystallogr D Biol Crystallogr, 2010. **66**(Pt 1): p. 12-21.
187. Krissinel, E., *Advances in PISA software for macromolecular assembly predictions from CCP4.* Acta Crystallographica a-Foundation and Advances, 2015. **71**: p. S40-S40.
188. Krissinel, E. and K. Henrick, *Inference of macromolecular assemblies from crystalline state.* J Mol Biol, 2007. **372**(3): p. 774-97.
189. Cui, N., et al., *Severe fever with thrombocytopenia syndrome bunyavirus-related human encephalitis.* J Infect, 2015. **70**(1): p. 52-9.
190. Yu, X.J., et al., *Fever with thrombocytopenia associated with a novel bunyavirus in China.* N Engl J Med, 2011. **364**(16): p. 1523-32.
191. Wang, Q., et al., *Neutralization mechanism of human monoclonal antibodies against Rift Valley fever virus.* Nat Microbiol, 2019. **4**(7): p. 1231-1241.
192. Ochoa, M.C., et al., *Antibody-dependent cell cytotoxicity: immunotherapy strategies enhancing effector NK cells.* Immunology and Cell Biology, 2017. **95**(4): p. 347-355.
193. Ober, R.J., et al., *Differences in promiscuity for antibody-FcRn interactions across species: implications for therapeutic antibodies.* Int Immunol, 2001. **13**(12): p. 1551-9.
194. Patino-Galindo, J.A. and F. Gonzalez-Candelas, *The substitution rate of HIV-1 subtypes: a genomic approach.* Virus Evol, 2017. **3**(2): p. vex029.

195. Rambaut, A., et al., *The genomic and epidemiological dynamics of human influenza A virus.* Nature, 2008. **453**(7195): p. 615-9.
196. Gray, R.R., et al., *The mode and tempo of hepatitis C virus evolution within and among hosts.* BMC Evol Biol, 2011. **11**: p. 131.
197. Thompson, C.P., et al., *A naturally protective epitope of limited variability as an influenza vaccine target.* Nat Commun, 2018. **9**(1): p. 3859.
198. Jin, Y., et al., *Human monoclonal antibodies as candidate therapeutics against emerging viruses.* Front Med, 2017. **11**(4): p. 462-470.
199. Qiu, X., et al., *Successful treatment of ebola virus-infected cynomolgus macaques with monoclonal antibodies.* Sci. Transl. Med., 2012. **4**(138): p. 138ra81.
200. Burton, D.R., *What Are the Most Powerful Immunogen Design Vaccine Strategies? Reverse Vaccinology 2.0 Shows Great Promise.* Cold Spring Harb Perspect Biol, 2017. **9**(11).
201. Dungu, B., B.A. Lubisi, and T. Ikegami, *Rift Valley fever vaccines: current and future needs.* Curr Opin Virol, 2018. **29**: p. 8-15.
202. Lopez-Gil, E., et al., *A single immunization with MVA expressing GnGc glycoproteins promotes epitope-specific CD8+-T cell activation and protects immune-competent mice against a lethal RVFV infection.* PLoS Negl Trop Dis, 2013. **7**(7): p. e2309.
203. Pan, R.M., et al., *Rabbit Anti-HIV-1 Monoclonal Antibodies Raised by Immunization Can Mimic the Antigen-Binding Modes of Antibodies Derived from HIV-1-Infected Humans.* Journal of Virology, 2013. **87**(18): p. 10221-10231.
204. Terwilliger, T.C., *Reciprocal-space solvent flattening.* Acta Crystallographica Section D-Biological Crystallography, 1999. **55**: p. 1863-1871.
205. Millican, D. and J.S. Porterfield, *Relationship between Glycoproteins of the Viral Envelope of Bunyaviruses and Antibody-Dependent Plaque Enhancement.* Journal of General Virology, 1982. **63**(Nov): p. 233-236.
206. Saphire, E.O., et al., *Antibody-mediated protection against Ebola virus.* Nature Immunology, 2018. **19**(11): p. 1169-1178.
207. Sutton, T.C., et al., *In Vitro Neutralization Is Not Predictive of Prophylactic Efficacy of Broadly Neutralizing Monoclonal Antibodies CR6261 and CR9114 against Lethal H2 Influenza Virus Challenge in Mice.* J Virol, 2017. **91**(24).
208. Olal, D., et al., *Structure of an Antibody in Complex with Its Mucin Domain Linear Epitope That Is Protective against Ebola Virus.* Journal of Virology, 2012. **86**(5): p. 2809-2816.
209. Henry Dunand, C.J., et al., *Both Neutralizing and Non-Neutralizing Human H7N9 Influenza Vaccine-Induced Monoclonal Antibodies Confer Protection.* Cell Host Microbe, 2016. **19**(6): p. 800-13.
210. Warimwe, G.M., et al., *Immunogenicity and efficacy of a chimpanzee adenovirus-vectored Rift Valley fever vaccine in mice.* Virol J, 2013. **10**: p. 349.
211. Warimwe, G.M., et al., *Chimpanzee Adenovirus Vaccine Provides Multispecies Protection against Rift Valley Fever.* Scientific Reports, 2016. **6**.
212. Ewer, K.J., et al., *Protective CD8+ T-cell immunity to human malaria induced by chimpanzee adenovirus-MVA immunisation.* Nat Commun, 2013. **4**: p. 2836.
213. Borthwick, N., et al., *Vaccine-elicited human T cells recognizing conserved protein regions inhibit HIV-1.* Mol Ther, 2014. **22**(2): p. 464-475.
214. Ewer, K., et al., *A Monovalent Chimpanzee Adenovirus Ebola Vaccine Boosted with MVA.* New England Journal of Medicine, 2016. **374**(17): p. 1635-1646.
215. Scott, G.R., et al., *Rift Valley Fever in Camels.* Journal of Pathology and Bacteriology, 1963. **86**(1): p. 229-+.
216. El Mamy, A.B.O., et al., *Unexpected Rift Valley Fever Outbreak, Northern Mauritania.* Emerging Infectious Diseases, 2011. **17**(10): p. 1894-1896.
217. Rissmann, M., et al., *Vaccination of alpacas against Rift Valley fever virus: Safety, immunogenicity and pathogenicity of MP-12 vaccine.* Vaccine, 2017. **35**(4): p. 655-662.
218. Muyldermans, S., C. Cambillau, and L. Wyns, *Recognition of antigens by single-domain antibody fragments: the superfluous luxury of paired domains.* Trends Biochem Sci, 2001. **26**(4): p. 230-5.

219. Muyldermans, S., *Nanobodies: natural single-domain antibodies.* Annu Rev Biochem, 2013. **82**: p. 775-97.
220. Pardon, E., et al., *A general protocol for the generation of Nanobodies for structural biology.* Nature Protocols, 2014. **9**(3): p. 674-693.
221. Rasmussen, S.G., et al., *Structure of a nanobody-stabilized active state of the beta(2) adrenoceptor.* Nature, 2011. **469**(7329): p. 175-80.
222. Lauwereys, M., et al., *Potent enzyme inhibitors derived from dromedary heavy-chain antibodies.* EMBO J, 1998. **17**(13): p. 3512-20.
223. De Genst, E., et al., *Molecular basis for the preferential cleft recognition by dromedary heavy-chain antibodies.* Proc Natl Acad Sci U S A, 2006. **103**(12): p. 4586-91.
224. Low, C., et al., *Nanobody mediated crystallization of an archeal mechanosensitive channel.* PLoS One, 2013. **8**(10): p. e77984.
225. Park, Y.J., et al., *Crystal structure of a heterodimer of editosome interaction proteins in complex with two copies of a cross-reacting nanobody.* Nucleic Acids Res, 2012. **40**(4): p. 1828-40.
226. Abskharon, R.N., et al., *Combining in-situ proteolysis and microseed matrix screening to promote crystallization of PrPc-nanobody complexes.* Protein Eng Des Sel, 2011. **24**(9): p. 737-41.
227. Desmyter, A., et al., *Crystal structure of a camel single-domain VH antibody fragment in complex with lysozyme.* Nat Struct Biol, 1996. **3**(9): p. 803-11.
228. Swadling, L., et al., *A human vaccine strategy based on chimpanzee adenoviral and MVA vectors that primes, boosts, and sustains functional HCV-specific T cell memory.* Science Translational Medicine, 2014. **6**(261).
229. Laverty, D., et al., *Cryo-EM structure of the human alpha1beta3gamma2 GABAA receptor in a lipid bilayer.* Nature, 2019. **565**(7740): p. 516-520.
230. Laursen, N.S., et al., *Universal protection against influenza infection by a multidomain antibody to influenza hemagglutinin.* Science, 2018. **362**(6414): p. 598-+.
231. Dessau, M. and Y. Modis, *Crystal structure of glycoprotein C from Rift Valley fever virus.* Proceedings of the National Academy of Sciences of the United States of America, 2013. **110**(5): p. 1696-1701.
232. Fairhead, M. and M. Howarth, *Site-specific biotinylation of purified proteins using BirA.* Methods Mol Biol, 2015. **1266**: p. 171-84.
233. Yadav, D.K., et al., *An insight into fusion technology aiding efficient recombinant protein production for functional proteomics.* Archives of Biochemistry and Biophysics, 2016. **612**: p. 57-77.
234. Jentsch, S. and G. Pyrowolakis, *Ubiquitin and its kin: how close are the family ties?* Trends in Cell Biology, 2000. **10**(8): p. 335-342.
235. Guardado-Calvo, P., et al., *A glycerophospholipid-specific pocket in the RVFV class II fusion protein drives target membrane insertion.* Science, 2017. **358**(6363): p. 663-667.
236. Ignatev, A., et al., *A size filtration approach to purify low affinity complexes for crystallization.* J Struct Biol, 2007. **159**(1): p. 154-7.
237. Elegheert, J., et al., *Lentiviral transduction of mammalian cells for fast, scalable and high-level production of soluble and membrane proteins.* Nat Protoc, 2018. **13**(12): p. 2991-3017.
238. Li, Y.T., et al., *Development and characterization of Rift Valley fever virus-like particles.* Genet Mol Res, 2016. **15**(1).
239. Daubney, R., J.R. Hudson, and P.C. Garnham, *Enzootic hepatitis or rift valley fever. An undescribed virus disease of sheep cattle and man from east africa.* The Journal of Pathology and Bacteriology, 1931. **34**(4): p. 545-579.
240. Ding, F., et al., *Epidemiologic features of severe fever with thrombocytopenia syndrome in China, 2011-2012.* Clin Infect Dis, 2013. **56**(11): p. 1682-3.
241. Tang, X., et al., *Human-to-human transmission of severe fever with thrombocytopenia syndrome bunyavirus through contact with infectious blood.* J Infect Dis, 2013. **207**(5): p. 736-9.
242. Gai, Z., et al., *Person-to-person transmission of severe fever with thrombocytopenia syndrome bunyavirus through blood contact.* Clin Infect Dis, 2012. **54**(2): p. 249-52.

243. Bosco-Lauth, A.M., et al., *Serological investigation of heartland virus (Bunyaviridae: Phlebovirus) exposure in wild and domestic animals adjacent to human case sites in Missouri 2012-2013.* Am J Trop Med Hyg, 2015. **92**(6): p. 1163-7.
244. Liu, R., et al., *Immunization with Recombinant SFTSV/NSs Protein Does Not Promote Virus Clearance in SFTSV-Infected C57BL/6J Mice.* Viral Immunology, 2015. **28**(2): p. 113-122.
245. Palacios, G., et al., *Characterization of the Uukuniemi Virus Group (Phlebovirus: Bunyaviridae): Evidence for Seven Distinct Species.* Journal of Virology, 2013. **87**(6): p. 3187-3195.
246. Goh, J.B. and S.K. Ng, *Impact of host cell line choice on glycan profile.* Critical Reviews in Biotechnology, 2018. **38**(6): p. 851-867.
247. Bowden, T.A., et al., *Unusual Molecular Architecture of the Machupo Virus Attachment Glycoprotein.* Journal of Virology, 2009. **83**(16): p. 8259-8265.
248. Crispin, M., et al., *A Human Embryonic Kidney 293T Cell Line Mutated at the Golgi alpha-Mannosidase II Locus.* Journal of Biological Chemistry, 2009. **284**(32): p. 21684-21695.
249. Chaudhary, S., et al., *Overexpressing human membrane proteins in stably transfected and clonal human embryonic kidney 293S cells.* Nature Protocols, 2012. **7**(3): p. 453-466.
250. Overby, A.K., et al., *Insights into bunyavirus architecture from electron cryotomography of Uukuniemi virus.* Proceedings of the National Academy of Sciences of the United States of America, 2008. **105**(7): p. 2375-2379.
251. Kim, K.H., et al., *An anti-Gn glycoprotein antibody from a convalescent patient potently inhibits the infection of severe fever with thrombocytopenia syndrome virus.* PLoS Pathog, 2019. **15**(2): p. e1007375.
252. Zhang, Y.Z., et al., *The ecology, genetic diversity, and phylogeny of Huaiyangshan virus in China.* J Virol, 2012. **86**(5): p. 2864-8.
253. Liu, Y., et al., *The Pathogenesis of Severe Fever with Thrombocytopenia Syndrome Virus Infection in Alpha/Beta Interferon Knockout Mice: Insights into the Pathologic Mechanisms of a New Viral Hemorrhagic Fever.* Journal of Virology, 2014. **88**(3): p. 1781-1786.
254. Jin, C., et al., *Pathogenesis of emerging severe fever with thrombocytopenia syndrome virus in C57/BL6 mouse model.* Proceedings of the National Academy of Sciences of the United States of America, 2012. **109**(25): p. 10053-10058.
255. Matsuno, K., et al., *Animal Models of Emerging Tick-Borne Phleboviruses: Determining Target Cells in a Lethal Model of SFTSV Infection.* Frontiers in Microbiology, 2017. **8**.
256. Bitto, D., et al., *Low pH and Anionic Lipid-dependent Fusion of Uukuniemi Phlebovirus to Liposomes.* J Biol Chem, 2016. **291**(12): p. 6412-22.
257. Zhu, Y., et al., *The Postfusion Structure of the Heartland Virus Gc Glycoprotein Supports Taxonomic Separation of the Bunyaviral Families Phenuiviridae and Hantaviridae.* J Virol, 2018. **92**(1).
258. Rambo, R.P. and J.A. Tainer, *Super-Resolution in Solution X-Ray Scattering and Its Applications to Structural Systems Biology.* Annual Review of Biophysics, Vol 42, 2013. **42**: p. 415-441.
259. Salazar, G., et al., *Antibody therapies for the prevention and treatment of viral infections.* Npj Vaccines, 2017. **2**.
260. Slon-Campos, J.L., et al., *A protective Zika virus E-dimer-based subunit vaccine engineered to abrogate antibody-dependent enhancement of dengue infection.* Nature Immunology, 2019. **20**(10): p. 1291-+.
261. Koukuntla, R., R.B. Mandell, and R. Flick, *Virus-Like Particle-Based Countermeasures Against Rift Valley Fever Virus.* Zoonoses and Public Health, 2012. **59**: p. 142-150.

Appendix 1.1 List of Abbreviations

Å	Ångströms = 10^{-10} metres
Ab	Antibody
ADCC	Antibody dependent cellular cytotoxicity
BALB/c	Bagg albino strain of inbred mouse
bp	Base pairs
C	Degrees centigrade
CDC	Centre of Disease control
CDR	Complementarity determining region
ch1	Constant region 1 of the antibody heavy chain
cL	Constant region of the antibody light chain
Cryo-EM	Cryogenic electron-microscopy
Cryo-ET	Cryogenic electron-tomography
Da	Daltons
DENV	Dengue virus
DMEM	Dulbecco's modified eagle medium
DMSO	Dimethyl sulphoxide
DNA	Deoxyribonucleic acid
E.coli	*Escherichia coli*
EBOV	Ebola virus
ELISA	Enzyme-linked immunosorbent assay
EDTA	Ethylenediaminetetraacetic acid
EF1	Endof1: Endoglycosidase-F1
Fab	Fragment antigen binding
FACS	Fluorescence activated cell sorting
Fc	Fragment crystallisable region of the antibody
FcR	Fc receptor
FCS	Foetal calf serum
g	Gram
Gc	Glycoprotein C
GlcNAc	N-acetyl glucosamine
Gn	Glycoprotein N
h	Hours
HC	Heavy chain
HEPES	(4-(2-hydroxyethyl)-1-piperazineethanesulfonic acid)
HEK293	Human Embryonic Kidney 293 cells
HIV	Human immunodeficiency virus
HRP	Horse-radish peroxidase
HRTV	Heartland virus
IC50	Inhibitory concentration 50%
IgG	Immunoglobulin G
IMAC	Immobilised metal affinity chromatography
IPTG	Isopropyl β-D-1-thiogalactopyranoside
k	Kilo (10^3)

Kb	Kilobase
KCL	Kings college london
L	Litre
LB	Luria broth
LC	Light chain
L-glut	L-glutamine
M	Molar
m	Metres
m	Milli (10^{-3})
mAb	Monoclonal antibody
Man	Mannose
MEM	Modified eagle media
MERS-CoV	Middle East respiratory syndrome coronavirus
MES	2-(N-morpholino)ethanesulfonic acid
min	Minutes
MPD	2-methyl-2,4-pentanediol
MS	Mass spectrometry
MWCO	Molecular weight cut-off
n	Nano
N	Nucleoprotein
nAb	Neutralising antibody
Nb	Nanobody
NCS	Non-crystallographic symmetry
NEAA	Non-essential amino acids
NsM	Non-structural protein of the M segment
NsS	Non-structural protein of the S segment
PBMC	Peripheral blood mononuclear cell
PBS	Phosphate buffered saline
PBS-T	PBS with Tween20
PCR	Polymerase chain reaction
PDB	Protein data bank
PEG	Polyethylene glycol
PEI	Polyethylenimine
pfu	Plaque forming units
PHE	Public Health England
RMSD	Root mean square deviation
RNA	Ribonucleic acid
rpm	Rotations per minute
RT	Room temperature =~25°c
RVFV	Rift Valley fever virus
s	Seconds
SDS-PAGE	Sodium dodecyl sulphate polyacrylamide gel electrophoresis
SEC	Size exclusion chromatography
SFTSV	Severe fever with thrombocytopenia syndrome virus
SOC	Super optimal broth
SP	Signal peptide
TAE	Tris Acetic acid EDTA

TBS	Tris buffered Saline (10 mm Tris pH 8.0, 150 mm NaCl)
Tm	Melting temperature (of DNA duplexes)
TM	Transmembrane
Tris	Tris(hydroxymethyl)aminomethane
µ	Micro (10^{-6})
UUKV	Uukuniemi virus
v/v	Volume per volume
Vh	Variable region of the antibody heavy chain
Vl	Variable region of the antibody light chain
w/v	Weight per volume
x g	Multiples of the standard gravity of earth, 9.8 ms^{-1}
ZIKV	Zika virus

Appendix 1.2: cDNA sequences of codon optimised genes by GeneArt (5' to 3')

Phlebovirus M-segments

RVFV

CGAATTGAAGGAAGGCCGTCAAGGCCGCATGAGCTCACCGGTATGTACGTGCTG
CTGACCATCCTGATCAGCGTGCTGGTGTGCGAGGCCGTGATCAGAGTGTCCCTGA
GCAGCACCCGGGAGGAAACCTGCTTCGGCGACAGCACCAACCCCGAGATGATCG
AGGGCGCCTGGGACAGCCTGCGGGAGGAAGAGATGCCCGAGGAACTGAGCTGC
AGCGTGTCCGGCATCCGGGAAGTGAAAACCAGCAGCCAGGAACTGTACCGGGCC
CTGAAGGCCATCATTGCCGCCGACGGCCTGAACAACATCACCTGTCACGGCAAG
AACCCCGAGGACAAGATCAGCCTGATCAAGGGCCCTCCCCACAAGAAACGCGTG
GGCATCGTGCGCTGCGAGCGGAGAAGGGACGCCAAGCAGATCGGCAGAGAAAC
CATGGCCGGCATTGCCATGACAGTGCTGCCCGCCCTGGCCGTGTTTGCTCTGGCC
CCCGTGGTGTTCGCCGAGGACCCCCACCTGAGAAACAGACCCGGCAAGGGCCAC
AACTACATCGACGGCATGACCCAGGAAGATGCCACTTGCAAGCCCGTGACCTAC
GCTGGCGCCTGCAGCAGCTTCGATGTGCTGCTGGAAAAGGGCAAGTTCCCCCTGT
TCCAGAGCTACGCCCACCACAGAACCCTGCTGGAAGCCGTGCACGACACCATTA
TCGCCAAGGCCGACCCCCCTAGCTGTGATCTGCAGAGCGCCCACGGCAACCCCT
GCATGAAAGAAAAGCTGGTGATGAAGACCCACTGCCCCAACGACTACCAGTCCG
CCCACTACCTGAACAACGACGGCAAGATGGCCAGCGTGAAGTGCCCCCCCAAGT
ACGAGCTGACCGAGGACTGCAACTTCTGTCGGCAGATGACCGGCGCCAGCCTGA
AGAAGGGCAGCTACCCACTGCAGGACCTGTTCTGCCAGAGCAGCGAGGACGACG
GCAGCAAGCTGAAAACAAAGATGAAGGGCGTGTGCGAAGTGGGCGTGCAGGCC
CTGAAGAAGTGCGACGGCCAGCTGAGCACAGCCCACGAGGTGGTGCCCTTCGCC
GTGTTCAAGAACAGCAAGAAGGTGTACCTGGACAAGCTGGACCTGAAAACCGAG
GAAAACCTGCTGCCCGACTCCTTCGTGTGCTTCGAGCACAAGGGCCAGTACAAG
GGCACCATGGACAGCGGCCAGACCAAGCGGGAGCTGAAGTCCTTCGACATCAGC
CAGTGCCCCAAGATCGGCGGCCACGGCAGCAAAAAGTGTACCGGCGACGCCGCC
TTCTGTAGCGCCTACGAGTGCACCGCCCAGTACGCCAACGCCTACTGCAGCCACG
CCAACGGCAGCGGCATCGTGCAGATCCAGGTGTCCGGCGTGTGGAAGAAACCCC
TGTGCGTGGGCTACGAGCGGGTGGTGGTGAAGAGAGAGCTGAGCGCCAAGCCCA
TCCAGAGAGTGGAGCCCTGCACCACCTGTATCACCAAGTGCGAGCCCCATGGCC
TGGTGGTGCGGAGCACCGGCTTCAAGATCAGCAGCGCCGTGGCCTGTGCTAGCG
GCGTGTGTGTGACCGGCAGCCAGAGCCCTAGCACCGAGATCACCCTGAAGTACC
CCGGCATCTCTCAGAGCAGCGGCGGAGACATCGGAGTGCACATGGCCCACGACG
ACCAGAGCGTGTCCAGCAAGATCGTGGCCCACTGCCCACCCCAGGATCCTTGCCT
GGTGCACGGCTGCATCGTGTGTGCCCACGGCCTGATCAACTACCAGTGCCACACC
GCCCTGAGCGCCTTCGTGGTGATCTTCGTGTTCAGCAGCACCGCCATCATCTGCC
TGGCCGTGCTGTATCGGGTGCTGAAGTGCCTGAAGATCGCCCCCAGAAAGGTGC
TGAACCCCCTGATGTGGATCACAGCCTTCATCCGCTGGGTGTACAAGAAAATGGT
GGCCCGGGTGGCCGACAACATCAACCAGGTGAACCGGGAGATCGGCTGGATGGA
AGGCGGACAGCTGGCCCTGGGCAACCCTGCCCCTATCCCCAGACACGCCCCCAT

CCCCCGGTACAGCACCTACCTGATGCTGCTGCTGATCGTGTCCTACGCCAGCGCT
TGCTCTGAGCTGATCCAGGCCAGCAGCCGGATCACCACATGCAGCACCGAGGGC
GTGAACACCAAGTGCAGACTGAGCGGCACTGCCCTGATCAGAGCTGGCTCTGTG
GGAGCCGAGGCCTGCCTGATGCTGAAAGGCGTGAAAGAGGACCAGACCAAGTTT
CTGAAGATCAAGACCGTGTCCAGCGAGCTGTCCTGCAGAGAGGGCCAGAGCTAC
TGGACCGGCAGCTTCAGCCCCAAGTGCCTGAGCAGCCGCAGATGTCACCTGGTG
GGCGAGTGCCACGTGAACAGATGCCTGAGCTGGCGGGACAACGAGACAAGCGC
CGAGTTCAGCTTCGTGGGCGAAAGCACCACCATGCGGGAGAACAAGTGCT
TTGAGCAGTGCGGCGGCTGGGGCTGCGGCTGCTTCAACGTGAACCCCAGCTGCCT
GTTCGTGCACACCTACCTGCAGAGCGTGCGGAAAGAGGCCCTGCGGGTGTTCAA
CTGCATCGACTGGGTGCACAAGCTGACCCTGGAAATCACCGACTTCGACGGCTCC
GTGAGCACAATCGACCTGGGCGCCAGCAGCTCCAGATTCACCAACTGGGGCTCC
GTGTCCCTGTCTCTGGACGCCGAGGGCATCAGCGGCAGCAACAGCTTCAGCTTCA
TCGAGAGCCCTGGCAAGGGCTACGCCATCGTGGACGAGCCCTTCAGCGAGATCC
CCAGGCAGGGCTTTCTGGGCGAGATCCGGTGCAACAGCGAGAGCAGCGTGCTGT
CCGCCCACGAGAGCTGCCTGAGAGCCCCCAACCTGGTGTCCTACAAGCCCATGA
TCGACCAGCTGGAATGCACCACCAACCTGATCGACCCCTTTGTGGTGTTCGAGAG
AGGCAGCCTGCCCCAGACCCGGAACGACAAGACCTTCGCCGCCAGCAAGGGCAA
TCGGGGGGTGCAGGCCTTTAGCAAGGGCTCCGTGCAGGCCGACCTGACCCTGAT
GTTCGACAACTTCGAGGTGGACTTCGTGGGAGCCGCCGTGAGCTGTGATGCCGCC
TTCCTGAACCTGACCGGCTGCTACAGCTGCAATGCCGGCGCTAGAGTGTGTCTGT
CCATCACCAGCACCGGCACAGGCACACTGAGCGCCCACAACAAGGACGGCAGCC
TGCACATCGTGCTGCCCAGCGAGAACGGCACCAAGGACCAGTGCCAGATCCTGC
ACTTCACCGTGCCCGAGGTGGAAGAGGAGTTCATGTACAGCTGCGACGGCGACG
AAAGACCCCTGCTGGTGAAGGGCACCCTGATCGCCATCGACCCTTTCGACGACA
GAAGAGAGGCTGGCGGCGAGTCCACCGTGGTGAACCCCAAGAGCGGCAGCTGG
AACTTCTTCGACTGGTTCAGCGGCCTGATGTCTTGGTTTGGCGGCCCTCTGAAAA
CCATCCTGCTGATCTGCCTGTACGTGGCCCTGAGCATCGGCCTGTTCTTTCTGCTG
ATCTATCTGGGACGGACCGGCCTGTCAAAAATGTGGCTGGCTGCCACCAAGAAG
GCTAGCGGTACCCTGGGCCTCATGGGCCTTCCTTTCACTGCC

SFTSV

CACTATAGGGCGAATTGAAGGAAGGCCGTCAAGGCCGCATACCGGTATGATGAA
AGTGATCTGGTTCAGCAGCCTGATCTGCTTCGTGATCCAGTGCAGCGGCGACAGC
GGCCCCATCATTTGTGCCGGCCCTATCCACAGCAACAAGAGCGCCGACATCCCCC
ATCTGCTGGGCTACAGCGAGAAGATCTGCCAGATCGACCGGCTGATCCACGTGT
CCAGCTGGCTGAGAAACCACAGCCAGTTCCAGGGCTACGTGGGACAGAGAGGCG
GCAGATCCCAGGTGTCCTACTACCCCGCCGAGAACAGCTACTCCAGGTGGAGCG
GACTGCTGAGCCCTTGCGACGCTGATTGGCTGGGCATGCTGGTCGTGAAGAAGG
CCAAGGGCAGCGACATGATCGTGCCTGGCCCTAGCTACAAGGGCAAGGTGTTCT
TCGAGCGGCCCACCTTCGACGGCTATGTGGGCTGGGGATGTGGCAGCGGCAAGA
GCAGAACAGAGTCCGGCGAGCTGTGCAGCAGCGATTCTGGCACAAGCAGCGGCC
TGCTGCCCAGCGATAGAGTGCTGTGGATCGGCGACGTGGCCTGCCAGCCTATGA
CCCCTATCCCCGAGGAAACCTTTCTGGAACTGAAGTCCTTCAGCCAGAGCGAGTT
CCCCGACATCTGCAAGATTGACGGCATCGTGTTCAACCAGTGCGAGGGCGAGAG
CCTGCCCCAGCCTTTTGATGTGGCCTGGATGGACGTGGGCCACTCCCACAAGATC

ATCATGCGCGAGCACAAGACCAAATGGGTGCAGGAAAGCAGCAGCAAGGACTT
CGTGTGCTACAAAGAGGGCACCGGCCCCTGCAGCGAGAGCGAGGAAAAGACCT
GCAAGACCAGCGGCAGCTGCAGAGGCGACATGCAGTTCTGCAAGGTGGCCGGAT
GCGAGCACGGCGAAGAGGCCAGCGAGGCCAAGTGCAGATGTAGCCTGGTGCAC
AAGCCCGGCGAGGTGGTGGTGTCTTACGGCGGCATGCGGATCCGGCCTAAGTGC
TACGGCTTCAGCCGGATGATGGCCACCCTGGAAGTGAACCAGCCCGAGCAGAGA
ATCGGCCAGTGCACCGGCTGCCACCTGGAATGCATCAATGGCGGCGTGCGGCTG
ATCACCCTGACCAGCGAACTGAAAAGCGCCACCGTGTGCGCCAGCCACTTCTGT
AGCAGCGCCACCTCCGGCAAGAAGTCCACCGAGATCCAGTTCCACAGCGGCTCC
CTCGTGGGCAAGACAGCCATCCATGTGAAGGGGGCCCTGGTGGACGGCACCGAG
TTTACCTTTGAGGGCTCCTGCATGTTCCCCGATGGCTGCGACGCCGTGGACTGTA
CCTTCTGCAGAGAGTTCCTGAAGAACCCCCAGTGCTACCCTGCCAAGAAATGGCT
GTTCATCATCATCGTGATCCTGCTGGGATACGCCGGCCTGATGCTGCTGACCAAC
GTGCTGAAGGCCATCGGCATCTGGGGCAGCTGGGTCATCGCCCCCGTGAAGCTG
ATGTTCGCCATCATCAAGAAACTGATGCGGACCGTGTCCTGCCTGATGGGCAAGC
TGATGGACCGGGGCAGACAAGTGATCCACGAGGAAATCGGCGAGAACAGAGAG
GGCAACCAGGACGACGTGCGGATCGAGATGGCCAGACCTAGAAGAGTGCGGCA
CTGGATGTACTCCCCAGTGATCCTGACCTTCCTGGCCATCGGACTGGCCGAGAGC
TGCGACGAAATGGTGCACGCCGACAGCAAGCTGGTGTCCTGCAGACAGGGCTCC
GGCAACATGAAGGAATGCGTGACCACCGGCAGAGCCCTGCTGCCTGCTGTGAAC
CCTGGACAGGAAGCCTGCCTGCACTTTACCGCCCCTGGCAGCCCTGACAGCAAGT
GCCTGAAGATCAAAGTGAAGCGGATCAACCTGAAGTGCAAGAAAAGCAGCTCCT
ACTTCGTGCCCGACGCCCGGTCCAGATGTACCAGCGTGCGGAGATGTAGATGGG
CTGGCGATTGCCAGAGCGGCTGCCCTCCTCACTTCACCAGCAACAGCTTCAGCGA
CGACTGGGCCGGCAAGATGGACAGAGCCGGACTGGGCTTTAGCGGCTGCTCTGA
TGGATGTGGCGGCGCTGCCTGCGGCTGCTTTAATGCCGCCCCTAGCTGCATCTTC
TGGCGGAAATGGGTGGAAAACCCCCACGGCATCATCTGGAAGGTGTCCCCATGT
GCCGCCTGGGTGCCATCTGCCGTGATCGAGCTGACAATGCCCAGCGGCGAAGTG
CGGACCTTCCACCCTATGAGCGGCATCCCCACCCAGGTGTTCAAGGGCGTGTCCG
TGACATACCTGGGCTCCGACATGGAAGTGTCCGGCCTGACCGACCTGTGCGAGA
TTGAGGAACTGAAATCCAAGAAGCTGGCCCTGGCCCCCTGTAACCAGGCCGGAA
TGGGAGTCGTGGGAAAAGTGGGCGAGATTCAGTGCAGCTCCGAGGAAAGCGCCC
GGACCATCAAGAAGGACGGCTGCATCTGGAACGCCGACCTCGTGGGAATTGAGC
TGAGAGTGGATGACGCCGTGTGTTACAGCAAGATCACCAGCGTGGAAGCCGTGG
CCAACTACAGCGCCATCCCTACCACAATCGGCGGCCTGAGATTCGAGCGGAGCC
ACGATAGCCAGGGCAAGATCAGCGGAAGCCCCCTGGACATCACCGCCATTAGAG
GCAGCTTCTCCGTGAACTACCGGGGCCTGAGACTGAGCCTGAGCGAGATCACAG
CCACCTGTACCGGGGAAGTGACCAATGTGTCCGGCTGTTACAGCTGCATGACCG
GCGCCAAGGTGTCCATCAAGCTGCACTCCAGCAAGAACAGCACCGCCCACGTGC
GGTGCAAGGGCGACGAGACAGCCTTCTCTGTGCTGGAAGGCGTGCACAGCTACA
CCGTGTCCCTGAGCTTCGACCACGCCGTGGTGGATGAGCAGTGCCAGCTGAATTG
TGGCGGCCACGAGTCCCAAGTGACCCTGAAGGGAAACCTGATCTTTCTGGACGT
GCCCAAGTTCGTGGACGGCTCCTACATGCAGACCTACCACAGCACCGTGCCCAC
AGGCGCCAACATCCCTAGCCCTACCGACTGGCTGAACGCCCTGTTCGGCAACGG
CCTGAGCAGATGGATCCTGGGCGTGATCGGAGTGCTGCTGGGAGGACTGGCCCT
GTTCTTTATGATCATGAGCCTGTTCAAGCTGGGCACCAAACAGGTGTTCCGGTCC
CGGACAAAGCTGGCCGGTACCCTGGGCCTCATGGGCCTTCCTTTCACTGCCCGCT
TTCCAG

HRTV

CACTATAGGGCGAATTGAAGGAAGGCCGTCAAGGCCGCATACCGGTATGATCGC
CCCCGTGGTGCTGTTCTTCACCCTGTGCCCTAGCCAGCTGAGCGCCTGGGGATCT
CCTGGCGATCCTATCGTGTGTGGCGTGCGGACCGAGACAAACAAGAGCATCCAG
ATCGAGTGGAAAGAGGGCCGCAGCGAGAAGCTGTGCCAGATCGATAGACTGGG
CCACGTGACCAGCTGGCTGCGGAACCACAGCAGCTTCCAGGGCCTGATCGGCCA
AGTGAAGGGCAGACCCAGCGTGTCCTACTTCCCTGAGGGCGCCAGCTACCCTAG
GTGGAGCGGACTGCTGAGCCCCTGTGATGCCGAATGGCTGGGACTGATCGCCGT
GTCCAAGGCCGGCGACACCGACATGATTGTGCCTGGCCCTACCTACAAGGGCAA
GATCTTCGTGGAAAGACCCACCTACAACGGCTATAAGGGCTGGGGCTGCGCCGA
CGGCAAGAGCCTGTCTCACAGCGGCACCTACTGCGAGACAGACAGCTCCGTGTC
CTCCGGCCTGATCCAGGGCGATAGAGTGCTGTGGGTGGGAGAGGTCGTGTGCCA
GAGGGGCACACCTGTGCCCGAGGATGTGTTCAGCGAGCTGATCTCCCTGAGCCA
GAGCGAGTTCCCCGACGTGTGCAAAGTGGATGGCGTGGCCCTGAACCAGTGCGA
GCAGGAATCCATCCCCCAGCCCCTGGATGTGGCCTGGATCGATGTGGGCAGATC
CCACAAGGTGCTGATGCGCGAGCACAAGACCAAATGGGTGCAGGAAAGCAGCG
CCAAGGACTTCGTGTGCTTCAAAGTGGGCCAGGGCCCCTGCAGCAAGCAGGAAG
AGGACGACTGCATGAGCAAGGGCAACTGCCACGGCGACGAGGTGTTCTGTAGAA
TGGCCGGCTGCAGCGCCCGGATGCAGGACAATCAGGAAGGCTGCCGCTGCGAGC
TGCTGCAGAAGCCTGGCGAGATCATCGTGAACTACGGCGGCGTGTCCGTGCGGC
CTACCTGCTACGGCTTCAGCAGAATGATGGCCACCCTGGAAGTGCACAAGCCCG
ACAGAGAGCTGACCGGCTGCACAGGCTGCCACCTGGAATGTATCGAGGGCGGCG
TGAAGATCGTGACCCTGACCTCCGAGCTGAGAAGCGCCACAGTGTGCGCCAGCC
ACTTTTGCGCCTCTGCCAAGGGCGGCAGCAAGACCACCGACATCCTGTTCCATAC
CGGCGCTCTCGTGGGCCCCAAGTCCATCAGAATCACCGGCCAGCTGCTGGACGG
CTCCAAGTTCAGCTTCGACGGCCACTGCATCTTCCCCGATGGCTGCATGGCCCTG
GACTGTACCTTCTGCAAAGAGTTCCTGAGAAACCCCCAGTGCTACCCCGTGAAGA
AATGGCTGTTCCTGGTCGTGGTCGTGATGTGCTGCTACTGCGCCCTGATGCTGCT
GACCAACATCCTGAGAGCCATCGGCGTGTGGGGCACCTGGGTGTTCGCCCCTATT
AAGCTGGTGCTGGCCCTGGGCCTGAGACTGGCCAAGCTGAGCAAGAAAGGCCTG
GTGGCCGTCGTGACCAGAGGCCAGATGATCGTGAATGACGAGCTGCACCAGATC
CGGGTGGAACGGGGAGAGCAGAACGAGGGCAGACTGGGACATGGCCCTAGAGG
ACCTGTGCGGCACTGGCTGTATAGCCCTGCCCTGATCCTGATTCTGACCACCAGC
ATCTGCAGCGGCTGCGACGAACTGGTGCACGCCGAGAGCAAGAGCATTACCTGC
AAGAGCGCCAGCGGCAACGAGAAAGAATGCAGCGTGACCGGCAGAGCCCTGCT
GCCTGCTGTGAACCCTGGACAGGAAGCCTGCCTGCACTTCAGCATGCCCGGCAG
CCCTGACAGCAAGTGCCTGAAGATCAAAGTGAAGTCTATCAACCTGCGGTGCAA
GCAGGCCAGCAGCTACTACGTGCCCGAAGCCAAGGCCAGGTGTACCAGCGTGCG
GAGATGTAGATGGGCTGGCGATTGCCAGAGCGGCTGCCCCACCTACTTCAGCAG
CAACAGCTTCAGCGACGATTGGGCCAACCGGATGGACAGAGCCGGCCTGGGCAT
GAGCGGATGTTCTGATGGCTGTGGCGGAGCCGCCTGCGGCTGCTTTAATGCCGCC
CCTAGCTGCATCTTTTGGCGGAAATGGGTGGAAAACCCCAGCAACAGAGTGTGG
AAGGTGTCCCCCTGTGCCTCCTGGGTGCTGGCTGCCATCATCGAGCTGACACTGC
CCAGCGGCGAAGTGAAAACCCTGGAACCTGTGACCGGCCAGGCCACCCAGATGT
TTAAGGGCGTGGCCATTACCTACCTGGGCAGCTCCATCGAGATCGTGGGCATGAC
CCGGCTGTGCGAGATGAAGGAAATGGGCACCGGCATCATGGCTCTGGCCCCCTG
CAATGATCCCGGGCACGCCATCATGGGCAACGTGGGCGAGATCCAGTGCTCCAG

CATCGAGTCCGCCAAGCACATTCGGAGCGACGGCTGCATCTGGAACGCCGACCT
CGTGGGAATTGAGCTGAGAGTGGACGACGCCGTGTGCTTTAGCAAGCTGACCAG
CGTGGAAGCCGTGGCCAACTTCAGCAAGATCCCCGCCATCATCAGCGGCGTCAG
ATTCGACCAGGGCAACCACGGCGAGAGCCGGATCTATGGCAGCCCCCTGGACAT
CACCAAGGTGTCCGGCGAGTTCTCCGTGTCTTTCCGGGGCATGAGACTGAAGCTG
AGCGAGATCTCCGCCTCCTGCACCGGGGAGATCACAAACGTGTCCGGATGCTAC
AGCTGCATGACCGGCGCCTCTGTGTCCATCAAGCTGCACAGCTCCAAGAACACC
ACCGGCCACCTGAAGTGCGACAGCGACGAGACAGCCTTCAGCGTGATGGAAGGC
ACCCACACCTACCGGCCCCACATGAGCTTCGACAAGGCCGTGGTGGACGAGGAA
TGCGTGCTGAACTGTGGCGGCCACTCCAGCAAGCTGCTGCTGAAAGGCAGCCTG
GTGTTCATGGACGTGCCCAGATTCGTGGACGGCAGCTACGTGCAGACCTACCAC
AGCAAGGTGCCCGCTGGCGGCAGAGTGCCCAATCCTGTGGATTGGCTGAACGCC
CTGTTCGGCGACGGCATCACCAGATGGATCCTGGGCATCATCGGAGTGCTGCTGG
CTTGCGTGCTGCTGTTTGTCGTGGTGGTGGCTATCACCAGACGGCTGATCAAGGG
CCTGACCCAGAGGGCTAAGGTGGCCGGTACCCTGGGCCTCATGGGCCTTCCTTTC
ACTGCCCGCTTTCCAG

Appendix 1.3 Rabbit Fab translated sequences

Heavy chain sequences

>RV-Gn8
QSLVESGGRLVTPGTPLTLTCTVSGIDLSSYAMIWVRQAPGKGLEWIGIIYGIGTTKY
ASWAKGRFTISKTSTTVDLKITSPTTEDTATYFCARGIYMIYDYPSRFNLWGQGTLVT
VSSGQPKAP
>RV-Gn20
QSLEESGGRLVAPGTPLTLTCTVSGFPLSSYAMTWVRQAPGKGLEWIGVVDIYNTIV
YASWAKGRFTISKTSSTTVDLKMTSPTTEDTATYFCVRSATAASTYTRLDLWGQGTL
VTVSSGQPKAPSV
> RV-Gn9
QSLVESGGRLVTPGTPLTLTCTVSGIDLSRHAMLWVRQAPGKGLEWIGYIWSGGSTD
YASWAKGRFTISKTSTTVDLKITSPTTEDTATYFCARSINENDGTVLWGQGTLVTVSS
GQPKAPSV
> RV-Gn10
QSLVESGGRLVTPGTPLTLTCTASGFSLSTHYMIWVRQAPGKGLEWIGYINTGGSAY
YASWAKGRFTISRTSTTVDLKMTSLTTEDTATYFCARDGATTGYYFDLWGQGTLVT
VSSGQPKAPX
> RV-Gn16
NSQSLVESGGRLVTPGTPLTLTCTVSGFSLNNYAMNWVRQAPGKGLEWIGIISSSGST
YYASWAKGRFTISKTSTTVDLKMTSPTTEDTATYFCARDAGSNYYAYYFNFWGQGT
LVTVSSGQPKAP
> RV-Gn11
NSQSLEESGGRLVTPGTPLTLTCTVSGIDLSSYAMGWVRQAPGEGLEWIGVVRHIGIT
YYASWAKGRFTISKSSTTVDLTLTSPTTEDTATYFCVRVMAGGCNLWGQGTLVTVS
SGQPKAP
>RV-Gn23
NSQSLEESGGRLVTPGTPLTLTCTVSGIDLNSRAMIWVRQAPGKGLEWIGIIWSGGGT
DYASWVKGRFTISKTSTTVDLRVASPTTEDTATYFCASWTPLDLWGQGTLVTVSSG
QPKAP
> RV-Gn14
NSQSLVESGGRLVTPGTPLTLTCTVSGFSLSNYAMSWVRQAPGKGLEWIGVIGSGGN
THYASWAKGRFTISKTSTTVDLKLTSSTTEDTATYFCARDAGSNYYAYYFDFWGQG
TLVTVSSGQPKAP
>RV-Gn26
NSQSLVESGGRLVTPGTPLTLTCTVSGIDLSSHAMSWVRQAPGRGLEWIGIIWSGGGT
DY
ASWAKGRFTISKTSTTVDLKVTSPTTEDTATYFCGSWTRLDLWGQGTLVTVSSGQPK
AP
> RV-Gn7
NSQSLVESGGRLVTPGTPLTLICTVSGIDLSSYAMGWVRQAPGKGLEYIGMLSTSGK
TYSANWAKGRFTISKTSSTTVELRIPSPTTEDTGTYFCARGGATYSSDGYALDYLDV
WGQGTLVTVSSGQPKAP
> RV-Gn18
NSQSLEESGGRLVTPGTPVTLTCTVSGFSLSSYTVSWVRQAPGKGLEWIGFISVSADT
YYASWARGRFTISNSPTTVDLKITSPTTEDTATYFCARDAGYSDYSLGLWGQGTLVT
VSSGQPKAPX

> RV-Gn17
NSQSLEESGGRLVTPGTPLTVTCTVSGFSLSNYAMSWVRQAPGKGLEWIGIISSSGST
YYTSWAKGRFTISKTSSTTVDLKMTSLTAADTATYFCARDAGSNYYAHYFDFWGQ
GTLVTVSSGQPKAP
> RV-Gn4
NSQSLVESGGRLVTPGTPLTLTCTVSGIDLSSYAMGWVRQAPGEGLEWIGVVRHIGIT
YYASWAKGRFTISKSSTTVDLTLTSPTTEDTATYFCVRIMAGGCNSWGQGTLVIVSS
GQPKAP
> RV-Gn15
NSQSLVESGGRLVTPGTPLTLSCTVSGFSLSNYAMSWVRQAPGKGLEWIGIISSSGSS
YYASWAKGRFTISKTSSTTVDLKMTSPTTEDTATYFCARDAGSNYYTYYFDFWGQG
TLVTVSSGQPKAP
> RV-Gn
6NSQSLEQSGGRLVTPGTPVTLTCTVSGFSLSNYAVSWVRQAPGKGLEWIGFISVSGD
TYYASWARGRFTISNSPTTVDLKITSPTTEDTATYFCVRDAGYSDYSLGLWGQGTLV
TVSSGQPKAP
>HC_C2_1 c1
NSQSLEESGGRLVTPGTPLTLTCTVSGIDLSSHAMIWVRQAPGSGLEWIGIIWSGGGT
DYASWVKGRFTISKTSTTVDLKVTSPTTEDTATYFCASWTRLDLWGQGTLVTVSSG
QPKAP
>RV-Gn22
NSQSLEESGGRLVKPGGSLTLICKVSGIDLSRDAMTWVRQAPGKGLEYIGIIWSGGSA
FYATWAKGRFTISRTSTTVDLKMTSLTTEDTATYFCARSFLDDTNGYYDLWGQGTL
VTVSSGQPKAP
> RV-Gn19
NSQSLEESGGRLVTPGTPVTLTCTVSGFSLSRYPVSWVRQAPGKGLEWIGFISVSADT
YYASWARGRFTISNSPTTVDLKITSPTTEDTATYFCARDGGHSDYSLGLWGQGTLVT
VSSGQPKAP
>RV-Gn21
NSQSLVESGGRLVTPGTPLTLTCTVSGFSLSNAGMGWVRQAPGEGLEWIGWISIGGT
PYYESWVNGRFTISKTSTTVDLKITXPTTEDTATYFCVRDLGYSXNLWGQGXLVTVS
SGQPKAP
> RV-Gn12
NSQSLEESGGRLVTPGTPLTLTCTVSGIDLSSYAMGWVRQAPGEGLEWIGVVRHIGIT
YYASWAKGRFTISKSSTTVDLTLTSPTTEDTATYFCVRIMAGGCNLWGQGTLVTVSS
GQPKAP
>RV-Gn25
NSQSLVESGGGLVTPGTSLTLTCTASGFSLSSYYMTWVRQAPGKGLEWIGIIYSGGST
YYSNWAKGRFTISRTSTTMDLKVTSLTAEDTATYFCARALDTIKNLWGQGTLVTVSS
GQPKAP
> RV-Gn3
NSQSLEESGGRLVTPGTPLTLTCTVSGIDPNSDHMSWVRQAPGKGLEWIAIIYASGTT
YYASWAKGRFTISKTSTTVDLRIASPTTEDTATYFCATYPNYPTDNLWGQGTLVTVS
SGQPKAP
> RV-Gn5
NSQSLVESGGRLVTPGTPLTLTCTVSGFDLSSYVMIWVRQAPGKGLEWIGMSRSPISI
YYASWAKGRFTISKTSTTVDLKITSPTTEDTATYFCGRAPYSRHVGYYICASLWGQG
TLVTVSSGQPKAP
> RV-Gn13
NSQSLEESGGRLVTPGTPLTLTCTVSGFSLRHYALSWVRQAPGKGLEWIGIISSGLTT

HYASWARGRFTISKTSATVDLKMTSLTTEDTATYFCARDAGSNYYAHYFDFWGQG
TLVTVSSGQPKAP
> RV-Gn1
ETGLRWLLLVAVLKGVQCQSLEESGGRLVTPGTPLTLTCTVSGIDPNSDHMSWVRQ
APGKGLEWIAIIYASGTTYYASWAKGRFTISKTSTTVDLRIASPTTEDTATYFCATYP
NYPTDNLWGQGTLVTVSSGQPKAPSVFPLAPCCGDX
>RV-Gn24
VAVLKGVQCQQLEQSGGGAEGGLVKPGGSLELCCKASGFIMSSTYWMCWVRQAPG
KGLEWIGCTAVRSGGRTTYASWVNGRFTLSRDVDQSTGCLQLNSLTVADTAIYFCG
RDRSTGTMDILDLWGQGTLVTVSSGQPKAPSVFPLAPCX
> RV-Gn2
ETGLRWLLLVAVLKGVQCQSLEESGGRLVTPGTPLTLTCTASGIDLNSDHMSWVRQ
APGKGLEWIAIIYASGTIYYASWAKGRFTISKTATTVDLRITSPTTEDTATYFCATYPN
YPTDNLWGQGTLVTVSSGQPKAPSVFPLAPCCGDX

Light chain sequences

> RV-Gn8
NSQVLTQTPASVSAAVRGTVTIKCQASQSIGNYLAWYQQKPGQPPSLLIYDATALES
GVPSRFKGSGSGTEFTLTISDLECADAATYYCQCTYGTASNTYGHAFGGGTEVVVRG
DPVAPSVLX
>RV-Gn20
NSQVMTQTPLPVSAAVGGTVTVSCQSSQSVYNYNNLAWFQQKSGQPPKLLIHSAST
LESGVPSRFKGSGSGTQFTLTISGVQCDDAATYYCLAIYADDADNGFGGGTEVVVRG
DPVAPSVLX
> RV-Gn9
NSQVLTQTPTSVSAAVGGTVTINCQASRSTSTALAWYQQKPGQRPQLLIYDAYTLAS
GVSSRFKGSGSGTQFTLTISDLECADAATYYCQSYYYSSSFTYGNVFGGGTKVVVRG
DPVAPSVLX
> RV-Gn10
NSQVLTQTPASVSEPVGGTVTIKCQASQSIGSDLAWYQQKPGQRPKLLIYKASTLAS
GVSSRFKGSGSGTQFTLAISGVQCDDAATYYCQQGFTLVNIDHAFGGGTKVVVRGD
PVAPSVLX
> RV-Gn16
NSQVMTQTPASVEAAVGGTVTIKCQASEDIYSLLAWYQQKPGQPPTLLIYSASTLAS
GVPPRFKGSGSGTQFTLTISDLECDDAATYYCQGGYYGYSYVVAFGGGTKVVVRGD
PVAPSVLX
> RV-Gn11
NSQVMTQTPPPVSAAVGGTVTINCQSSQSVYGNNWLAWYQQKPGQPPKLLIYQASK
LASGVPSRFKGSGSGTQFTLTISGVQCDDAATYYCQGSDYGSGWYFAFGGGTEVVV
RGDPVAPSVLX
>RV-Gn21
NSQVMTQTPASVSEPVGGTVTIKCQASQSISSWLAWYQQKPGQPPKLLMYDTSTLAS
GVPSRFRGSGSGTEFTLTISDLECADAATYYCQCHTYSSANTYGNLFGGGTKVVVRG
DPVAPSVLX
> RV-Gn14
NSQVMTQTPASVSAAVGGTVTINCQASESIYSNLAWYQQKPGQPPKLLIYCASTPAS

GVPSRFKGSGSGTQFTLTISDLECDDAATYYCQGGYYGDSYVVAFGGGTKVVVRGD
PVAPSVLX
>RV-Gn24
NSQVMTQTPSSVSEPVGGTVTIKCQASESISSWLAWYQQKPGQPPKLLIYDASDLAS
GVPSRFIGSGSGTQFTLTISDLECADAASYYCQCHTYSSANSYGNLFGGGTEVVVRG
DPVAPSVLX
> RV-Gn7
NSQVLTQTPSSVSAGVGGTVSISCQASQSVYTNNLLSWYQQKPGQPPKLLIYYASTL
ESGVPSRFKGSGSGTQFTLTISDLECDDVAIYYCLGGYHTSTTDTTFGGGTEVVVRGD
PVAPSVLX
> RV-Gn18
NSQVMTQTPASVEAAVGGTVTIKCQASQSIGSYLAWYQQKPGQPPKLLIYSASTLES
GVPSRFKGSGSGTEFTLTISDLECADAAAYYCQCSEFGIYYLGAFGGGTEVVVRGDP
VAPSVLX
> RV-Gn17
NSQVMTQTPASVSEPVGGTVTIKCQASENIYSLLAWYQQKPGQPPKLLIYHASTLAS
GVPSRFKGSGSGTQFTLTISDLECDDVATYYCQGGNYDDSYVVAFGGGTEVVVRGD
PVAPSVLX
> RV-Gn4
NSQVMTQTPSPVSAAVGGTVTINCQSSQTVYGNNWLSWYQQKPGQPPKLLIYQASK
LASGVPSRFKGSGSGTQFTLTISGVQCDDAATYYCQGSDYGSGWYFTFGGGTEVVV
RGDPVAPSVLX
> RV-Gn15
NSQVMTQTPSSVSAAVGGTVTIKCQASENIYSLLAWYQQKPGQPPKLLIYYASTLAS
GVPSRFSGSGSGTQFTLTISDLECDDAATYYCQGGGYDDSYVVAFGGGTEVVVRGD
PVAPSVLX
> RV-Gn6
NSQVLTQTPASVEAAVGGTVTIKCQASERIGSYLAWYQQKSGQPPKLLIYSASTLAS
GVSSRFEGSGSGTEFTLTISDLECADAASYYCQCSEFGIYYLGGFGGGTEVVVRGDPV
APSVLX
>RV-Gn25
NSQVLTQTPVSVSEPVGGTVTIKCQASESISSWLAWYQQKPGQPPKLLIYDVSTLASG
VPSRFKGSGSGTEFTLTISDLECADAATYYCQCHTYSSANSYGNLFGGGTKVVVRGD
PVAPSVLX
>RV-Gn22
NSQVLTQTPSSVEAAVGGTVTIKCQASQSIYRNLAWYQQKSGQRPRLLIFGASNLAS
GVSSRFKGSGFGTEFTLTISDLECADAATYYCQSYAGSSSDTLAFGGGTKVVVRGDP
VAPSVLX
> RV-Gn19
NSQVLTQTPASVEAAVGGTVTIKCQASQSIGSYLAWYQQKPGQPPKLLIYSASTLAS
GVSSRFKGSGSGTEFTLTISDLECADAAAYYCQCSEFGTYYLGAFGGGTEVVVRGDP
VAPSVLX
>RV-Gn26
NSQVLTQTPASVSEPVGGTVTIKCQASESIGSRLAWYQQKPGQPPKLLIYDASDLASG
VPSRFKGSGSGTEFTLTISDLECADAATYVCQGGIYGSSYRVAFGGGTKVVVRGDPV
APSVLX
> RV-Gn12
NSQVLTQTPSPVSAAVGGTVTINCQSSQTVYGNNWLSWYQQKPGQPPKLLIYQASK
LASGVPSRFKGSGSGTQFTLTISGVQCDDAATYYCQGSDYGSGWYFTFGGGTEVVV
RGDPVAPSVLX

>RV-Gn23
NSQVMTQTPSPVSAAVGGTVTISCQSSQSVHKGKYLSWYQQKPGQPPKLLIHDASTL
ASGVPSRFSGSGSGTEFTLTISGVQCDDAATYYCLGLYDDDSENGFGGGTKVVVRG
DPVAPSVLX
> RV-Gn3
NSQVMTQTPSPVSAAVGGTVTIKCQASQSVYNNNLLSWFQQKPGQPPKRLIYSTSTL
ASGVSSRFKGSGSGTHFTLTISDVQCDDAATYYCLGSYDGNSANCLVFGGGTKVVV
RGDPVAPSVLX
> RV-Gn5
NSQVMTQTPSPVSVAVGGTVTIECQSSQSVYNSDSLAWYQQKLGQPPKLLIYEASNL
ASGVPDRFSGSGSGTQFTLTISGVQCDDAATYYCLGGFDDDADNAFGGGTKVVVRG
DPVAPSVLX
> RV-Gn13
NSQVMTQTPSPVSAAVGGTVTINCQASEDIYRLVAWYQQKPGQPPKPLIYSASTLAS
GVPSRFSGSGSGTQFTLTISDLECADAATYYCQGGYYGDSYVVAFGGGTKVVVRGD
PVAPSVLX
> RV-Gn1
MTQTPSPVSAAVGGTVTINCQASQSVYNNYLLSWYQQKPGQPPKRLIYSASTLASGV
SSRFKGSGSGTQFTLTISDVQCDDAATYYCLGSYDGNSADCLAFGGGTEVVVKGDP
VAPTVLIFPPAADQVATGTVTIVCVANKYFPDVTVTWEVDGTTQTX
> RV-Gn2
APELDMTQTPPSVSAAVGDTVTIKCQSSQSVGDVNELSWYQQKPGQPPKLLVYRAS
NLASGIPSRFKGSGSGTQFTLAINGVDCDDAATYYCQGTYYTSDWYLAFGGGTEVV
VKGDPVAPTVLIFPPAADQVATGTVTIVCVANKYFPDVTVTWEVDGTTQTTGIX
>RV-Gn3
MTQTPSPVSAAVGGTVTIKCQASQSVYNNNLLSWFQQKPGQPPKRLIYSTSTLASGV
PSRFKGSGSGTHFTLTISDVQCDDAATYYCLGSYDGNSADCLAFGGGTEVVVKGDP
VAPTVLIFPPAADQVATGTVTIVCVANKYFPDVTVTWEVDGTTX

Appendix 1.4 Nanobody sequences

>Nb1
QVQLVESGGGLVQAGGSLTLACAASRRSLSSYVMGWFRQAPGKEREIVATMSWIGD
SGYY
ADSVKGRFTMSRGSADNTVSLQMGSLEPEDTAVYYCAAGRRSTGRDYLSASAYDY
WGQGT
QVTVSSHHHHHHEPEA
>Nb2
QVQLVESGGGLVQAGGSLTLACAGSGRSLSSYVMGWFRQAPGKEREIVATMSWIG
DSGYY
VDSVKGRFTMSRGSADNTVSLQMGSLEPEDTAVYYCAAGRRSTGRNYLSASAYDY
WGQGT
QVTVSSHHHHHHEPEA
>Nb3
QVQLVESGGGLVQAGGSLTLACAASGHSLTSYVTGWFRQAPGKEREILATMSWIGD
SGYY
ADSVKGRFTMSRGSADNMVSLQMGSLEPEDTAVYYCAAGRRSTGRNYLSASAYDY
WGQGT
QVTVSSHHHHHHEPEA
>Nb4
QVQLVESGGGLVQPGDSLRLSCAASGRSLSSYVMGWFRQAPGKEREIVATMSWIGD
SGYY
ADSVKGRFTMSRGSADNTVSLQMGSLEPEDTAVYYCAAGRRSTGRNYLSASAYDY
WGQGT
QVTVSSHHHHHHEPEA
>Nb5
QVQLVESGGGLVQAGGSLSLSCAASGGSFSPYVVGWFRQAPGKEREFVSVINWGGD
STSY
GDSVKGRFTLSRDNAKRTVTLQMNSLKPEDTAVYFCAASRIYIADATFYDYWGQGT
QVTV
SSHHHHHHEPEA
>Nb6
QVQLVESGGGLVQAGGSLSLSCAASGRTFSPYVVGWFRQAPGKEREFVSVINWGGD
NTSY
GDSVKGRFTLSRDNAKRTVTLQMNSLKPEDTAVYFCAASRIYIDDARLYDYWGQGT
QVTV
SSHHHHHHEPEA
>Nb7
QVQLVESGGGLVQSGGSLRLSCAASGMRFSSHTAGWYRQAPGSEERDLVATITAAG
TPDY
ADSVKGRFAIARDNAVGTVSLQMNSLRPEDTAVYYCWVFDYWGQGTQVTVSSHH
HHHHEPEA
>Nb8
QVQLVESGGGLVQPGGSLRLSCTASGLFSGDMITTMHWNRQAPGLQRELVALVMR
EGSTK
YVDSVKGRFTISMDKTKNTVYLQMNSLRPDDTAVYNCNAQVVRSGTTYHYWGQG
TQVTVS
SHHHHHHEPEA
>Nb9

QVQLVESGGGLVQAGGSLRLSCTASGLFSGDMITTMHWNRQAPGLQRELVALVMR
EGSTK
YVDSVKGRFTISMDKTKNTVYLQMNSLRPDDTAVYNCNAQVVRSGTTYHYWGQG
TQVTVS
SHHHHHHEPEA
>Nb10
QVQLVESGGGSVQAGGSLRLSCTASGLFSGDMITTMHWNRQAPGLQRELVALVMR
EGSTK
YVDSVKGRFTISMDKTKNTVYLQMNSLRPDDTAVYNCNAQVVRSGTTYHYWGQG
TQVTVS
SHHHHHHEPEA
>Nb11
QVQLVESGGGSVQAGGSLRLSCTASGLFSGDMITTMHWNRQAPGLQRELDALVMR
EGSTK
YVDSVKGRFTISMDKTKNTVYLQMNSLRPDDTAVYNCNAQVVRSGTTYHYWGQG
TQVTVS
SHHHHHHEPEA
>Nb12
QVQLVESGGGSVQAGGSLRLSCTASGLFSGDMITTMHWNRQAPGKQRELVALVMR
EGSTK
YTESVKGRFTISMDNAKNTVYLQMNSLRPDDTAVYNCNAQVVRSGTTYHYWGQGT
QVTVS
SHHHHHHEPEA
>Nb13
QVQLVESGGGSVQAGGSLRLSCTASGLISGDMITTMHWNRQAPGHQRGLVAVVMR
GGSTK
YADSVKGRFTISMDNAQNTVYLQMNSLRPDDTAVYNCNAQVVRSGTTYHYWGQG
TQVTVS
SHHHHHHEPEA
>Nb14
QVQLVESGGGSVQAGGSLRLSCTASGLISGDMVMTMHWNRQAPGKQRELVALVSR
DGSTK
YEDSVKGRFTISMDNAKNTVYLQMNSLKPDDTAVYNCNAQVVRSGTTYYYWGQG
TQVTVS
SHHHHHHEPEA
>Nb15
QVQLVESGGGLVQPGGSLRLTCAASGNIVNLIDMAWYRQVPGKEREQVASLTSYGA
ADYA
DFVKGRFTISKDNAKNTVYLQMNNLRPEDTAVYVCNVFAHTRESGTTASSLAHYW
GQGTQ
VTVSSHHHHHHEPEA
>Nb19
QVQLVESGGGLEQPGGSLRLSCAASGFIFQNYPMSWVRQAPGKGPEWVSTIYAHDN
TTHY
ADSVKGRFTISRDNAKNMLYLQMNSLKPEDTAVYYCARGGYISNPRQRANDWGPG
TQVTV
SSHHHHHHEPEA
>Nb18
QVQLVESGGSLEQPGGSLRLSCAASGFIFKNYPMSWVRQAPGKGPEWVSTIYAHDN
TTHY

ADSVKGRFTISRDNAKNMLYLQMNSLKPEDTAVYYCARGGYISNPRQRANDWGPG
TQVTV
SSHHHHHHEPEA
>Nb17
QVQLVESGGGLEQPGGSLRLSCAASGFIFKNYPMSWVRQAPGKGPEWVSTIYAHDN
TTHY
ADSVKGRFTISRDNAKNMLYLQMNSLKPEDTAVYYCARGGYVSNPRQRANDWGPG
TQVTV
SSHHHHHHEPEA
>Nb20
QVQLVESGGGLEQPGGSLRLSCAASGFIFRNSPMSWVRQAPGKGPEWVSTIYAHDG
TTDY
ADSVKGRFTISRDNAKNTLHLQMNNLKPEDTAVYYCARGGYKSNPRQRANDWGPG
TQVTV
SSHHHHHHEPEA
>Nb21
QVQLVESGGGLEQPGGSLRLSCAASGFTFVNYPMSWVRQAPGKGPEWVSTIYADSV
TTHY
ADSVKGRFTISRDNAKNTLYLQMDNLKPEDTAMYFCARGGYISNPRQRANDWGPG
TQVTV
SSHHHHHHEPEA
>Nb22
QVQLVESGGGLVQPGGSLRLSCAASGFSFSTTAMSWVRQAPGKGPEWVSSIYNSAD
NTRY
ADSVKGRFTISRDNAKNTLYLQMSSLKPEDTAMYYCTRGAYSSNPKQRTPDWGPGT
QVTV
SSHHHHHHEPEA
>Nb23
QVQLVESGGGLVQPGGSLRLSCAASGFSFSTTAMSWVRQAPGKGPEWVSSIYNSAD
NTRY
ADSVKGRFTISRDNAKNTLYLQMNTLEPEDTAMYYCTRGAYSSNPRQRTPDWGPGT
QVTV
SSHHHHHHEPEA
>Nb24
QVQLVESGGGLVQPGGSLRLSCAASGFSFSTTAMSWVRQAPGKGPEWVSSIYNSAD
NTRY
ADSVKGRFTISRDNAKNTLLLQMNNLKPEDTAMYYCTRGAYSSNPRQRTPDWGPGT
QVTV
SSHHHHHHEPEA
>Nb25
QVQLVESGGGLVQAGGSLRLSCVASGFSFSTSAMSWVRQAPGKGPEWVSSIYNSAD
NTRY
ADSVKGRFTISRDNAKNTLYLQMSSLKPEDTAMYYCTRGAYSSNPKQRTPDWGPGT
QVTV
SSHHHHHHEPEA
> Nb26
QVQLVESGGGLVPAGGSRRLSCVASGFSFSTSAMSWVRQAPGKGPEWVSSIYNSAD
NTRY
ADSVKGRFTISRDNAKNTLYLQMNSLKPEDTAMYYCTLGAYSTNPRQRTPYWGPGT
QVTV

SSHHHHHHEPEA
> Nb27
QVQLVESGGGLEQSGGSLRLSCLASGFTFRDYPMSWVRQAPGKGPEWVSTIYKDGT
TDYP
NSMKGRFTISRDNAKNTVFLQMNNLKPDDTAVYSCARGGYRSDPRLRANDWGPGT
QVTVS
SHHHHHHEPEA
> Nb28
QVQLVESGGGLVQPGGSLRLSCAASGMIFSDNAMAWYRQAPGKQRELLAVITSGGV
ANYL
DSVKGRFAISRDNAKNTLYLQMNSLKPEDTAVYYCHAGSFPNVLHGTARYWGQGT
QVTVS
SHHHHHHEPEA
> Nb29
QVQLVESGGGLVQPGGSLRLSCQASGSIYNNHMGWYRQAPGKQREFVAVVTSGDT
TSYAD
SAKGRFTISRDNEKNTVYLQMNSLKPEDTAAYYCNTWPANWYWGQGTQVTVSSHH
HHHHE
PEA
> Nb30
QVQLVESGGGLVQPGESLRLSCAVSGRISRIEAMGWYRQAPGKQRDFVALLTAGGS
TTYA
DSVKGRFTISKDNAKSYLYLQMNSLKPEDTAVYYCYGNLTIYRGAYYTDNYWGQG
TQVTV
SSHHHHHHEPEA
> Nb31
QVQLVESGGGLVQAGGSLRLACAASGGGFSIDGMGWYRQAPGKQRELVAFMDQN
LNTNYT
DSVKGRFTISRSEAGDTLYLQMNALKTEDTAVYYCSAAVRLTRYASPTIYWGQGTQ
VTVS
SHHHHHHEPEA
> Nb32
QVQLVESGGGLVQAGDSLTLSCAVSGRTASTVAVGWFRQATGKERESVAAIRWIGS
NTYY
ADSVKGRFTVSKNNAKTTFYLQMNSLKPEDTANYYCAAASAWWNSMWYDDRSYN
YWGQGT
QVTVSSHHHHHHEPEA
> Nb33
QVQLVESGGGLVQAGGSLSLSCAGSGRTFSRYTMGWFRQAPGNEREFVAAVTWDG
RGSTY
YADSVKGRFTISMGGSRDKNTLTLQMNNLKPEDTAVYYCASSSSPGRRVGAGEYDY
WGRG
TQVTVSSHHHHHHEPEA
> Nb34
QVQLVESGGGLVQAGGSLRLSCELQGRIRNISAVGWYRQAPGQERELVAALTSTGST
TYT
DSVKGRFTISTDNLYNILYLQMTSLKPEDTALYYCYAHLRASGTTSFNKYWGQGTQ
VTVS
SHHHHHHEPEA

Negative Control
>Nb16
QVQLQESGGGLVQPGGSLRLSCAPSGPFSPNSMGWYRQAPGKQRELVAVMTIDGRT
NYQD
SVKGRFTISRDYVKNTAYLQMNNLKPDDTAVYICNAETRGFMHWGQGTQVTVSSH
HHHHHEPEA

Appendix 1.4:Nanobody sequence alignment

(A) Nb selected against RVFV Gn and (B) Nb selected against RVFV Gc

A

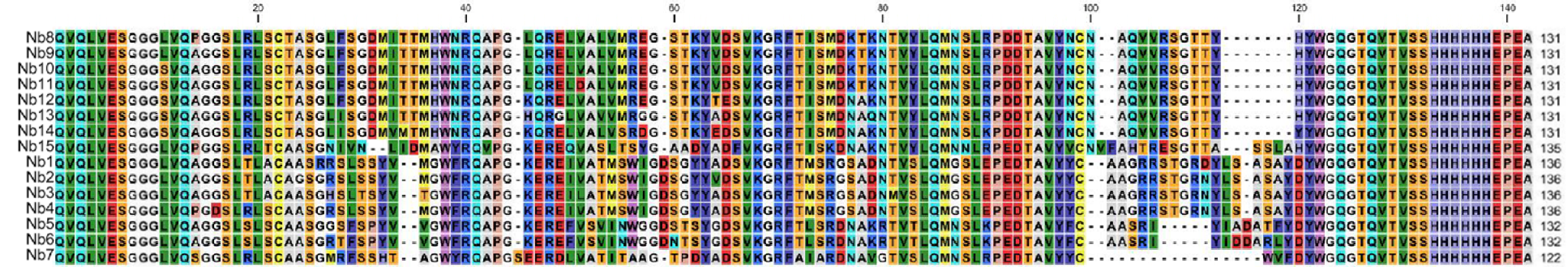

B

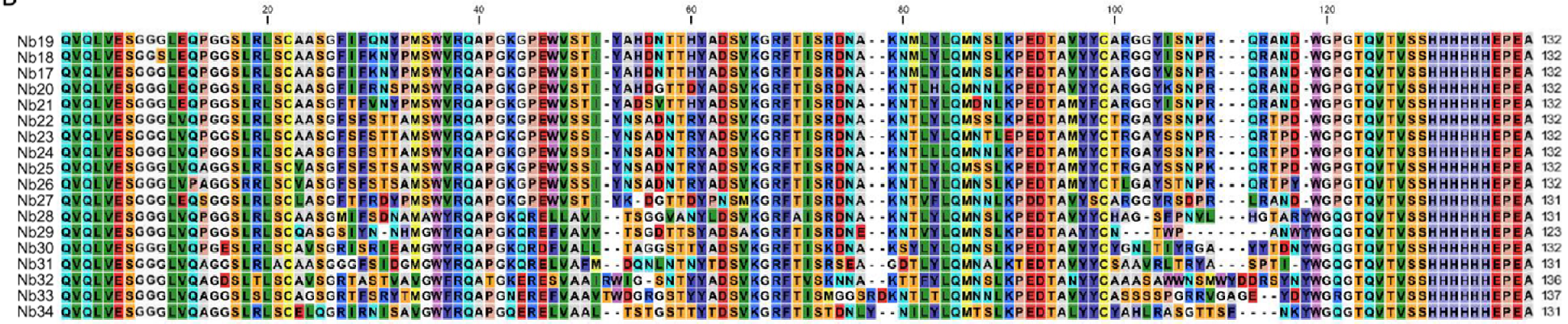

Appendix 1.4 Phenuivirus Gn sequence alignment

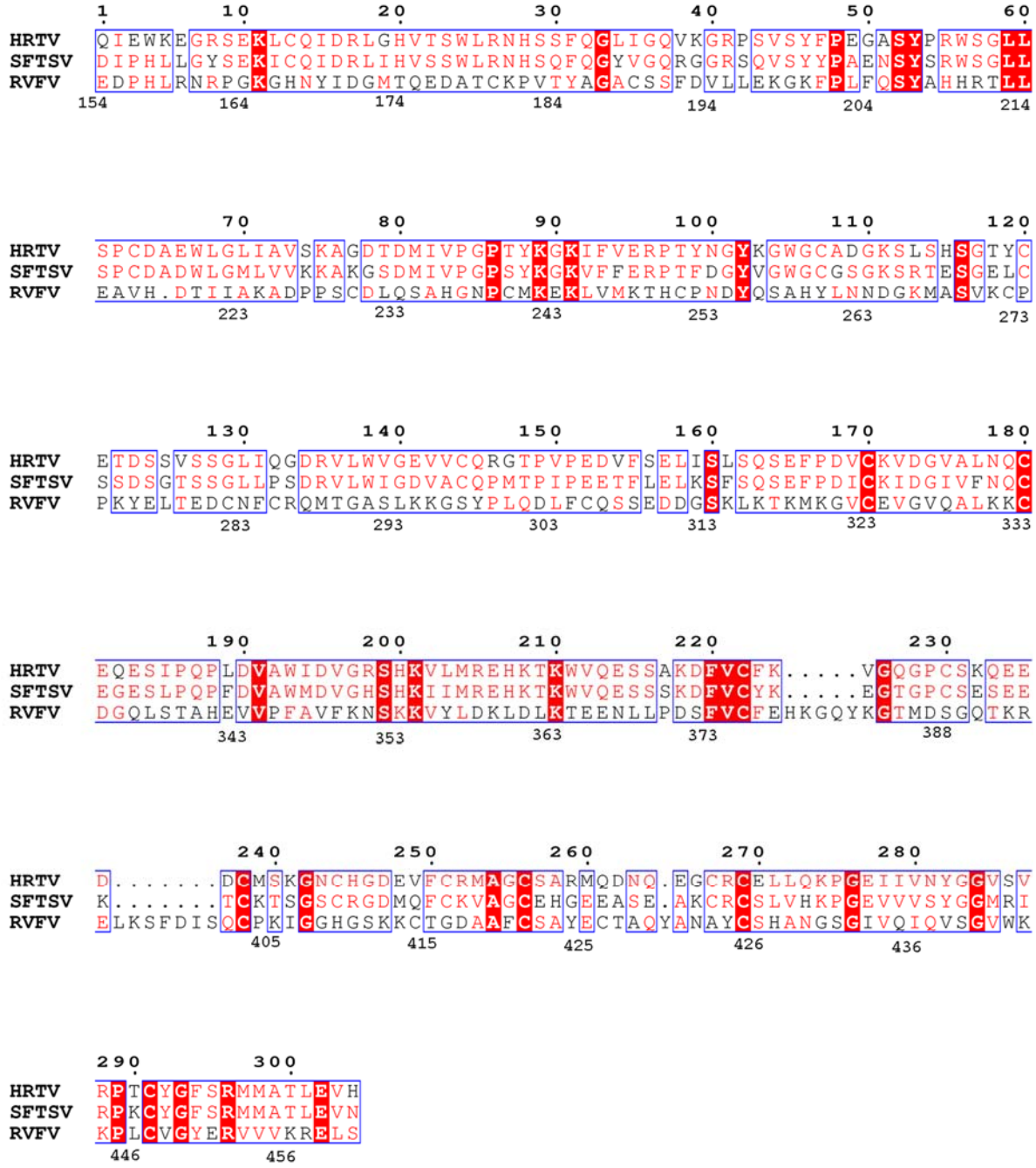

The sequence alignment was determined using Clustal Omega [179] and plotted with ESPRIPT[174]. Numbers above indicate residue numbers for SFTSV and HRTV, and numbers below indicate residue numbers for RVFV.

Appendix 1.6 Primers

Table of constructs and primers for RVFV Gn, HRTV Gn and SFTSV Gn

Construct	Start site – end site (length)[a]	Forward primer sequence (5' to 3')[b,c]	
RVFV GnX	E154 – D560 (407)	cgcaccggtGAGGACCCCCACCTGAGAAACAG	cgcggtaccATCCTGGGGTGGGCAGTGGG
RVFV GnL	E154 – S469 (316)	cgcaccggtGAGGACCCCCACCTGAGAAACAG	cgcggtaccATGGGGCTCGCACTTGGTGATACA
SFTSV	D21 – N342 (322)	cgcaccggtGACAGCGGCCCCATCATTTGTGC	cgcggtaccGTTCACTTCCAGGGTGGCCATCAT
HRTV Gn	C27 – K358 (332)	cgcaccggtGACGTGGCCTGCCAGCCTATGA	cgcggtaccCTTGTGCACTTCCAGGGTGGCC
HRTV Gn	C140 – P420 (281)	cgcaccggtTGCGCCGACGGCAAGAGCCT	cgcggtaccAGAGGCGCAAAAGTGGCTGGCG
	K164 – P420 (257)	cgcaccggtAAGAGCCTGTCTCACAGCGGCAC	cgcggtaccAGAGGCGCAAAAGTGGCTGGCG
	S177 – P420 (244)	cgcaccggtAGCTCCGTGTCCTCCGGCCT	cgcggtaccAGAGGCGCAAAAGTGGCTGGCG
	C140 – S469 (330)	cgcaccggtTGCGCCGACGGCAAGAGCCT	cgcggtaccTTTCTTCACGGGGTAGCAC
	K164 – S469 (305)	cgcaccggtAAGAGCCTGTCTCACAGCGGCAC	cgcggtaccTTTCTTCACGGGGTAGCAC
	S177 – S469 (293)	cgcaccggtAGCTCCGTGTCCTCCGGCCT	cgcggtaccTTTCTTCACGGGGTAGCAC
	E48 – K358 (311)	cgcaccggtGAGACAAACAAGAGCATCCAGATCGAGT	cgcggtaccCTTGTGCACTTCCAGGGTGGCC
	C140 – K358 (219)	cgcaccggtTGCGCCGACGGCAAGAGCCT	cgcggtaccCTTGTGCACTTCCAGGGTGGCC
	K164 – K358 (343)	cgcaccggtAAGAGCCTGTCTCACAGCGGCAC	cgcggtaccCTTGTGCACTTCCAGGGTGGCC

[a] Start and end site numbers are based on amino acid sequences M-segments of RVFV, HRTV and SFTSV.

[b] Underlined nucleotide sequence corresponds to restriction sites: Forward primer contains *Age* I restriction site and reverse primer contains *Kpn*I restriction site.

[c] Lowercase nucleotide sequences contains the stabilising flanking region (cgc) and restriction site, while the uppercase sequence is complimentary to region on cDNA

Primers

Nanobody sequencing primer: TTATGCTTCCGGCTCGTATG

pHLSec sequencing primers:
forward CACCAGCCACCACCTTCTGATAG
reverse GCTGGTTGTTGTGCTGTCTCATC

2rabHCAgeI f 2	GTAGCTGAAACCGGTCAGAGCCTGGAGGAGTCCGG
2rabHCAgeI f 4	GTAGCTGAAACCGGTCAGAGCCTGGTGGAGTCCGG
2rabHCAgeI f 5	GTAGCTGAAACCGGTCAGAGCCTGGTGGAGTCCGGA
2rabHCAgeI f 6	GTAGCTGAAACCGGTCAGAGCCTGGAGCAGTCCGG
2rabHCkpnI R	GTGGTGCTTGGTACCGCTGCATGTCGAGGGCGCAAC
rRLC FW1AgeI f1	GTAGCTGAAACCGGTCAGGTGCTGACCCAGACTCC
rRLC FW1 AgeI f2	GTAGCTGAAACCGGTCAGGTGCTGACCCAAACACC
rRLC FW1 AgeI f4	GTAGCTGAAACCGGTCAGGTGATGACCCAGACACC
rRLC FW1 AgeI f5	GTAGCTGAAACCGGTCAGGTGATGACCCAGACTCC
2rabLCxhoI R	GATACTAGTCTCGAGTTACTAGCAGTCACCCCTATTGAAG

Table of primers for InFusion cloning of rabbit Fabs

Appendix 1.7 Antigen specific B cell sorting gates.

B cell sorting, day 41

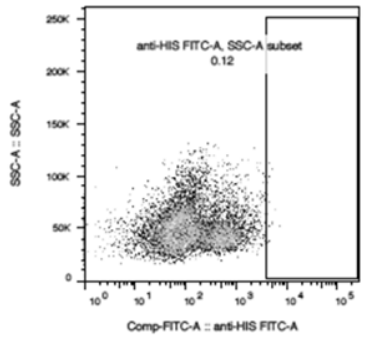

Mouse 10/HRTV-FITC

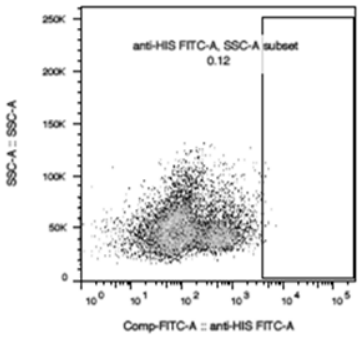

Mouse 6/HRTV-FITC

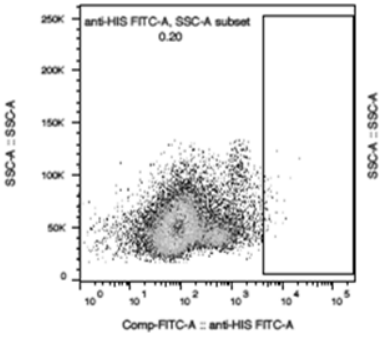

Mouse 10/SFTSV-FITC

B cell sorting day 58

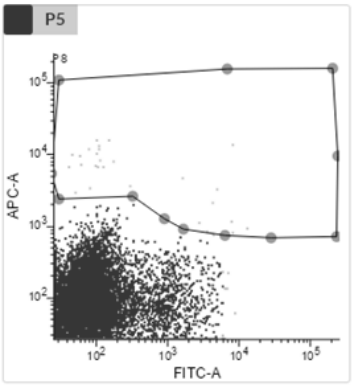

Mouse 7: HRTV Gn-APC + SFTSV Gn-FITC

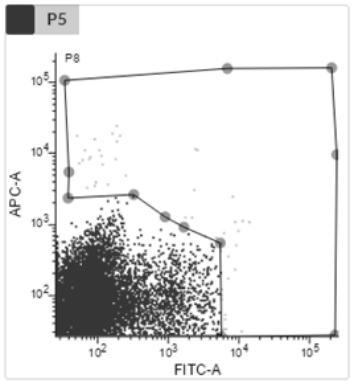

Mouse 7: HRTV Gn-APC +SFTSV Gn-FITC

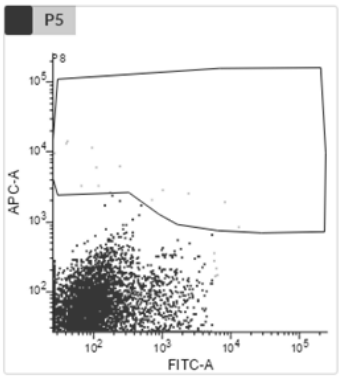

Mouse 12: HRTV Gn-APC +SFTSV Gn-FITC

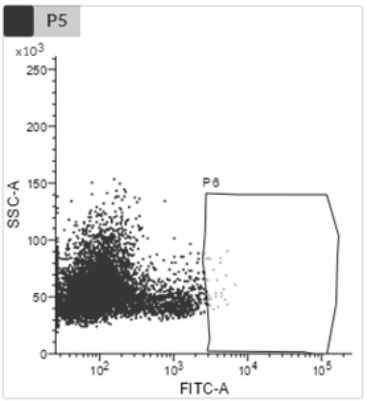

Mouse 13: SFTSV-FITC

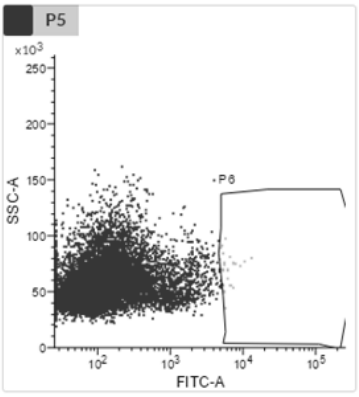

Mouse 13: HRTV-FITC

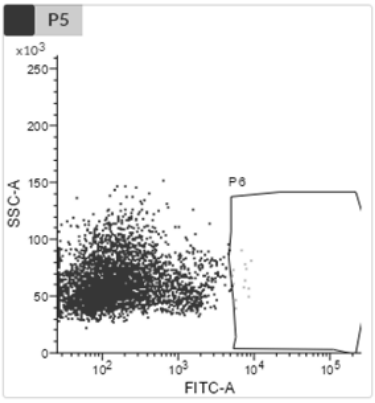

Mouse 13: RVFV-FITC